THE UNIVERSITY *of* EDINBURGH

Molecular Information Ratchets

Adam Wilson

Degree of Doctor of Philosophy

School of Chemistry

The University of Edinburgh

January 2012

For my parents.

Table of Contents

Chapter One:
Ratchet Mechanisms in Chemistry

Chapter Two:
A Three-Compartment Chemical Information Ratchet

Chapter Three:
Synthesis, Operation and Analysis of an Extended Three-Compartment Molecular Information Ratchet

Chapter Four:
Progress Towards Highly Extended Information Ratchets

Abstract and Layout of Thesis

In the emerging field of molecular machines, a molecular ratchet is a chemical system that allows the positional displacement of a submolecular component of be captured and directionally released. In information ratchets, the track over which a Brownian particle is to be transported is able to respond to the particle's position. By raising energetic barriers to translation selectively behind the particle, it is possible to move the particle in a forward direction. This Thesis describes the development of a series of chemically-driven information ratchets based on rotaxane architectures. Acylation of the rotaxane thread presents an impassible kinetic barrier to macrocycle shuttling. The incorporation of chiral centres into the thread allows the macrocycle's position to have an effect on the kinetics of acylation in a chiral environment, with the result that the macrocycle is transported by successive acylation reactions in a direction specified by the handedness of a chiral.

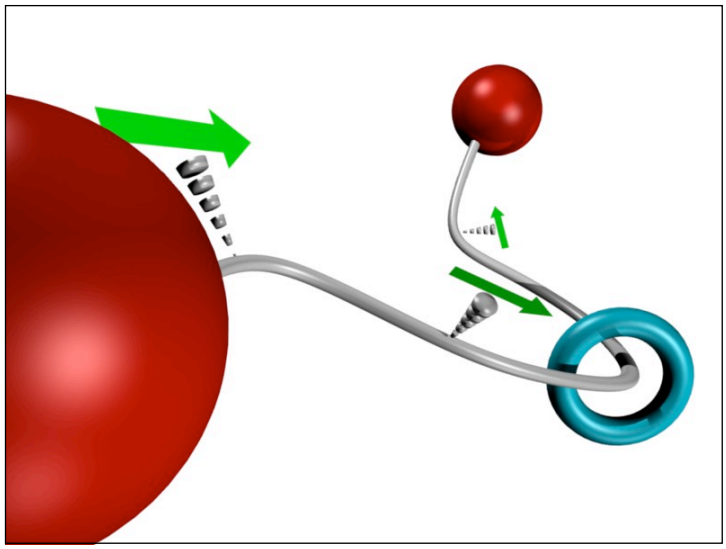

Figure 0.1. Cartoon representation of a rotaxane-based information ratchet, in which the direction of travel of the macrocycle is determined by chiral 'signposts' incorporated into the thread.

In Chapter One the physical principles of molecular motors are examined. It is shown that molecular motors are a subset of the much broader class of "triangular" reactions investigated by Onsager in 1931. Progress in the exciting field of artificial chemical ratchets and motors is reviewed, and the deep connections between molecular motors and the cyclic reaction networks postulated to explain the origin of biological homochirality are explored.

Chapter Two describes the synthesis and operation of a three-compartment rotaxane information ratchet in which the macrocycle can be transported along a thread in either direction depending on the handedness of a chiral catalyst. Internal mechanisms of operation are elucidated by treating the system as a hidden Markov process.

Chapter Three describes the synthesis and operation of a second-generation three-compartment information ratchet. A comparison between this system and that of the previous chapter sheds light on the complicated trade-offs between kinetics and thermodynamics when these molecular ratchets are operated.

In Chapter Four the ongoing efforts to construct extended information ratchets, incorporating many repeat units, are described. The synthesis of a five-compartment information ratchet proved unexpectedly difficult owing to problems of solubility. A four-compartment rotaxane was easier to synthesise. Preliminary findings suggest that an information ratchet mechanism is operating in this four-compartment system.

Declaration

The scientific work described in this thesis was carried out in the School of Chemistry at the University of Edinburgh between September 2008 and January 2012. Unless otherwise stated, it is the work of the author and has not been submitted in whole or in part in support of an application for another degree or qualification at this or any other University or institute of learning.

Signed:

Date:

Meetings Attended and Presentations Given

1. **Organic Research Seminars**, School of Chemistry, University of Edinburgh, United Kingdom, 2008–2011.
    (a) *Linear Information Ratchet Motor*, 10th October 2008
    (b) *Linear Information Ratchet Motor*, 7th November 2010
    (c) *Linear Information Ratchet Motors*, 5th April 2011

2. **School of Chemistry Visiting Speaker Colloquia**, School of Chemistry, University of Edinburgh, United Kingdom, 2008–2011.

3. **Special Symposium in Honour of David Reinhoudt**, University of Edinburgh, United Kingdom, 11th November 2008.
    Poster presentation: *Towards Molecular Information Ratchet Motors*.

4. **20th SCI Postgraduate Symposium**, School of Chemistry, University of St Andrews, United Kingdom, 2nd April 2009.

5. **School of Chemistry, Organic Section Firbush Symposium**, Firbush Point Centre, University of Edinburgh, UK, 12th April 2010.
    Poster presentation: *Towards a Linear Information Ratchet Motor*.

6. **Bruker Avance and TopSpin™ Training Course**, five-day onsite training at the Bruker UK headquarters, Coventry, United Kingdom,10th–14th May 2010.

7. **39th RSC Scottish Regional Meeting of the Organic Chemistry Division**, University of Edinburgh, 14th December 2010.
    Poster presentation: *A Linear Information Ratchet Motor*.

8. **School of Chemistry, Organic Section Firbush Symposium**, Firbush Point Centre, University of Edinburgh, UK, 5th April 2011.

   Oral presentation: *Linear Information Ratchet Motors*.

9. **22nd SCI Regional Graduate Symposium on Novel Organic Chemistry**, University of Edinburgh, 3rd May 2011.

10. **Challenges in Organic Materials & Supramolecular Chemistry (ISACS6)**, Beijing, China, 2nd–5th September 2011.

    Poster presentation: *Molecular Machines: A Linear Information Ratchet Motor*

11. **40th RSC Scottish Organic Division Meeting**, University of Strathclyde, 14th December 2011.

Acknowledgements

First of all I would like to thank Dave, both for creating a such a wonderful environment in which to work, and for letting me join it. It's not often one gets such an opportunity to work on such fascinating projects and with such extraordinary people, and it is a time I will never forget.

When I first came to the group everything I touched either smashed, spilled, fell apart, stopped working or disappeared altogether. The person with the unenviable task of containing this vortex of destruction was Nathalie, and she bore it with the kind of patience not even Job could muster. By the time the responsibility passed to Armando things had quietened down a bit, but that's not to say he had an easy job of it either. Our sessions of wrestling with theories, rushing down blind alleys and coming up with new solutions were some of the most exasperating and enjoyable parts of my time here. Between them, Nathalie and Armando taught me everything I know about practical organic synthesis, and I thank and continue to admire them. In the latter stages of my PhD I had the pleasure of working with two extremely talented chemists: Jordi, the eternal optimist, and Miriam, the original autonomous machine. They took broken instruments and made them sing.

The fourth bay from the left was a fun place to work, as well as an exciting forum of political, social and musical debate. Thank you Bartek, Francesco, Jon B, Jordi (again), Nathalie (again), Romen and Tao; also Sonja, to whom I bequeathed my fume hood and a lot of excess entropy. Thanks, too, to the people I shared a lab with, past and present: Alan, Amaya, Ángel, Anthony, Ara, Aurélien, Barney, Barry, Bea, Chris, Christoph, Clint, Costanza, Craig, Daniel, Dave H, David, Dominik, Rock Star Chemist Edzard, Emily, Eva, Fabien, Francesca, Guillaume, Gus, Hei-Man, Jhenyi (travel companion on the epic China trek), John, Jon D, Jonas, Jeff, Kat, Kathleen, the inimitable Kevin, Léo, Lily,

Marcus, Maria, Marius, Mark, Max, Mike, Mustafa, Patrick, Paul, Philipp, Roy, Sarah P, Sarah T, Satoshi, Steffen, Steve, Steven, Takeshi, Teresa, Ula and Victor.

Thanks to Louise and Stuart for keeping our lab from falling apart; thanks again to the NMR and LCMS monkeys Bartek, Dave H, Miriam, Paul and Sonja. The wizards who run the department machines were absolutely invaluable: for NMR, Juraj, Lorna and Marika; for mass spec, Alan Taylor and Logan Mackay. Thanks to the support staff, Amanda and Annette, Tim, Derek, Raymond and John, who kept things running smoothly.

When I first came to Edinburgh I moved in with complete strangers and struck gold. Thank you Koosha, Taraneh and Vandana, for putting up with me for these three-and-a-bit years, for cooking for me when I was down, for not minding the harmonica too much.

Special thanks to the group who played a major role in maintaining my sanity throughout this period: Ben, Cathryn, Charlotte, Dan T and Jamie. Thanks for the Scrabble.

Artemis, thank you for your love and kindness. You took days that were just days, and made them into good days. مرسی عزیزم

I'd like to express my profound appreciation for the good people over at the Blender Foundation, who made a free, open-source program that lets you draw interlocked structures without needing to delete things behind other things or add masking layers or any of that nonsense. This thesis (indeed, this entire PhD) would have taken twice as long without it. I should also mention that the idea of

using hidden Markov models came not from anything to do with chemistry but from reading *The Language Instinct* by Steven Pinker,[1] so thanks to him too.

And finally, I thank my family – Luke, and especially my parents – for their endless support and encouragement over the years, for cakes and cards. This thesis is for you.

[1] In which I also learned that the average American high-school leaver has a vocabulary of over 60,000 words. Think about that a second: that's a new word learned *every ninety waking minutes* on average. Could you imagine memorising phone numbers at that rate, and remembering them for the rest of your life? It's incredible. But I digress.

List of Abbreviations

δ	chemical shift
Boc	*tert*-butoxycarbonyl
Bz	benzoyl
dba	dibenzylammonium
DCM	dichloromethane
DIPEA	diisopropylethylamine
DMAP	4-dimethylaminopyridine
DMF	dimethylformamide
DMSO	dimethylsulfoxide
DNA	deoxyribonucleic acid
eq	equivalents
ESI	electrospray ionisation
fum	fumaramide
HF·py	hydrogen fluoride as a solution in pyridine
HMM	Hidden Markov Model
HPLC	High Performance Liquid Chromatography
HOBt	hydroxybenzotriazole
HR-MS	High Resolution Mass Spectrometry
IPA	2-propanol (isopropyl alcohol)
LR-MS	Low Resolution Mass Spectrometry
mal	maleimide
MALDI	Matrix-Assisted Laser Desorption Ionisation
mba	monobenzylammonium

M.p.	Melting point
NMR	Nuclear Magnetic Resonance
PE	Petroleum Ether (60–80 °C)
PMB	*para*-methoxybenzyl ether
ppm	parts per million
quant.	quantitative yield
Ref.	Reference
rt	Room Temperature (298 K)
succ	succinamide
TBAF	tetrabutylammonium fluoride
TBDMS	*tert*-butyldimethylsilyl
TBDPS	*tert*-butyldiphenylsilyl
TBTU	*O*-(Benzotriazol-1-yl)-*N*,*N*,*N*′,*N*′-tetramethyluronium tetrafluoroborate
TFA	trifluoroacetic acid
THF	tetrahydrofuran
TIPS	triisopropylsilane
TLC	Thin Layer Chromatography
TMSOMe	Methoxytrimethylsilane
vol	volume
wt.	weight

Conventional abbreviations for units and physical quantities and constants are not included.

General Remarks on Experimental Data

Unless otherwise stated, all reagents were purchased from commercial sources and used without further purification. Anhydrous solvents (DCM, $CHCl_3$) were obtained by passing the solvent through an activated alumina column on a PureSolv™ solvent purification system (Innovative Technologies, Inc., MA). Anhydrous dimethylformamide and tetrahydrofuran were purchased from Aldrich. Flash column chromatography was carried out using Kieselgel C60 (Merck, Germany) as the stationary phase. Analytical thin layer chromatography was performed on 0.25 mm thick precoated silica gel plates ($60F_{254}$, Merck, Germany) as the stationary phase. Preparative thin layer chromatography was performed on 500 μm or 1500 μm thick precoated silica gel plates (Analtech, Germany). Compounds were visualised under UV light or using ninhydrin or permanganate dips. ^{1}H and ^{13}C NMR spectra were recorded on Bruker AV 400 or AV 500 instruments as indicated, at a constant temperature of 300 K unless otherwise stated. Chemical shifts (δ) are reported in parts per million (ppm) and referenced to the residual solvent peak. When mixtures $CD_3OD/CDCl_3$ were used, the former was chosen as the reference. Coupling constants (*J*) are reported in hertz (Hz). Standard abbreviations indicating multiplicity are given: br = broad, d = doublet, q = quartet, quint = quintet, s = singlet, t = triplet. Assignments of the ^{1}H NMR signals was accomplished by two-dimensional NMR spectroscopy (COSY, NOESY, HSQC, HMBC). Carbon NMR spectra were recorded as "pendant" experiments. LCMS analysis was performed on an Agilent Technologies 1200 LC system with 6130 single quadrupole. Melting points were determined using a Sanyo Gallenkamp apparatus and are uncorrected. ESI accurate mass spectroscopy was carried out by the mass spectrometry services at the EPSRC National Mass Spectrometry Centre in Swansea (Wales). Optical rotations were recorded on a Polaar 20 polarimeter at 589 nm (sodium D line) at 20 °C in the concentration (g / 100 mL) and solvent indicated in each case. MALDI mass spectrometry was carried out on a solariXFTCIR mass spectrometer equipped with a 12 T superconducting magnet (Bruker Daltonics).

Chapter One

Ratchet Mechanisms in Chemistry

Acknowledgements

Dr Bartosz Lewandowski is gratefully acknowledged for examining and proofreading this Chapter.

Synopsis

Biology employs a bewildering array of extraordinary molecular motors to perform the countless tasks necessary for life. However, it is only recently that chemists have been able to devise artificial chemical systems capable of performing cumulative work on the molecular level. The coupling of synthetic molecular motors to other chemical systems or the outside world so that their fuelled motions can be used to perform useful tasks has still not been achieved. The development of molecular rotary and linear motors depends crucially on ratchet mechanisms, the means by which random Brownian motion can be harnessed and converted into directed molecular movement. This Chapter discusses the development of some of the first true molecular motors, and shows how such molecular machines are a special case of the general class of the cyclic or "triangular" reactions famously investigated by Onsager. Deep connections exist between the physics and chemistry of molecular motors and recent research into the origins of homochirality in life on Earth.

Molecular machines are able to exist in a number of states corresponding to positional displacements of submolecular components; external stimuli may be used to move these components from one position to another. Consideration of the principles of detailed balance and microscopic reversibility shows that no net flux between these positional states is possible at equilibrium. Nevertheless, ratchet mechanisms allow the machine's reversible positional displacements to be coupled to an energetically favourable consumption of fuel. By maintaining a far-from-equilibrium environment, detailed balance is broken and the system can be made to cycle between positional states with net directionality. By ensuring that the machine returns to its starting state via *a different path to the one which it set out upon, these ratcheted cyclic reactions allow the work done to persist after the thermodynamic driving force has been removed; this is a requirement both for*

molecular motors that must do repetitive work over many cycles, and for the reaction networks proposed for the enantioenrichment of a primordial chiral pool.

This Chapter discusses the physics of ratchet mechanisms in molecular machines and elsewhere. Many artificial chemical systems have been prepared to study ratchets in isolation; these have afforded valuable insights into the thermodynamic and kinetic processes involved in their operation. In parallel with these more theoretical studies, complex rotary or linear molecular motors have been synthesised. In each system, one finds the necessary requirements for the maintenance of directional flux in a cyclic reaction network. It is hoped that the fields of molecular machines and origin of homochirality will both benefit from an appreciation that the theoretical constraints faced by each discipline are in fact common to both, and that advances in one field will continue to shed light upon the other.

1.1 Introduction

Recent years have seen the emergence of chemical systems in which some mechanical task is performed solely by the stimulus-induced positional displacement of submolecular components. The most striking of these have demonstrated that a molecular-level conformational change can be harnessed to cause the lifting,[1] turning[2] and directional transport[3] of objects large enough to be seen with the naked eye. Nevertheless, in each of these pioneering examples the molecules responsible for the macroscopic motion are simple chemical switches; as such, they are unable to perform cumulative work. After performing one work cycle a switch cannot be reset to do more work without undoing the work it did previously.

In order to progress beyond simple switches and develop motors capable of cumulative or progressive mechanical work, it is vital to appreciate the fundamental differences between controlling motion in the macroscopic and nanoscopic worlds (in the words of Astumian, molecular machines must "walk in a hurricane and swim in molasses").[4] Machines that work under such conditions must operate not by fighting Brownian motion but by exploiting it as a randomising element necessary for stochastic conformational pumping. The design principles for such molecular motors must therefore be deeply rooted in the theories of statistical thermodynamics. Consideration of the principles of detailed balance and microscopic reversibility reveals that far-from-equilibrium conditions must be maintained in order for directional flux to be possible. The fundamental theories from which these conclusions are derived have also found use in the fascinating research on the origin of biological homochirality. By treating motion with net directionality as a type of triangular reaction, deep connections between molecular machines and the problem of primordial enantioenrichment become apparent.

1.2 Molecular Machines and the Principle of Detailed Balance

The crucial difference between a motor and a switch is that a switch influences a system as a function of state; returning the switch to its original position will undo any work the switch has done.[5] A motor, on the other hand, influences a system as a function of the trajectory of its components or the substrate.[5] As such, completion of a motor's cycle of operation will reset the motor without undoing its mechanical effect on the system. This ability of a motor to return to its starting state *via* a different pathway to the one it set out upon may be visualised in terms of a cyclic reaction: whereas a switch may be defined as a system that proceeds from state A to state B along a certain pathway and can only proceed from B back to A *via* a reversal of that pathway, a motor is able to cycle through (at least) three states in the manner of A→B→C→A. Conceived in this way, it is apparent that molecular motors represent a special case of the more general class of cyclic or triangular reactions famously investigated by Onsager.[6,7] In 1931 Onsager demonstrated that cyclic reactions (and consequently molecular motors) will show no net directional flux at equilibrium. This result follows from a consideration of the concepts of microscopic reversibility and detailed balance.

The principle of detailed balance states that for a system of species i and j in dynamic exchange *at equilibrium*, the number of transitions from state i to state j is equal to the number of transitions in the reverse direction, or

$$N_i P_{ij} = N_j P_{ji}$$

where N_i is the number of particles in state i and P_{ij} is the probability of transition to state j for a given molecule in state i.[8] Directional cycling of the

type A→B→C→A cannot proceed adiabatically, because at equilibrium the number of transitions in the opposite direction (A→C→B→A) would occur with equal frequency. An appeal might be made to the idea of using energetically favourable reactions to force the cyclic reaction to proceed in one direction only, but this is forbidden by the second law of thermodynamics. In an isolated system, no reaction is truly irreversible, a consequence of the time-reversal invariance of molecular interactions, and analysis of putative adiabatic A→B→C→A systems shows that contributions from the reverse reactions will always negate any directional flux unless energy is added to the system (Figure 1.1).[9,10]

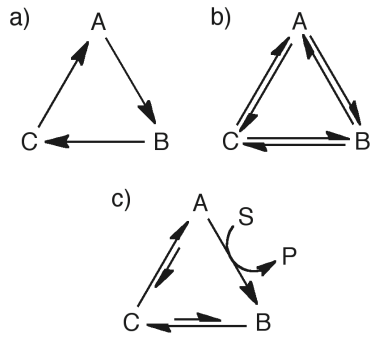

Figure 1.1 Triangular processes such as (a) cannot be sustained adiabatically; in the absence of an energy input an equilibrium with no net flux will result (b). Only when the forward reaction is coupled to an energetically favourable consumption of fuel (S→P) can a cyclic reaction be maintained (c).

A treatment by Astumian demonstrates that net directional circumrotation of small macrocycles around a larger one (see Figure 1.2) is possible only when coupled to a non-equilibrium reaction that converts a starting material S into a product P.[11] The reaction between S and P is itself mechanically reversible in that a movie of the macrocycles rotating backwards coupled to the reaction P→S would still make sense – indeed, *at equilibrium* these processes would occur at the same rate with no net work done, in accordance with the principle of detailed balance. However, by ensuring that the system is kept away from

equilibrium by constant addition of S (or removal of P), a catenane motor can be made to rotate in one direction only.

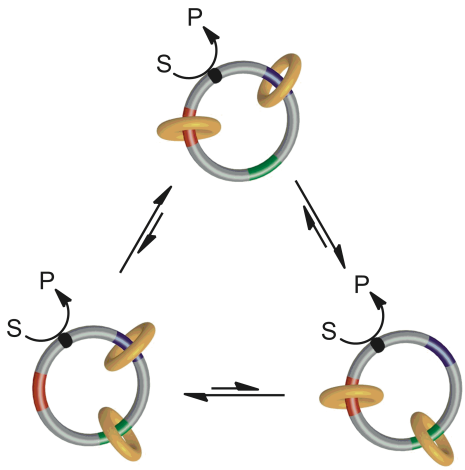

Figure 1.2 A triangular reaction may be made to proceed directionally only if coupled to an energy input, such as consumption of a fuel during a chemical reaction (S⟶P).[6,7,11]

In order for cumulative and progressive work to be done by a molecular system, it is useful that local environments that are out of equilibrium are preserved by some form of compartmentalisation.[5] These compartments may be demarcated by addition of an impassable kinetic barrier to dynamic exchange; alternatively, very short timescales of reaction might be employed, in which there is not sufficient time for the system to reach its global equilibrium. The [3]catenane discussed by Astumian is self-compartmentalising, in that the motion of one macrocycle is restricted by the presence of the other; a [2]catenane with one macrocycle moving sequentially between three binding sites would not demonstrate directional rotation because there is no barrier to the equally probable transitions in the reverse direction.

1.3 The Role of Triangular Reactions in the Origin of Biological Homochirality

Fundamental thermodynamic principles, related to those required for a molecular machine to do work, have been studied in research relating to the origin of biological homochirality. In 1953, Frank described an autocatalytic reaction in which metastable dimers (LL or DD) catalyse the formation of one enantiomer (L or D) while suppressing the other.[12] A theoretical treatment demonstrated that such a network would result in the amplification of a very small enantiomeric excess, ultimately leading to the near-complete conversion of the reactants into the major enantiomer. Experimental verification came in 1995 with the discovery of the Soai reaction, in which a secondary alcohol (close to racemic; seeded with a small amount of one enantiomer) in the presence of diisopropylzinc and an achiral aldehyde results in dramatic enantioenrichment after only a few cycles (Figure 1.3a).[13] A more direct link to the origin of homochirality in biological or prebiotic systems came with the elucidation, by Huber and Wächtershäuser, of reaction networks between certain amino acids under hot, anaerobic, aqueous conditions believed to be representative of primordial Earth.[14,15] On addition of water and carbon monoxide, and in the presence of (Ni,Fe)S and hydrogen sulfide, dipeptides were found to form (Figure 1.3b). Importantly, for some amino acids (L-phenylalanine and L-tyrosine), racemisation was observed. The relevance of this system to homochirality was seen by Plasson *et al.*,[16] who hypothesised that if the dipeptides were able to act as chirally selective autocatalysts, a slight enantiomeric excess in starting materials would be enhanced at the expense of the minority enantiomer exactly as Frank predicted. Theoretical consideration of these networks has also demonstrated that they actually lead to *reduction* of the enantiomeric excess if there is no energy input.[17] The triangular reactions that make up the networks must obey the principle of microscopic reversibility, and unless they are coupled to an energetically favourable process such as the

conversion of a fuel to waste products, the contribution of reverse reactions increase until equilibrium is reached and no net flux is generated (Figure 1.4).

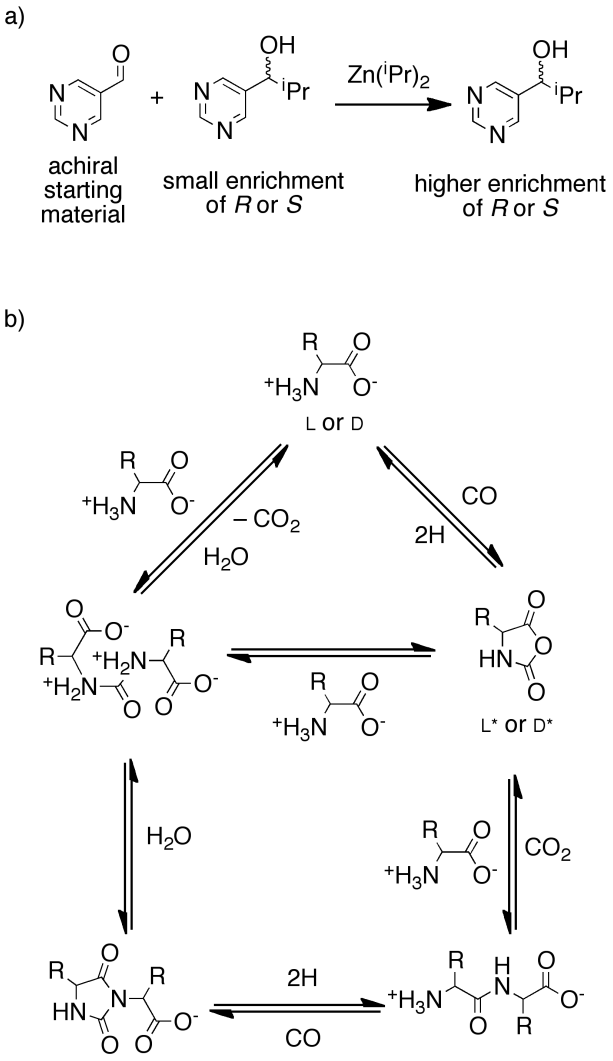

Figure 1.3 a) the Soai reaction;[13] b) the peptide formation and degradation reaction described by Wächtershäuser and co-workers.[14]

The enantioenrichment achieved by these systems is related to the mechanical work that can be done by a molecular motor: in both cases, triangular networks of reactions, coupled to an external source of energy, are used to perform a task (enantioenrichment or positional displacement) that is not undone (racemisation or retrograde positional displacement) when the reacting species return to their original states.

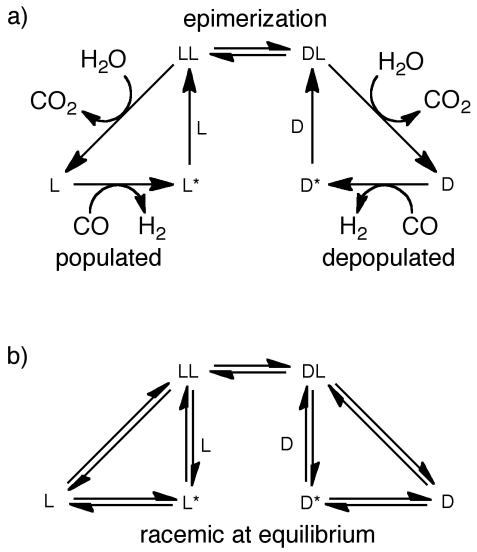

Figure 1.4 Reaction network for the Wächtershäuser system: a) mass flow (H_2O and CO in; CO_2 and H_2 out) results in far-from equilibrium directional flux and enantioenrichment; b) without mass flow, a racemic equilibrium eventually results.[15,17]

While these reaction networks require a steady supply of chemical fuel, directional flux may be maintained in the absence of mass flow, as long as the energy input is not subject to microscopic reversibility. Such energy sources include external magnetic fields, Coriolis forces and photochemical reactions.[15] The light-fuelled rotary motors published by the Feringa group (discussed in detail below) illustrate this point. Simply heating the system generates no net flux, but directional rotation is possible on irradiation with light because the motor is able to convert photons (fuel) into heat (waste) (Figure 1.5).

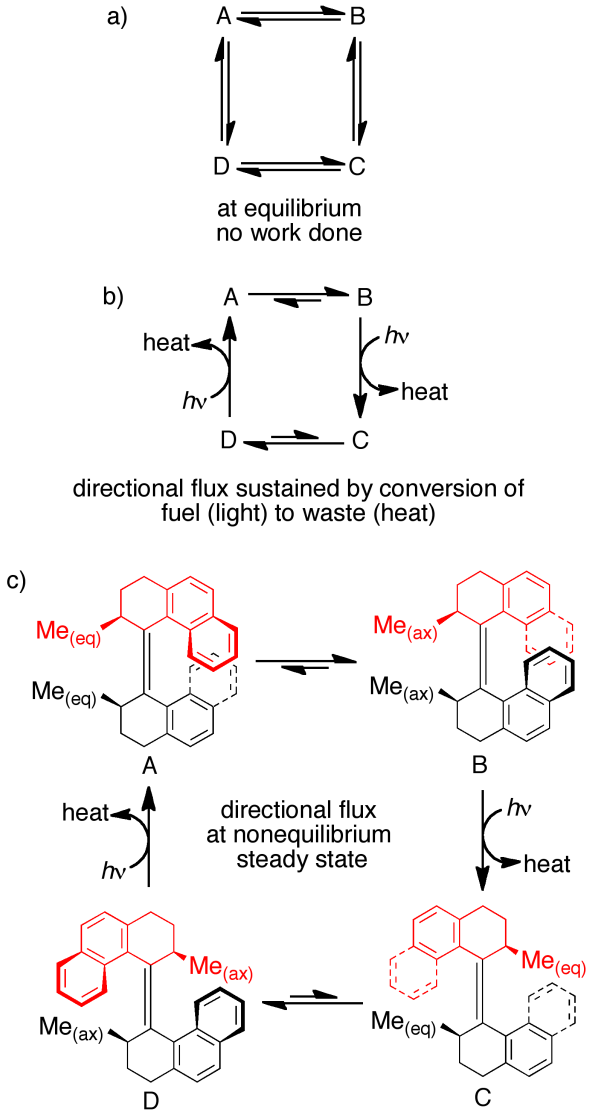

Figure 1.5 (a) A four-state reaction network at equilibrium cannot do net work; (b) conversion of fuel (light) to waste (heat) can provide the necessary energy input for directional cycling between states; (c) Feringa *et al.*'s light-driven rotary motor is a realisation of this principle (for an in-depth discussion see Section 1.5.1).

Research into the development of molecular motors has required an understanding of mechanisms known in the physics literature as "Brownian ratchets".[18,19] Ratcheting has been described as "the capturing of a positional displacement of a substrate through the imposition of a kinetic energy barrier which prevents the displacement being reversed when the thermodynamic driving force is removed."[5] In fact, more generally, it is the coupling of an

energetically favourable process to a reversible one (or a network of reversible processes) in order to drive the reversible process directionally. In the special case of molecular machines, the process to be driven is positional displacement of a substrate. The ways of transporting a Brownian particle directionally along a compartmentalised potential energy surface fall broadly into two categories: energy ratchets and information ratchets.[4,5,18,19] In energy ratchets, transport is achieved by a periodic, repetitive raising and lowering of the surface's minima and maxima; this cyclic fluctuation takes place irrespective of the position of the particle on that surface. In information ratchets, kinetic barriers to translation are raised and lowered locally depending on the position of the particle.

1.4 Examples of Simple Ratchets

In interlocked architectures at least, the development of molecular ratchets has its origins in the pioneering work on bistable positional switches by the groups of Stoddart,[20–23] Sauvage[24–26] and others. It was soon seen that by incorporating orthogonal switching mechanisms to prevent a return to the system's initial state when the first switch was reversed, true ratchet mechanisms could be produced. While chemical ratchets are essential components of molecular motors, they can also be studied in isolation, affording insights into how directional discrimination occurs at a single site. In many cases, study of these simple ratchets points directly to how they may be incorporated into a molecular motor.

1.4.1 Energy Ratchets

In a landmark study by Leigh *et al.* in 2006, a Brownian particle (the macrocycle component of a rotaxane) was driven energetically uphill into the less favourable of two binding sites by the use of an energy ratchet process (Scheme 1.1).[27] Rotaxane **1** was prepared as a single positional isomer with the entire population of the macrocycle residing over the fumaramide residue. On removal of the kinetic barrier to shuttling, the equilibrium distribution at room temperature is 85% *fum*-*E*-**1**, 15% *succ*-*E*-**1**, and although macrocycles are free to exchange between the two compartments (the compartments are "linked"[5,28]), the principle of detailed balance dictates that no net flux can occur. Detailed balance is broken by light-induced $E \rightarrow Z$ isomerisation which reduces the affinity of the macrocycle for this binding site: net flux is generated as the system relaxes into a new equilibrium with 56% of the macrocycles over the (now preferred) succinamide residue. Exchange between the two compartments is halted by an unlinking stimulus – the addition of a silyl protecting group that acts as a barrier to shuttling. Thermal $Z \rightarrow E$ isomerisation then returns the fumaramide residue to its original configuration. Through operation of this cycle (balanced and unlinked, unbalanced and unlinked, unbalanced and linked, balanced and linked, and finally returning to its original unlinked state with the macrocycle distribution altered) the population of macrocycles kinetically locked into the least favourable compartment increases from 15% to 56%. The kinetic barrier prevents the "ratcheted" macrocycles from returning to the equilibrium distribution once the thermodynamic driving force is removed.

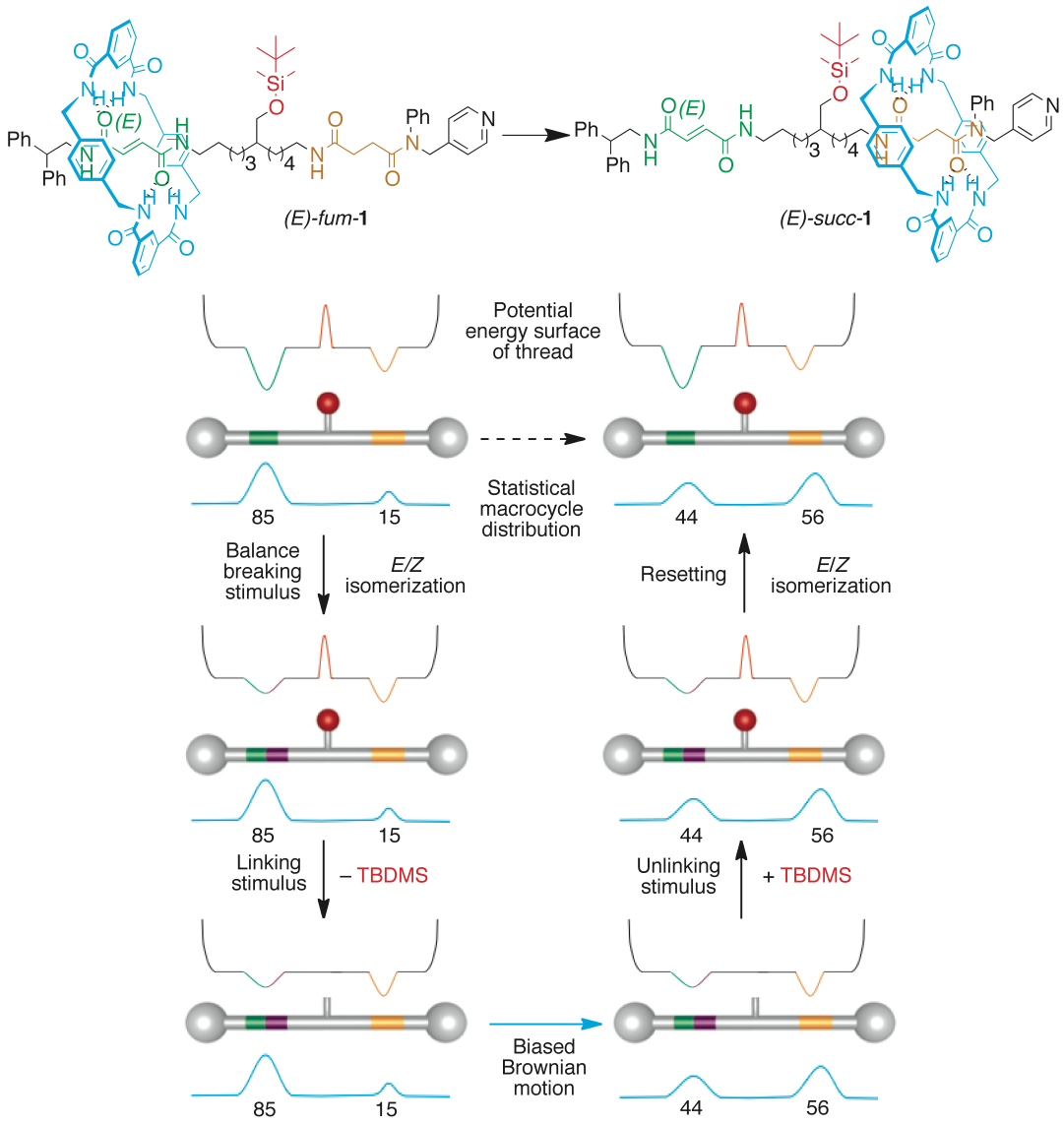

Scheme 1.1 An energy ratchet that transports a particle enthalpically uphill.[27]

1.4.2 Information Ratchets

Rotaxane **2**, published by Leigh *et al.* in 2007, makes use of an information ratchet mechanism to induce a far-from-equilibrium macrocycle distribution (Scheme 1.2).[18] The α-methyl stilbene group acts as a gate that either permits

(*E*-configuration) or prevents (*Z*-configuration) the macrocycle from shuttling between the dibenzylammonium compartment (dba, *left*) and the monobenzylammonium compartment (mba, *right*). On irradiation in the presence of photosensitiser benzil the gate is mostly closed, but energy transfer from a benzophenone moiety incorporated into the macrocycle is able to induce $Z \rightarrow E$ photoisomerisation. The distance dependence of this energy transfer, together with the inherent asymmetry of the thread, allows the macrocycle to "signal" its location to the gate, thereby selectively lowering the barrier to shuttling when the macrocycle is in the left-hand compartment. When the macrocycle is in the right-hand compartment (far from the gate), the benzil-sensitised reaction dominates and the gate remains mostly closed. In this way, the macrocycle distribution is driven away from its equilibrium value of 65:35 dba-**2**:mba-**2** to a maximum ratio of 45:55 without the affinity for either compartment ever varying. The energy input needed for this directional transport[29] is provided by the photons of light, which may be considered as serving to erase information regarding the macrocycle's (probable) location and pay the energetic cost of the information transfer process.

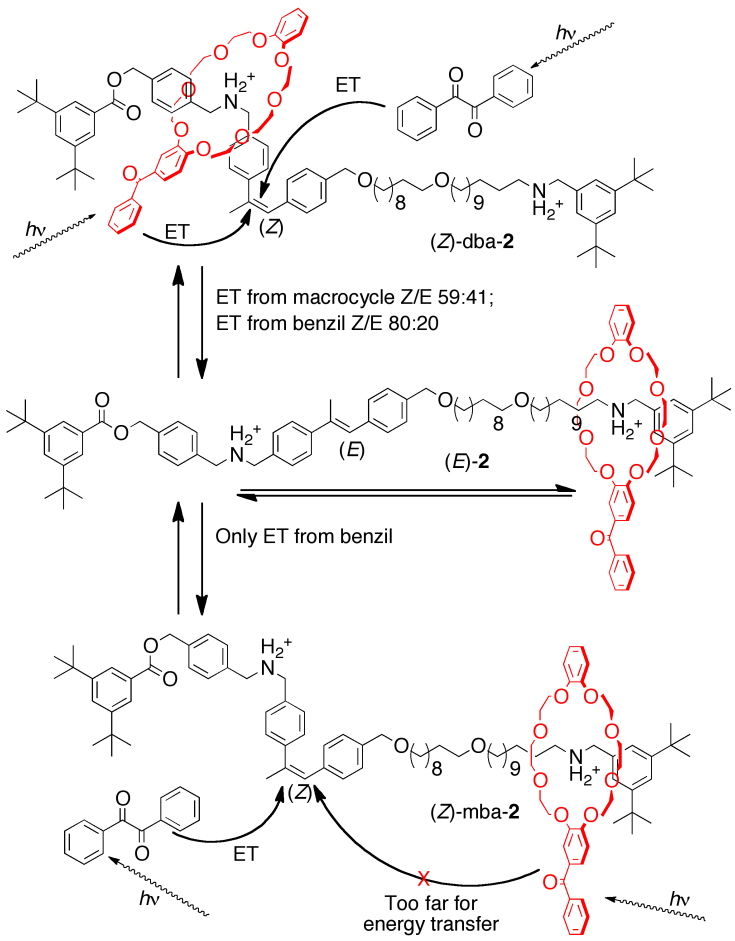

Scheme 1.2 A light-powered molecular information ratchet.[18]

An information ratchet fuelled by chemical energy, rotaxane **3**, was published by Leigh *et al.* in 2008 (Scheme 1.3).[30] The presence of the macrocycle on one side or the other of the central carbon atom lends chirality to the system. The rotaxane with a freely shuttling macrocycle is best thought of as a pair of enantiomers in equilibrium. As such, **3** is amenable to enantioenrichment by dynamic kinetic resolution in a chiral environment. A chiral acylation catalyst is used to drive the system from its equilibrium ratio of 50:50 *left*-**3**:*right*-**3** to an unequal distribution of 33:66. This proceeds by raising a kinetic barrier to shuttling preferentially behind the macrocycle; the binding affinity for the two compartments is unchanged throughout the process. Use of the catalyst's chiral antipode gives the expected equal and opposite ratio of 66:33 *left*-**4**:*right*-**4**.

Movement away from a 50:50 ratio represents a decrease in the entropy of the system, the energy penalty for which is paid by the conversion of a high-energy fuel (benzoic anhydride) into lower-energy products.

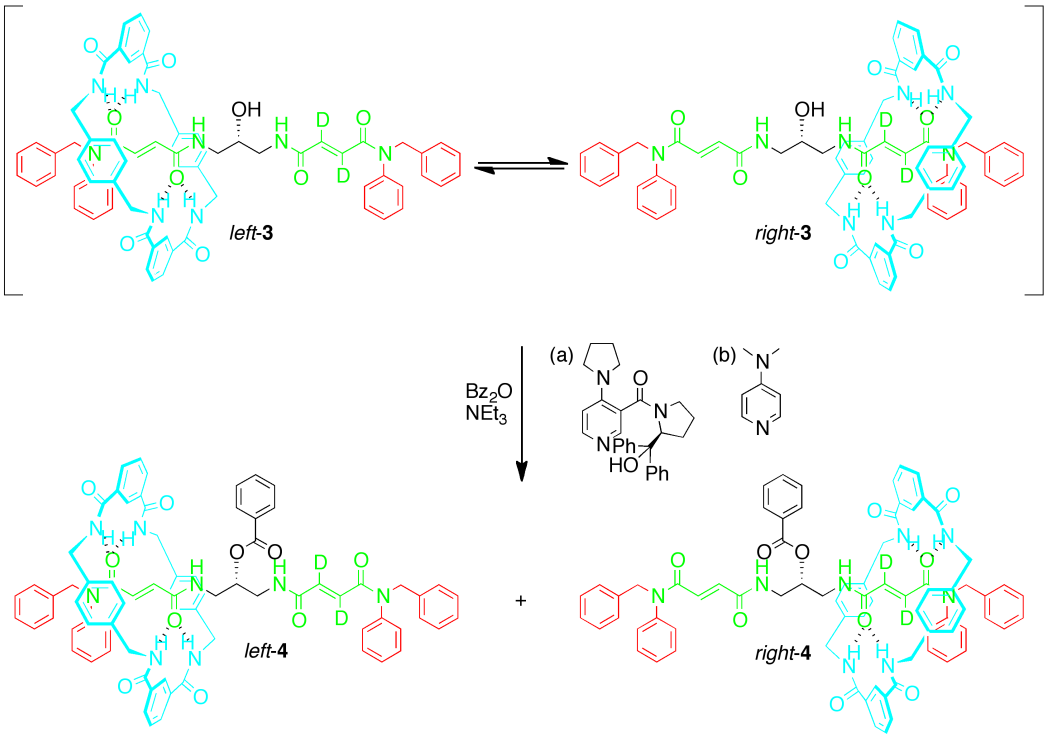

Scheme 1.3 A chemically fuelled molecular information ratchet.[30]

The same methodology was employed to ratchet the unsymmetrical rotaxane **5** uphill in terms of enthalpy: by selectively acylating when the macrocycle is on one side of a chiral centre, the distribution can be shifted from its equilibrium value of ~75:25 *fum*-**5**:*succ*-**5** to a value of 63:37, corresponding to a transportation of 15% of the macrocycles from an energetically favourable fumaramide binding environment into an unfavourable succinamic binding environment. The process may be readily understood in terms of the Curtin-Hammett principle: the final ratio of products is determined, not so much by the equilibrium distribution of the rapidly converting intermediates **5**, but by the

differences in energy of the two transition states made accessible by the chiral catalyst.

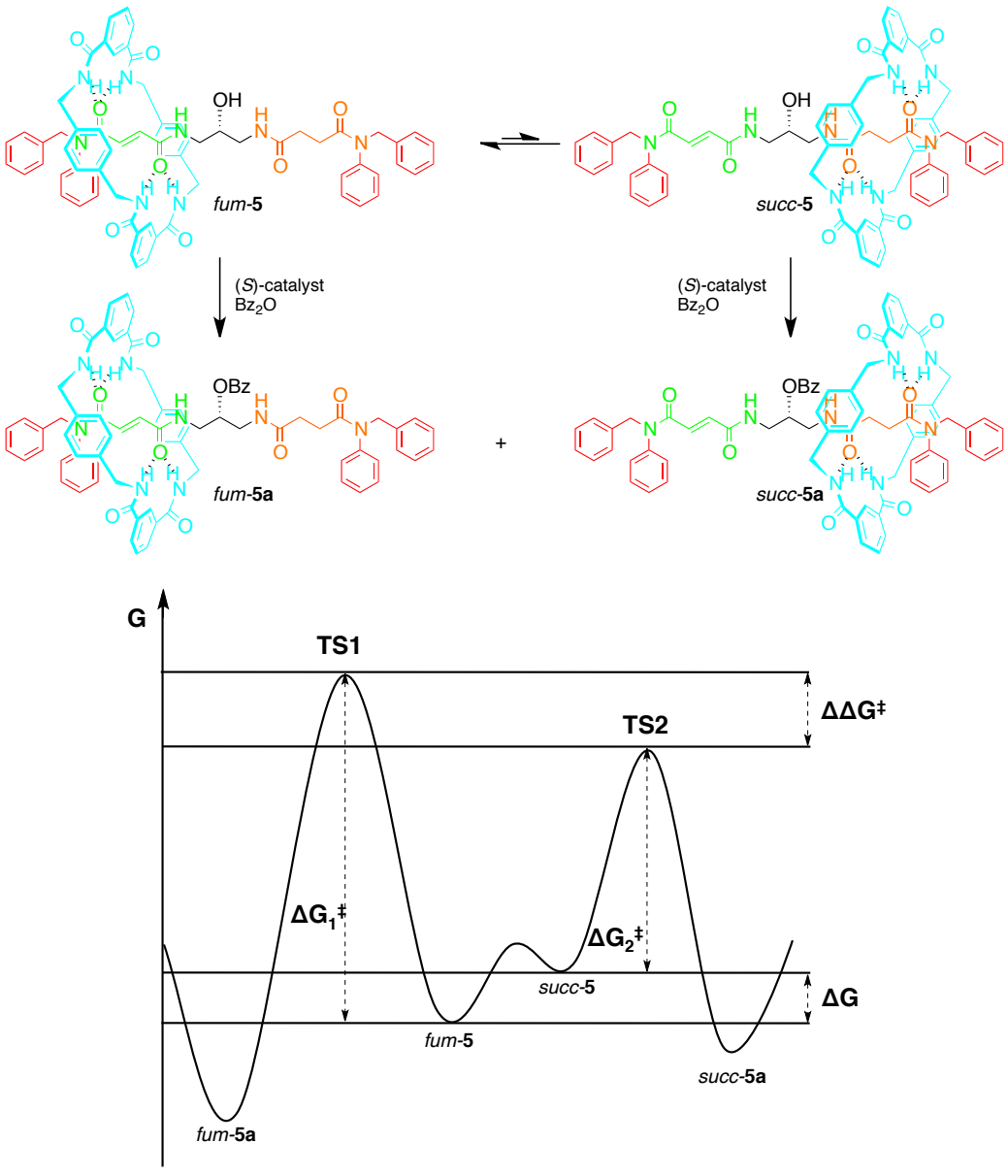

Figure 1.6. A molecular information ratchet capable of ratcheting a Brownian particle enthalpically uphill.[30] The product ratio depends both on the equilibrium distribution of starting material **5** and the relative heights of the energy barriers to the final products, in accordance with the Curtin-Hammett principle.

1.4.3 Diffusion Ratchets

What each of the above ratchets has in common is that compartmentalisation is achieved through the introduction of kinetic gates that present effectively infinitely high barriers to shuttling. An alternative means of compartmentalisation is temporal: the particle can be confined to a small portion of the potential energy surface if it is only allowed to explore this surface diffusively for a brief period of time (the theoretical description of this kind of machine is a *temperature* or *diffusion* ratchet).[5,31] This is demonstrated in a system recently published by Takata and coworkers (Scheme 1.4).[32] In pseudorotaxane **6**H$^+$, the crown ether macrocycle is bound to a secondary ammonium moiety sufficiently strongly that the rate of dethreading is negligible on the experimental timescale. Deprotonation of the ammonium salt significantly weakens the binding and allows for slow dethreading (movement to right) under thermodynamic control. However, acylation of the secondary amine occurs preferentially with the macrocycle on the left hand side, for reasons attributed to sterics by the authors. By careful choice of reagents to control the timescale of the reaction, it is possible to control the direction of motion of the macrocycle.

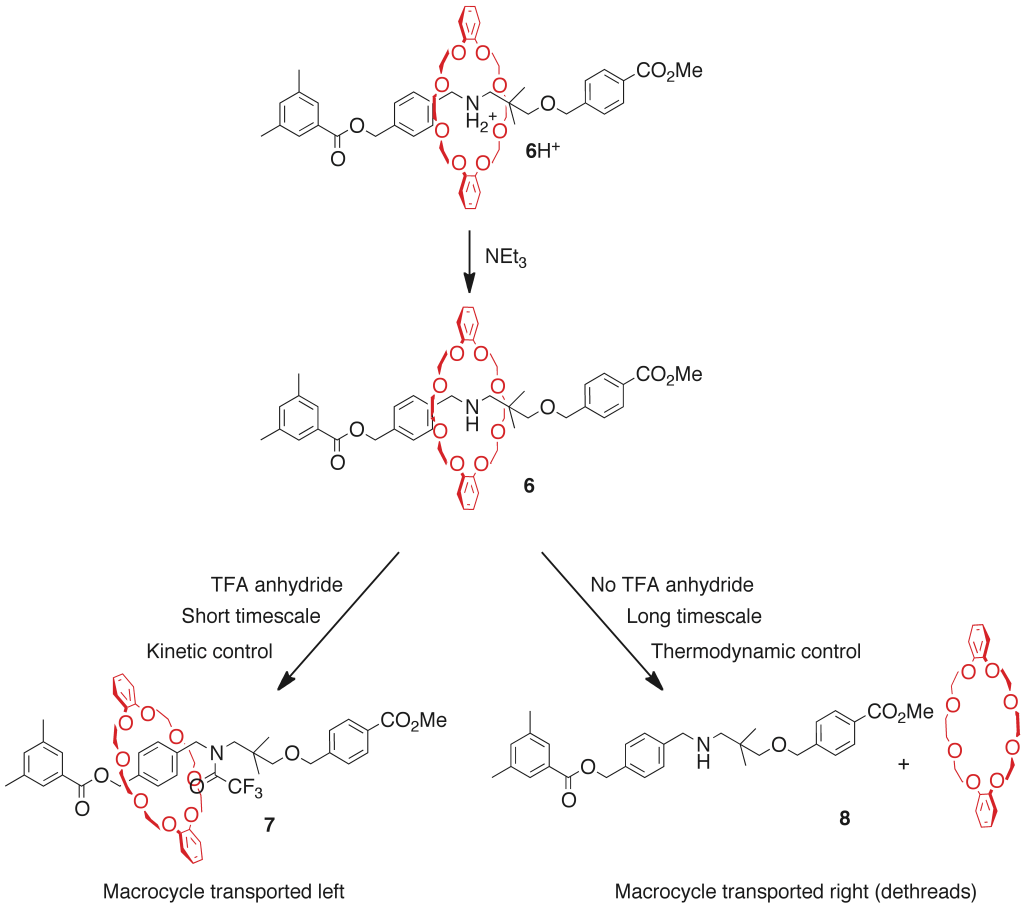

Scheme 1.4 Directional transport by varying the timescale of a reaction.[25]

1.5 Incorporation of Ratchets into Motors

Recent years have witnessed much progress in the field of molecular machines. Those systems designed to act as motors, and not simple chemical switches, have incorporated ratchet mechanisms into their design.

1.5.1 Rotary Motors

One of the first attempts at a directional molecular rotary motor was made in 1999 by Kelly *et al.* (Figure 1.7).[33,34] Their molecular "cog wheel" **9** consists of a triptycene "rotor" unit bound to a helicene "stator", and is a molecular realisation of the adiabatic ratchet and pawl mechanism expounded by Feynman in his celebrated lectures on thermodynamics.[35] Although computational studies demonstrated the presence of an asymmetric potential energy surface (a requirement for the operation of a molecular motor), analysis by ^{1}H NMR spectroscopy showed equal contributions from 'forward' and 'backward' rotational motion. The system at equilibrium was incapable of performing net work, in accordance with the principle of detailed balance.

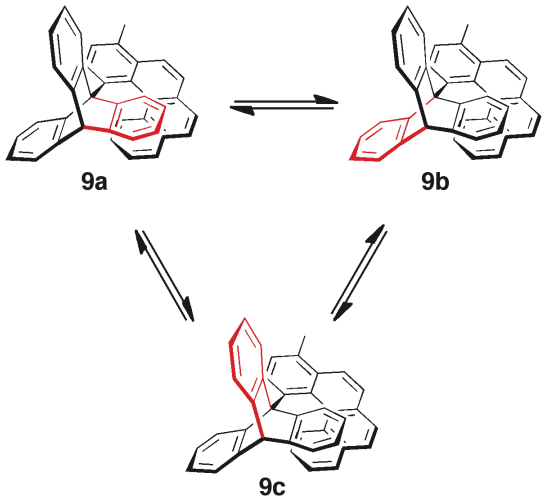

Figure 1.7 Kelly's first-generation molecular "cog wheel".[33] At equilibrium no work can be done by the molecule.

In order to overcome this hurdle and realise a true directional motor, an amine group was incorporated into the triptycene unit (**10**, Scheme 1.5). Conversion of the low-energy amine into a more reactive isocyanate **11** provided the energy input to power the reaction. An alcohol moiety on the helicene stator unit was able to react with the nearby isocyanate (**12**), allowing the system to relax into a

new potential energy minimum by overcoming the steric barrier to rotation. This ratchet mechanism produced a 120° turn of the rotor unit relative to the stator; hydrolysis of the amide linker completed the cycle of operation. Although it only performs one third of a full turn (**10a**→**10b**), this molecular machine incorporates both the asymmetry and input of energy necessary for cumulative mechanical work, and represents a major advance in the field.

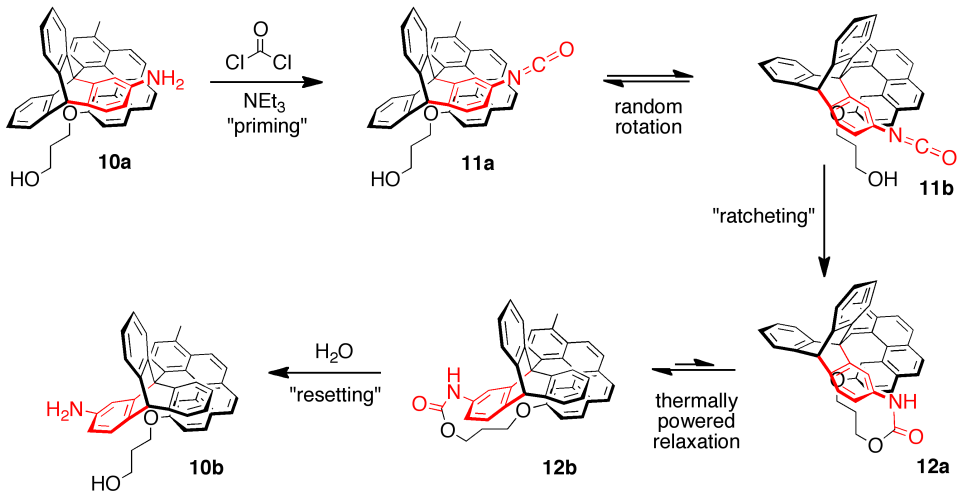

Scheme 1.5 120° rotation about a C–C bond powered by chemical energy.[34]

In the same year, Feringa *et al.* published a system that is capable of repeated 360° directional rotations powered by light (Scheme 1.6).[36] Irradiation of (3*R*-3′*R*)-(*P*,*P*)-*trans*-**13** (wavelength λ ≥ 280 nm) causes photoisomerisation of the olefin moiety resulting in a directional part-rotation of the rotor relative to the stator. This isomer (3*R*-3′*R*)-(*M*,*M*)-*cis*-**13** possesses two methyl groups in unfavourable equatorial positions, and at room temperature a thermally activated helical inversion allows the molecule to relax into (3*R*-3′*R*)-(*P*,*P*)-*cis*-**13**, a lower-energy isomer whose methyl groups are in more favourable axial positions. A second irradiation (wavelength λ ≥ 380 nm) induces a second isomerisation (*cis* to *trans*), and subsequent helix inversion ((3*R*-3′*R*)-(*M*,*M*)-*trans*-**13** to (3*R*-3′*R*)-(*P*,*P*)-*trans*-**13**, this time requiring heating to a temperature greater than 60 °C) returns the molecule to its starting

configuration. Remarkably, sustained irradiation at wavelengths λ ≥ 280 nm at a temperature greater than 60 °C results in continuous rotation with net directionality. Under these conditions a steady state is obtained in which the distribution of isomers does not change, but this steady state is not an adiabatic equilibrium. Continuous input of energy in the form of heat and light allow the maintenance of a cyclic reaction A→B→C→D→A with net directional flux between these states. Refinements in the design of **13** resulted in a million-fold increase of rate of rotation reported for less-hindered motor **14** (Figure 1.8).[37] Later applications have included the incorporation of related molecular machines onto gold surfaces,[38] into liquid crystal films[2] and, more recently, into a system that achieves directional motion across a surface by a paddlewheel-like rotation of four submolecular rotors[39] (in this last case, the olefin isomerisation is achieved electrochemically, not through photoirradiation).

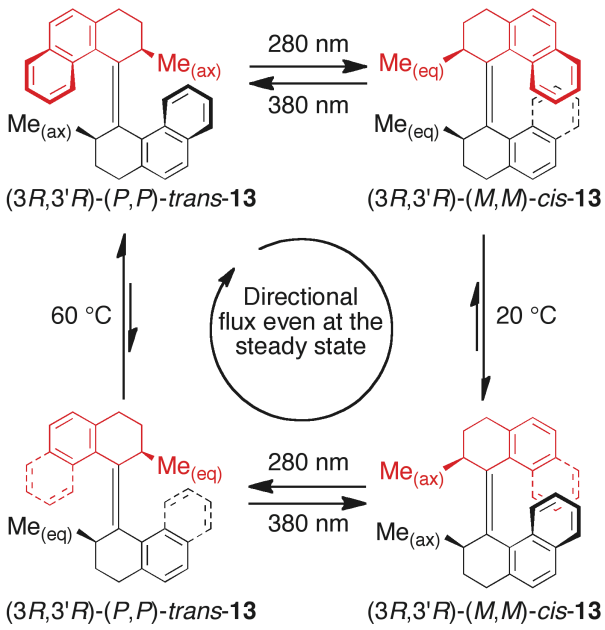

Scheme 1.6 The first light-powered directional molecular motor.[36]

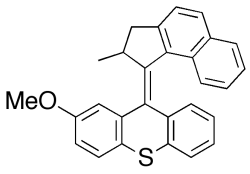

14

Figure 1.8 A directional rotary motor capable of 3 MHz rotation at room temperature.[37]

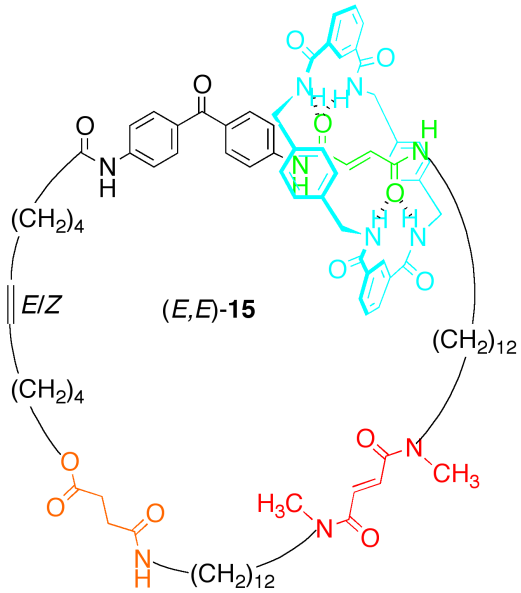

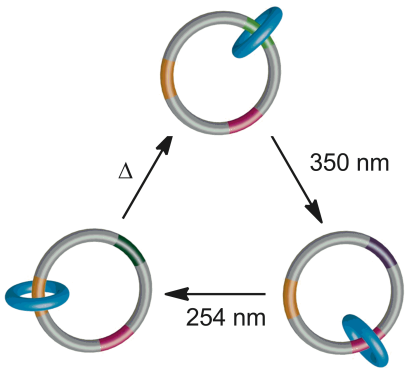

$K_{light\ green} > K_{pink} > K_{orange}$

$K_{pink} > K_{orange} > K_{blue}$

$K_{orange} > K_{blue} > K_{dark\ green}$

Figure 1.9 The small macrocycle in [2]catenane **15** can be sent to the three stations sequentially, but this movement proceeds with no net directionality.[40]

A molecular realisation of the [3]catenane system treated theoretically by Astumian was published by Leigh and coworkers in 2003.[40] Initial studies on model compounds demonstrated that the small amide macrocycle in [2]catenane **15** (Figure 1.9) shows excellent discrimination for a number of pairs of binding sites, and that the affinity for these binding sites can be varied by photoisomerisation to induce steric clash or loss of hydrogen bonding efficiency. These balance-breaking stimuli serve to create new potential energy minima for the system to relax into. Although photochemical stimulation can be used to make the macrocycle bind to each of the three "stations" in turn, this circumrotation does not proceed with net directionality: on its journey from an unfavourable station to a preferred one, the macrocycle is equally likely to travel clockwise as anticlockwise, resulting in no net work. Missing from this model are linking/unlinking steps to impose restrictions on the pathway the system can take to reach equilibrium. Directional circumrotation was achieved in self-compartmentalising [3]catenane **16** (Figure 1.10), in which each small macrocycle serves to control the circumrotation of the other. The sequence of operation for this directional motor is as follows. First, irradiation of (*E*,*E*)-**16** at 350 nm isomerises the light green nonmethylated fumaramide station from *E* to *Z* geometry, creating a new equilibrium position for the blue macrocycle (residing over the succinamide station shown in orange) that is accessible only through an anticlockwise 180° circumrotation. Irradiation of the resulting (*Z*,*E*)-**16** at 254 nm isomerises the methylated fumaramide station, forcing the purple macrocycle into the next most favourable binding site, the single amide (dark green), again in an anticlockwise direction. This step immediately causes the blue macrocycle to migrate in a 90° clockwise circumrotation to the now available methylated fumaramide station (which is energetically more favourable than the succinamide station). Returning the fumaramide residues to their original (*E*,*E*) geometries effects yet another circumrotation of the purple macrocycle. After these three steps (*E*,*E*)-**16** has been regenerated, but with the positions of the two macrocycles swapped; a second cycle of these three steps is required to return the macrocycles to their original positions and complete the 360° movement.

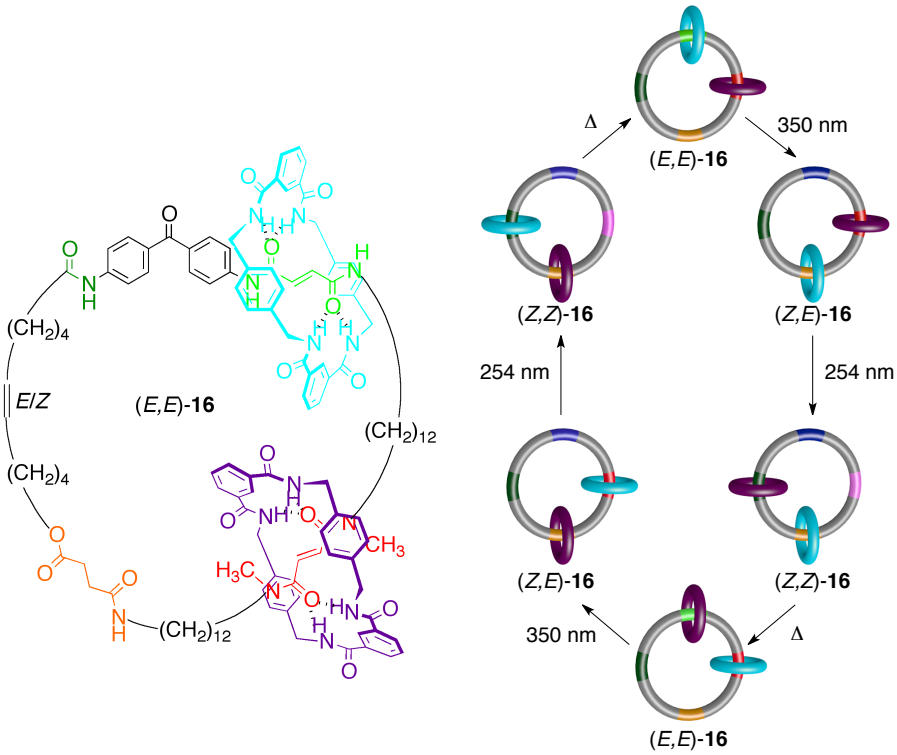

Figure 1.10 Directional 360° circumrotation of the two small rings in [3]catenane **16**.[40]

In 2004, a reversible synthetic rotary molecular motor was published by Leigh *et al.* (Figure 1.11).[28] In [2]catenane **17** the use of two orthogonal linking/unlinking reactions (desilylation/silylation and detritylation/tritylation) and two balance-breaking reactions (olefin isomerisation from *E* to *Z* and from *Z* to *E*) allows for the direction of rotation to be reversed simply by reversing the order in which the protecting groups are cleaved. As previously stated, directional rotation (in either direction) requires an energy input, whereas nondirectional rotation is random and may proceed adiabatically. Analysis of **17** shows that the directional rotation is powered by the *E*→*Z* photoisomerisation step, which is inherently endothermic as it requires disruption of the hydrogen bonding with the macrocycle; this added energy is converted into heat when the olefin returns to its original position and hydrogen bonding to the macrocycle is restored.

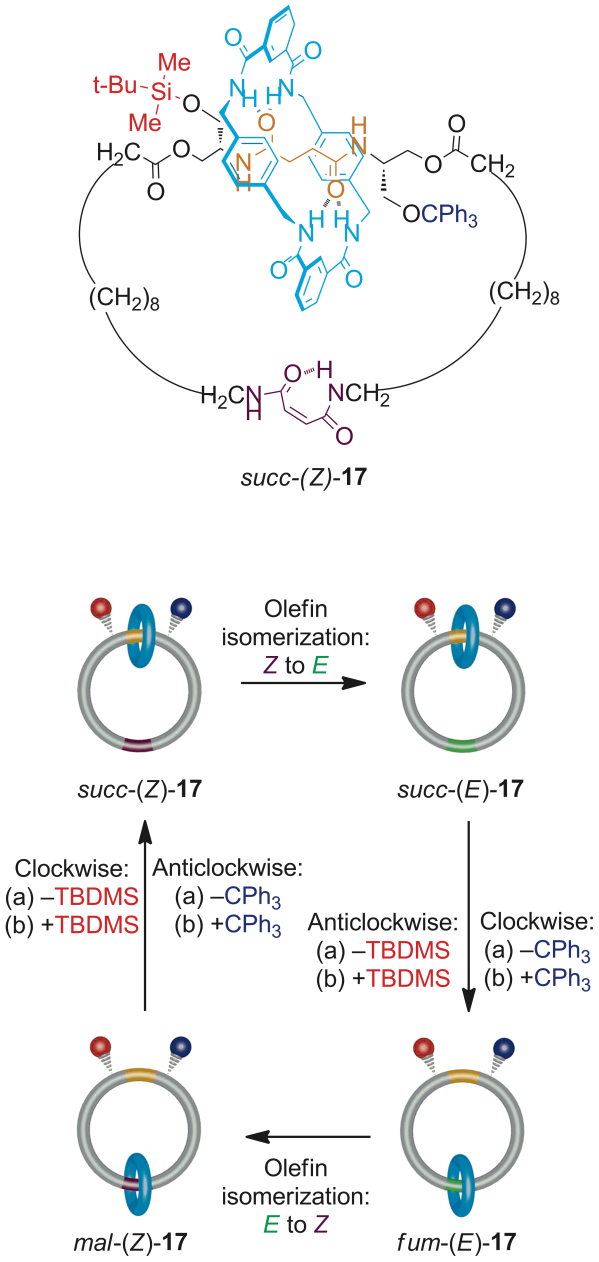

Figure 1.11 Reversible 360° circumrotation in [2]catenane **17**.[28]

A rotary motor published by Feringa *et al.* in 2005 operates by an information ratchet mechanism and derives its energy input from chemical sources.[41] Biaryl lactone **18** (Scheme 1.7) exists as a pair of enantiomers in equilibrium owing to the low energetic barrier to small-amplitude pivoting about the aryl-aryl bond. The chiral catalyst (*S*)-2-methyl-CBS-oxazaborolidine is employed in a stereoselective ring-opening reaction (**18**→**19a**) that induces a 90° rotation of

the rotor unit (top half as drawn); this dynamic kinetic resolution is reminiscent of the minimalist information ratchet published by the Leigh group in 2008.[30] The energetic cost of this resolution is paid for by the consumption of borane., and reverse rotation is rendered unfavourable by the increased steric bulk of the allyl substituent in an *ortho* position. Oxidation of the stator unit's alcohol to a carboxylic acid (**19a**→**19b**), followed by the removal of the PMB group, results in spontaneous lactonisation coupled to a further 90° rotation of the stator (**19b**→**20**). A second chiral catalyst-promoted stereoselective ring-opening, followed by deprotection and subsequent lactonisation with restricted rotation, completes the turn and regenerates **18**. Use of the catalyst's chiral antipode favours ring-opening on the other side, resulting in a reversal of the direction of rotation.

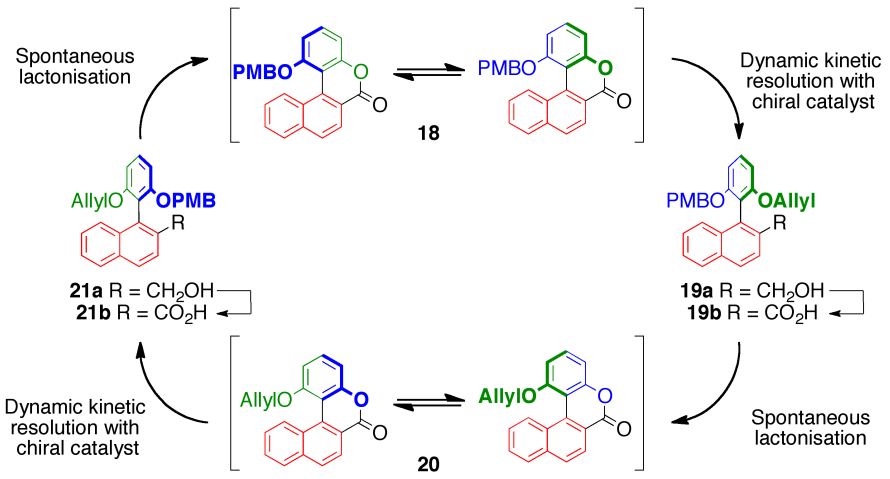

Scheme 1.7 Rotation with net directionality about an aryl-aryl bond *via* an information ratchet mechanism.[41]

A system published recently by Haberhauer achieves directional rotation of a submolecular "blade" through a cycle of metal complexation events and *cis*/*trans* isomerisation of an azobenzene unit (Scheme 1.8).[42] In its starting state, *trans*-(*P*)-**22** has an N–C–C–N dihedral angle of approximately 180° in the 2,2'-bipyridine units and the azobenzene unit is present in a *trans*/*cis* ratio of 80:20.

UV irradiation (355 nm) of this species at 20 °C results in isomerisation of the diazo moiety (42:58 *trans*/*cis* at the photostationary state). A balance-breaking stimulus is then added in the form of Zn^{2+}. In order to coordinate to these ions, the part of the molecule bearing the "blade" undergoes a rotation about the bipyridine's C–C bond. Computational analysis confirms that steric bulk on one side of the molecule poses an impassable barrier to rotation in that direction, and the complexation step occurs by way of a 180° bond rotation that is essentially unidirectional. The resulting dizinc complex *cis*-(*M*)-**22**-Zn_2 is then returned to its initial *trans*/*cis* ratio by irradiation with visible light, and removal of the Zn^{2+} ions restores the molecule to its original state having rotated the blade through a full 360° turn about a virtual axis.

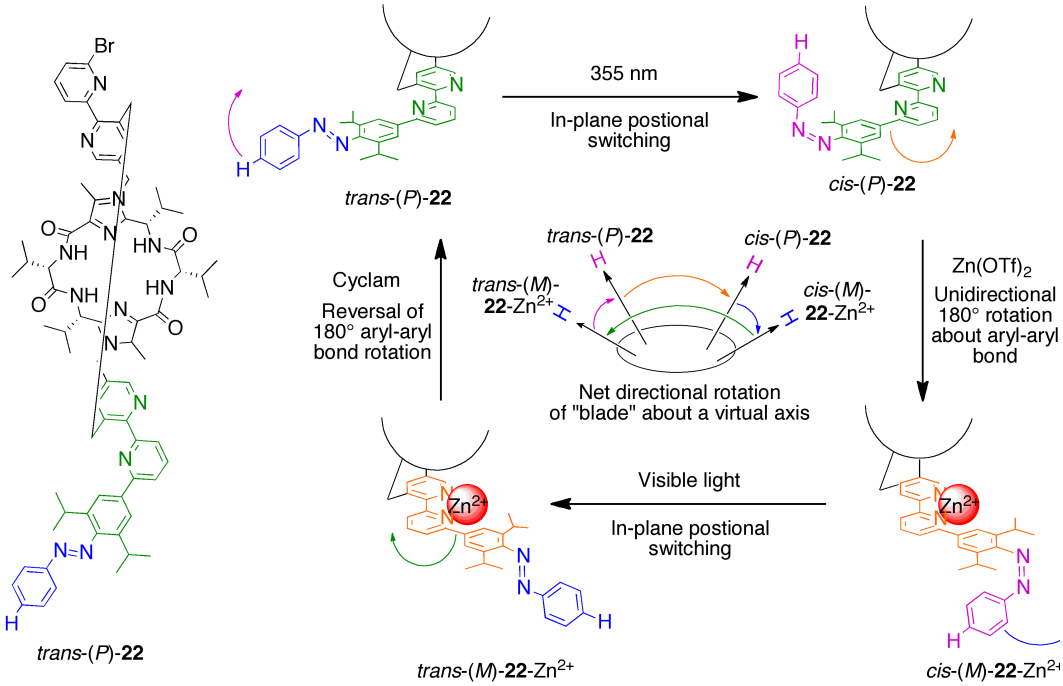

Scheme 1.8 Directional rotation of a submolecular component about a virtual axis by irradiation and metal complexation.[42]

Haberhauer's molecular motor consists of two independently operable positional switches that move the "blade" in different planes. By using these switching mechanisms alternately, the blade moves through four positions and returns to its starting state *via* a different pathway to the one it set out upon.

The system makes use of non-reciprocal motion to perform directional work, a concept expounded on by Purcell in his celebrated talk "Life at Low Reynolds Number."[43] The point is also made by Lehn in a conceptual study of imines,[44] in which he proposes a rotary motor based on a chiral imine that exploits the different pathways of double bond isomerisation under UV irradiation (an out-of-plane bond rotation) and thermal heating (an in-plane nitrogen inversion *via* a linear transitional state). Lehn conjectures that a chiral centre could be used to force directionality in the photoisomerisation step, thus ensuring non-reciprocal motion and and net directional motion.

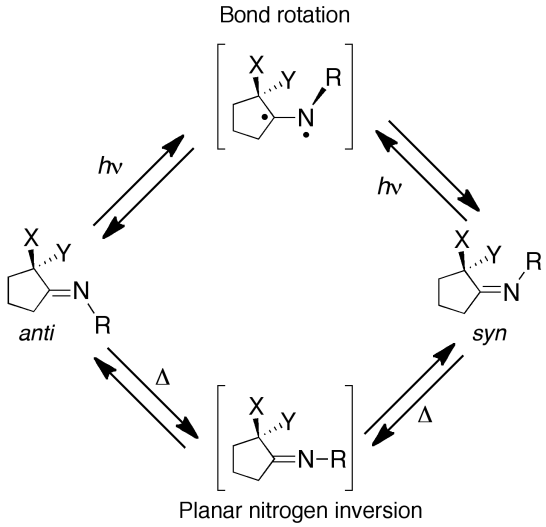

Figure 1.12 Lehn's conjectural imine rotary motor.[44]

1.5.2 Walkers

While the above has focused on rotary motors, the technical description of motors also applies to linear systems and "walkers", systems that exhibit the four fundamental characteristics of progressive, repetitive, processive and directional motion along a track. Like Leigh *et al.*'s [3]catenane **13**, walker units act as self-compartmentalising Brownian particles in that having one "foot"

kinetically fixed to the track restricts the number of linked binding sites accessible to the labile foot. (For a recent review see *Ref.* 45)

1.5.3 DNA-based Walkers

Since 2004, a number of linear motors have emerged that use DNA as a construction material for all or part of the machine. The first example of a walker based entirely on DNA,[46] published by Sherman and Seeman,[47] takes one 2 nm step along a three-foothold track *via* an "inchworm" gait (in which one foot is always the leading foot).[5] The sequence of operation is shown in Scheme 1.9. The walker unit begins attached to its track *via* two "anchor strands" that bind through 20 cooperative base pair interactions. Addition of a "fuel strand" competitively unzips the anchor strand between the leading foot and its foothold; addition of a second anchor strand binds the now labile foot to the next foothold along. A second unzipping/hybridisation cycle moves the trailing foot onto the foothold vacated by the leading foot. The establishment of eight new base pairs per fuel strand consumed provides the energetically favourable process required to drive the reversible walking directionally.

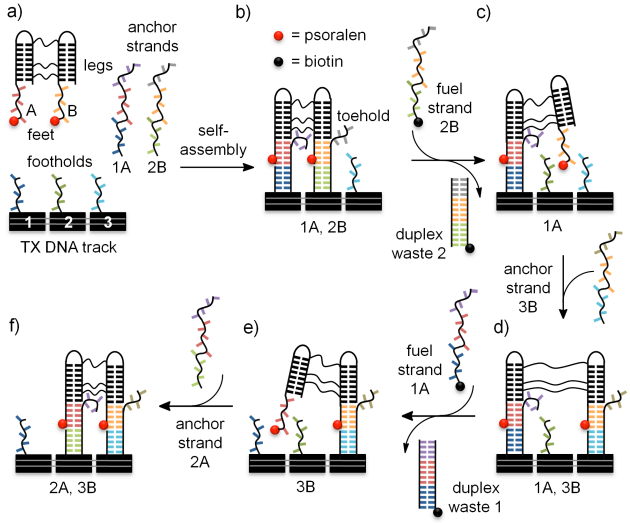

Scheme 1.9 Sherman, Seeman *et al.*'s non-autonomous inchworm walker.[47] Adapted with permission from *Ref.* 45.

A conceptually similar walker by the group of Shin and Pierce published later that year proceeds *via* a "passing-leg" gait (in which each step causes the trailing foot to become the leading foot and vice versa).[48] The year 2004 also saw the appearance of DNA walkers able to perform directional walking autonomously. Turberfield and coworkers' six-nucleotide walker unit was passed between three footholds with net directionality; the energy input comes from ATP hydrolysis of the restriction enzyme used to cut the walker from the foothold.[49] An enzyme-mediated autonomous walker that ensures directionality by irreversibly altering the track behind itself (a "burnt-bridges" mechanism) was published by Turberfield *et al.* in 2005.[50] A conceptually similar system by Mao *et al.* performs directional transport of a DNAzyme walker fragment autonomously without the use of external enzymes.[51] The first enzyme-free, autonomous, processive and directional walker was published by Turberfield in 2008, an ingenious system in which the trailing foot and leading foot are chemically inequivalent at every position on the track (Scheme 1.10).[52] The fuel strands that power locomotion are consumed at different rates by the two feet, resulting in a tendency for the trailing foot to overstep the leading foot more often than the reverse.[53]

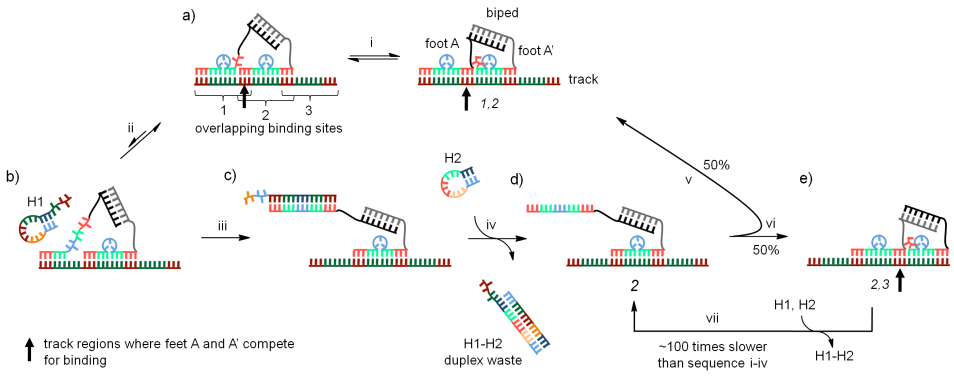

Scheme 1.10 An autonomous, directional, enzyme-free DNA walker by Turberfield *et al.*[52] Adapted with permission from *Ref.* 45.

Recent developments in this exciting field have seen DNA-based molecular machines walk along surfaces responding robotically to instructions such as "start", "stop" and "turn",[54] and perform consecutive synthesis of polypeptide chains.[55] An impressive demonstration of the power of such DNA-based devices was reported by Seeman and coworkers in 2010: a tensegrity triangle organisation with four "feet" uses its three "hands" to sequentially pick up DNA-functionalised gold nanoparticles from three independently programmable donor sites.[56] This proximity-based transfer process could be used to load the triangular walker with three nanoparticle cargoes in one of eight (2^3) combinations.

1.5.4 Small-Molecule Walkers

An additional advance in the miniaturisation of linear motors came with the publication by Leigh *et al.* of a minimalist small-molecule walker.[57,58] In **23**, a 21-atom fragment shown in red is transported directionally from one side of the track to the other by an information ratchet mechanism (Figure 1.13). The two feet are able to bind to footholds on the track *via* disulfide and hydrazone covalent bonds; although kinetically stable under most conditions, these feet can be made labile selectively by addition of acid (detaching the hydrazone foot) or base (detaching the disulfide foot). In each case, the labile foot is free to exchange between the linked footholds until the unlinking stimulus (return of the pH to within certain boundaries) is applied, kinetically locking the foot. Repeated cycling of these linking and unlinking steps allows the walker to reach a steady state of four positional isomers (one of which, *1,4*-**23**, is an "overstepping" isomer resulting from the flexibility of the track). That this is the steady state was elegantly confirmed by synthesising the molecule with the walker fragment occupying the *3,4* position; the same distribution of walkers was shown to be reached irrespective of where on the track the walker fragment starts from.

While operating a sample of pristine *1,2*-**23** will result in migration of some of the walker to the opposite end of the track, this should not be considered true directional walking because the system is moving towards its energetic minimum (detailed balance has been broken not through some external stimulus but as a result of the route taken in the synthesis). In order to drive the system away from its steady-state distribution and perform useful work, it was necessary to lend directional character to one of the steps. This was achieved by replacing the reversible disulfide exchange reaction with a redox reaction in which the kinetically locked product is generated by rapid oxidation in the presence of iodine. This kinetically-controlled, nearly instantaneous step results in a migration of 34% of the walker to the *3,4* position after only 1.5 cycles, a substantial improvement on the 19% *3,4*-**23** present at the steady state. This directional linear motor operates *via* an information ratchet mechanism; the directional discrimination depends on the kinetic accessibility of the sulfur-containing foot, which itself depends on the walker fragment's position on the track.

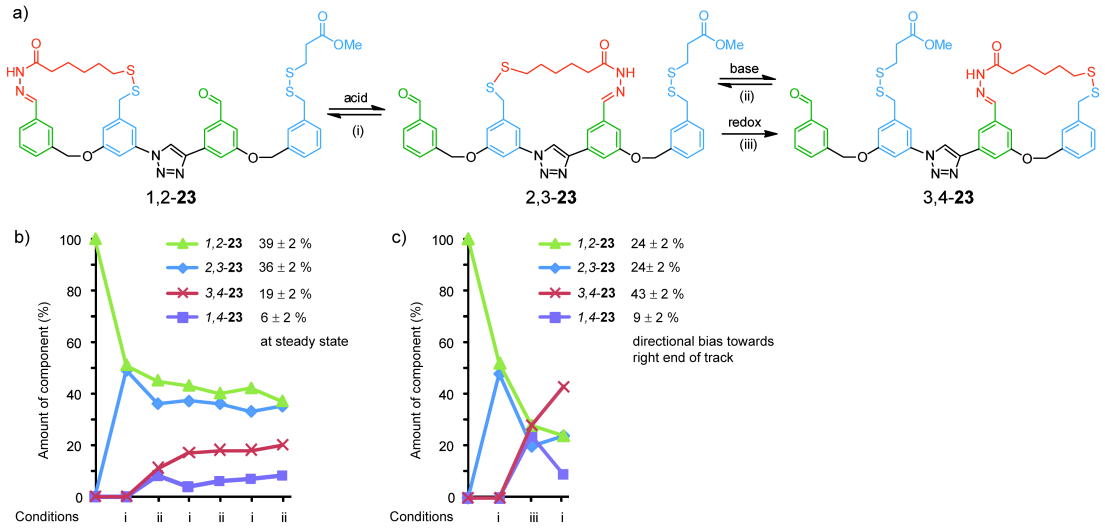

Figure 1.13 (a) Operation of a synthetic small-molecule walker;[57,58] (b) A steady state is arrived at after a number of operation cycles; (c) Directional transport under information ratchet conditions. Adapted with permission from *Ref.* 45.

A conceptually related system published by Leigh *et al.* in 2011 explores the idea of incorporating an energy ratchet mechanism into a small-molecule walker (Figure 1.14).[59] Walker **24** again makes use of hydrazone and disulfide linkages as independently addressable feet, but also includes in the track a stilbene moiety that may be isomerised to induce or relieve ring strain in any macrocycle incorporating it. The formation of *2,3*-**24** was found to be more favourable with the stilbene in the *Z* configuration; *E*→*Z* photoisomerisation provides a driving force for the walker to "step" from the *1,2* position to the *2,3* position when the disulfide exchange conditions were employed. Neutralisation traps the majority of walker fragments in the *2,3* position. *Z*→*E* isomerisation then provides an impetus for the walker to "step" from the *2,3* position to the *3,4* position on labilisation of the hydrazone foot. The addition or removal of kinetic barriers to migration (through addition of acid or base), coupled with the raising and lowering of thermodynamic minima (through light-induced changes in ring strain) causes the walker fragment to be directionally transported, *via* an energy ratchet mechanism, in either direction depending on the order in which the stimuli are applied.

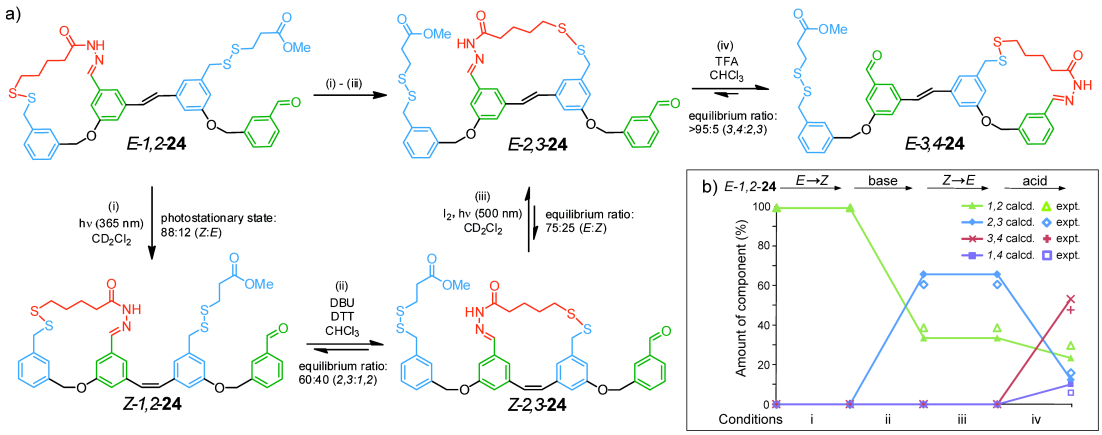

Figure 1.14 (a) Operation of an energy ratchet small-molecule walker;[59] (b) Manipulation of energetic minima leads to directional migration of the walker fragment. Adapted with permission from *Ref.* 45.

1.6 Summary and Outlook

This brief survey of the field of synthetic molecular motors has demonstrated the remarkable diversity both of the types of machines that have been synthesised and the ways in which their motion is produced. Nevertheless, consideration of these motors as chemical species obeying the laws of thermodynamics shows that much of this diversity is superficial. Where cumulative directional motion is observed on the molecular scale, one finds balance breaking stimuli that push the system out of equilibrium; a randomising element, provided by Brownian motion; and an input of energy, often in the form of a chemical fuel, so that such motion does not violate the second law of thermodynamics. One can even see how the principle of microscopic reversibility dictates what kinds of energy input can be used to drive a system, and what kinds can not. Most importantly, everywhere in the field of molecular motors one sees ratchet mechanisms, whose purpose is to couple a reversible process to an energy source to drive a reaction network with net directionality. Many of these phenomena appear in the current theories to explain the intriguing phenomenon of biological homochirality. The thermodynamic principles that allow rotation with net directionality in a molecular motor are also those that allow enantioenrichment in simulations of primordial reaction mixtures. Discoveries in one field continue to provide inspiration for advances in the other, and it is hoped that this feedback will increase and strengthen as understanding of the fundamental similarities involved grows.

1.7 References and Notes

1. Morimoto, M.; Irie, M. A diarylethene cocrystal that converts light into mechanical work. *J. Am. Chem. Soc.* **2010**, *132*, 14172–14178.

2. Eelkema, R.; Pollard, M. M.; Vicario, J.; Katsonis, N.; Ramon, B. S.; Bastiaansen, C. W. M.; Broer, D. J.; Feringa, B. L. Nanomotor rotates microscale objects. *Nature* **2006**, *440*, 163.

3. Berná, J.; Leigh, D. A.; Lubomska, M.; Mendoza, S. M.; Pérez, E. M.; Rudolf, P.; Teobaldi, G.; Zerbetto, F. Macroscopic transport by synthetic molecular machines. *Nat. Mater.* **2005**, *4*, 704–710.

4. Astumian, R. D. Design principles for Brownian molecular machines: how to swim in molasses and walk in a hurricane. *Phys. Chem. Chem. Phys.* **2007**, *9*, 5067–5083.

5. Kay, E. R.; Leigh, D. A.; Zerbetto, F. Synthetic molecular motors and mechanical machines. *Angew. Chem. Int. Ed.* **2007**, *46*, 72–191.

6. Onsager, L. Reciprocal relations in irreversible processes. I. *Phys. Rev.* **1931**, *37,* 405–426.

7. Onsager, L. Reciprocal relations in irreversible processes. II. *Phys. Rev.* **1931**, *38*, 2265–2279.

8. Morrissey, B. W. Microcscopic reversibility and detailed balance – Overview. *J. Chem. Educ.* **1975**, *52*, 296–298.

9. Blackmond, D. G. "If Pigs Could Fly" chemistry: a tutorial on the principle of microscopic reversibility. *Angew. Chem. Int. Ed.* **2009**, *48*, 2648–2654.

10. Alberty, R. A. Principle of detailed balance in kinetics. *J. Chem. Educ.* **2004**, *81*, 1206–1209.

11. Astumian, R. D. Microscopic reversibility and reciprocal relations for Brownian molecular machines. *Tetrahedron* **2008**, *64*, 8287–8291.

12. Frank, F. C. On spontaneous asymmetric synthesis. *Biochim. Biophys. Acta* **1953**, *11*, 459–463.

13. Soai, K.; Shibata, T.; Morioka, H.; Choji, K. Asymmetric autocatalysis and amplification of enantiomeric excess of a chiral molecule. *Nature* **1995**, *378*, 767–768.

14. Huber, C.; Wächtershäuser, G. Peptides by activation of amino acids with CO on (Ni,Fe)S surfaces: implications for the origin of life. *Science* **1998**, *281*, 670–672.

15. Blackmond, D. G.; Matar, O. K. Re-examination of reversibility in reaction models for the spontaneous emergence of homochirality. *J. Phys. Chem. B* **2008**, *112*, 5098–5104.

16. Plasson, R.; Bersini, H.; Cornmeyras, A. Recycling Frank: spontaneous emergence of homochirality in noncatalytic systems. *Proc. Natl. Acad. Sci. U.S.A.* **2004**, *101*, 16733–16738.

17. Blackmond, D. G. Response to "Comment on 'A Re-examination of reversibility in reaction models for the spontaneous emergence of homochirality'". *J. Phys. Chem. B* **2008**, *112*, 9553–9555.

18. Serreli, V.; Lee, C.-F.; Kay, E. R.; Leigh, D. A. A molecular information ratchet. *Nature* **2007**, *445*, 523–527.

19. Astumian, R. D.; Derényi, I. Fluctuation driven transport and models of molecular motors and pumps. *Eur. Biophys. J.* **1998**, *27*, 474–489.

20. Anelli, P. L.; Spencer, N.; Stoddart, J.F. *J. Am. Chem. Soc.* **1991**, *113*, 5131–5133.

21. Bissell, R. A.; Córdova, E.; Kaifer, A. E.; Stoddart, J. F. A chemically and electrochemically switchable molecular shuttle. *Nature* **1994**, *369*, 133–137.

22. Vignon, S. A.; Jarrosson, T.; Iijima, T.; Tseng, H.-R.; Sanders, J. K. M.; Stoddart, J. F. *J. Am. Chem. Soc.* **2004**, *126*, 9884–9885.

23. Badjić, J. D.; Balzani, V.; Credi, A.; Silvi, S.; Stoddart, J. F. A molecular elevator. *Science* **2004**, *303*, 1845–1849.

24. Dietrich-Buchecker, C. O.; Sauvage, J.-P.; Kintzinger, J. P. *Tetrahedron Lett.* **1983**, *24*, 5095–5098.

25. Livoreil, A.; Dietrich-Buchecker, C. O.; Sauvage, J.-P. *J. Am. Chem. Soc.* **1994**, *116*, 9399–9400.

26. Sauvage, J.–P. *Acc. Chem. Res.* **1998**, *31*, 611–619.

27. Chatterjee, M. N.; Kay, E. R.; Leigh, D. A. Beyond switches: ratcheting a particle energetically uphill with a compartmentalized molecular machine. *J. Am. Chem. Soc.* **2006**, *128*, 4058–4073.

28. Hernández, J. V.; Kay, E. R.; Leigh, D. A. A reversible synthetic rotary molecular motor. *Science* **2004**, *306*, 1532–1537.

29. Bennett, C. H. The thermodynamics of computation – a review. *Int. J. Theor. Phys.* **1982**, *21*, 905–940.

30. Alvarez-Pérez, M.; Goldup, S. M.; Leigh, D. A.; Slawin, A. M. Z. A chemically-driven molecular information ratchet. *J. Am. Chem. Soc.* **2008**, *130*, 1836–1838.

31. Reimann, P. Brownian motors: noisy transport far from equilibrium. *Phys. Rep.* **2002**, *361*, 57–265.

32. Makita, Y.; Kihara, N.; Takata, T. Quantitative active transport in [2]rotaxane using a one-shot acylation reaction toward the linear molecular motor. *J. Org. Chem.* **2008**, *73*, 9245–9250.

33. Kelly, T. R.; De Silva, H.; Silva, R. A. Unidirectional rotary motion in a molecular system. *Nature* **1999**, *401*, 150–152.

34. Kelly, T. R.; Cai, X.; Damkaci, F.; Panicker, S. B.; Tu, B.; Bushell, S. M.; Cornella, I.; Piggott, M. J.; Salives, R.; Cavero, M.; Zhao, Y.; Jasmin, S. Progress toward a rationally designed, chemically powered rotary molecular motor. *J. Am. Chem. Soc.* **2007**, *129*, 376–386.

35. Feynman, R. P.; Leighton, R. B.; Sands, M. Ratchet and pawl. In *The Feynman Lectures on Physics*; Addison-Wesley: Reading, MA, 1963; Vol. 1, Chapter 46.

36. Koumura, N.; Zijlstra, R. W. J.; van Delden, R. A.; Harada, N.; Feringa, B. L. Light-driven monodirectional molecular rotor. *Nature* **1999**, *401*, 152–155.

37. Klok, M.; Boyle, N.; Pryce, M. T.; Meetsma, A.; Browne, W. R.; Feringa, B. L. MHz unidirectional rotation of molecular rotary motors. *J. Am. Chem. Soc.* **2008**, *130*, 10484–10485.

38. van Delden, R. A.; ter Wiel, M. K. J.; Pollard, M. M.; Vicario, J.; Koumura, N.; Feringa, B. L. Unidirectional molecular motor on a gold surface. *Nature* **2005**, *437*, 1337–1340.

39. Kudernac, T.; Ruangsupapichat, N.; Parschau, M.; Maciá, B.; Katsonis, N.; Harutyunyan, S. R.; Ernst, K.-H.; Feringa, B. L. Electrically driven directional motion of a four-wheeled molecule on a metal surface. *Nature* **2011**, *479*, 208–211.

40. Leigh, D. A.; Wong, J. K. Y.; Dehez, F.; Zerbetto, F. Unidirectional rotation in a mechanically interlocked molecular rotor. *Nature* **2003**, *424*, 174–179.

41. Fletcher, S. P.; Dumur, F.; Pollard, M. M.; Feringa, B. L. A reversible, unidirectional molecular rotary motor driven by chemical energy. *Science* **2005**, *310*, 80–82.

42. Haberhauer, G. A molecular four-stroke motor. *Angew. Chem. Int. Ed.* **2011**, *50*, 6415–6418.

43. Purcell, E. M. Life at low Reynolds number. *Am. J. Phys.* **1977**, *45*, 3–11.

44. Lehn, J.-M. Conjecture: imines as unidirectional photodriven molecular motors – Motional and constitutional dynamic devices. *Chem. Eur. J.* **2006**, *12*, 5910–5915.

45. von Delius, M.; Leigh, D. A. Walking molecules. *Chem. Soc. Rev.* **2011**, *40*, 3656–3676.

46. The psoralen and biotin tags used for analysis and purification may be excluded because they were not necessary for walking.

47. Sherman, W. B.; Seeman, N. C. A precisely controlled DNA biped walking device. *Nano Lett.* **2004**, *4*, 1203–1207.

48. Shin, J.-S.; Pierce, N. A. A synthetic DNA walker for molecular transport. *J. Am. Chem. Soc.* **2004**, *126*, 10834–10835.

49. Yin, P.; Yan, H.; Daniell, X. G.; Turberfield, A. J.; Reif, J. H. A unidirectional DNA walker that moves autonomously along a track. *Angew. Chem. Int. Ed.* **2004**, *43*, 4906–4911.

50. Bath, J.; Green, S. J.; Turberfield, A. J. A free-running DNA motor powered by a nicking enzyme. *Angew. Chem. Int. Ed.* **2005**, *44*, 4358–4361.

51. Tian, Y.; He, Y.; Chen, Y.; Yin, P.; Mao, C. A DNAzyme that walks processively and autonomously along a one-dimensional track. *Angew. Chem. Int. Ed.* **2005**, *44*, 4355–4358.

52. Green, S. J.; Bath, J.; Turberfield, A. J. Coordinated chemomechanical cycles: a mechanism for autonomous molecular motion. *Phys. Rev. Lett.* **2008**, *101*, 238101.

53. Bath, J.; Green, S. J.; Allen, K. E.; Turberfield, A. J. Mechanism for a directional, processive, and reversible DNA motor. *Small* **2009**, *5*, 1513–1516.

54. Lund, K.; Manzo, A. J.; Dabby, N.; Michelotti, N.; Johnson-Buck, A.; Nangreave, J.; Taylor, S.; Pei, R.; Stojanovic, M. N.; Walter, N. G.; Winfree, E.; Yan, H. Molecular robots guided by prescriptive landscapes. *Nature* **2010**, *465*, 206–210.

55. He, Y.; Liu, D. R. Autonomous multistep organic synthesis in a single isothermal solution mediated by a DNA walker. *Nat. Nano.* **2010**, *5*, 778–782.

56. Gu, H.; Chao, J.; Xiao, S.-J.; Seeman, N. C. A proximity-based programmable DNA nanoscale assembly line. *Nature* **2010**, *465*, 202–205.

57. von Delius, M.; Geertsema, E. M.; Leigh, D. A. A synthetic small molecule that can walk down a track. *Nat. Chem.* **2010**, *2*, 96–101.

58. von Delius, M.; Geertsema, E. M.; Leigh, D. A.; Tang, D.-T. D. Design, synthesis, and operation of small molecules that walk along tracks. *J. Am. Chem. Soc.* **2010**, *132*, 16134–16145.

59. Barrell, M. J.; Campaña, A. G.; von Delius, M.; Geertsema, E. M.; Leigh, D. A. Light-driven transport of a molecular walker in either direction along a molecular track. *Angew. Chem. Int. Ed.* **2011**, *50*, 285–290.

Chapter Two

A Three-Compartment Chemical Information Ratchet

Acknowledgements

Dr Armando Carlone and Dr Nathalie Lebrasseur provided stocks of **34** and **35**, as well as much discussion that contributed greatly to the final form of the theory presented here. Professor Stephen Connon is thanked for his generous donation of (*S*)-**42**. Dr Craig Robertson is gratefully acknowledged for the examination and proofreading of this Chapter.

Synopsis

This Chapter describes a three-compartment rotaxane information ratchet in which the macrocycle can be directionally transported in either direction along an achiral (other than isotopic labeling) track depending on the handedness of the chiral catalyst used to promote a benzolyation reaction that ratchets the displacement of the macrocycle. Chiral DMAP-based catalysts transport the macrocycle to the particular end compartment determined by the handedness of the catalyst. Modelling the system as a hidden Markov process reveals that the mechanism of directional transport involves the benzoylation reactions occurring preferentially to one side of the macrocycle, according to the handedness of the catalyst.

2.1 Introduction

Nature uses molecular motors to drive chemical systems away from equilibrium, to perform mechanical tasks at the molecular level, and to transport cargoes directionally.[1] Synthetic chemists have developed many types of molecular switches (sometimes somewhat misleadingly called 'motors' or 'motor-molecules').[2-7] However, simple positional changes in the components of molecular systems are insufficient for directional transport to occur (and work to be done) cumulatively and progressively by a molecular machine.[8-21] The advance from switch to motor requires a ratchet mechanism that prevents the work that is done in one step being undone as the machine is reset. Recently, a chemically-driven molecular information ratchet by Leigh and coworkers was demonstrated[16] using a [2]rotaxane in which two "compartments" of the thread were separated by a prochiral hydroxyl group. Directional transport of the macrocycle between the compartments could be achieved by dynamic kinetic resolution with the required energy input[22] provided by benzoic anhydride.

In an information ratchet, the potential energy surface responds to the position of the particle being transported. Directional transport is achieved by selectively raising barriers to translation behind the particle, preventing retrograde motion. One way of achieving this selectivity is for the position of the Brownian particle to have an effect on the chirality of the molecule; then, in a chiral environment, the different positional isomers become chemically distinguishable. This technique, demonstrated in simple ratchet **3** (see Scheme 1.3), has been employed in the design of a rotary motor,[13] and has also been used to drive a synthetic small-molecule walker.[18] As yet, however, there have been no instances of small-molecule systems incorporating multiple information ratchet sites of discrimination for cumulative, directional transport across a one-dimensional track.

The incorporation of multiple sites of directional discrimination into a single molecule would constitute a significant advance over simple ratchet systems, and an important step in the progress towards linear molecular motors capable of doing useful mechanical work on a molecular level. This Chapter describes the synthesis, operation and analysis of a molecule designed to meet this challenge.

2.2 Design

The proposed design for a three-compartment chemical information ratchet is shown in Figure 2.1.

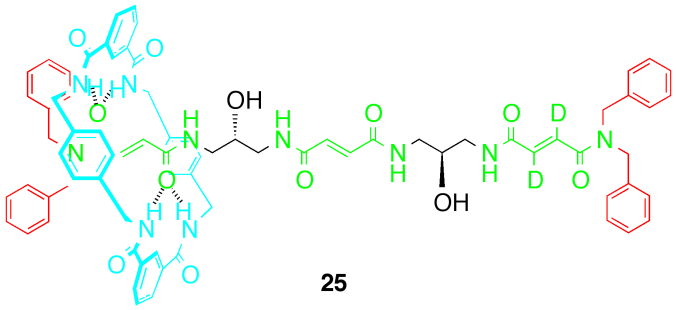

Figure 2.1 A three-compartment chemical information ratchet.

[2]Rotaxane diol **25** employs several of the structural motifs of the two-compartment information ratchet **3** (see Scheme 1.3). Fumaramide residues are incorporated as binding sites for an amide macrocycle; they also serve as a template for the initial formation of the macrocycle under conditions developed by Leigh and coworkers.[16] The inter-binding site spacers were chosen to prevent folding of the thread and to inhibit the macrocycle binding to more than one fumaramide group at a time. In its diol form, the macrocycle of **25** would be able to shuttle freely between the three compartments, but benzoylation of the

hydroxyl groups would provide a steric barrier over which the macrocycle would be unable to pass.

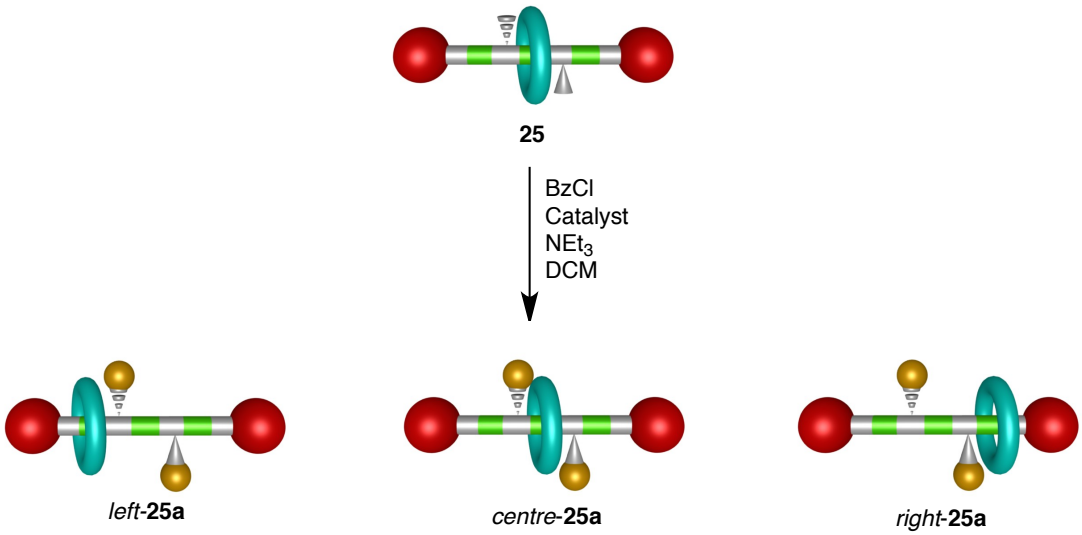

Figure 2.2 The double benzoylation of **25** would result in three positional isomers (*left*-**25a**, *centre*-**25a** and *right*-**25a**) with the macrocycle locked into different compartments.

Double benzoylation of diol **25** would lead to three positional isomers as shown in Figure 2.2. The rotaxane with the centrally positioned macrocycle (*centre*-**25a**) would be chemically different from the two with the macrocycle in the terminal compartments (*left*-**25a** and *right*-**25a**), and could theoretically be separated by chromatographic techniques. The products with the macrocycle locked in the left or right compartments would probably be too similar for such a separation to be effected. For this reason, **25** was designed so that the ratio of products formed could be determined by non-chromatographic techniques. It has been demonstrated that a macrocycle residing over a fumaramide binding site causes a significant upfield shift in the ^{1}H NMR spectroscopy signals for the fumaric protons.[16] The relative integral of the shielded fumaric protons, referenced to an internal standard in the molecule, would be used to calculate the fraction of macrocycles that are near the protons being shielded. In the design of **25**, the right-hand compartment has been labelled with deuterium in

order to distinguish between *left*-**25a** and *right*-**25a**.

One structural difference between **25** and two-compartment system **3** is the stopper design. The decision to base **25**'s stoppers on dibenzylamine rather than *N*-phenybenzylamine was made for two reasons. Firstly, by removing the hydrogen bonding potential of the NH protons it was envisaged that the solubility penalty for introducing an extra fumaramide unit would be at least partially offset. Secondly, an anticipated problem was that π-stacking interactions between the macrocycle and an *N*-phenylbenzylamine stopper would disfavour the macrocycle residing in the central compartment. It has been shown from crystal structures that increasing the distance with an additional CH_2 group reduces the tendency for π-stacking.[23] By changing the stoppers in this way, the three binding sites would be rendered more chemically similar to each other, reducing any thermodynamic preference for the terminal compartments over the central one.

2.3 Retrosynthesis

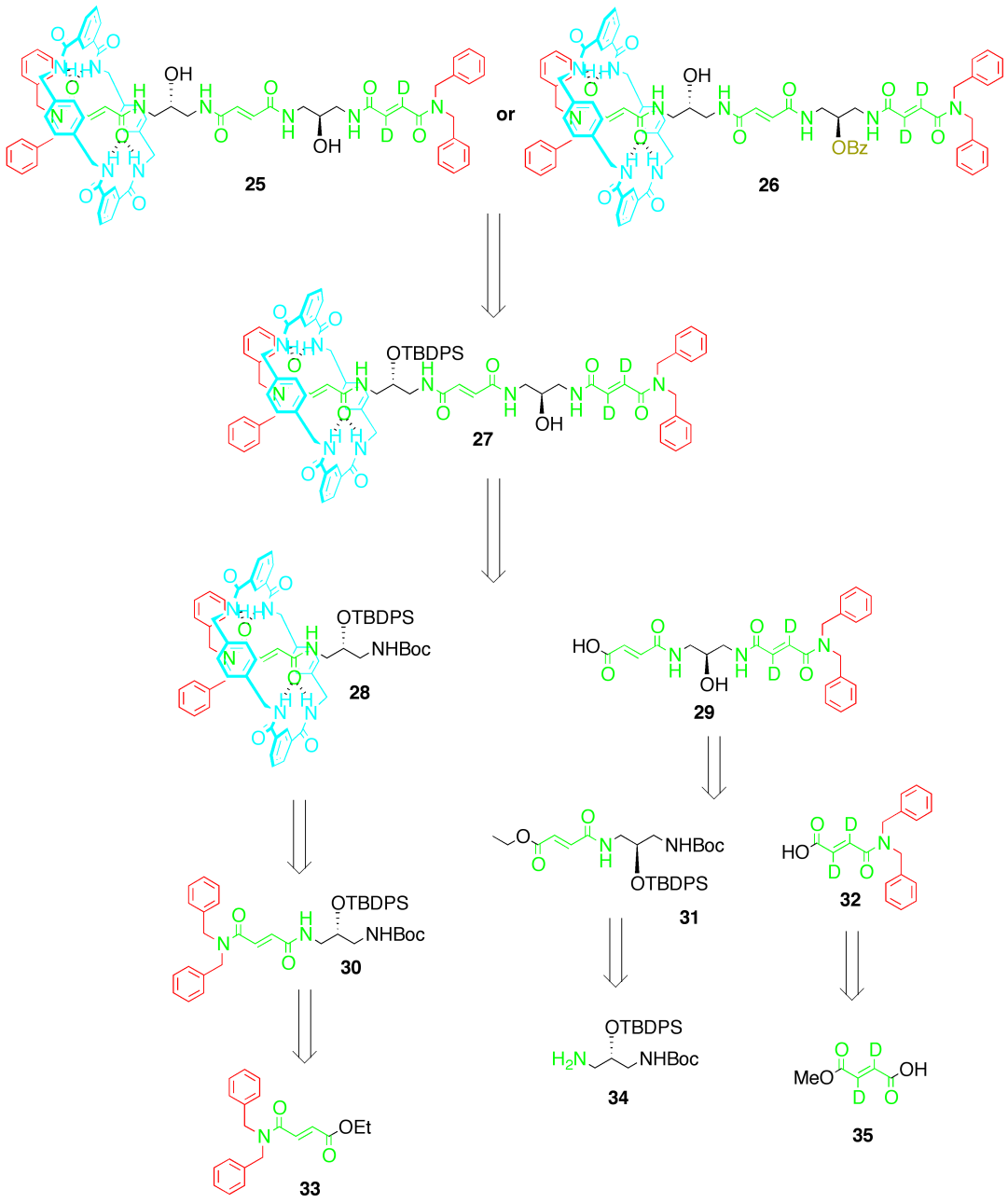

Scheme 2.1 Retrosynthesis of diol rotaxane **25** and mono-benzoylated form **26**.

Both diol **25** and its mono-benzoylated analogue **26** were considered to be desirable targets, since benzoylation of **26** was expected to afford valuable insights into the directional discrimination occurring at a single site. The chiral building block **34** is known in the literature[16] and can be prepared from

commercially available (*R*)-3-amino-1,2-propanediol in six steps. Peptidic couplings performed with TBTU, HOBt and DIPEA would be used to assemble the target molecules. This technique has the advantage that the coupling agents are soluble in water and may be removed with a simple aqueous wash. TBDPS was chosen as a protecting group for the secondary alcohols because of its ease of cleavage, with fluoride, in the presence of a Boc group. Carboxylic acids were to be masked as methyl or ethyl esters, allowing the free acids to be obtained by saponification with lithium hydroxide when desired.

2.4 Synthesis

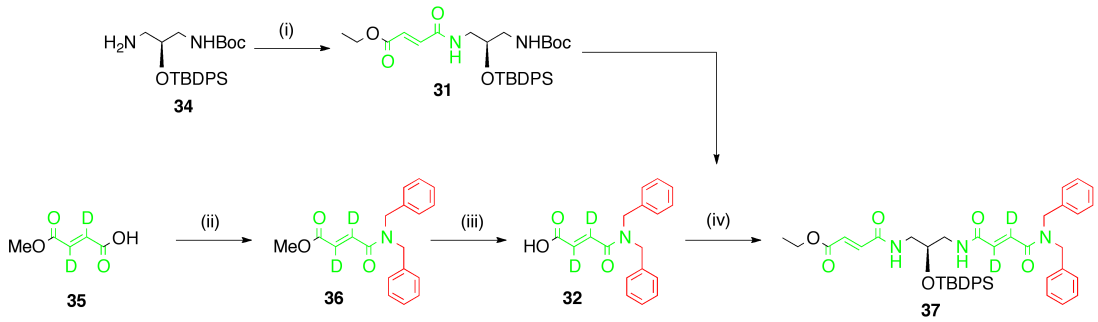

Scheme 2.2 (i) Mono-ethyl fumarate, TBTU, HOBt, DIPEA, DMF, 0 °C to rt, 16 h, 94%; (ii) Dibenzylamine, TBTU, HOBt, DIPEA, DMF, 0 °C to rt, 16 h, 40%; (iii) $LiOH{\cdot}H_2O$, 3:1 THF/H_2O, rt, 1 h, *quant.*; (iv) (a) Amide **31**, 4:1 DCM/TFA, rt, 16 h, 92%; (b) Acid **32**, TBTU, HOBt, DIPEA, DMF, 0 °C to rt, 16 h, 58% (over two steps).

Acid **35** was prepared from dimethyl acetylenedicarboxylate by *trans*-deuteration with heavy water[24] followed by a desymmetrisation[25] and was used without further purification in a peptidic coupling reaction with a slight excess of dibenzylamine. The coupling agents chosen were TBTU and HOBt, with 1.2 equivalents of DIPEA present as a base. In such coupling reactions a common byproduct was tetramethylurea, which could easily be removed by trituration with hexane either before or after column chromatography. Amide **36** was

obtained as a white solid in 40% yield. Saponification of **36** with lithium hydroxide in a THF/water mixture proceeded quantitatively and completed after less than an hour. An acidic work-up furnished **32** in excellent purity as determined by NMR spectroscopy and mass spectrometry, and it was possible to use the material without further purification.

Amine **34** was prepared in six steps from (*R*)-3-amino-1,2-propanediol according to a literature procedure.[16] A peptidic coupling with mono-ethyl fumarate afforded **31** in an excellent yield. Boc-deprotection of amide **31** was carried out by dissolving it in a 4:1 DCM/TFA mixture in a loosely-sealed flask at room temperature, with stirring, overnight. After a basic work-up the resulting primary amine was immediately coupled to acid **32** to give amide **37** in 58% yield.

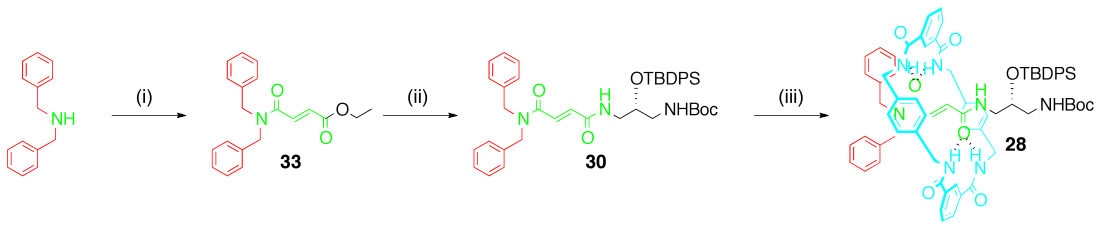

Scheme 2.3 (i) Mono-ethyl fumarate, TBTU, HOBt, DIPEA, DMF, 0 °C to rt, 16 h, 87%; (ii) (a) $LiOH{\cdot}H_2O$, 3:1 THF/H_2O, rt, 1 h, *quant.*; (b) Amine **34**, TBTU, HOBt, DIPEA, DMF, 0 °C to rt, 16 h, 94%; (iii) Isophthaloyl chloride, *p*-xylylene diamine, NEt_3, $CHCl_3$, rt, 3 h, 62%.

A peptidic coupling reaction between mono-ethyl fumarate and dibenzylamine afforded ester **33** in good yield. This compound was then saponified with lithium hydroxide and coupled to a slight excess of amine **34** without further purification. Column chromatography of the peptidic coupling afforded **30**, which was an ideal template for macrocycle formation as it comprised a fumaramide binding site between two structural moieties sufficiently bulky to prevent macrocycle dethreading. In order to form the rotaxane **28**, thread **30** was dissolved in chloroform with triethylamine at high dilution. To this reaction

mixture was added simultaneously and slowly, using two syringe pumps, isophthaloyl chloride in chloroform in one syringe, and a mixture of *p*-xylylene diamine and triethylamine in the second syringe, also in chloroform. After a few minutes of addition, the reaction mixture became opaque from the formation of oligomeric species. The addition finished after three hours, upon which the reaction mixture was passed through a glass sintered funnel to remove oligomers and worked up with acidic and then basic aqueous washes. The crude product was purified by column chromatography to afford rotaxane **28** in 62% yield; the unreacted thread **30** was also easily recovered and reused.

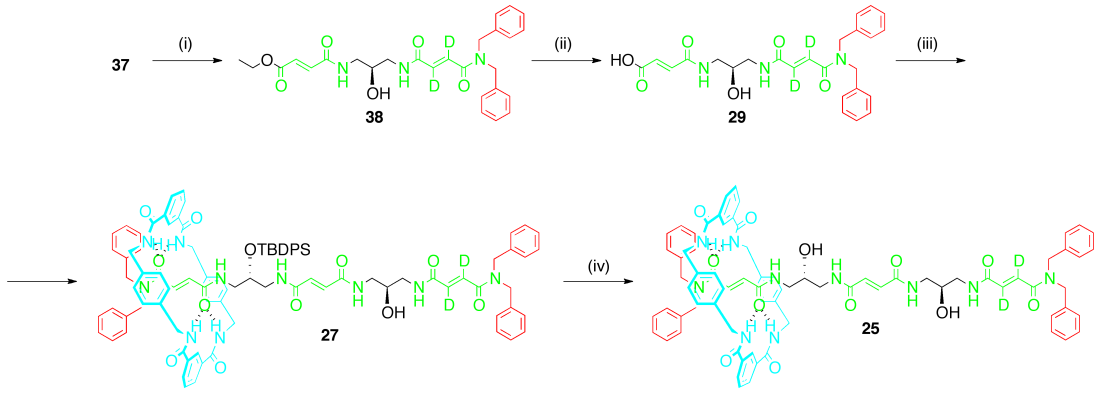

Scheme 2.4 (i) TBAF, THF, rt, 16 h, 81%; (ii) LiOH·H_2O, 3:1 THF/H_2O, rt, 25 min, *quant.*; (iii) (a) Rotaxane **28**, 4:1 DCM/TFA, rt, 16 h, 91%; (b) Acid **29**, TBTU, HOBt, DIPEA, 0 °C to rt, 16 h, 85%; (iv) HF·py, THF, rt, 16 h, 83%.

Amide **37** was treated with TBAF to cleave the TBDPS group. The reaction proceeded smoothly, and after an acidic work-up and several washes with sodium citrate to remove tetrabutylammonium salts, column chromatography afforded ester **38** in 81% yield. Saponification of **38** proved to be problematic, as the standard treatment with lithium hydroxide in 3:1 THF/water led rapidly to decomposition, but the problem was largely circumvented by quenching the reaction with 1 M HCl after 20 minutes. The resulting acid **29** was highly insoluble in organic solvents, perhaps unsurprisingly for a carboxylic acid with so many hydrogen-bonding groups. For this reason no attempt was made to

remove the very minor decomposition product, and **29** was used without further purification.

The Boc group on rotaxane **28** was cleaved with TFA. After a basic work-up the resulting primary amine was coupled under standard conditions to acid **29**, affording rotaxane **27** in excellent yield. Removal of the TBDPS protecting group proceeded smoothly with TBAF but generated salts that were difficult to remove by either aqueous washing or chromatography. Some success was had using a technique published by Kaburagi and Kishi[26] in which a sulfonic acid resin and calcium carbonate are added to the crude reaction mixture and removed by filtration. This technique proved quite effective at removing the salts, but ultimately hydrogen fluoride as a solution in pyridine was adopted as a synthetically much cleaner deprotection agent. The reaction was quenched with methoxytrimethylsilane and was followed by an acidic work-up. Column chromatography afforded the target diol rotaxane **25** in 83% yield.

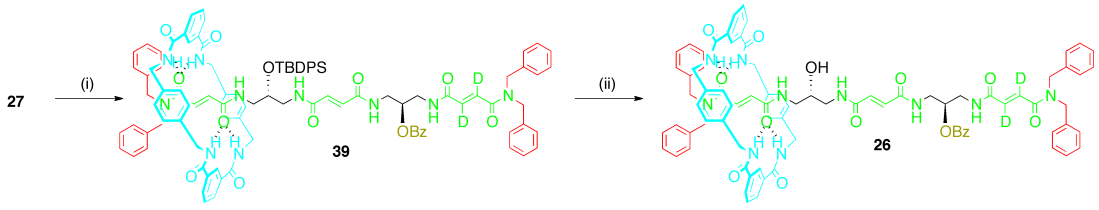

Scheme 2.5 (i) BzCl, DMAP, NEt_3, DCM, rt, 1 h, 87%; (ii) HF·py, THF, rt, 16 h, *quant.*

Rotaxane **27** also served as a precursor for mono-benzoylated rotaxane **26**. The free secondary alcohol was benzoylated with benzoyl chloride in the presence of DMAP, a reaction that proceeded very smoothly and completed in less than an hour. After purification by column chromatography, rotaxane **39** was treated with HF in pyridine to afford **26** in quantitative yield.

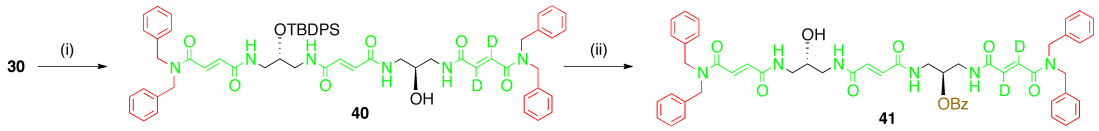

Scheme 2.6 (i) (a) TFA, DCM, 16 h, *quant.*; (b) Acid **29**, TBTU, HOBt, DIPEA, DMF, 0 °C to rt, 16 h, 79%; (ii) BzCl, DMAP, NEt_3, DCM, then HF·py, DCM, 16 h, 24% (over 2 steps).

Exactly the same procedure was employed using thread **30** in place of rotaxane **28** to obtain a thread molecule for the purpose of comparison by NMR spectroscopy. The low isolated yield of 24% for **41** is not a reflection of the efficacy of the benzoylation or desilylation reactions, which probably proceeded quantitatively, but rather of the difficulty in purifying such a powerful organogelator. To our surprise, even solutions in dichloromethane as dilute as 5 mg in 5 mL (0.8% wt.) left standing for several days were found to pass the gel inversion test. The combination, on a linear molecule, of multiple hydrogen-bonding units with chiral centres that reduce the number of possible spatial configurations, are likely to have contributed strongly to this gelation effect.[27,28] Thread **41** was eventually purified by a combination of column chromatography and preparative TLC.

2.5 Operation and Analysis of Molecular Information Ratchets

The acylation reactions were performed in the presence of a modified version of the catalyst[28] used by Leigh and coworkers in 2008. The DMAP analogue **42** was found by Connon and coworkers to be more effective at the asymmetric acylation of secondary alcohols,[29] and could be prepared in two steps from commercially available α,α-bis-(3,5-ditrifluoromethylphenyl)-L-prolinol and 4-chloronicotinic acid; this catalyst was chosen instead. The standard procedure for operation was to dissolve or suspend the information ratchet in dry dichloromethane (10 mM), and then add sequentially the acylation catalyst, triethylamine and benzoyl chloride (2 equivalents per hydroxyl group to be acylated). Reactions proceeded quickly and quantitatively, typically completing in less than fifteen minutes at room temperature. After the disappearance of diol **25** was confirmed by TLC analysis using an eluent of 40:60 DCM/acetone, the solvent was removed under reduced pressure, and the crude product was triturated once with diethyl ether to remove the catalyst and unreacted benzoyl chloride (the ratio of products was unaffected by this process).

The result of benzoylation was a mixture of kinetically locked positional isomers *left*-**43**, *centre*-**43** and *right*-**43**. The efficacy of the information ratchet mechanism would be determined from the distribution of products, and the extent to which this depended on the catalyst employed. In order to determine the ratios of positional isomers, it was first necessary to obtain pure samples of each of the kinetically locked products *left*-**43**, *centre*-**43** and *right*-**43**.

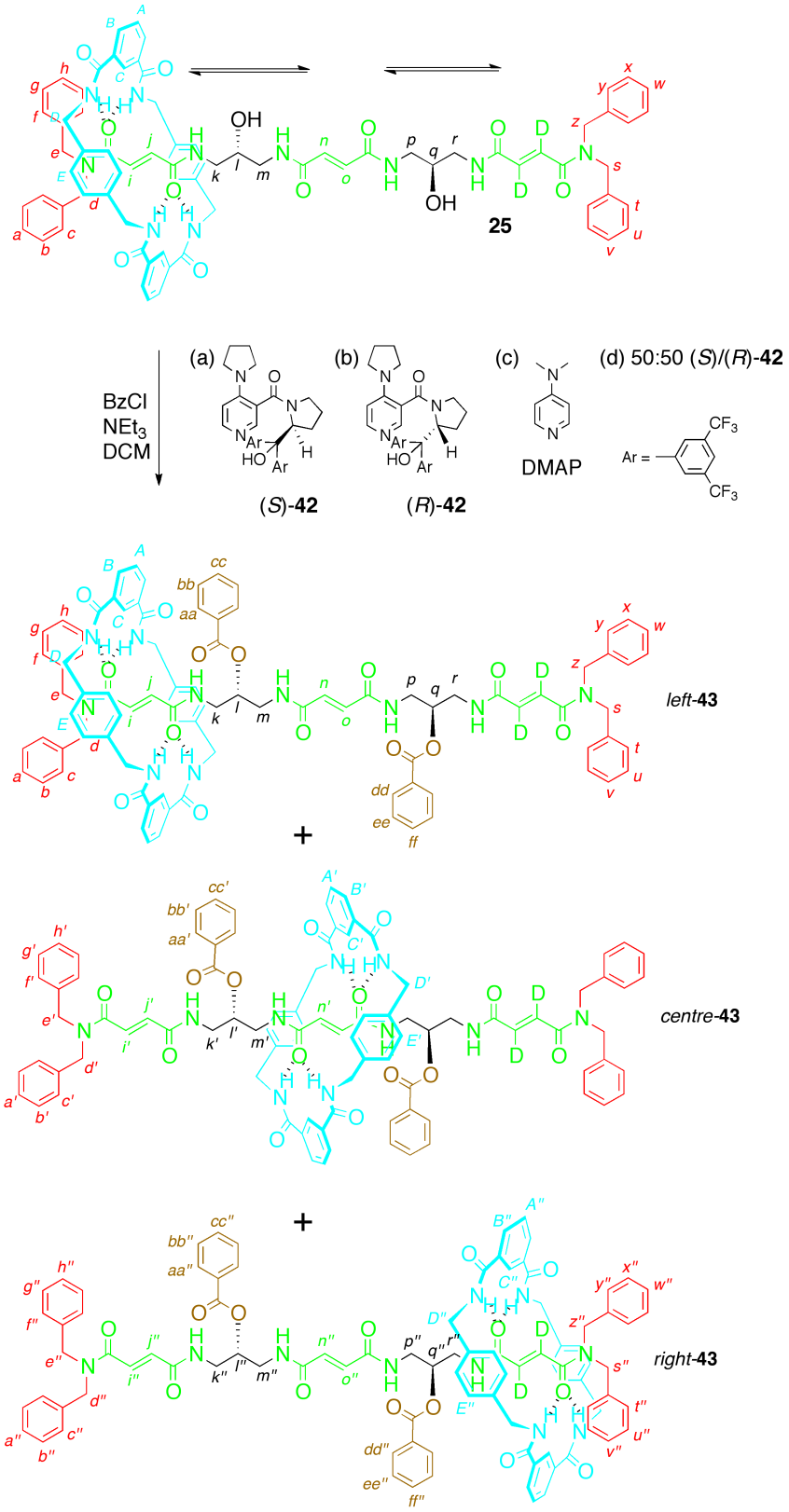

Scheme 2.7 Operation of molecular information ratchet **25**. Reagents and conditions: BzCl (4 equivalents), NEt_3 (4 equivalents), (*S*)-**42** or (*R*)-**42** or DMAP or 50:50 (*S*)/(*R*)-**42** mixture (4 equivalents), DCM, 10 mM, rt, 2 h.

The benzoylation of the hydroxy groups on **25** and **26** had unexpected effects on the molecules' solubility. While the rotaxane products bearing a terminally positioned macrocycle (*left*-**43** and *right*-**43**) were readily soluble in mixtures of methanol and chloroform, the more symmetrical positional isomer *centre*-**43** was found to be soluble only in DMSO. This proved advantageous for purification purposes, since a mixture of *left*-**43** and *right*-**43** could be separated easily from *centre*-**43** by selective precipitation from methanol/chloroform mixtures; unfortunately, the radical difference in solubilities also meant that the ratios of positional isomers could only be determined in certain solvents. When an NMR spectrum was taken in a methanol/chloroform mixture, precipitation of *centre*-**43** meant that the ratio of compounds present in solution changed over time, and did not reflect the true ratio of products formed. The problem was circumvented by taking the spectra in DMSO-d_6.

Fortuitously, each enantiomer of the chiral catalyst seemed to produce either a *left*-**43**/*centre*-**43** mixture with negligible amounts of *right*-**43** (using (*R*)-**42**), or a *right*-**43**/*centre*-**43** mixture with negligible amounts of *left*-**43** (using (*S*)-**42**). This meant that there was no need to employ a method such as chiral HPLC to obtain pure samples of *left*-**43** or *right*-**43**: all that was needed was to operate the machine under chiral conditions, remove the *centre*-**43** by trituration, and use either column chromatography or preparative TLC to obtain a sample of the desired terminal isomer that had no detectable trace of the undesired terminal isomer.

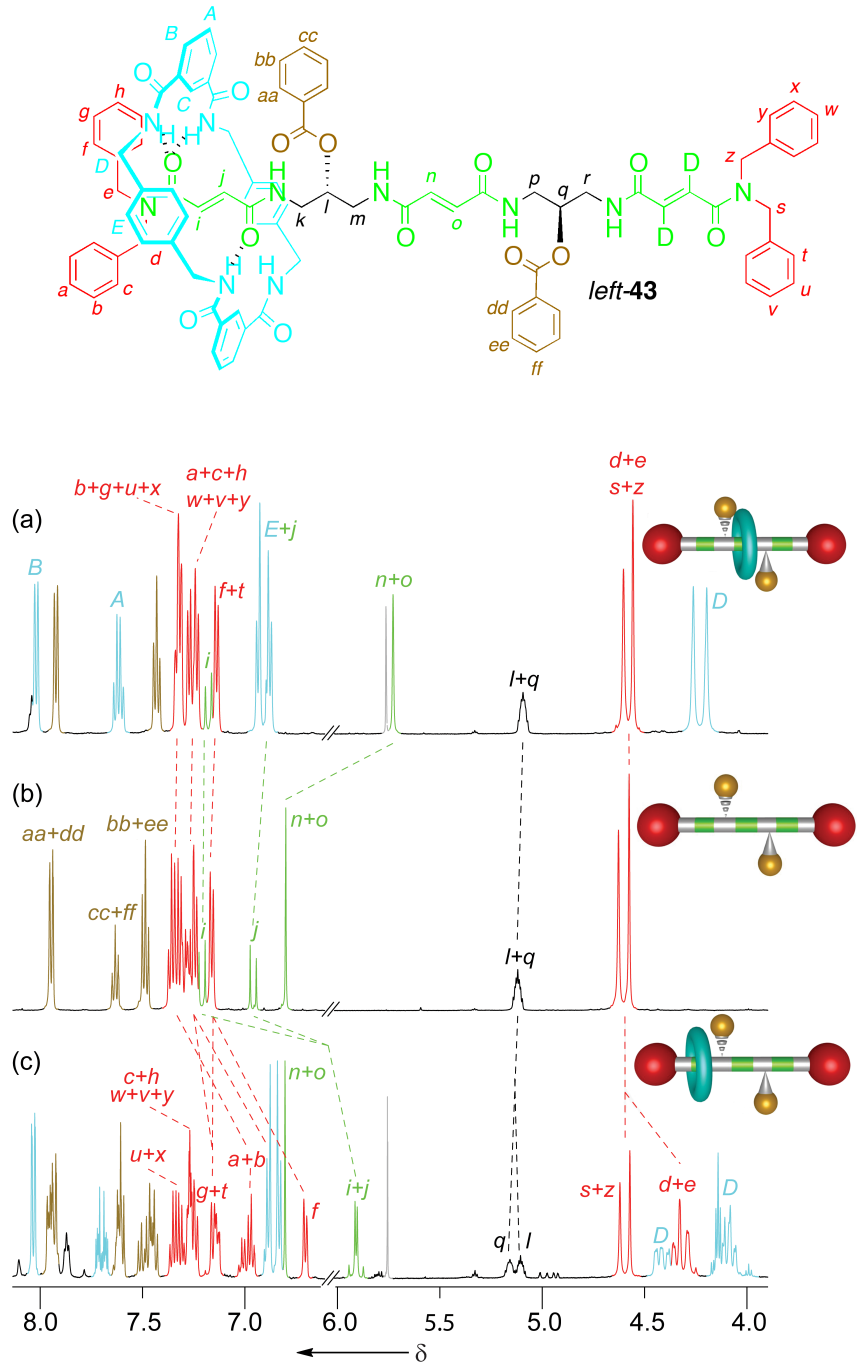

Figure 2.3 Partial ^{1}H NMR spectra (500 MHz, DMSO-d_6, 300 K) of (a) *centre*-**43**, (b) thread, (c) *left*-**43**. Residual solvent peaks are shown in grey. For full spectral assignments, see the experimental section.

Analysis by NMR spectroscopy of *centre*-**43** (Figure 2.3a) revealed the molecule to be highly symmetrical as expected. The signals for the macrocyclic *D* protons (blue) existed as a pair of singlets, as did the signals for the stopper protons *d, e, s* and *z* (red). When the macrocycle is locked into a terminal compartment

(Figure 2.3c), this symmetry is lost. The close proximity of the macrocycle to *one* set of stopper protons causes a splitting of the signals for both the macrocycle and the nearby stopper, while leaving the signals for the more distant stopper protons unchanged. This shielding effect was exploited for the characterisation of the product mixtures. The region of 6.0 ppm to 3.5 ppm was treated as an analysis region with various overlapping signals. Once the spectra were fully assigned, and once it was known which positional isomers contributed to which signals, it was possible to determine the ratios of products, without the need for separation, by integrating the overlapping regions and solving simultaneous equations (see Figure 2.4 for analysis regions). The results obtained for the double benzoylation of diol **25** (as depicted in Scheme 2.7) are given in Table 2.1. Values are cited as ±4% to account for variability in the integration of the analysis regions.

	Catalyst	**Product Distribution (±4%)** *left*-**43**:*centre*-**43**:*right*-**43**
(a)	(*S*)-**42**	<1:21:79
(b)	(*R*)-**42**	75:25:<1
(c)	DMAP	39:18:43
(d)	50:50 (*S*)/(*R*)-**42**	10:77:13

Table 2.1 Product distribution on double benzoylation of **25** using various catalysts. Reagents and conditions: BzCl (4 equivalents), NEt_3 (4 equivalents), (*S*)-**42** or (*R*)-**42** or DMAP or 50:50 (*S*)/(*R*)-**42** mixture (4 equivalents), DCM, 10 mM, rt, 2 h.

When diol **25** was treated with benzoyl chloride and triethylamine in the presence of chiral acylation catalyst (*S*)-**42**, the dibenzoylation kinetically locked the macrocycle predominantly in the right-hand compartment (<1:21:79 *left*-**43**/centre-**43**/right-**43**). Use of the antipode catalyst, (*R*)-**42**, led to an equal and opposite distribution (75:25:<1 *left*-**43**/centre-**43**/right-**43**), showing that the direction of net movement depends on the handedness of the chiral catalyst

employed. Benzoylation of **25** with the achiral acylation catalyst DMAP (c) yielded the benzoylated rotaxanes with the macrocycles trapped preferentially on the two terminal stations. Unexpectedly, use of a racemic mixture of catalysts (d) had the opposite effect to DMAP, and the product formed in the greatest quantity was *centre*-**43**.

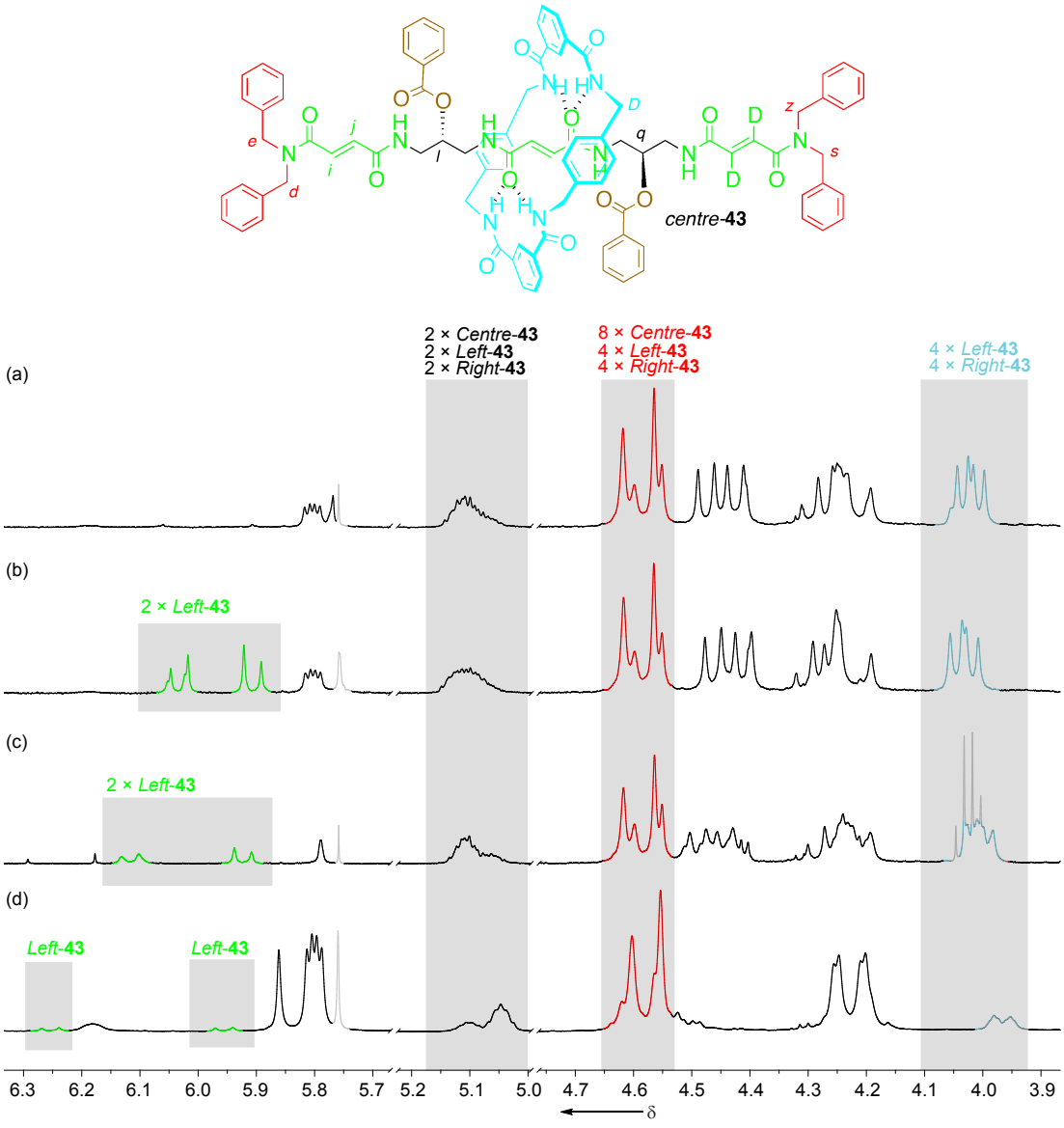

Figure 2.4 Partial ^{1}H NMR spectra (500 MHz, DMSO-d_6, 300 K) of double benzoylation of **25** in the presence of (a) (*S*)-**42**, (b) (*R*)-**42**, (c) DMAP and (d) a 50:50 (*S*)/(*R*)-**42** mixture. Residual solvent peaks are shown in grey. Peaks in highlighted analysis regions, from left to right, are as follows: fumaramide protons *i* and *j* when shielded by macrocycle (green); *l* and *q* (black); stopper protons *d*, *e*, *s* and *z* when far from macrocycle (red); and macrocyclic *D* protons when close to a stopper (blue).

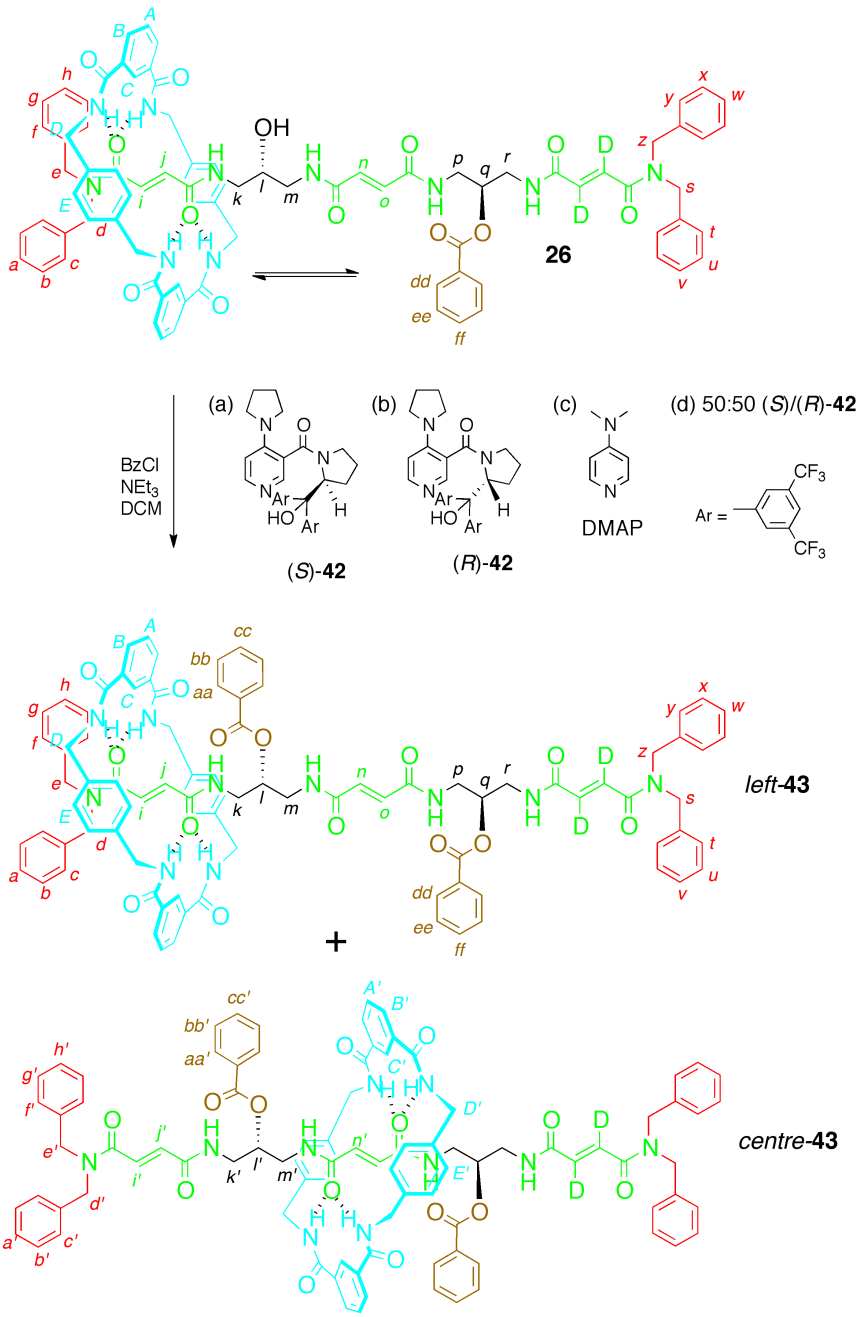

Scheme 2.8 Operation of molecular information ratchet **26**. Reagents and conditions: BzCl (2 equivalents), NEt_3 (2 equivalents), (*S*)-**42** or (*R*)-**42** or DMAP or 50:50 (*S*)/(*R*)-**42** mixture (2 equivalents), DCM, 10 mM, rt, 2 h.

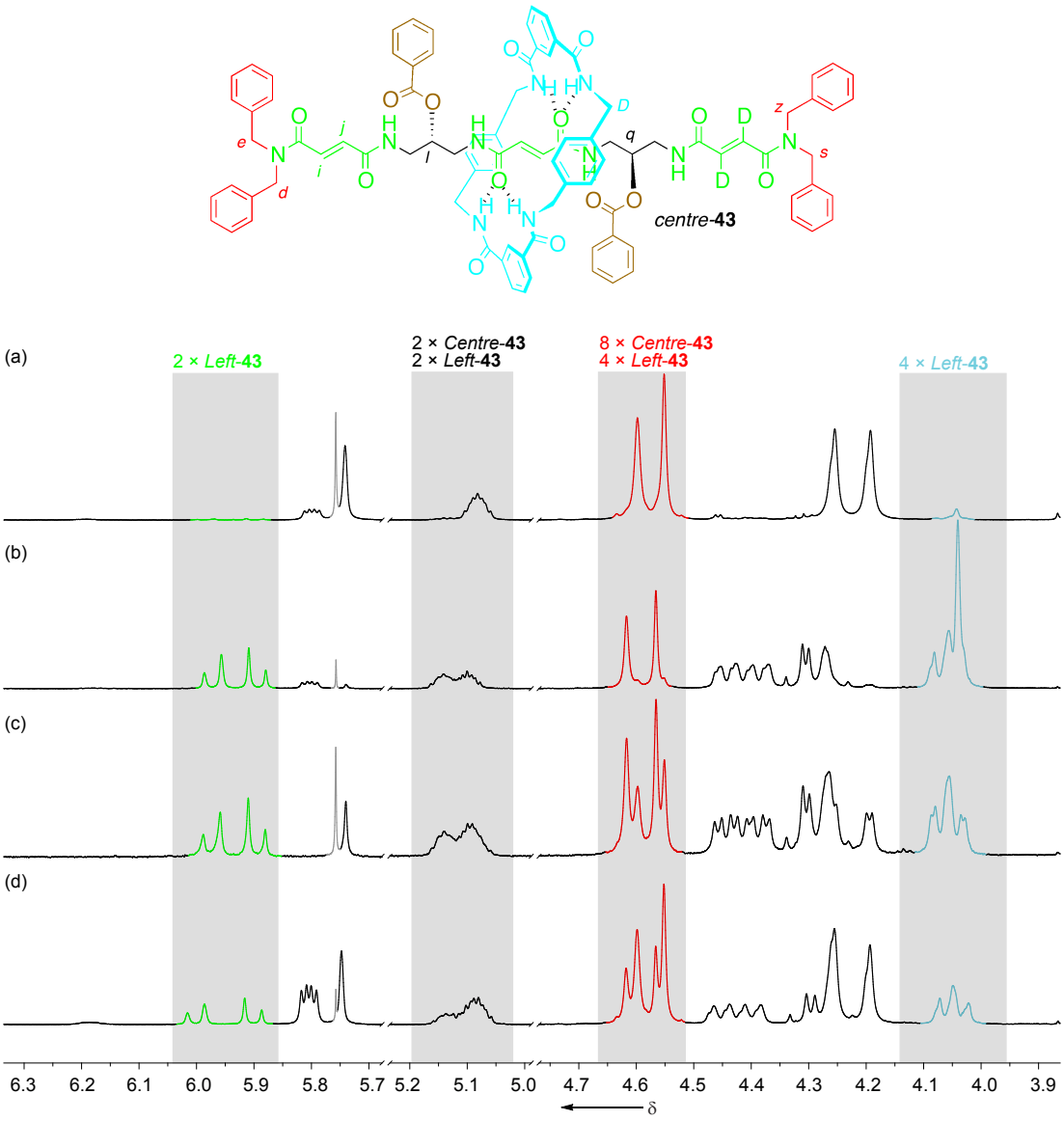

Figure 2.5 Partial ^{1}H NMR spectra (500 MHz, DMSO-d_6, 300 K) of benzoylation of **26** in the presence of (a) (*S*)-**42**, (b) (*R*)-**42**, (c) DMAP and (d) a 50:50 (*S*)/(*R*)-**42** mixture. Residual solvent peaks are shown in grey. Peaks in highlighted analysis regions, from left to right, are as follows: fumaramide protons *i* and *j* when shielded by macrocycle (green); *l* and *q* (black); stopper protons *d*, *e*, *s* and *z* when far from the macrocycle (red); and macrocyclic *D* protons when close to a stopper (blue).

To gain further insights into the mechanism of the process, the mono-benzoylated rotaxane **26** was also operated under the same conditions. The presence of a benzoyl blocking group already on the thread meant that the ratios produced were unambiguously the result of directional discrimination occurring at a single site; the macrocycle was forced to choose between the left

and centre compartments. The results of single benzoylation of **26** in the presence of various catalysts are shown in Table 2.2. Use of (*S*)-**42** and (*R*)-**42** individually gave ratios of products that were opposite but not equal (13:87 and 96:4 *left*-**43**/*centre*-**43** respectively). With **26**, as for **25**, DMAP preferentially catalysed the acylation reaction when the macrocycle was in a terminal binding environment. The slight majority of *centre*-**43** formed when a racemic mixture of catalysts was used also reflected the tendency of **25** to form *centre*-**43** under similar conditions.

	Catalyst	**Product Distribution (±4%)** *left*-**43**:*centre*-**43**
(a)	(*S*)-**42**	13:87
(b)	(*R*)-**42**	96:4
(c)	DMAP	64:36
(d)	50:50 (*S*)/(*R*)-**42**	45:55

Table 2.2 Product distribution on double benzoylation of **26** using various catalysts. Reagents and conditions: BzCl (2 equivalents), NEt_3 (2 equivalents), (*S*)-**42** or (*R*)-**42** or DMAP or 50:50 (*S*)/(*R*)-**42** mixture (2 equivalents), DCM, 10 mM, rt, 2 h.

It was evident that there were common traits in the operation of **25** and **26**. In both cases the benzoylation reactions were taking place selectively behind the macrocycle, with a forward direction specified by the handedness of the catalyst: left for (*R*)-**42**, right for (*S*)-**42**. It also appeared that this directional discrimination occurred in parallel with a pre-existing bias for the macrocycle occupying the terminal compartments. This effect could be seen in the single benzoylation of **26**, where the pre-existing bias was added to in the case of catalysis by (*R*)-**42**, resulting in a very effective (96%) macrocycle transport, or opposed, in the case of (*S*)-**42**, resulting a transport of reduced efficacy (87%). This hypothesis is borne out by NMR-spectroscopic analysis of the starting materials.

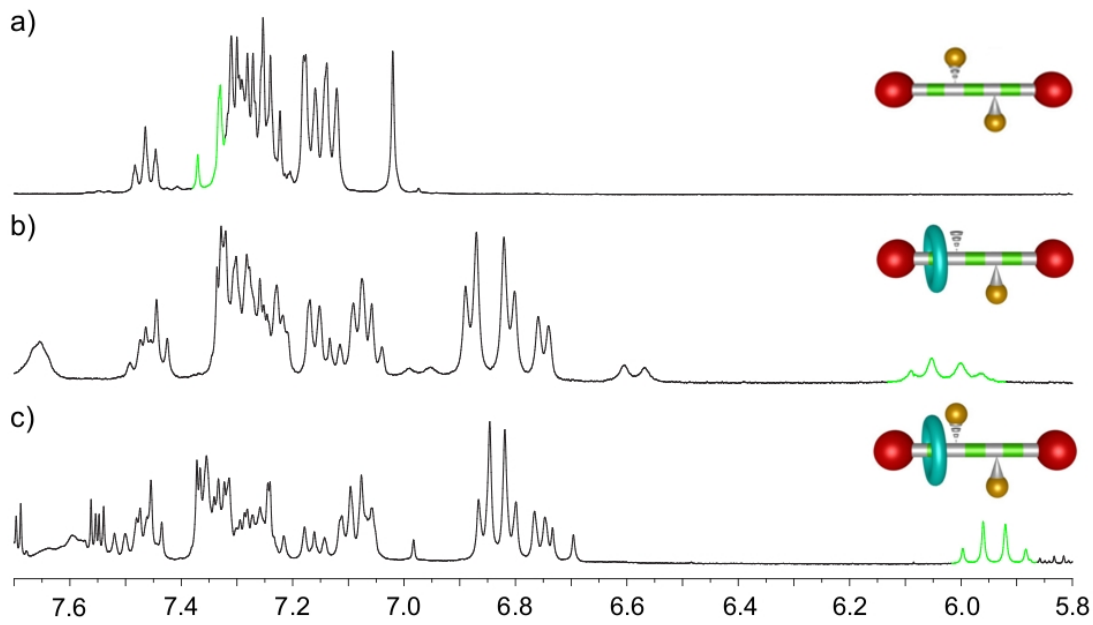

Figure 2.6 Partial ^{1}H NMR spectra (400 MHz, DCM-d_2, 298 K) of (a) bare thread, (b) singly benzoylated rotaxane **26**, (c) *left*-**43**; signals corresponding to the fumaric protons in the left-hand terminal compartment are highlighted in green.

Figure 2.6 shows a partial ^{1}H NMR spectrum of mono-benzoylated rotaxane **26**, with thread and *left*-**43** for comparison. Since the equilibrium distribution is likely to depend on the solvent and the temperature, the spectra were all obtained in the standard reaction solvent, DCM, at room temperature, so that the macrocycle distribution would be the same for the analysis as for the operation. The partial shielding of the fumaric protons suggests that the macrocycle is in fast exchange between the two binding sites, and at equilibrium the protons appear to spend much more of their time shielded by the macrocycle than not. While it is difficult to determine the equilibrium distribution exactly from such analytical methods, it is clear that in the case of the mono-benzoylated rotaxane, the principal contribution is from the macrocycle positioned on the terminal station rather than the central one.

The difference between the product ratios obtained with DMAP and the racemic **42** mixture remained perplexing, however. It was unsurprising that the ratios

obtained were not identical; DMAP and **42** are different compounds, presumably with different reactivities towards benzoyl chloride and secondary alcohol groups. Nevertheless, it was unexpected that DMAP preferred to benzoylate with the macrocycle in the terminal compartment, and that the racemate, though showing little preference, appeared to benzoylate more often when the macrocycle was in the centre. The difficulties in resolving the problem were exacerbated by the impossibility of observing the benzoylation in real time (the reaction occurred too quickly for the process to be observed by NMR spectroscopy), or of knowing the outcome of a single benzoylation on a diol thread (the mixtures of products obtained using one equivalent of benzoyl chloride would have been too complex to analyse).

While a totally satisfactory explanation of the internal mechanisms of action did not emerge until comparisons could be made with related systems (see the next Chapter), important clues were provided by a mathematical technique that allowed the outcome of unobservable reactions to be inferred. This technique involved modelling the reaction as a hidden Markov process.

2.6 Markov Modelling

In the double benzoylation of **25**, starting material **25** is converted in a stepwise fashion into its kinetically locked products, *via* certain allowed transitions, passing through a set of four transient singly-benzoylated intermediates which are not observable under the experimental conditions. Because this benzoylation is stochastic and memoryless it may be described as a hidden Markov process,[30] and represented as a transition diagram as in Schemes 2.9, 2.11 and 2.13. The arrows represent the probabilities of transitions from one state to another. Although these transitions cannot be quantified by direct observation, they may be inferred from information gleaned from single-

benzoylation experiments. The ratio of products formed on single benzoylation of **26** gives values for transitions that can be entered into the diagram for double benzoylation of **25**. The remaining transitions can be calculated by a number of techniques, as described in detail below. In the transition diagrams that follow, arrows in red show transitions whose probabilities have been observed directly through experiments; transitions whose probabilities have been calculated indirectly are marked in black. The maximum error for the transitions is ±4%, a consequence of the error in NMR spectroscopy measurements.

2.6.1 Modelling of Information Ratchet 25 in the Presence of DMAP

The benzoylation of **25** in the presence of DMAP is illustrated schematically in Scheme 2.9. The initial benzoylation reaction can occur at one of two available hydroxyl groups, and the macrocycle can be either on one side or the other of the site of benzoylation, giving rise to four possible singly-benzoylated intermediates. These intermediates may then go on to react with a second molecule of benzoyl chloride, resulting in three possible final products.

For some of the intermediates, the outcome is fixed as soon as the first benzoylation has taken place: the macrocycle has been locked into a compartment by the first benzoylation and its position can in no way be influenced by the second, a consequence of the irreversibility of the benzoylation reactions. For this reason the probabilities of transitions V(a) and X(a) are set at 100%.

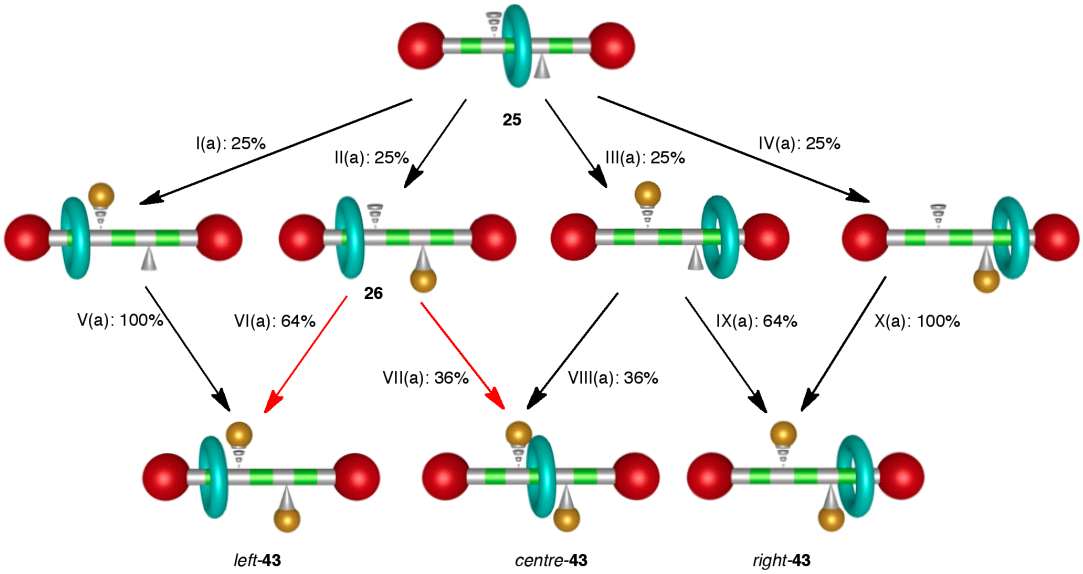

Scheme 2.9 Transition diagram of the operation of information ratchet **25** in the presence of DMAP. Values for I(a) and II(a) were determined from experimental results; values for III(a) and IV(a) are taken to be equal to values II(a) and I(a) respectively; values for V(a) and X(a) must logically be 100% under irreversible benzoylation conditions; values for VI(a) and VII(a) were obtained experimentally by single benzoylation of **26**; values for VIII(a) and IX(a) are taken to be equal to values for VII(a) and VI(a) respectively. Values for transitions shown in red were determined directly through experiment; values for transitions shown in black were inferred through indirect methods.

One of the singly-benzoylated intermediates has already been synthesised as **26**. Single-benzoylation experiments on **26** allow that part of the Markov model to be explored in isolation from the rest. Values for transitions VI(a) and VII(a) are given by the single benzoylation of **26**, and are found to be 64% and 36% respectively; this reflects the thermodynamic preference for the macrocycle occupying the terminal stations. Given the achirality of DMAP and the symmetry of **25**, a mirror-image version of **26** would be expected to produce mirror-image ratios of products: transitions VIII(a) and IX(a) therefore have probabilities of 36% and 64% respectively.

With these values firmly established, the probabilities of transitions I(a) and II (a) and their mirror images III(a) and IV(a) could be obtained by adjusting

their values until a good fit with experimental data for the double benzoylation of **25** was achieved. Thus it was inferred that the first benzoylation of **25**, catalysed by DMAP, has a 50% probability of trapping the macrocycle in one of the terminal compartments, and a 50% probability of occurring in a way that leaves the macrocycle free to shuttle between the two remaining compartments. A comparison between experimental and calculated ratios is given in Scheme 2.10.

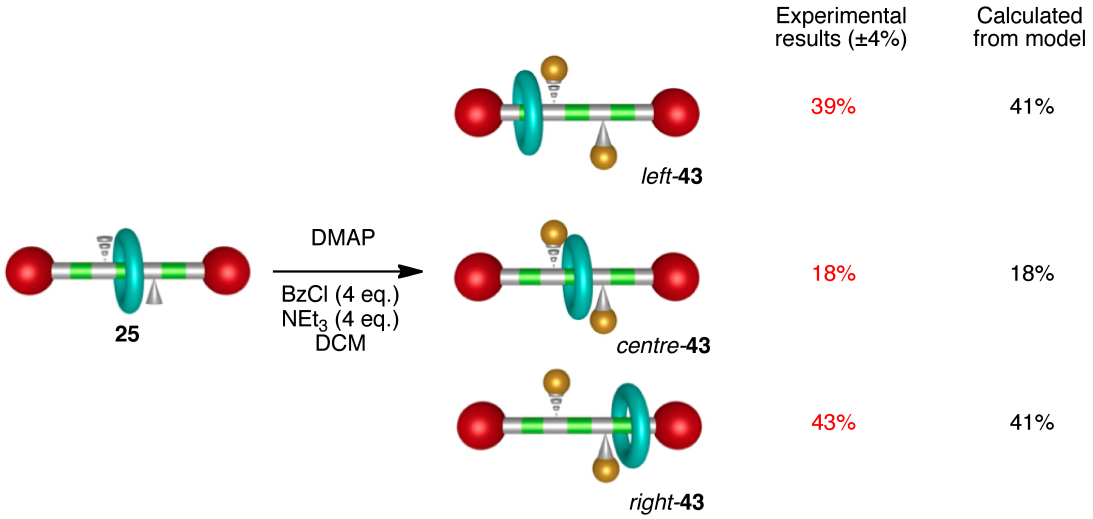

Scheme 2.10 Comparison of experimental results obtained for double benzoylation of **25** in the presence of DMAP with the results obtained with the model in Scheme 2.9.

2.6.2 Modelling of Information Ratchet 25 in the Presence of a 50:50 (*S*)/(*R*)-42 Mixture

The ratios of *left*-**43** to *centre*-**43** given by benzoylation of **26** in the presence of a 50:50 (*S*)/(*R*)-**42** mixture correspond to the probabilities of transitions VI(b) and VII(b), 45% and 55% respectively. Since treatment of diol **25** in the presence of the racemic **42** mixture produces equal amounts of *left*-**43** and *right*-**43**, transitions VIII(b) and IX(b) are assumed to be mirror images of VI(b) and VII(b), and have probabilities of 55% and 44% respectively. Transitions

II(b) and III(b) are mirror images of each other and so must be equiprobable under racemic conditions.

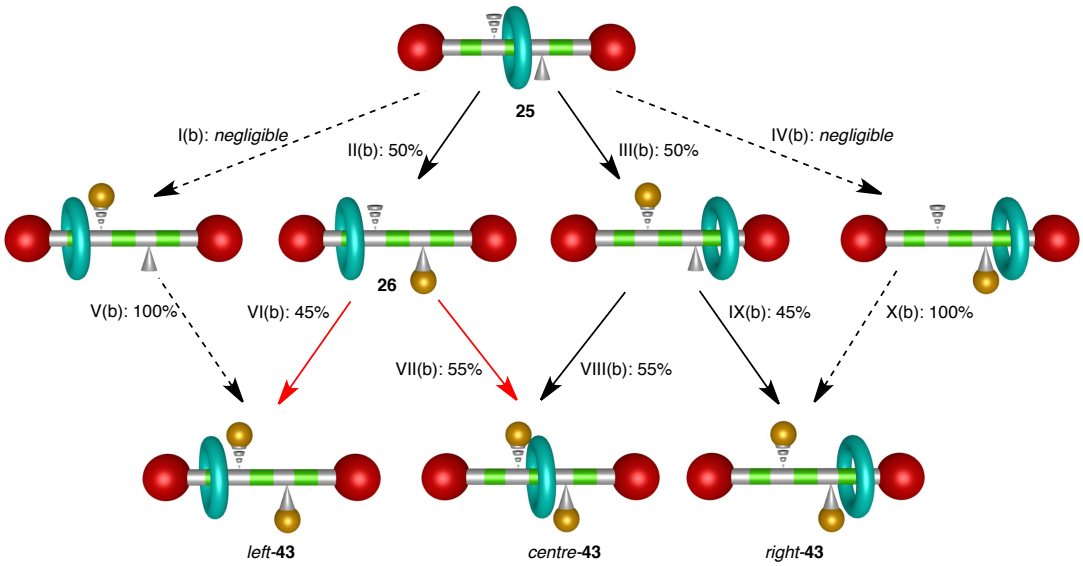

Scheme 2.11 Markov model of the operation of information ratchet **25** in the presence of 50:50 (*S*)/(*R*)-**42** mixture. Values for I(b) and II(b) were calculated by fitting to experimental results of diol benzoylation; values for III(b) and IV(b) are taken to be equal to values II(b) and I(b) respectively; values for V(b) and X(b) must logically be 100% under irreversible benzoylation conditions; values for VI(b) and VII(b) obtained experimentally by single benzoylation of **26**; values for VIII(b) and IX(b) taken to be equal to values for VII(b) and VI(b) respectively. Values for transitions shown in red were determined directly through experiment; values for transitions shown in black were inferred through indirect methods. Dashed arrows indicate transitions that were explored to a negligible extent.

These transitions already account for the large amount of *centre*-**43** formed under racemic conditions. Since processes resulting from transitions I(b) and IV(b) can only lead to the formation of *left*-**43** and *right*-**43** at the expense of *centre*-**43**, the contribution from these pathways must be negligible; wherever possible, benzoylation reactions catalysed by either enantiomer of **42** occur in a way that leaves the macrocycle free to shuttle, and do not, in the first instance, trap the macrocycle into either of the terminal compartments. This effect may be the result of steric clash with the bulky (*S*)-**42**, an effect not seen with the smaller molecule DMAP (this theory is elaborated upon in the following Chapter). Transitions V(b) and X(b) must logically take values of 100% under

irreversible benzoylation conditions, although they are not explored to any detectable extent. Modelling **25** in this way gives the closest fit with its experimentally observed behaviour in the presence of a 50:50 (*S*)/(*R*)-**42** mixture. A comparison between experimental and calculated ratios is given in Scheme 2.12.

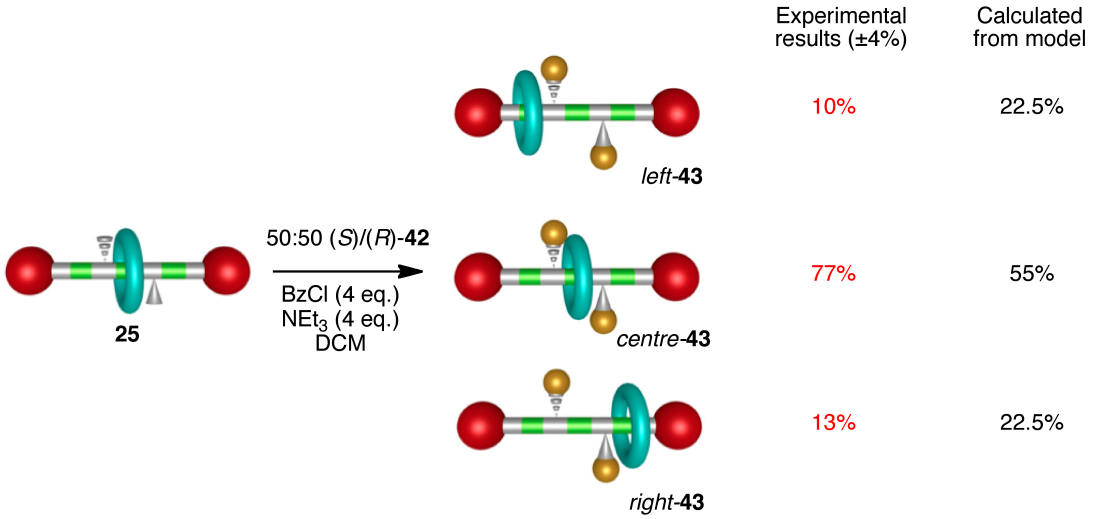

Scheme 2.12 Comparison of experimental results obtained for double benzoylation of **25** in the presence of 50:50 (*S*)/(*R*)-**42** mixture with the results obtained with the model in Scheme 2.11.

2.6.3 Modelling of Information Ratchet 25 in the Presence of (*S*)-42

As in the previous examples, single benzoylation of **26** revealed the values of VI(c) and VII(c) to be 13% and 87% respectively; however, because reactions at the two chiral centres of **25** are inequivalent under chiral conditions, IX(c) and VIII(c) can no longer be taken to be mirror images of VI(c) and VII(c). Rather than synthesise **26a** and perform a single benzoylation in the presence of (*S*)-**42**, it was found more expedient to use the ratios obtained by benzoylation of **26** in the presence of (*R*)-**42**. Since this resulted in the formation of 4%

centre-**43** and 96% *left*-**43**, the values of VIII(c) and IX(c) are 4% and 96% respectively. These results serve further to confirm that there exists a thermodynamic bias towards formation of rotaxane with the macrocycle in the terminal compartments, and that the bias introduced by the chiral catalyst can act in concert with this (as in the benzoylation of **26a**, where the directional transport is 96% effective) or in opposition to this (as in the benzoylation of **26**, where directional transport is less effective at 87%).

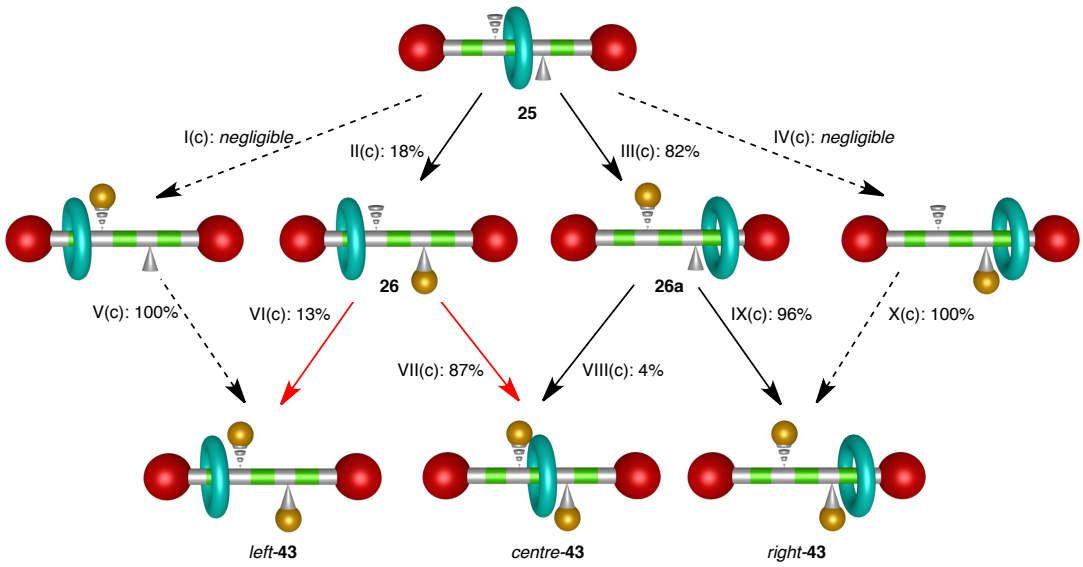

Scheme 2.13 Markov model of the operation of information ratchet **25** in the presence of (*S*)-**42**. Contributions from I(c) and IV(c) are known to be negligible when either enantiomer of **42** is used as an acylation catalyst; values for II(c) and III(c) were calculated by fitting to experimental data of benzoylation of **25**; values for V(c) and X(c) must logically be 100% under irreversible benzoylation conditions; values for VI(c) and VII(c) obtained experimentally by single benzoylation of **26** in the presence of (*S*)-**42**; values for VIII(c) and IX(c) obtained by benzoylation of **26** in the presence of (*R*)-**42**. Values for transitions shown in red were determined directly through experiment; values for transitions shown in black were inferred through indirect methods. Dashed arrows indicate transitions that were explored to a negligible extent.

If the contribution of a transition is negligible in the presence a 50:50 (S)/(R)-**42** mixture it must also be negligible in the presence of (*S*)-**42** or (*R*)-**42** individually; therefore contributions from I(c) and IV(c) are negligible, and

transitions V(c) and X(c), though logically valued at 100%, are not explored under these conditions. Based on these values, the values of II(c) and III(c) can be obtained by fitting them against the experimental ratios obtained on double benzoylation of **25** in the presence of (*S*)-**42**. Macrocycle shuttling is likely to be rapid on the acylation timescale; even though the macrocycle is believed to reside primarily in the terminal compartments, enough of its time is spent near the site of benzoylation to ensure that the chiral centres are well-expressed. Because of this, benzoylation reactions II(c) and III(c), at (*R*)- and (*S*)-centres respectively,[31] take place at very different rates. A comparison between experimental and calculated ratios is given in Scheme 2.14.

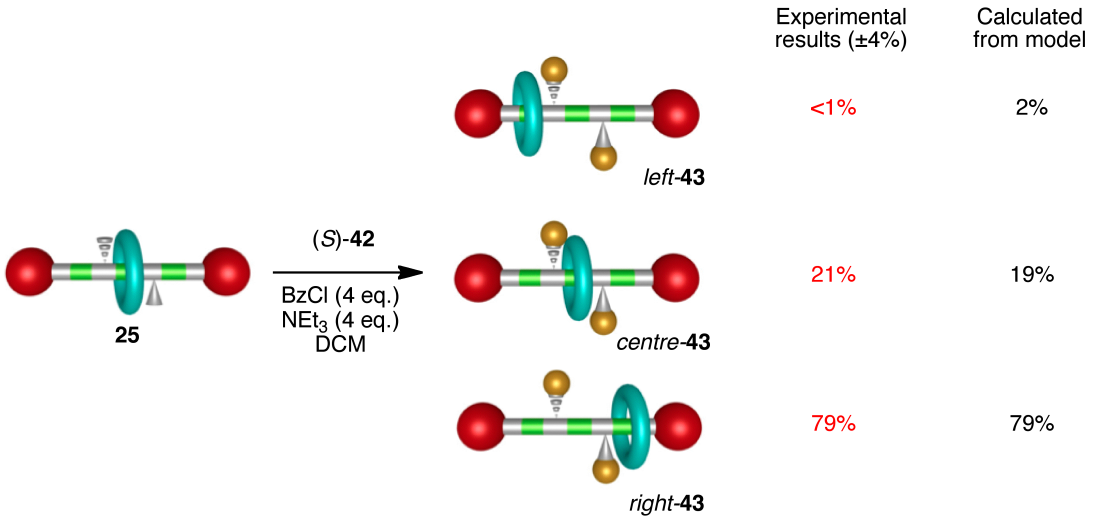

Scheme 2.14 Comparison of experimental results obtained for double benzoylation of **25** in the presence of (*S*)-**42** with the results obtained with the model (Scheme 2.13).

2.7 Overview: the Information Ratchet Mechanism in **25**

In the case of **25** it was found that, in the presence of (*S*)-**42**, the contribution from reactions that trap the macrocycle into the right-hand compartment are negligible, despite the strong thermodynamic bias for the macrocycle occupying that binding site. Reactions that trap the macrocycle into a terminal compartment in the first instance appear to be kinetically unfavourable. Instead, the most likely outcome (82%) of a single benzoylation of **25** is mono-benzoylated rotaxane **44** (see Scheme 2.15). This ratcheting step leaves the macrocycle free to shuttle between the central and right-hand stations, but bars the macrocycle from slipping backwards. When **44** is itself benzoylated, again in the presence of (*S*)-**42**, the most likely outcome (96%) is *right*-**43**. The directional transport is highly efficient in this second benzoylation because the macrocycle exhibits a strong thermodynamic preference for occupying terminal binding sites. Over two benzoylation reactions, a high proportion of **25** (>75%) is successfully converted into *right*-**43** because reactions that take place ahead of the macrocycle, blocking the direction of travel, are the least likely to occur under the chosen conditions. The direction of transport, and all ratios, are reversed when the antipode catalyst (*R*)-**42** is employed.

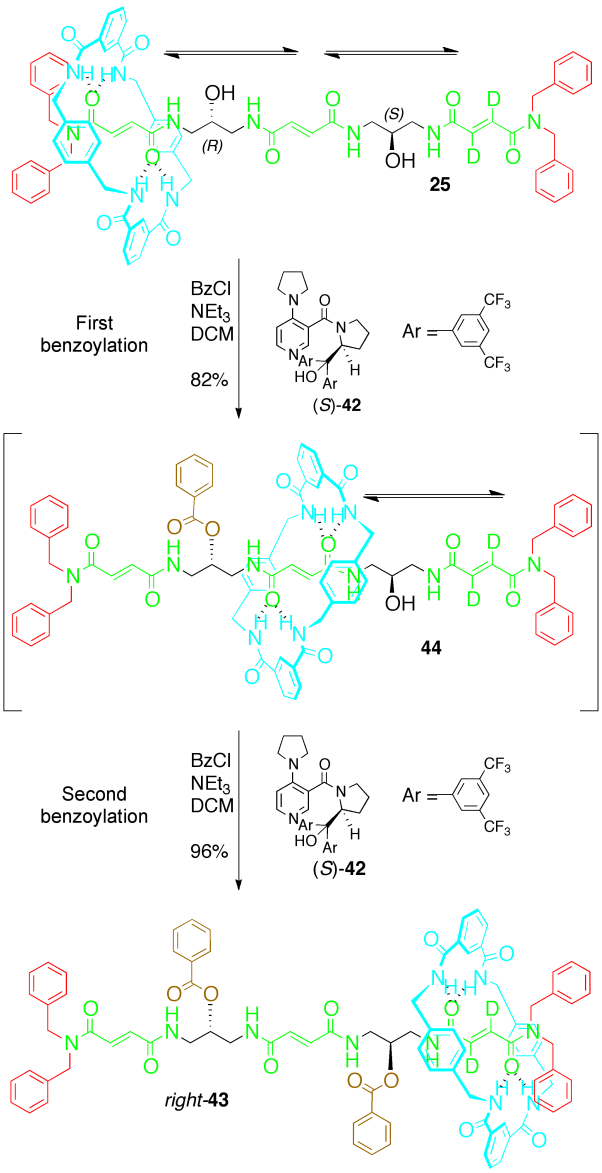

Scheme 2.15 The most likely fate of a molecule of **25** doubly benzoylated in the presence of (*S*)-**42**. Benzoylation reactions occur successively on the left of the macrocycle, resulting in rightward motion. The direction of transport is reversed by using (*R*)-**42**.

2.8 Summary and Outlook

Diol rotaxane **25** has been demonstrated to be information ratchet system that is able to directionally transport its macrocycle with remarkable efficiency to either end of its three-compartment thread. The two end compartments are identical, other than isotopic labels to distinguish them for analysis purposes, and yet the macrocycle can be driven to either end of the track by acylation reactions in the presence of a chiral catalyst. Stereochemical information is used to make benzoylation reactions take place preferentially behind the macrocycle; net directional transport results. Understanding the behaviour of this system in terms of contributions from many different processes provides insights into the statistical nature of molecular machines; it is hoped that these findings will prove useful in designing more extended rotaxanes in which the macrocycles are able to move directionally over greater distances and a higher number of compartments.

2.9 Experimental Section

Many of the compounds documented in this Chapter are chiral or adopt chiral conformations. The resulting inequivalent nuclei are in some instances observed as a complex series of signals, although the same compound may also exhibit simpler signals under different conditions (different solvent, temperature, concentration, etc). Where possible, the signals have been assigned unambiguously and where non-equivalence occurred it is noted in the experimental assignments. Signals for carbons adjacent to deuterons on fumaramide residues were not observed by ^{13}C NMR spectroscopy.

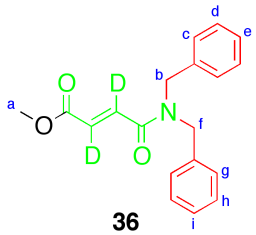

36

To a stirred, cooled (0 °C) solution of **35** (170 mg, 12.9 mmol) in anhydrous DMF (12.5 mL) under N_2 was added sequentially dibenzylamine (1.2 eq, 1.55 mmol, 0.25 mL), DIPEA (1.2 eq, 1.55 mmol, 0.26 mL), HOBt (1.2 eq, 1.55 mmol, 209 mg), TBTU (1.2 eq, 1.55 mmol, 496 mg). The mixture was stirred and allowed to reach room temperature over 12 h, then diluted with saturated $NaHCO_3$ (20 mL) and extracted into Et_2O (3 × 20 mL). The combined ethereal fractions were washed with saturated $NaHCO_3$ (3 × 10 mL), HCl (1 M, 3 × 10 mL) and brine (3 × 10 mL), then dried over $MgSO_4$ and concentrated under reduced pressure. Flash chromatography (5:1 PE/EtOAc) gave **36** as a colourless oil that solidified on standing (169 mg, 54%). ^{1}H NMR (400 MHz, $CDCl_3$): δ = 7.31-7.18 (m, 6H, H_d + H_e + H_h + H_i), 7.18-7.12 (m, 2H, H_c), 7.06 (d, 2H, J = 6.9, H_g), 4.55 (s, 2H, H_f), 4.43 (s, 2H, H_b), 3.67 (s, 3H, H_a); ^{13}C NMR (100 MHz, $CDCl_3$): δ = 166.0 (C), 165.2 (C), 136.6 (C), 135.8 (C), 129.1 (CH), 128.8 (CH), 128.4 (CH), 128.0 (CH), 127.7 (CH), 126.7 (CH), 52.2 (CH_3), 50.1 (CH_2), 48.4 (CH_2). LR-MS (ESI):

m/z 312 $[M+H]^+$; HR-MS (ESI): m/z = 312.1557 $[M+H]^+$ (calculated for $C_{19}H_{18}D_2NO_3$ = 312.1563).

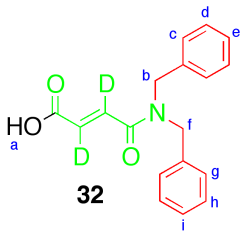

32

To a stirred solution of **36** (350 mg, 1.25 mmol) in 3:1 THF/H_2O (13.3 mL) was added LiOH·H_2O (2 eq, 2.5 mmol, 105 mg). After 1 h the mixture was diluted with HCl (1 M, 15 mL) and extracted into Et_2O (3 × 30 mL). The combined ethereal fractions were washed with HCl (1 M, 3 × 15 mL) and brine (3 × 15 mL), then dried over $MgSO_4$ and concentrated at reduced pressure to give acid **32** as a colourless oil that solidified on standing (344 mg, *quant*). ^1H NMR (400 MHz, $CDCl_3$): δ = 8.99 (br, 1H, H_a), 7.33-7.18 (m, 6H, H_d + H_e + H_h + H_i), 7.18 (d, 2H, *J* = 6.6, H_c), 7.07 (d, 2H, *J* = 7.0, H_g), 4.57 (s, 2H, H_b), 4.44 (s, 2H, H_f); ^{13}C NMR (100 MHz, $CDCl_3$): δ = 169.5 (C), 165.3 (C), 136.3 (C), 135.7 (C), 135.2 (CH), 129.1 (CH), 128.8 (CH), 128.5 (CH), 127.8 (CH), 126.7 (CH), 50.2 (CH_2), 48.5 (CH_2). LR-MS (ESI): m/z 298 $[M+H]^+$; HR-MS (ESI): m/z = 298.1403 $[M+H]^+$ (calculated for $C_{18}H_{16}D_2NO_3$ = 298.1407).

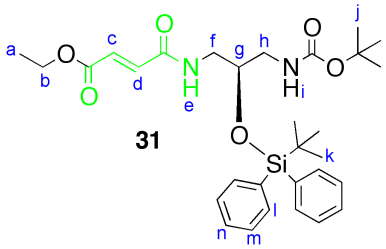

31

To a stirred, cooled (0 °C) solution of mono-ethyl fumarate (330 mg, 2.30 mmol) in anhydrous DMF (23 mL) under N_2 were added sequentially amine **34** (1.2 eq, 2.76 mmol, 1.18 g), DIPEA (1.2 eq, 0.47 mL, 2.76 mmol), HOBt (1.2 eq, 0.56

mmol, 75 mg) and TBTU (1.2 eq, 2.76 mmol, 886 mg). The reaction was allowed to reach room temperature with stirring over 12 h and diluted with saturated $NaHCO_3$ (30 mL). The aqueous fraction was extracted with Et_2O (3 × 30 mL) and the combined ethereal fractions were washed with saturated $NaHCO_3$ (3 × 15 mL), HCl (1 M, 3 × 15 mL) and brine (3 × 15 mL), then dried over $MgSO_4$ and concentrated under reduced pressure. Flash chromatography (2% acetone in DCM) gave **31** as a white solid (1.95 g, 94%). M.p. 142–144 °C. $[\alpha]_D^{20}$ = +29.9 (c = 0.33, DCM). ^{1}H NMR (400 MHz, $CDCl_3$): δ = 7.59 (t, 4H, *J* = 7.6, H_m), 7.42-7.28 (m, 6H, H_l + H_n), 6.72-6.61 (m, 2H, H_c + H_d), 6.54 (t, *J* = 6.4, 1H, H_e), 4.79 (t, *J* = 6.5, 1H, H_i), 4.17 (q, *J* = 7.1, 2H, H_b), 3.88-3.79 (m, 1H, H_g), 3.61-3.50 (m, 1H, H_f), 3.24 (ddd, 1H, *J* = 14.3, 8.1, 3.5, H_h), 3.07-2.95 (m, 1H, H_f), 2.92-2.80 (m, 1H, H_h), 2.10 (s, 9H, H_j), 1.24 (t, 3H, *J* = 7.1, H_a), 1.02 (s, 9H, H_k); ^{13}C NMR (100 MHz, $CDCl_3$): δ = 165.6 (C), 163.8 (C), 156.8 (C), 136.3 (CH), 135.7 (CH), 133.4 (C), 130.1 (CH ×2), 128.0 (CH), 79.8 (CH_2), 70.6 (CH), 61.1 (C), 43.0 (CH_2), 41.6 (CH_2), 28.3 (CH_3), 27.0 (CH_3), 19.3 (C), 14.2 (CH_3). LR-MS (ESI): m/z 555 $[M+H]^+$; HR-MS (ESI): m/z = 555.2883 $[M+H]^+$ (calculated for $C_{30}H_{43}O_6N_2Si$ = 555.2885).

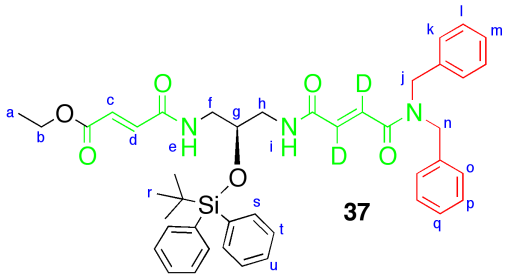

37

To a stirred solution of **31** (470 mg, 0.85 mmol) in anhydrous DCM (2 mL) in a loosely-sealed round-bottomed flask was added TFA (0.86 mL). After 20 h the mixture was diluted with aqueous NaOH (1 M) until basic and extracted into DCM (3 × 20 mL). The combined organic fractions were dried over $MgSO_4$ and the solvent was removed under reduced pressure. The obtained residue was redissolved in anhydrous DMF (7.8 mL) under N_2 and cooled to 0 °C. Acid **32** (1.2 eq, 0.94 mmol, 278 mg), DIPEA (1.2 eq, 0.94 mmol, 0.16 mL), HOBt (1.2 eq,

0.94 mmol, 127 mg) and TBTU (1.2 eq, 0.94 mmol, 302 mg) were added. After allowing the reaction to reach room temperature with stirring over 16 h the reaction mixture was diluted with saturated $NaHCO_3$ (10 mL) and extracted into DCM (4 × 15 mL). The combined organic fractions were washed with saturated $NaHCO_3$ (3 × 10 mL), HCl (1 M, 3 × 10 mL) and brine (3 × 10 mL), then dried over $MgSO_4$ and the solvent was removed under reduced pressure. Flash chromatography (1.5:1 PE/EtOAc) gave **37** as a colourless foam (414 mg, 72%). $[\alpha]_D^{20}$ = –7.3 (c = 1.10, DCM). ^1H NMR (400 MHz, $CDCl_3$): δ = 7.68 (m, 4H, H_s), 7.51-7.27 (m, 12H, $H_l + H_m + H_p + H_q + H_t + H_u$), 7.24 (d, 2H, *J* = 6.5, H_k), 7.17 (d, 2H, *J* = 7.0, H_o), 6.70 (d, *J* = 15.4, 1H, H_c), 6.63 (d, *J* = 15.4, 1H, H_d), 6.69-6.56 (m, 2H, $H_e + H_i$), 4.64 (s, 2H, H_j), 4.56 (s, 2H, H_n), 4.24 (q, 2H, *J* = 7.1, H_b), 4.06-3.98 (m, 1H, H_g), 3.71-3.61 (m, 2H, H_f), 3.05-2.95 (m, 2H, H_h), 1.32 (t, 3H, *J* = 7.1, H_a), 1.11 (s, 9H, H_r); ^{13}C NMR (100 MHz, $CDCl_3$): δ = 165.7 (C), 165.5 (C), 165.0 (C), 164.1 (C), 136.6 (C), 136.2 (CH), 135.8 (C), 135.7 (CH), 133.3 (C), 133.4 (CH), 130.2 (CH), 129.0 (CH), 128.8 (CH), 128.3 (CH), 128.0 (CH×2), 127.7 (CH), 126.8 (CH), 70.2 (CH), 61.1 (CH_2), 50.1 (CH_2), 48.4 (CH_2), 42.2 (CH_2), 41.9 (CH_2), 38.6 (CH_3), 27.0 (CH_3), 19.3 (C). LR-MS (ESI): m/z 734 $[M+H]^+$; HR-MS (ESI): m/z = 734.3601 $[M+H]^+$ (calculated for $C_{43}H_{48}D_2N_3O_6Si$ = 734.3595).

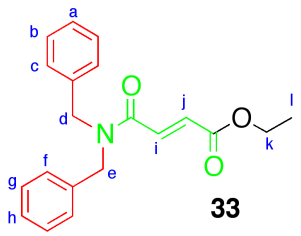

33

To a stirred, cooled (0 °C) solution of monoethylfumarate (0.61 g, 4.29 mmol) in anhydrous DMF (41 mL) under N_2 was added sequentially dibenzylamine (1.2 eq, 5.08 mmol, 0.83 mL), DIPEA (1.2 eq, 5.08 mmol, 0.86 mL), HOBt (1.2 eq, 5.08 mmol, 686 mg) and TBTU (1.2 eq, 5.08 mmol, 1.63 g). The mixture was allowed to reach room temperature with stirring over 12 h, diluted with saturated $NaHCO_3$ (40 mL) and extracted into Et_2O (3 × 50 mL). The combined ethereal fractions were washed with saturated $NaHCO_3$ (3 × 25 mL), HCl (1 M, 3 × 25 mL) and brine (3 × 25 mL), then dried over $MgSO_4$ and concentrated under reduced

pressure. Flash chromatography (5:1 PE/EtOAc) gave **33** as a colourless oil (1.28 g, 92%). ^{1}H NMR (400 MHz, $CDCl_3$): δ = 7.37 (d, 1H, *J* = 15.3, H_j), 7.33-7.19 (m, 6H, H_a + H_b + H_g + H_h), 7.19-7.13 (m, 2H, H_f), 7.08 (d, 2H, *J* = 7.0, H_c), 6.87 (d, 1H, *J* = 15.2, H_i), 4.57 (s, 2H, H_e), 4.46 (s, 2H, H_d), 4.15 (q, 2H, *J* = 7.1, H_k), 1.22 (t, 3H, *J* = 7.1, H_l); ^{13}C NMR (100 MHz, $CDCl_3$): δ = 165.4 (C), 165.1 (C), 136.3 (C), 135.6 (C), 133.5 (CH), 132.2 (CH), 128.8 (CH), 128.5 (CH), 128.2, (CH) 127.8 (CH), 127.5 (CH), 126.5 (CH), 61.0 (CH_2), 49.9 (CH_2), 48.2 (CH_2), 13.9 (CH_3). LR-MS (ESI): m/z 324 $[M+H]^+$; HR-MS (ESI): m/z = 324.1592 $[M+H]^+$ (calculated for $C_{20}H_{22}O_3N$ = 324.1594).

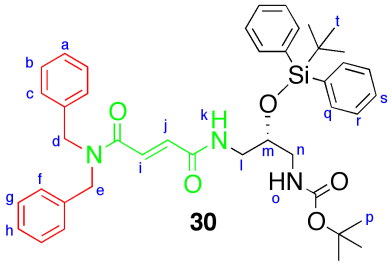

30

To a stirred solution of **33** (0.99 g, 3.07 mmol) in 3:1 THF/H_2O (32 mL) was added LiOH·H_2O (2 eq, 6.14 mmol, 0.26 g). After 1 h the mixture was diluted with HCl (1 M, 30 mL) and extracted into Et_2O (3 × 30 mL). The combined ethereal fractions were washed with HCl (1 M, 3 × 15 mL) and brine (3 × 15 mL), dried over $MgSO_4$ and concentrated under reduced pressure. The obtained residue (905 mg) was redissolved in anhydrous DMF (30 mL) under N_2 and the solution was cooled (0 °C). Amine **34** (1.09 eq, 3.68 mmol, 1.44 g), DIPEA (1.2 eq, 3.68 mmol, 0.63 mL), HOBt (1.2 eq, 3.68 mmol, 497 mg) and TBTU (1.2 eq, 3.68 mmol, 1.18 g) were sequentially added. The mixture was allowed to reach room temperature with stirring over 12 h then diluted with saturated $NaHCO_3$ (30 mL) and extracted into Et_2O (3 × 30 mL). The combined ethereal fractions were washed with saturated $NaHCO_3$ (3 × 15 mL), HCl (1 M, 3 × 15 mL) and brine (3 × 15 mL), then dried over $MgSO_4$ and concentrated under reduced pressure. Flash chromatography (2% acetone in DCM) gave **30** as colourless foam (1.28 g, 94%). $[\alpha]_D^{20}$ = +39.0 (c = 0.21, DCM). ^{1}H NMR (400 MHz, $CDCl_3$): δ = 7.58 (td, 4H, *J* = 7.8, 1.5, H_q), 7.40-7.18 (m, 13H, H_a + H_b + H_g + H_h + H_i + H_r +

H_s), 7.18-7.13 (m, 2H, H_f), 7.07 (d, 2H, J = 6.9, H_c), 6.85 (d, 1H, J = 14.7, H_j), 6.57-6.48 (m, 1H, H_k), 4.82-4.73 (m, 1H, H_o), 4.64 (q, 2H, J = 14.7, H_e), 4.51-4.39 (m, 2H, H_d), 3.82 (dt, 1H, J = 9.8, 4.7, H_m), 3.63-3.52 (m, 1H, H_l), 3.29-3.18 (m, 1H, H_n), 3.00-2.89 (m, 1H, H_l), 2.82 (dt, 1H, J = 14.3, 5.1, H_n), 1.34 (s, 9H, H_t), 1.01 (s, 9H, H_p); ^{13}C NMR (100 MHz, $CDCl_3$): δ = 166.4 (C), 164.9 (C), 157.3 (C), 137.3 (C), 136.5 (C), 136.3 (CH), 136.0 (CH), 134.0 (C), 130.9 (CH), 130.6 (CH), 129.6 (CH), 129.3 (CH), 129.0 (CH), 128.6 (CH), 128.5 (CH), 128.2 (CH), 127.3 (CH), 80.4 (C), 71.2 (CH), 50.6 (CH_2), 48.9 (CH_2), 43.5 (CH_2), 42.1 (CH_2), 28.9 (CH_3), 27.6 (CH_3), 19.9 (C). LR-MS (ESI): m/z = 706 $[M+H]^+$; HR-MS (ESI): m/z = 706.3670 $[M+H]^+$ (calculated for $C_{42}H_{52}O_5N_3Si$ = 706.3671).

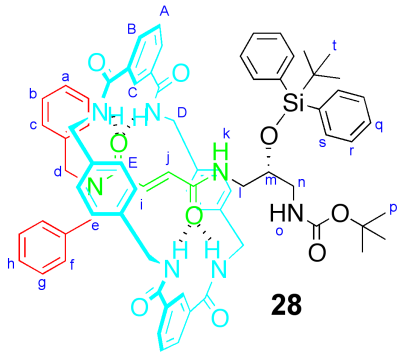

28

To a stirred solution of **30** (300 mg, 0.43 mmol) and triethylamine (3.3 eq, 1.42 mmol, 0.2 mL) in anhydrous chloroform (150 mL) under N_2 was added simultaneously a solution of isophthaloyl chloride (8 eq, 3.44 mmol, 600 mg) in anhydrous chloroform (43 mL) and a solution of *p*-xylylene diamine (8 eq, 3.44 mmol, 468 mg) and triethylamine (14.6 eq, 6.28 mmol, 0.87 mL) in anhydrous chloroform (43 mL) over 3 h using syringe pumps. The mixture was filtered through a sinter and the residue was washed with chloroform (3 × 50 mL). The combined organic phase was washed with saturated $NaHCO_3$ (3 × 100 mL) then dried over $MgSO_4$ and concentrated under reduced pressure. Flash chromatography (1.5:1 PE/EtOAc) gave **28** as a white solid (334 mg, 62%). M.p. 150–152 °C. $[\alpha]_D^{20}$ = 0.0 (c = 0.47, DCM). ^{1}H NMR (400 MHz, $CDCl_3$): δ = 8.33 (s, 2H, H_C), 8.17 (t, 4H, J = 8.7, H_B), 7.60-7.48 (m, 6H, H_r + NH), 7.44 (dd, 1H, J = 8.3,

4.3, H_k), 7.41-7.32 (m, 4H, H_A + NH), 7.30-7.22 (m, 6H, H_a + H_b), 7.22-7.11 (m, 5H, H_a + H_c + H_q), 7.06 (t, 1H, *J* = 7.4, H_h), 6.94 (t, 2H, *J* = 7.6, H_g), 6.75 (d, 4H, *J* = 7.9, H_E), 6.66-6.51 (m, 6H, H_E + H_f), 5.81 (d, 1H, *J* = 14.6, H_i), 5.70 (d, 1H, *J* = 14.6, H_j), 4.88 (dd, 1H, *J* = 8.7, 4.6, H_o), 4.66-3.91 (m, 12H, H_D + H_d + H_e), 3.63-3.50 (m, 1H, H_m), 3.44 (ddd, 1H, *J* = 13.7, 8.7, 5.0, H_l), 3.12 (ddd, 1H, *J* = 14.7, 8.9, 2.5, H_n), 3.00-2.87 (m, 1H, H_n), 2.69 (ddd, 1H, *J* = 13.7, 8.9, 2.5, H_l), 1.12 (s, 9H, H_p), 0.96 (s, 9H, H_t); ^{13}C NMR (100 MHz, $CDCl_3$): δ = 166.1 (C), 165.9 (C), 165.4 (C), 164.9 (C), 137.5 (C), 135.9 (C), 135.6 (CH), 135.5 (CH), 134.9 (C), 133.6 (C), 133.3 (CH), 132.9 (C), 131.8 (CH), 130.3 (CH), 129.3 (CH), 129.0 (CH), 128.8 (CH ×2), 128.4 (CH), 128.1 (CH), 127.9 (CH ×2), 126.4 (CH), 125.4 (CH), 80.6 (C), 70.2 (CH), 60.4 (CH_2), 51.1 (CH_2), 43.7 (CH_2), 43.5 (CH_2), 41.1 (CH_2), 28.0 (CH_3), 26.9 (CH_3), 19.2 (C). LR-MS (ESI): m/z = 1238 $[M+H]^+$; HR-MS (ESI): m/z = 1255.6043 $[M+NH_4]^+$ (calculated for $C_{74}H_{83}N_8O_9Si$ = 1255.6047).

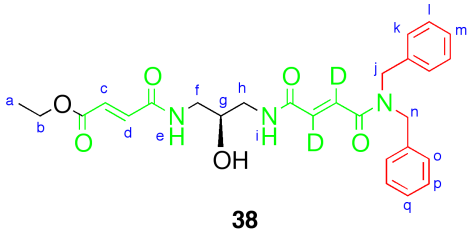

38

To a stirred solution of **37** (414 mg, 0.56 mmol) in dry THF (5 mL) was added TBAF (2 eq, 1.13 mmol, 1.13 mL of 1 M solution in THF). After 18 h the reaction mixture was diluted with saturated ammonium chloride solution (10 mL) and extracted into DCM (4 × 15 mL). The combined organic fractions were washed with saturated ammonium chloride solution (3 × 10 mL), saturated sodium citrate solution (3 × 10 mL) and water (3 × 10 mL), then dried over $MgSO_4$ and concentrated under reduced pressure. Flash chromatography (1.5:1 PE/EtOAc increasing to pure EtOAc) gave **38** as a colourless solid (203 mg, 73%). M.p. 163–165 °C. $[\alpha]_D^{20}$ = +200 (c = 0.21, DMSO). ^1H NMR (400 MHz, $CDCl_3$): δ = 7.33-7.21 (m, 7H, H_l + H_m + H_p + H_q + NH), 7.17-7.12 (m, 2H, H_k), 7.09 (d, 2H, *J* = 6.9, H_o), 6.96 (t, 1H, *J* = 6.0, NH), 6.91 (d, 1H, *J* = 15.4, H_c), 6.71 (d, 1H, *J* = 15.4, H_d), 4.58 (s, 2H, H_j), 4.50 (s, 2H, H_n), 4.16 (q, 2H, *J* = 7.1, H_b), 3.80-3.72 (m, 1H,

H_g), 3.39-3.22 (m, 4H, H_f + H_h), 1.23 (t, 3H, *J* = 7.1, H_a); ^{13}C NMR (100 MHz, $CDCl_3$): δ = 166.0 (C), 165.6 (C,×2), 164.9 (C), 136.3 (C), 136.2 (CH), 135.7 (C), 135.2 (CH), 130.6 (CH), 129.1 (CH), 128.8 (CH), 128.0 (CH), 127.7 (CH), 126.8 (CH), 69.5 (CH), 61.2 (CH_2), 52.3 (CH_2), 50.3 (CH_2), 48.6 (CH_2), 43.0 (CH_2), 42.8 (CH_3). LR-MS (ESI): m/z = 496 $[M+H]^+$; HR-MS (ESI): m/z = 496.2413 $[M+H]^+$ (calculated for $C_{27}H_{30}D_2O_6N_3$ = 496.2411).

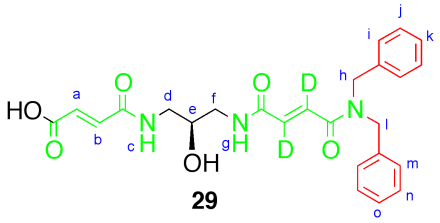

29

To a stirred solution of ester **38** (662 mg, 1.34 mmol) in 3:1 THF/H_2O (13.3 mL) was added LiOH·H_2O (2 eq, 2.68 mmol, 112 mg). After 25 minutes the reaction mixture was diluted with HCl (1 M, 15 mL) and extracted into 3:1 $CHCl_3$/IPA (4 × 50 mL). The combined organic fractions were washed with H_2O (3 × 20 mL) and dried over $MgSO_4$ then concentrated under reduced pressure to give acid **29** as a white solid (624 mg, *quant*). M.p. 165–167 °C. $[\alpha]_D^{20}$ = +66.7 (c = 0.27, DMSO). ^{1}H NMR (400 MHz, 3:1 $CD_3OD/CDCl_3$): δ = 7.41-7.26 (m, 6H, H_k + H_j + H_n + H_o), 7.26-2.21 (m, 2H, H_i), 7.18 (d, 2H, *J* = 7.1, H_m), 7.00 (d, 1H, *J* = 15.5, H_a), 6.71 (d, 1H, *J* = 15.5, H_b), 4.71-4.56 (m, 4H, H_h + H_l), 3.88-3.79 (m, 1H, H_e), 3.44-3.26 (m, 4H, H_d + H_f); ^{13}C NMR (100 MHz, 3:1 $CD_3OD/CDCl_3$): δ = 168.2 (C), 167.3 (C), 166.4 (C), 165.9 (C), 137.1 (C), 136.7 (C), 131.3 (CH), 130.3 (CH), 129.7 (CH), 129.4 (CH), 128.8 (CH), 128.6 (CH), 128.4 (CH), 127.4 (CH), 69.4 (CH), 51.1 (CH_2), 49.5 (CH_2), 44.0 (CH_2 ×2). LR-MS (ESI): m/z = 468 $[M+H]^+$; HR-MS (ESI): m/z = 468.2090 $[M+H]^+$ (calculated for $C_{25}H_{26}D_2N_3O_6$ = 468.2098).

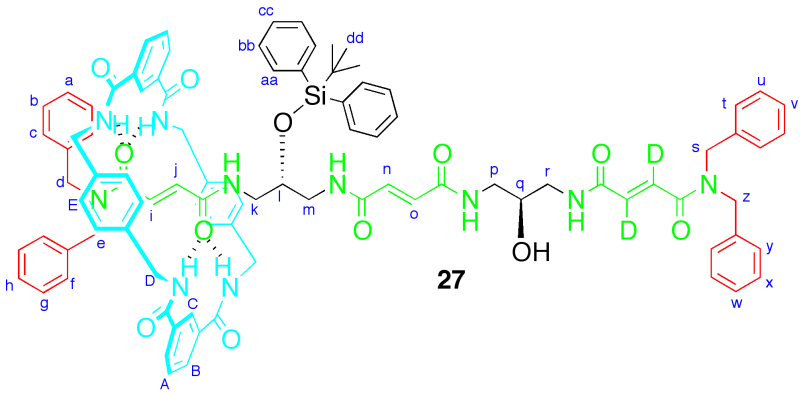

27

To a stirred solution of **28** (545 mg, 0.44 mmol) in anhydrous DCM (10 mL) in a loosely-sealed round-bottomed flask was added TFA (2.5 mL). After 16 h the mixture was diluted with aqueous NaOH (1 M) until basic and extracted into EtOAc (3 × 30 mL). The combined organic fractions were washed with HCl (1 M, 3 × 10 mL), saturated $NaHCO_3$ solution (3 × 10 mL) and brine (3 × 10 mL) then dried over $MgSO_4$ and concentrated under reduced pressure. The obtained residue (371 mg, 326 µmol) was redissolved in anhydrous DMF (2.71 mL) and cooled to 0 °C under N_2. Acid **29** (0.83 eq, 271 µmol, 127 mg), DIPEA (1 eq, 326 µmol, 55 µL), HOBt (1 eq, 326 µmol, 44 mg) and TBTU (1 eq, 326 µmol, 104 mg) were added sequentially. The reaction mixture was allowed to reach room temperature with stirring over 16 h then was diluted with saturated $NaHCO_3$ solution (10 mL) and extracted into 3:1 $CHCl_3$/IPA (3 × 30 mL). The combined organic fractions were washed with saturated $NaHCO_3$ (3 × 10 mL), HCl (1 M, 3 × 10 mL) and brine (3 × 10 mL) then dried over $MgSO_4$ and concentrated under reduced pressure. Flash chromatography (3:2 THF/hexane, then 1:9 MeOH/ DCM) gave **27** as a white solid (366 mg, 85%). M.p. 142–143 °C. $[\alpha]_D^{20}$ = +10.7 (c = 0.38, DCM). ^{1}H NMR (400 MHz, 3:1 $CD_3OD/CDCl_3$): δ = 8.33 (s, 2H, H_C), 8.08-8.02 (m, 4H, H_B), 7.58-7.48 (m, 6H, H_A + H_{bb}), 7.72-7.10 (m, 17H, H_h + H_g + H_t + H_u + H_v + H_x + H_w + H_{aa} + H_{cc}), 7.06 (t, 4H, *J* = 5.9, H_f + H_y), 6.97 (t, 1H, *J* = 7.3, H_a), 6.90 (t, 2H, *J* = 7.4, H_b), 6.81 (d, 1H, *J* = 15.1, H_n), 6.77-6.63 (m, 9H, H_E + H_o), 6.59 (d, 2H, *J* = 7.3, H_c), 5.83-5.69 (m, 2H, H_i + H_j), 4.56-4.47 (m, 4H, H_s + H_z), 4.39-3.92 (m, 12H, H_D + H_d + H_e), 3.88-3.74 (m, 2H, H_l + H_q), 3.39-3.16 (m, 7H, H_k + H_m + H_p + H_r), 2.89 (dd, 1H, *J* = 13.3, 9.4, H_k), 0.92 (s, 9H, H_{dd}); ^{13}C NMR (100 MHz, 3:1 $CD_3OD/CDCl_3$): δ = 166.4 (C), 166.3 (C), 165.9 (C), 165.7 (C), 165.1 (C),

165.0 (C), 164.8 (C), 136.5 (C), 136.4 (C), 135.9 (C), 135.5 (C), 135.1 (CH), 134.8 (C), 133.0 (C), 132.7 (C), 132.6 (CH), 131.6 (CH), 130.9 (CH ×2), 129.6 (CH), 129.5 (CH), 128.7 (CH ×2), 128.6 (CH), 128.3 (CH ×2), 128.2 (CH), 128.0 (CH ×2), 127.4 (CH), 127.2 (CH), 127.1 (CH), 127.0 (CH), 126.1 (CH), 126.0 (CH), 124.9 (CH), 123.7 (CH), 69.6 (CH), 68.1 (CH), 67.2 (CH_2), 51.0 (CH_2), 50.8 (CH_2), 49.8 (CH_2), 42.9 (CH_2), 42.8 (CH_2 ×2), 41.6 (CH_2), 25.9 (CH_3), 24.8 (CH_2), 18.3 (C). LR-MS (ESI): m/z = 1587 $[M+H]^+$; HR-MS (ESI): m/z = 794.3626 $[M+2H]^{2+}$ (calculated for $C_{94}H_{96}D_2N_{10}O_{12}Si$ = 794.3625).

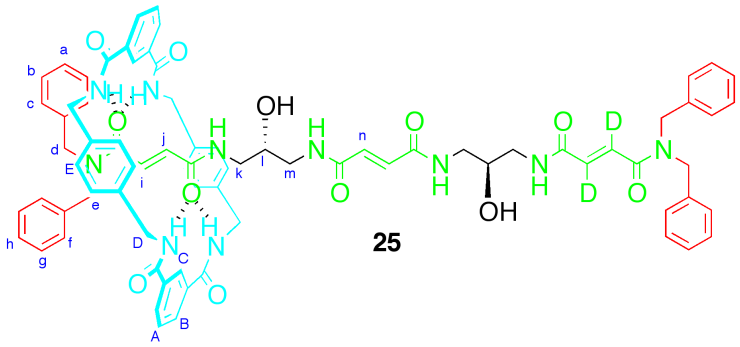

25

To a stirred solution of **27** (100 mg, 63 µmol) in DCM (0.59 mL) was added HF·py (40% vol, 0.38 mL of a 70% in pyridine solution) and the mixture was stirred for 16 h, then cooled to 0 °C and diluted with DCM (10 mL). TMSOMe (3.4 mL) was added followed by HCl (1 M, 10 mL), and the mixture was extracted into 3:1 $CHCl_3$/IPA (3 × 30 mL). The combined organic fractions were dried over $MgSO_4$ and concentrated under reduced pressure. Flash chromatography (5% MeOH in DCM, increased to 10% MeOH in DCM) gave diol **25** as a colourless solid (71 mg, 83%). On measuring the melting point the compound decomposed at 254 °C. ^{1}H NMR (400 MHz, 3:1 $CD_3OD/CDCl_3$): δ = 8.53-8.44 (m, 2H, H_C), 8.02 (dd, 4H, J = 7.8, 1.6, H_B), 7.51 (t, 2H, J = 7.8, H_A), 7.26-7.16 (m, 6H, H_b + H_h), 7.15-7.05 (m, 10H, H_a + H_c + H_g), 6.93 (s, 8H, H_E), 6.90-6.84 (m, 4H, H_f + H_n), 6.69 (br d, 1H, J = 15.0, H_i), 6.60 (s, 2H, H_n), 6.51 (d, 1H, J = 14.7, H_j), 4.42, (d, 8H, J = 14.6, H_d + H_e), 4.28 (dd, 8H, J = 4.5, 2.6, H_D), 3.79-3.69 (m, 2H, H_l), 3.36-3.06 (m, 8H, H_k + H_m); ^{13}C NMR (100 MHz, DMSO-d_6): δ = 165.9 (C), 165.8 (C), 165.6 (C), 164.8 (C), 137.7, 137.2 (×2), 134.5, 132.1,

131.3 (×2), 129.4, 129.2, 129.1 (×2), 128.9, 128.6, 127.8 (×2), 126.6, 125.0, 68.6 (C), 55.4 (CH_2), 50.8 (CH_2), 49.8 (CH_2), 31.2 (CH_2), 27.7 (CH_2). LR-MS (ESI): m/z = 1348 $[M+H]^+$; HR-MS (ESI): m/z = 675.3031 $[M+2H]^{2+}$ (calc. for $C_{78}H_{78}D_2N_{10}O_{12}$ = 675.3036).

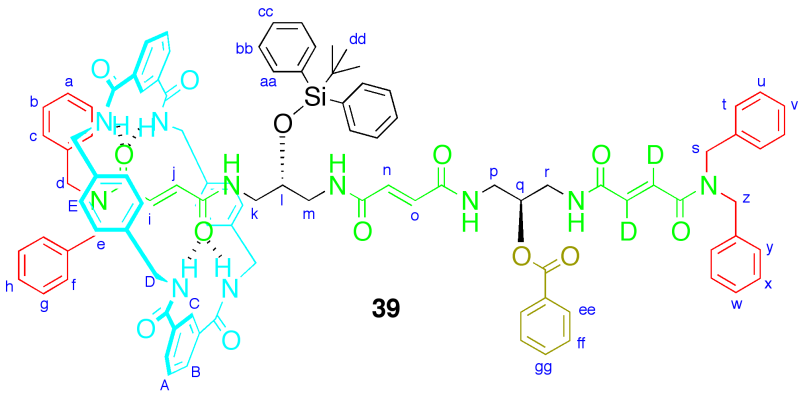

To a stirred solution of **27** (124 mg, 78 µmol), DMAP (2 eq, 156 µmol, 19 mg) and triethylamine (2 eq, 156 µmol, 15.8 mg) in DCM (0.9 mL) was added benzoyl chloride (2 eq, 156 µmol, 22 mg). After 5 h the mixture was concentrated under reduced pressure. Flash chromatography (5% MeOH in DCM) gave **39** as a colourless solid (115 mg, 87%). M.p. 126–128 °C. $[\alpha]_D^{20}$ = +8.0 (c = 0.25, DCM). ^{1}H NMR (500 MHz, 3:1 $CD_3OD/CDCl_3$): δ = 8.44 (s, 2H, H_C), 8.13 (m, 4H, H_B), 8.01 (dd, 2H, *J* = 8.4, 1.4, H_{ee}), 7.65 (m, 4H, H_{bb}), 7.60 (t, 2H, *J* = 7.8, H_A), 7.52 (t, 1H, *J* = 7.5, H_{gg}), 7.37-7.24 (m, 17H, H_h + H_g + H_t + H_u + H_v + H_w + H_x + H_{aa} + H_{cc}), 7.21 (m, 4H, H_f + H_y), 7.15 (d, 2H, *J* = 7.1, H_{ff}), 7.09 (t, 1H, *J* = 7.4, H_a), 7.01 (t, 2H, *J* = 7.5, H_b), 6.90 (d, 1H, *J* = 15.1, H_o), 6.83 (d, 4H, *J* = 8.1, H_E), 6.77-6.68 (m, 7H, H_E + H_c + H_n), 5.83 (s, 2H, H_i + H_j), 5.41 (m, 1H, H_q), 4.63 (s, 2H, H_s or H_z), 4.60 (s, 2H, H_s or H_z), 4.51-4.38 (m, 4H, H_D), 4.34-4.21 (m, 4H, H_d + H_e), 4.17-4.03 (m, 4H, H_D), 3.38 (m 1H, H_l), 3.77-3.61 (m, 4H, H_p + H_r), 3.46-3.38 (m, 2H, H_k + H_m), 3.37-3.31 (m, 1H, H_m), 2.87 (dd, 1H, *J* = 13.5, 9.3, H_k), 1.03 (s, 9H, H_{dd}); ^{13}C NMR (100 MHz, 3:1 $CD_3OD/CDCl_3$): δ = 168.4 (C), 168.3 (C), 167.8 (C), 167.6 (C), 167.0 (CH ×2C ×2), 166.7 (C), 166.6 (C), 138.3 (C), 137.9 (C), 137.7 (C), 137.3 (C), 137.0 (CH), 136.8 (C), 135.0 (C + CD), 134.4 (C), 134.6 (CH), 134.4

(C + CH), 133.5 (CH), 132.8 (CH), 132.7 (CH), 131.4 (CH ×2), 131.0 (CH), 130.6 (CH), 130.5 (CH), 130.2 (CH ×2), 130.1 (CH), 129.9 (CH) 129.5 (CH), 129.4 (CH), 129.3 (CH), 129.1 (CH), 129.0 (CH ×2), 128.9 (CH), 128.0 (CH), 127.9 (CH), 126.8 (CH), 125.6 (CH), 73.2 (CH), 71.4 (CH), 53.0 (CH_2), 52.8 (CH_2), 51.6 (CH_2), 44.7 (CH_2), 46.7 (CH_2), 43.1 (CH_2), 43.0 (CH_2), 41.9 (CH_2), 41.8 (CH_2), 27.7 (CH_3), 20.2 (C). LR-MS (ESI): m/z = 846 $[M+2H]^{2+}$; HR-MS (ESI): m/z = 1691.7406 $[M+H]^+$ (calculated for $C_{101}H_{99}D_2N_{10}O_{13}Si$ = 1691.7439).

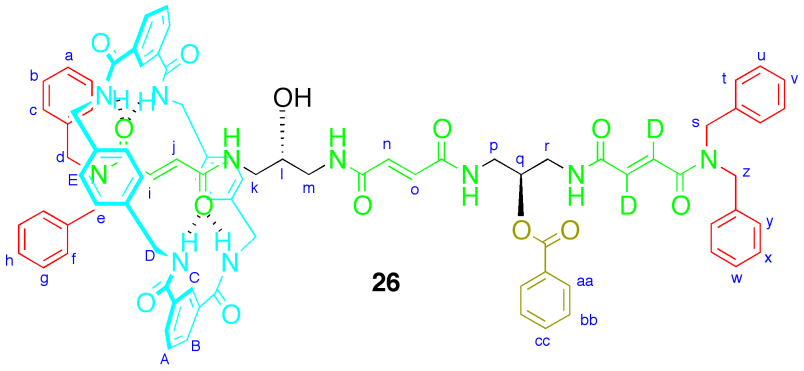

To a stirred solution of **39** (97 mg, 57 µmol) in DCM (0.59 mL) was added HF·py (40% vol, 1.0 mL of a 70% in pyridine solution) and the mixture was stirred for 16 h, then cooled to 0 °C and diluted with DCM (10 mL). TMSOMe (3.4 mL) was added followed by HCl (1 M, 10 mL), and the mixture was extracted into 3:1 $CHCl_{3\times}$/IPA (3 × 30 mL). The combined organic fractions were dried over $MgSO_4$ and concentrated under reduced pressure. Flash chromatography (2% MeOH in DCM, increased to 6% MeOH in DCM) gave mono-benzoylated rotaxane **26** as a colourless solid (83 mg, *quant*). M.p. 155–158 °C. $[\alpha]_D^{20}$ = –9.9 (c = 0.41, DCM). ^{1}H NMR (400 MHz, 3:1 $CD_3OD/CDCl_3$): δ = 8.67 (t, 1H, *J* = 5.92, NH), 8.54 (t, 1H, *J* = 5.7, NH), 8.51-8.38 (m, 4H, H_C + NH), 8.00 (d, 4H, *J* = 7.9, H_B), 7.94 (br s, 4H, NH), 7.89 (d, 2H, *J* = 7.2, H_{aa}), 7.52-7.40 (m, 3H, H_A + H_{cc}), 7.33-6.96 (m, 20H, H_a + H_b + H_f + H_g + H_h + H_t + H_u + H_v + H_w + H_x + H_y + H_{bb}), 6.96-6.84 (m, 8H, H_E), 6.73 (d, 2H, *J* = 6.4, H_c), 6.53-6.35 (m, 2H, H_n + H_o), 6.28-6.11 (m, 2H, H_i + H_j), 5.25-5.13 (m, 1H, H_q), 4.51 (s, 2H, H_s or H_z), 4.47 (s, 2H, H_s or H_z), 4.41-4.27 (m, 8H, H_d + H_e + H_D), 4.20 (dd, 4H, *J* = 14.1, 4.4, H_D), 3.80-3.66 (m, 1H, H_l), 3.63-3.35 (m, 4H, H_k + H_m), 3.30-3.04 (m, 4H, H_p + H_r); ^{13}C NMR (100 MHz, 3:1 CD_3OD/

$CDCl_3$): δ = 168.0 (C), 167.4 (C), 167.2 (C), 167.0 (C), 166.8 (C), 166.7 (C ×2), 166.6 (C), 138.1 (C), 138.0 (C), 137.3 (C), 137.0 (C), 136.3 (C), 134.6 (C), 134.5 (CH), 133.9 (CH), 132.8 (CH), 132.7 (CH), 132.1 (CH), 130.6 (C), 130.3 (CH), 129.9 (CH), 129.8 (CH), 129.7 (CH), 129.6 (CH), 129.5 (CH), 129.3 (CH ×2), 129.0 (CH), 128.7 (CH), 128.6 (CH), 128.5 (CH ×2), 128.2 (CH), 128.0 (CH), 127.4 (CH), 126.6 (CH), 125.2 (CH), 72.7 (CH), 69.4 (CH), 52.0 (CH_2), 51.3 (CH_2), 51.1 (CH_2), 47.4 (CH_2), 44.3 (CH_2 ×2), 44.1 (CH_2), 41.2 (CH_2), 30.3 (CH_2). LR-MS (ESI): m/z = 1475 $[M+Na]^+$; HR-MS (ESI): m/z = 1475.6122 $[M+Na]^+$ (calculated for $C_{85}H_{80}D_2N_{10}O_{13}Na$ = 1475.6081).

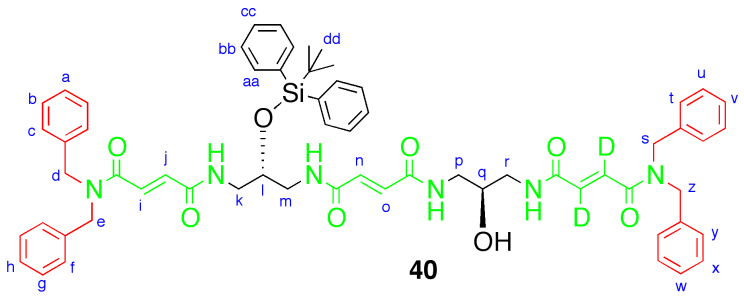

40

Procedure followed as for **27**. By using **30** (710 mg, 1.00 mmol) instead of **28**, **40** was obtained as a colourless foam (360 mg, 79% over two steps). $[\alpha]_D^{20}$ = 25.0 (c = 0.5, DCM). ^{1}H NMR (500 MHz, 3:1 $CD_3OD/CDCl_3$): δ = 7.70 – 7.64 (m, 4H, H_{bb}), 7.46-7.27 (m, 19H, H_a + H_b + H_g + H_h + H_i + H_u + H_v + H_w + H_x + H_{aa} + H_{cc}), 7.26-7.22 (m, 4H, H_f + H_t), 7.21-7.15 (m, 4H, H_c + H_y), 6.94 (d, 1H, *J* = 15.0, H_j), 6.83 (d, *J* = 15.2, H_n), 6.79 (d, *J* = 15.2 1H, H_o), 4.70-4.57 (m, 8H, H_d + H_e + H_s + H_z), 4.08-3.99 (m, 1H, H_l), 3.88-3.78 (m, 1H, H_q), 3.49-3.17 (m, 8H, H_k + H_m + H_p + H_r), 1.07 (s, 9H, H_{dd}); ^{13}C NMR (125 MHz, 3:1 $CD_3OD/CDCl_3$): δ = 167.5 (C), 167.4 (C), 166.7 (C), 166.6 (C), 166.5 (C), 166.4 (C), 137.4 (×2), 137.0, 136.7, 135.9, 135.7, 134.2 (×1), 133.5 (×2), 133.3, 131.4, 133.0, 130.8 (×3), 129.8, 129.5, 128.9, 128.7, 128.6 (×2), 128.5 (×2), 127.6, 69.8, 69.6, 51.3 (CH_2), 44.2 (CH_2 ×2), 43.8 (CH_2 ×2), 30.4 (CH_2 ×2), 27.9 (CH_2), 27.4 (CH_3), 19.9 (C). LR-MS (ESI): m/z = 1055 $[M+H]^+$; HR-MS (ESI): m/z = 1055.5057 $[M+H]^+$ (calculated for $C_{62}H_{67}D_2N_6O_8Si$ = 1055.5066).

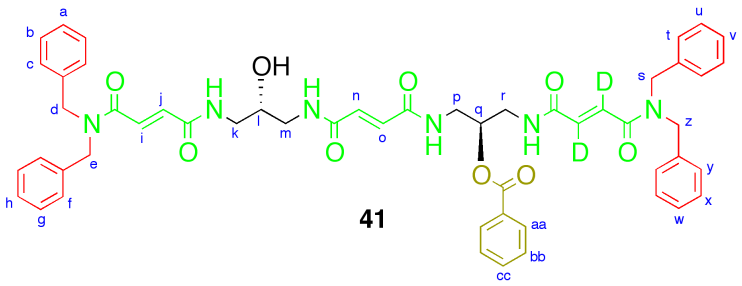

41

Procedure followed as for **26**. By using **40** (360 mg, 0.34 mmol) instead of **27**, **41** was obtained as a colourless solid (57 mg, 24% over two steps). M.p. 158–161 °C. $[\alpha]_D^{20}$ = –428.6 (c = 0.07, DCM). ^{1}H NMR (500 MHz, 3:1 $CD_3OD/CDCl_3$): δ = 8.02 (d, 2H, *J* = 7.2, H_{aa}), 7.57 (t, 1H, *J* = 7.5, H_{cc}), 7.48-7.39 (m, 3H, H_i + H_{bb}), 7.39-7.26 (m, 12H, H_a + H_b + H_g + H_h + H_u + H_v + H_w + H_x), 7.27 – 7.21 (m, 4H, H_f + H_t), 7.20 – 7.15 (m, 4H, H_c + H_y), 7.04 (d, 1H, *J* = 15.0, H_j), 6.89 (d, *J* = 15.4, 1H, H_n), 6.87 (d, *J* = 15.4, 1H, H_o), 5.37-5.26 (m, 1H, H_q), 4.69-4.55 (m, 8H, H_d + H_e + H_s + H_z), 3.87-3.78 (m, 1H, H_l), 3.72-3.56 (m, 4H, H_p + H_r), 3.43-3.26 (m, 4H, H_k + H_m); ^{13}C NMR (125 MHz, 3:1 $CD_3OD/CDCl_3$): δ = 167.6 (C), 167.5 (C), 167.3 (C), 166.9 (C), 166.8 (C), 166.7 (C), 166.6 (C), 137.4 (×2), 137.0 (×2), 136.0 (×2), 134.1, 133.9, 133.8, 133.5, 133.4, 131.0, 130.8, 130.6, 130.5, 129.8, 129.5, 129.2, 129.0, 128.7, 128.5, 127.6 (×2), 72.9 (CH), 69.7 (CH), 51.3 (CH_2 ×2), 44.3 (CH_2 ×2), 41.4 (CH_2 ×2), 32.8 (CH_2), 30.5 (CH_2). LR-MS (ESI): m/z = 921 $[M+H]^+$; HR-MS (ESI): m/z = 921.4145 $[M+H]^+$ (calculated for $C_{53}H_{53}D_2N_6O_9$ = 921.4151).

2.9.1 General Method for Operation of Molecular Information Ratchet 25

To a stirred suspension of diol **25** (5 mg, 3.71 µmol) in DCM (0.37 mL) was added catalyst ((*S*)-**42** or (*R*)-**42** or DMAP or 50:50 (*S*)/(*R*)-**42** mixture, 4 eq, 14.8 µmol), triethylamine (4 eq, 14.8 µmol, 1.5 mg) and benzoyl chloride (4 eq, 14.8 µmol, 2.1 mg). After 2 h the reaction mixture was concentrated under

reduced pressure and triturated with Et_2O (1 × 2 mL). Residual Et_2O was removed under reduced pressure and the entire crude mixture was dissolved in DMSO-d_6 for NMR analysis.

2.9.2 General Method for Operation of Molecular Information Ratchet 26

To a stirred suspension of mono-benzoylated rotaxane **26** (5 mg, 3.44 μmol) in DCM (0.344 mL) was added catalyst ((*S*)-**42** or (*R*)-**42** or DMAP or 50:50 (*S*)/(*R*)-**42** mixture, 2 eq, 6.88 μmol), triethylamine (2 eq, 6.88 μmol, 0.70 mg) and benzoyl chloride (2 eq, 6.88 μmol, 0.97 mg). After 2 h the reaction mixture was concentrated under reduced pressure and triturated with Et_2O (1 × 2 mL). Residual Et_2O was removed under reduced pressure and the entire crude mixture was dissolved in DMSO-d_6 for NMR analysis.

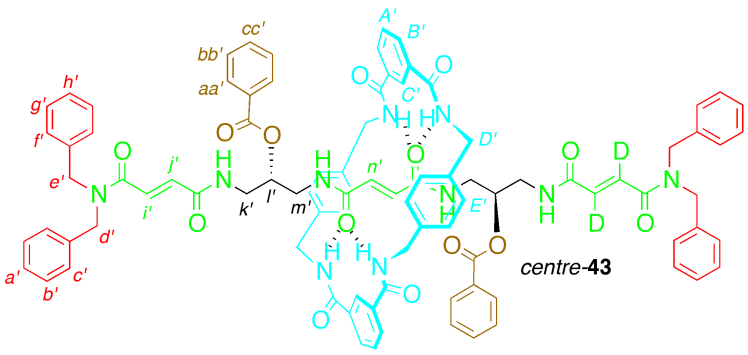

A pure sample of *centre*-**43** was obtained by successive triturations with 3:1 MeOH/$CHCl_3$ of the crude mixture of products from benzoylation of **26** in the presence of (*S*)-**42**. On measuring the melting point the compound decomposed at 257 °C. ^{1}H NMR (500 MHz, DMSO-d_6): δ = 8.51 (s, 2H, $H_{C'}$), 8.02 (d, 4H, J = 7.8, $H_{B'}$), 7.93 (d, 4H, J = 7.9, $H_{aa'}$), 7.63 (t, 2H, J = 7.9, $H_{A`}$ or $H_{cc`}$), 7.61 (t, 2H, J = 7.8, $H_{A`}$ or $H_{cc`}$), 7.44 (t, 4H, J = 7.6, $H_{bb`}$), 7.37-7.30 (m, 8H, $H_{b'}$ + $H_{g'}$), 7.26 (m, 8H, $H_{a'}$ + $H_{c'}$ + $H_{h'}$), 7.18 (d, 1H, J = 14.9, $H_{i'}$), 7.14 (d, 4H, J = 7.5, H_{f}), 6.94 (d, 4H, J = 8.0,

$H_{E'}$), 6.92-6.85 (m, 5H, $H_{E'}$ + $H_{j'}$), 5.73 (s, 2H, $H_{n'}$), 5.14-5.06 (m, 2H, $H_{l'}$), 4.61 (s, 4H, $H_{e'}$ or $H_{d'}$), 4.56 (s, 4H, $H_{e'}$ or $H_{d'}$), 4.27 (s, 4H, $H_{D'}$), 4.20 (s, 4H, $H_{D'}$), 3.56-3.23 (m, 8H, $H_{k'}$ + $H_{m'}$); ^{13}C NMR (125 MHz, DMSO-d_6): δ = 167.3 (C), 167.2 (C), 166.1 (C), 165.5 (C), 162.2 (C), 137.1 (C), 136.2 (C), 135.6 (C), 135.0, 134.0 (C), 133.9 (C), 133.5, 131.1, 131.0, 130.7, 130.0, 129.6, 129.2, 129.0, 128.7, 128.4, 128.1, 128.0, 127.7, 126.6, 124.8, 71.5 (CH), 50.2 (CH_2), 43.8 (CH_2 ×2), 40.3 (CH_2), 40.1 (CH_2). LR-MS (ESI): m/z = 1558 $[M+H]^+$; HR-MS (ESI): m/z = 1558.6508 $[M+H]^+$ (calculated for $C_{92}H_{85}D_2N_{10}O_{14}$ = 1558.6555).

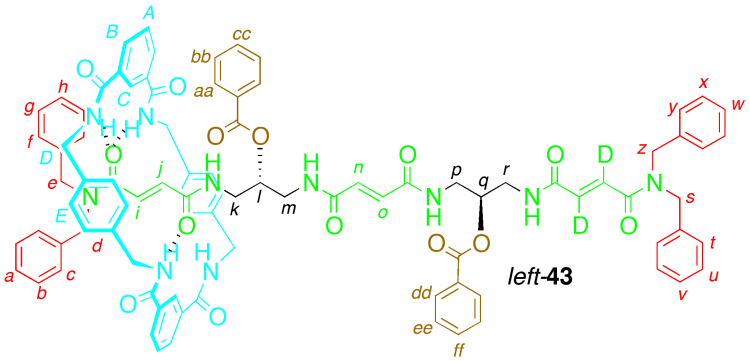

A pure sample of *left*-**43** was obtained by preparative TLC (EtOAc, × 4) of the crude mixture of products from benzoylation of **26** in the presence of (*R*)-**42**. M.p. 163–164 °C. $[\alpha]_D^{20}$ = +155.6 (c = 0.18, MeOH). ^{1}H NMR (500 MHz, DMSO-d_6): δ = 8.40 (s, 2H, H_C), 8.03 (dd, 4H, *J* = 7.7, H_B), 7.97-7.89 (m, 4H, H_{aa} + H_{dd}), 7.73-7.65 (m, 2H, H_{cc} + H_{ff}), 7.63-7.57 (m, 2H, H_A), 7.53-7.41 (m, 4H, H_{bb} + H_{ee}), 7.38-7.30 (m, 4H, Hu + Hx), 7.30-7.21 (m, 7H H_c + H_h + H_v + H_w + H_y), 7.17-7.10 (m, 4H, H_g + H_t), 7.04-6.93 (m, 3H, H_a + H_b), 6.91-6.81 (m, 8H, H_E), 6.80 (s, 2H, H_n + H_o), 6.70 (d, 2H, *J* = 7.0, H_f), 5.93 (d, 1H, *J* = 14.8, H_i), 5.89 (d, 1H, *J* = 14.8, H_j), 5.19-5.05 (m, 2H, H_l + H_q), 4.63 (s, 2H, H_s or H_z), 4.58 (s, 2H, H_s or H_z), 4.47-4.21 (m, 8H, H_D + H_d + H_e), 4.19-4.01 (4H, H_D), 3.65-3.18 (m, 8H, H_k + H_m + H_p + H_r); ^{13}C NMR (125 MHz, DMSO-d_6): δ = 166.9 (C), 165.6 (C), 165.3 (C), 165.2 (C, ×4), 165.0 (C ×2), 137.2, 137.1, 136.8 (×2), 136.7 (×2), 135.7, 135.4, 133.8 (×2), 131.7, 130.8, 129.7, 129.4 (×2), 129.2, 129.0, 128.8, 128.7, 128.6, 128.5 (×2),

128.4 (×2), 128.2 (×2), 127.7, 127.5, 127.4, 127.1, 126.4, 125.5, 125.1, 124.0, 67.3 (CH ×2), 43.0 (CH_2), 31.3 (CH_2), 29.8 (CH_2), 29.0 (CH_2 ×2), 28.7 (CH_2), 28.4 (CH_2), 23.2 (CH_2), 22.4 (CH_2). LR-MS (ESI): m/z 779 $[M+2H]^{2+}$; HR-MS (ESI): m/z = 1558.6505 $[M+H]^+$ (calculated for $C_{92}H_{85}D_2N_{10}O_{14}$ = 1558.6555).

2.10 References and Notes

1. Schliwa, M.; Woehlke, G. Molecular motors. *Nature* **2003**, *422*, 759–765.

2. Kelly, T. R.; De Silva, H.; Silva, R. A. Unidirectional rotary motion in a molecular system. *Nature* **1999**, *401*, 150–152.

3. Thordarson, P.; Bijsterveld, E. J. A.; Rowan, A. E.; Nolte, R. J. M. Epoxidation of polybutadiene by a topologically linked catalyst. *Nature* **2003**, *424*, 915–918.

4. Balzani, V.; Clemente-Leon, M.; Credi, A.; Ferrer, B.; Venturi, M.; Flood, A. H.; Stoddart, J. F. Autonomous artificial nanomotor powered by sunlight. *Proc. Natl. Acad. Sci. U.S.A.* **2006**, *103*, 1178–1183.

5. Muraoka, T.; Kinbara, K.; Aida, T. Mechanical twisting of a guest by a photoresponsive host. *Nature* **2006**, *440*, 512–515.

6. Pijper, D.; Feringa, B. L. Molecular transmission: Controlling the twist sense of a helical polymer with a single light-driven molecular motor. *Angew. Chem. Int. Ed.* **2007**, *46*, 3693–3696.

7. Panman, M. R.; Bodis, P.; Shaw, D. J.; Bakker, B. H.; Newton, A. C.; Kay, E. R.; Brouwer, A. M.; Buma, W. J.; Leigh, D. A.; Woutersen, S. Operation mechanism of a molecular machine revealed using time-resolved vibrational spectroscopy. *Science* **2010**, *328*, 1255–1258.

8. Kay, E. R.; Leigh, D. A.; Zerbetto, F. Synthetic molecular motors and mechanical machines. *Angew. Chem. Int. Ed.* **2007**, *46*, 72–191.

9. Koumura, N.; Zijlstra, R. W. J.; van Delden, R. A.; Harada, N.; Feringa, B. L. Light-driven monodirectional molecular rotor. *Nature* **1999**, *401*, 152–155.

10. Leigh, D. A.; Wong, J. K. Y.; Dehez, F.; Zerbetto, F. Unidirectional rotation in a mechanically interlocked molecular rotor. *Nature* **2003**, *424*, 174–179.

11. Hernández, J. V.; Kay, E. R.; Leigh, D. A. A reversible synthetic rotary molecular motor. *Science* **2004**, *306*, 1532–1537.

12. van Delden, R. A.; ter Wiel, M. K. J.; Pollard, M. M.; Vicario, J.; Koumura, N.; Feringa, B. L. Unidirectional Molecular Motor on a Gold Surface. *Nature* **2005**, *437*, 1337–1340.

13. Fletcher, S. P.; Dumur, F.; Pollard, M. M.; Feringa, B. L. A reversible, unidirectional molecular rotary motor driven by chemical energy. *Science* **2005**, *310*, 80–82.

14. Eelkema, R.; Pollard, M. M.; Vicario, J.; Katsonis, N.; Ramon, B. S.; Bastiaansen, C. W. M.; Broer, D. J.; Feringa, B. L. Nanomotor rotates microscale objects. *Nature* **2006**, *440*, 163.

15. Serreli, V.; Lee, C.-F.; Kay, E. R.; Leigh, D. A. A molecular information ratchet. *Nature* **2007**, *445*, 523–527.

16. Alvarez-Pérez, M.; Goldup, S. M.; Leigh, D. A.; Slawin, A. M. Z. A chemically-driven molecular information ratchet. *J. Am. Chem. Soc.* **2008**, *130*, 1836–1838.

17. Klok, M.; Boyle, N.; Pryce, M. T.; Meetsma, A.; Browne, W. R.; Feringa, B. L. MHz unidirectional rotation of molecular rotary motors. *J. Am. Chem. Soc.* **2008**, *130*, 10484–10485.

18. von Delius, M.; Geertsema, E. M.; Leigh, D. A. A synthetic small molecule that can walk down a track. *Nat. Chem.* **2010**, *2*, 96–101.

19. Barrell, M. J.; Campaña, A. G.; von Delius, M.; Geertsema, E. M.; Leigh, D. A. Light-driven transport of a molecular walker in either direction along a molecular track. *Angew. Chem. Int. Ed.* **2011**, *50*, 285–290.

20. von Delius, M.; Geertsema, E. M.; Leigh, D. A.; Tang, D.-T. D. Design, synthesis, and operation of small molecules that walk along tracks. *J. Am. Chem. Soc.* **2010**, *132*, 16134–16145.

21. Haberhauer, G. A Molecular four-stroke motor. *Angew. Chem. Int. Ed.* **2011**, *50*, 6415–6418.

22. Bennett, C. H. The thermodynamics of computation – a review. *Int. J. Theor. Phys.* **1982**, *21*, 905–940.

23. Brouwer, A. M.; Frochot, C.; Gatti, F. G.; Leigh, D. A.; Mottier, L.; Paolucci, F.; Roffia, S.; Wurpel, G. W. H. Photoinduction of fast, reversible translational motion in a hydrogen-bonded molecular shuttle. *Science* **2001**, *291*, 2124–2128.

24. Lee, K.-M.; Ramalingam, K.; Son, J.-K.; Woodard, R. W. A highly efficient and large-scale synthesis of (2*S*,3*S*)-[2,3-$^{2}H_{2}$]- and (2*S*,3*R*)-[3-^{2}H]aspartic acids via an immobilised aspartase-containing microbial cell system. *J. Org. Chem.* **1989**, *54*, 3195–3198.

25. Niwayama, S. Highly efficient selective monohydrolysis of symmetric diesters. *J. Org. Chem.* **2000**, *65*, 5834–5836.

26. Kaburagi, Y.; Kishi, Y. Operationally simple and efficient workup procedure for TBAF-mediated desilylation: application to halichondrin synthesis. *Org. Lett.* **2007**, *9*, 723–726.

27. Stanley, C. E.; Clarke, N.; Anderson, K. M.; Elder, J. A.; Lenthall, J. T.; Steed, J. W. Anion binding inhibition of the formation of a helical organogel. *Chem. Commun.* **2006**, 3199–3201.

28. Lloyd, G. O.; Steed, J. W. Anion-tuning of supramolecular gel properties. *Nat. Chem.* **2009**, *1*, 437–442.

29. Dalaigh, C. O.; Hynes, S. J.; O'Brien, J. E.; McCabe, T.; Maher, D. J.; Watson, G. W.; Connon, S. J. Asymmetric acyl-transfer promoted by readily assembled chiral 4-*N*,*N*-dialkylaminopyridine derivatives. *Organic & Biomolecular Chemistry* **2006**, *4*, 2785–2793.

30. Peschiulli, A.; Quigley, C.; Tallon, S.; Gun'ko, Y. K.; Connon, S. J. Organocatalytic asymmetric addition of alcohols and thiols to activated electrophiles: efficient dynamic kinetic resolution and desymmetrization Protocols. *J. Org. Chem.* **2008**, *73*, 6409–6412.

31. Gillespie, D. T. *Markov processes: an introduction for physical scientists*; Academic Press, Inc.: San Diego, 1992, p xi.

32. Neglecting deuterium, which has been demonstrated not to noticeably affect the ratio of products observed on operation of this type of information ratchet (see *Ref*. 16).

Chapter Three

Synthesis, Operation and Analysis of an Extended Three-Compartment Molecular Information Ratchet

Acknowledgements

Dr Craig Robertson is gratefully acknowledged for his examination and proofreading of this Chapter.

Synopsis

The successful operation of a three-compartment molecular information ratchet was an important milestone in the evolution of this project; it showed that multiple sites of directional discrimination could be combined to effect long-distance transport of a macrocycle along a linear track.

From our experience with these compounds, it appeared that the limit on how far this technology might be extended is determined by the molecules' solubility. As a step towards the ultimate goal of directional transport of a macrocyclic Brownian particle over many tens of nanometres, it was first necessary to redesign the system so as to increase its solubility in organic solvents.

This Chapter details the synthesis and operation of a molecule intended to act as an effective model for longer systems. The techniques of analysis developed earlier in the project proved invaluable once again, and comparison of this Chapter's system with the one previously described afforded a much deeper insight into the behaviour of these fascinating molecular machines.

3.1 Introduction

In a molecular machine in which a submolecular component is to be moved along a predefined track, it is possible to imagine some metrics by which the efficacy and utility of a given molecular machine might be informally quantified:

1. *Efficiency of delivery.* The percentage of particles to be transported that successfully reach their destination.

2. *Physical distance covered.* The straight-line distance separating the particles' starting position and their destination.

3. *Difficulty of the terrain.* The energy barriers that must be overcome in order to transport the particle.

4. *Degree of external control.* How much control the chemist has over the final position of the particle, in terms of the number of possible end-states available and the ease of chemist in inducing each one selectively.

The chemically-driven two-compartment information ratchet published by Leigh and coworkers in 2008 achieves an efficiency of delivery of 66% over a distance of approximately 0.82 nm (the measured straight-line distance between fumaramide groups in the molecule's crystal structure).[1] When operating the machine the chemist, through catalyst selection, has the ability to direct the macrocycle into one of two possible destinations: either the left compartment or the right (deuterated) one.

The system described in the previous Chapter extends and enhances this technology by changing the catalyst and incorporating an extra chiral centre at

which directional discrimination can take place. Efficiency of delivery has been increased to greater than 80%; the distance over which the macrocycle is transported has also increased by the length of one fumaramide binding site. The operator of the three-compartment machine is no longer limited to sending the macrocycle only to the left or right of the molecule: while (*R*)- and (*S*)-**42** direct the macrocycle to the left and right respectively as before, use of DMAP also sends the macrocycle mostly into the two terminal stations, while a racemic mixture of **42** gives access to the central compartment. Additionally, acknowledging that the central compartment represents a different chemical environment for the macrocycle from the terminal compartments, it has been shown that the macrocycle can be transported both *into* and *out of* whatever potential energy minima are presented by the topology of the thread; in terms of the metrics established above, the difficulties of the terrain have been overcome.

Despite these advances, there is much room for improvement. The distances over which directional transport occurs can still be increased, though not without a change in design to address the problems of solubility. Experimentation with new designs will not only produce more efficient machines as measured by the above metrics; they will also allow us, by way of comparison, to discover the general rules that these machines follow, and will shed light on what other changes might be made to increase the efficiency of these molecular information ratchets.

3.2 Design

The previous Chapter demonstrated how the system published by Leigh and coworkers in 2008 could be made one station longer by the incorporation of one extra fumaramide binding site and chiral unit. The most obvious next step to increase the length of the system even further might be simply to introduce yet another of these repeat units; however, our experience with the synthesis of the previous Chapter's system and its intermediates suggested that this approach would not be feasible, for reasons of solubility. While rotaxane **3** was readily soluble in dichloromethane, **25** was only sparingly soluble in its diol form. Many of the precursors for the synthesis of rotaxane **25** were also highly insoluble in common organic solvents. Without finding some means of offsetting the solubility penalty of incorporating extra fumaramide residues, extended systems like **45** are likely to be synthetically unreachable.

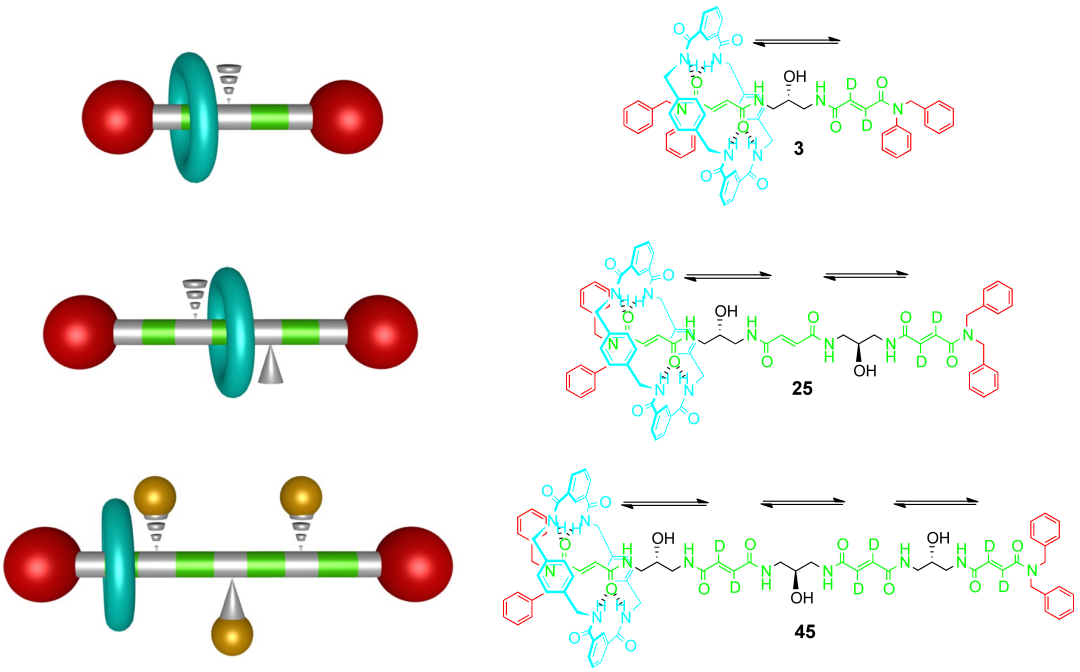

Figure 3.1 From top: Leigh and coworkers' two-compartment chemical information ratchet **3**;[1] the previous Chapter's three-compartment information ratchet **25**; and a four-compartment extension of the structure, likely to be extremely difficult to synthesise for reasons of solubility.

In order to ensure that an increase in length does not entail a decrease in solubility below the level at which synthesis is feasible, a solubilising group must be incorporated into the structure; for example, long alkyl chains might be added to the stoppers. While there is a good chance that such a modification would improve the molecule's solubility, it would in a sense be only a temporary solution, because further extension of the system would eventually overcome the solubilising effects of whatever group was chosen. The desired property is nicely captured by the term *extensibility* borrowed from computer programming.[2] An extensible design is one that makes allowances for future growth; an increase in size in an extensible system entails neither an increase in the system's complexity nor a major change of architecture.

If the ultimate intention is to construct rotaxanes capable of transporting macrocycles over very long distances, with multiple chiral centres at which directional control may be exerted, then the principle of extensibility must be built into any model systems. For this reason a decane spacer was incorporated into the repeat unit itself. The expectation was that this approach would help to offset the solubility penalty for each new fumaramide group introduced.

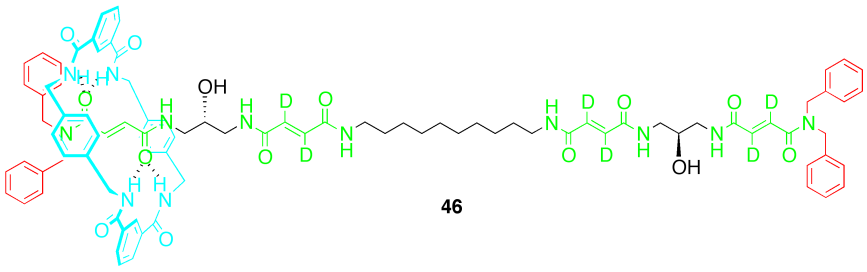

Figure 3.2 Diol **46**: an extended three-compartment information ratchet.

Operation of **46** would result in three doubly-protected positional isomers analogous to those generated by the previous system. One important difference

is that the central compartment contains two fumaramide binding sites, not one. Two important consequences are:

1. In the positional isomer with the macrocycle locked into the central compartment, the macrocycle will not be confined to binding with a single fumaramide group, but instead will be free to shuttle between two degenerate binding sites.

2. Because it has two binding sites rather than the usual one, the central compartment treated as a unit may represent a greater thermodynamic sink than the central compartment of the previous system. This change in the shape of the potential energy surface is likely to have a noticeable impact on the ratios generated on operation.

Rather than being disadvantages, these differences from the previous Chapter's system will allow us, by comparison, to gain a more complete understanding of the internal mechanism of action for this type of molecular machine.

3.3 Retrosynthesis

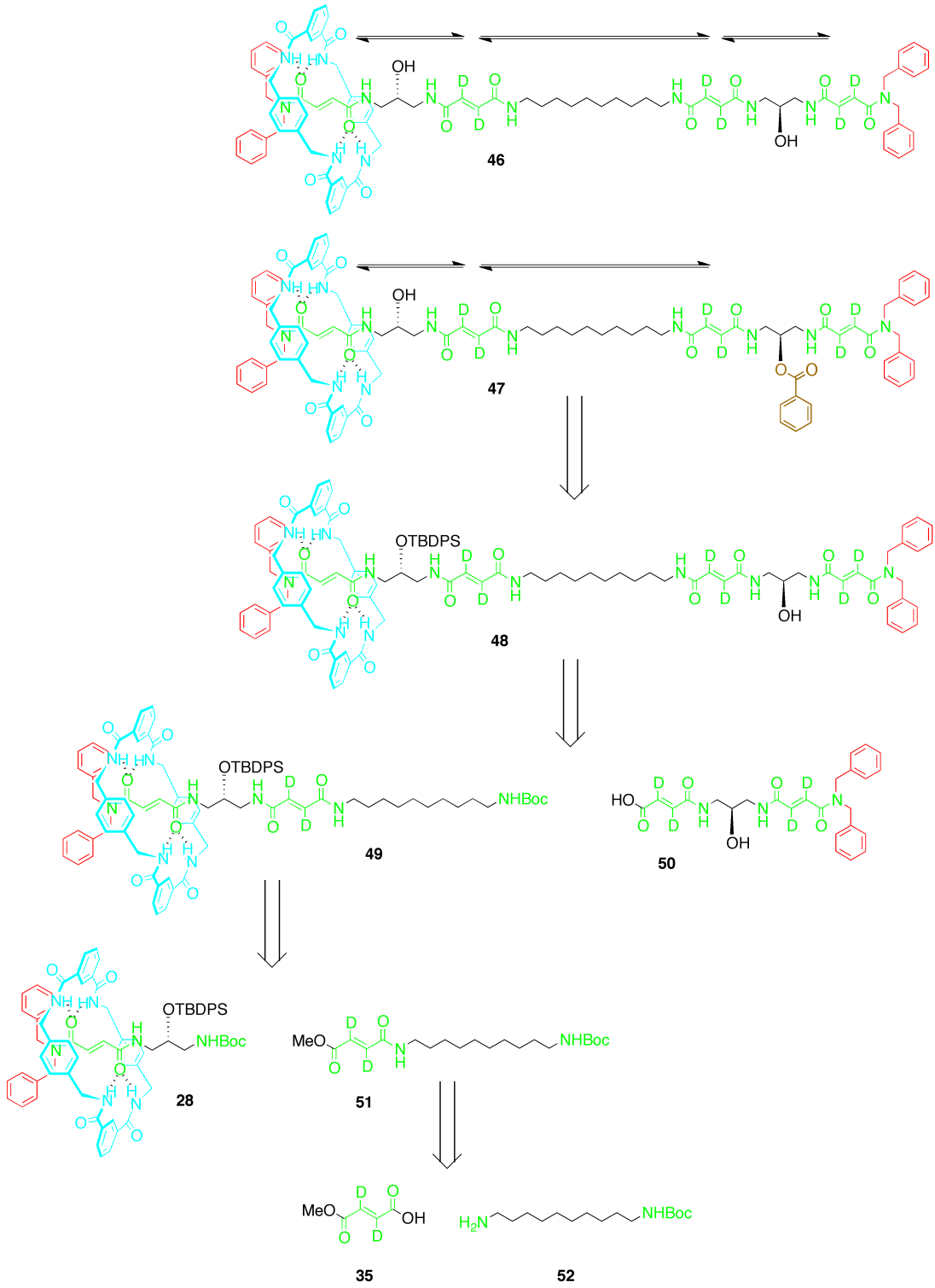

Scheme 3.1 Retrosynthetic analysis of **46**.

The synthetic efforts of the previous Chapter afforded both a supply of readily available building blocks and an appreciation of the best way that they might be employed. A retrosynthetic analysis of **46** is presented in Scheme 3.1.

As in the previous Chapter, both the diol **46** and its mono-benzoylated form **47** were both desirable targets, as only by operating the two in conjunction would the internal mechanisms of action be elucidated. Both forms were to be obtained from rotaxane **48** – either a desilylation to give **46**, or a benzoylation of the free hydroxyl group followed by desilylation to give mono-benzoylated **47**. Rotaxane **47** would be constructed from acid **50**, which differs from the previous Chapter's acid **29** only in the pattern of deuteration, and so was readily accessible. The amide groups, as well as being important hydrogen bonding motifs for macrocycle binding, also suggested that the molecule could be most easily be prepared as a series of peptidic couplings promoted by TBTU and HOBt. Amines would be protected with Boc, which experience has demonstrated can be cleaved with TFA without affecting the silyl groups. The carboxylic acids would be obtained from saponification of the corresponding methyl or ethyl esters.

Rotaxane **49** was to be prepared by coupling previously synthesised rotaxane intermediate **28** to spacer unit **51**, which was itself to be formed from a peptidic coupling between acid **35** and amine **52**, both of which are found in the chemical literature: Ghanem and coworkers describe a protocol for the desymmetrisation of 1,10-diaminodecane;[3] Niwayama describes a the technique already used in the preceding Chapter for the synthesis of **35**.[4]

3.4 Synthesis

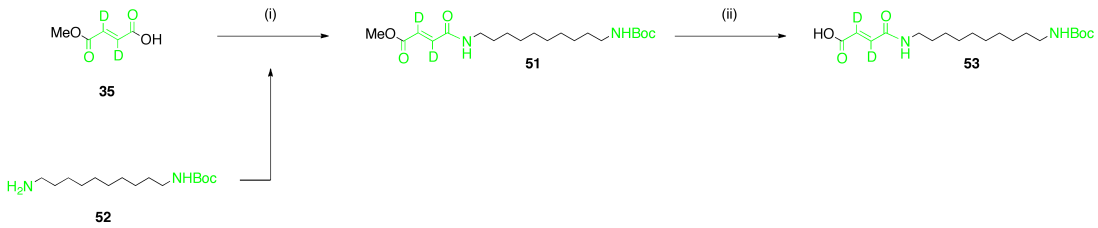

Scheme 3.2 (i) Amine 52, TBTU, HOBt, DIPEA, DMF, 0 °C to rt, 16 h, 90%; (ii) LiOH·H_2O, 3:1 THF/H_2O, rt, 1 h, *quant*.

Both acid **35** and amine **52** were prepared by desymmetrisation reactions described in the literature,[3,4] and were used without further purification. As a consequence, **51** was formed in the presence of a number of impurities resulting from traces of doubly-deprotected starting materials, the most significant of which, **51a**, came from double addition of **35** to unreacted diamine; this impurity was rather apolar and could be removed easily by column chromatography, as shown in Scheme 3.3.

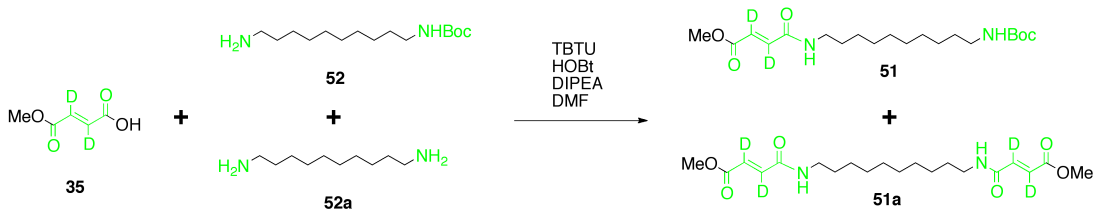

Scheme 3.3 The presence of unreacted diamine **52a** results in a doubly-coupled impurity **51a** that is easily removed by column chromatography.

Amide **51** was obtained as a white solid in a yield of 90% relative to **35**. Saponification of **51** was performed quantitatively using two equivalents of lithium hydroxide in a 3:1 THF/water mixture over one hour.

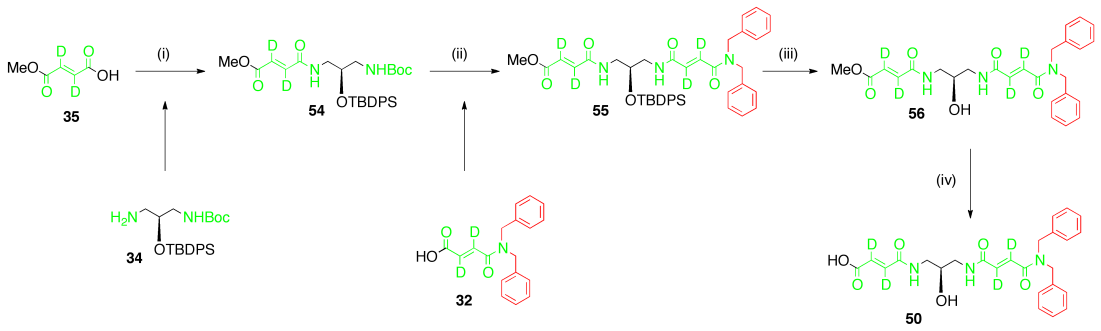

Scheme 3.4 (i) Amine **34**, TBTU, HOBt, DIPEA, DMF, 0 °C to rt, 78%; (ii) (a) TFA, DCM, 16 h, rt, *quant.*; (b) Acid **32**, TBTU, HOBt, DIPEA, DMF, 16 h, 0 °C to rt, 85%; (iii) TBAF, THF, rt, 16 h, *quant.*; (iv) LiOH·H_2O, 3:1, THF/H_2O, rt, 20 min, *quant.*

Acid **35**, again without prior purification, was coupled to a slight molar excess of chiral amine **34** to afford **54** as a white solid in 85% yield. The Boc group was cleaved by stirring overnight in a loosely-sealed vessel with a 4:1 DCM/TFA mixture. After a basic work-up the crude reaction mixture was coupled directly to **32**, a stopper molecule prepared for the previous Chapter, to give **55** in 85% yield. The silyl protecting group was cleaved by stirring overnight with TBAF in THF. A silica plug was sufficient to remove the resulting TBDPS-fluoride byproduct, and **56** was obtained in quantitative yield.

Amide **56** was saponified under standard conditions, with extra care taken to quench the reaction immediately to prevent the decomposition seen with saponification of **38**. The resulting highly insoluble acid **50** was used without further purification.

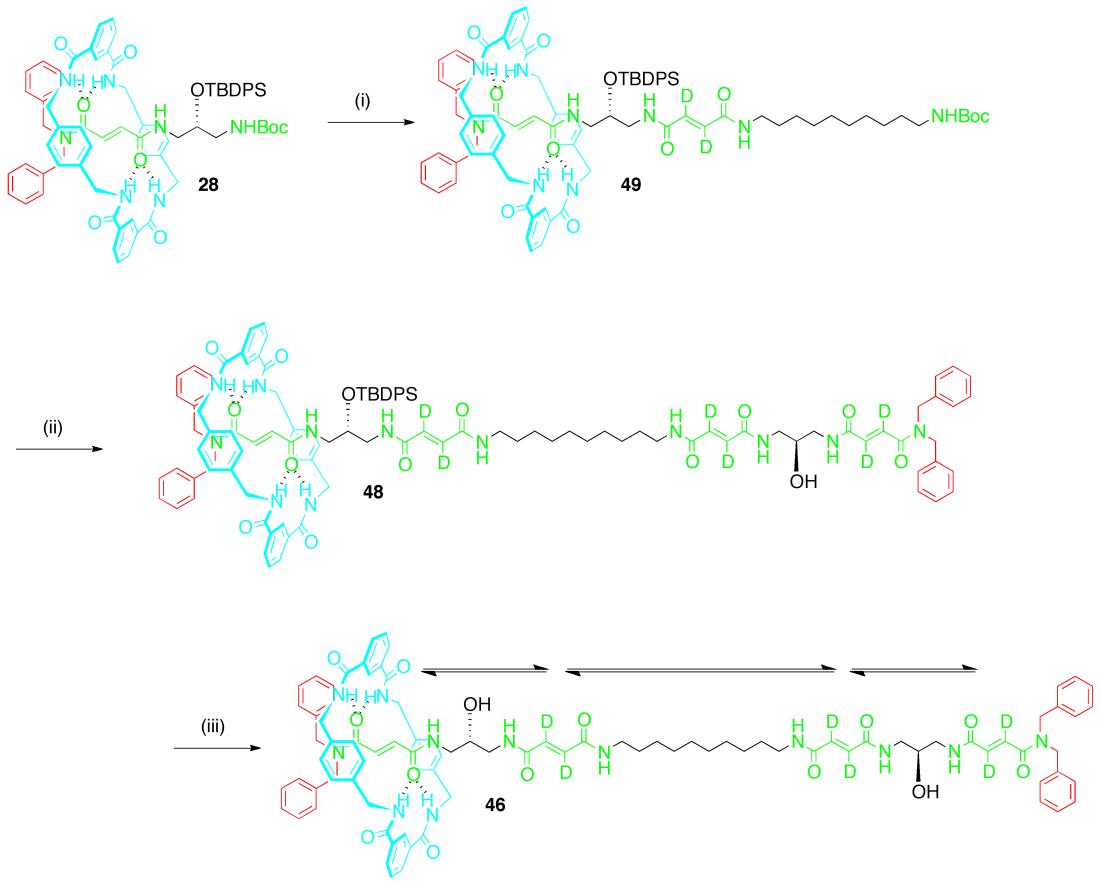

Scheme 3.5 (i) (a) TFA, DCM, rt, 16 h; (b) Acid **53**, TBTU, HOBt, DIPEA, DMF, 0 °C to rt, 56%; (ii) (a) TFA, DCM, rt, 16 h; (b) Acid **50**, TBTU, HOBt, DIPEA, DMF, 0 °C to rt, 90%; (iii) HF·py, DCM, rt, 16 h, 84%.

Rotaxane **28**, a building-block from the previous Chapter, was treated with a 4:1 DCM/TFA mixture to cleave the Boc group, and the resulting primary amine was coupled to spacer unit **53** in the presence of TBTU and HOBt to give **49** in 56% yield on purification. Cleavage of **49**'s Boc group, followed by a peptidic coupling reaction with **50**, gave rotaxane **48** in 90% yield. Treatment of **48** with a solution of HF in pyridine successfully cleaved the TBDPS protecting group, and a short column afforded the desired target molecule **46** in 84% yield.

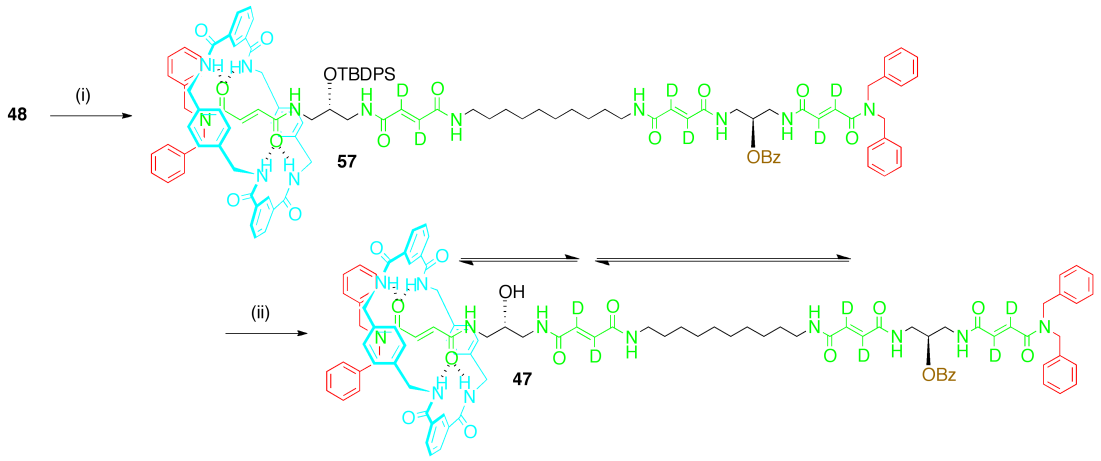

Scheme 3.6 (i) Rotaxane **48**, BzCl, DMAP, DCM, 1 h, rt, 30%; (ii) HF·py, DCM, rt, 16 h, 66%.

Integration of resonance peaks for the benzoyl group by ^{1}H NMR spectroscopy suggests that the benzoylation of **48** proceeded quantitatively; indeed, acylation reactions catalysed by DMAP or DMAP analogues are the core of this project and generally do not present problems. Nevertheless, the purification of **57** by column chromatography always incurred heavy losses. Whether this loss was the result of low solubility or decomposition on silica was uncertain, but yields above 30% were not obtained. The final step, removal of the TBDPS group with hydrogen fluoride in pyridine, proceeded much more effectively and afforded mono-benzoylated rotaxane **47** as a white solid in 66% yield.

3.5 Operation of Diol Information Ratchet 46

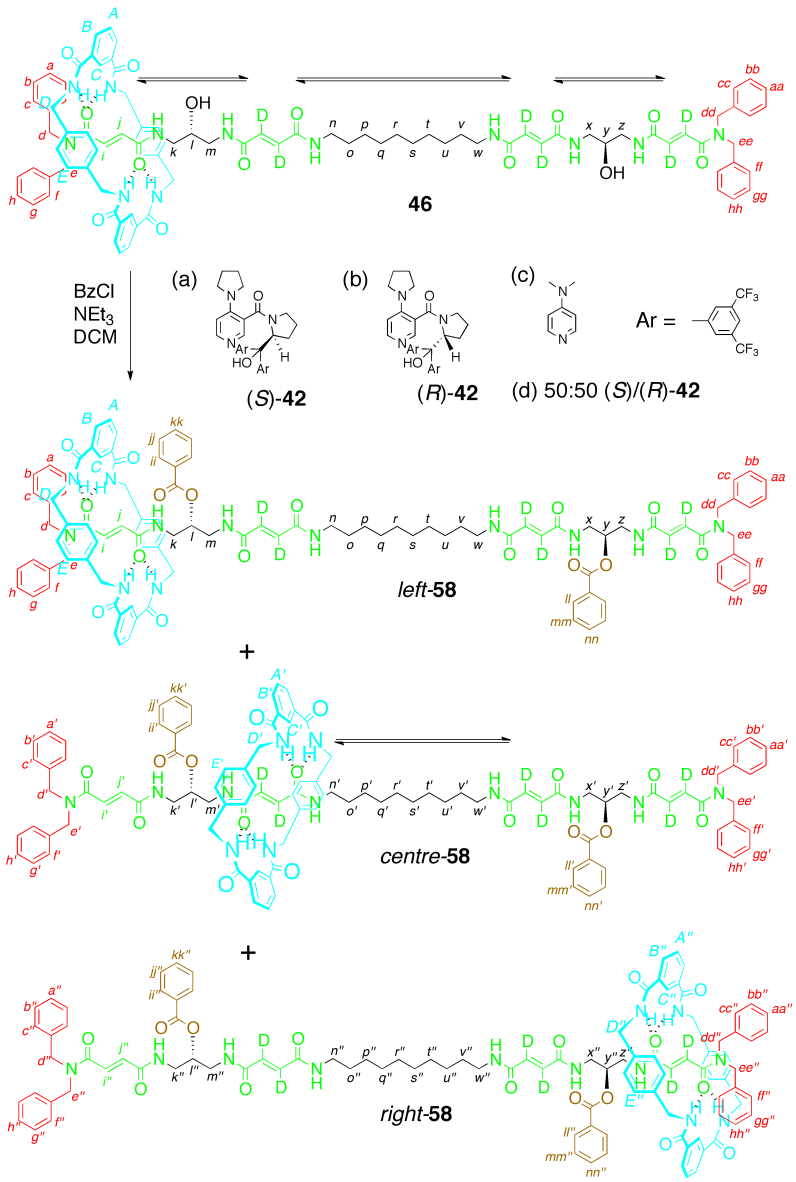

Scheme 3.7 Operation of diol information ratchet **46**. Reagents and conditions: BzCl (4 eq), NEt_3 (4 eq), (*S*)-**42** or (*R*)-**42** or DMAP or 50:50 (*S*)/(*R*)-**42** mixture (4 eq), DCM, 10 mM, rt, 2 h.

The procedure described in the previous Chapter was employed for the double benzoylation of **46** and the analysis of its products. Diol **46** was suspended in dichloromethane (0.1 M). To this suspension was added sequentially the catalyst (4 eq – 2 equivalents per hydroxyl group), triethylamine (4 eq) and benzoyl chloride (4 eq). After stirring for one hour, the solvent was removed by

rotary evaporation. Trituration with diethyl ether was used to remove the catalyst and excess benzoyl chloride, and the resulting solid was dissolved in DMSO-d_6 for analysis by NMR spectroscopy.

By solving simultaneous equations as described in the previous Chapter (section 2.6), the doubly-benzoylated products were found to be formed in the following ratios:

	Catalyst	**Product Distribution (±4%)** *left*-**58**:*centre*-**58**:*right*-**58**
(a)	(*S*)-**42**	<1:23:77
(b)	(*R*)-**42**	74:26:<1
(c)	DMAP	20:52:28
(d)	50:50 (*S*)/(*R*)-**42**	15:70:15

Table 3.1 Product distribution on double benzoylation of **21** using various catalysts. Reagents and conditions: BzCl (4 eq), NEt_3 (4 eq), (*S*)-**42** or (*R*)-**42** or DMAP or 50:50 (*S*)/(*R*)-**42** mixture (4 eq), DCM, 10 mM, rt, 2 h.

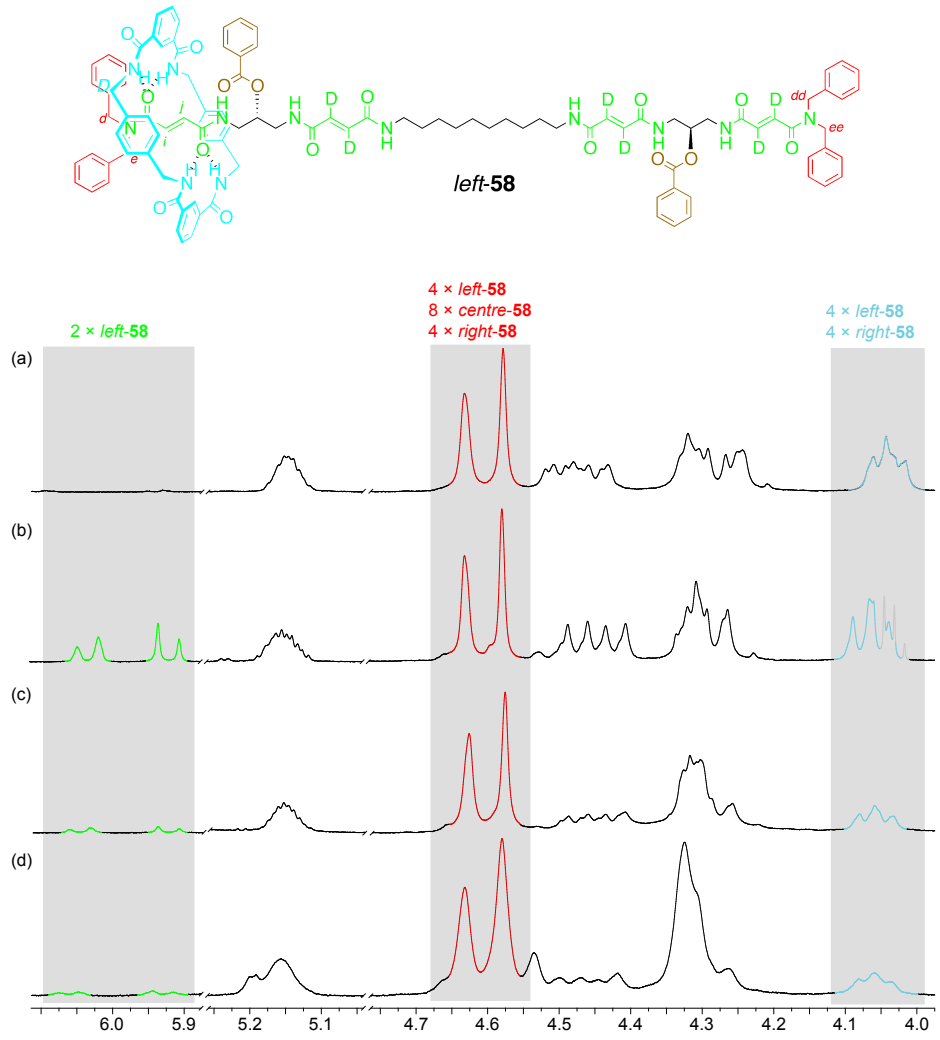

Figure 3.3 Partial ^{1}H NMR spectra (500 MHz, DMSO-d_6, 300 K) of double benzoylation of **46** in the presence of (a) (*S*)-**42**, (b) (*R*)-**42**, (c) DMAP and (d) a 50:50 (*S*)/(*R*)-**42** mixture. Residual solvent peaks are shown in grey. The peaks in the highlighted analysis regions, from left to right, correspond to the following protons: *i* and *j* when shielded by macrocycle (green); *d*, *e*, *dd* and *ee* when far from the macrocycle (red); macrocyclic D protons when near the stoppers (blue).

3.6 Operation of Mono-Benzoylated Information Ratchet 47

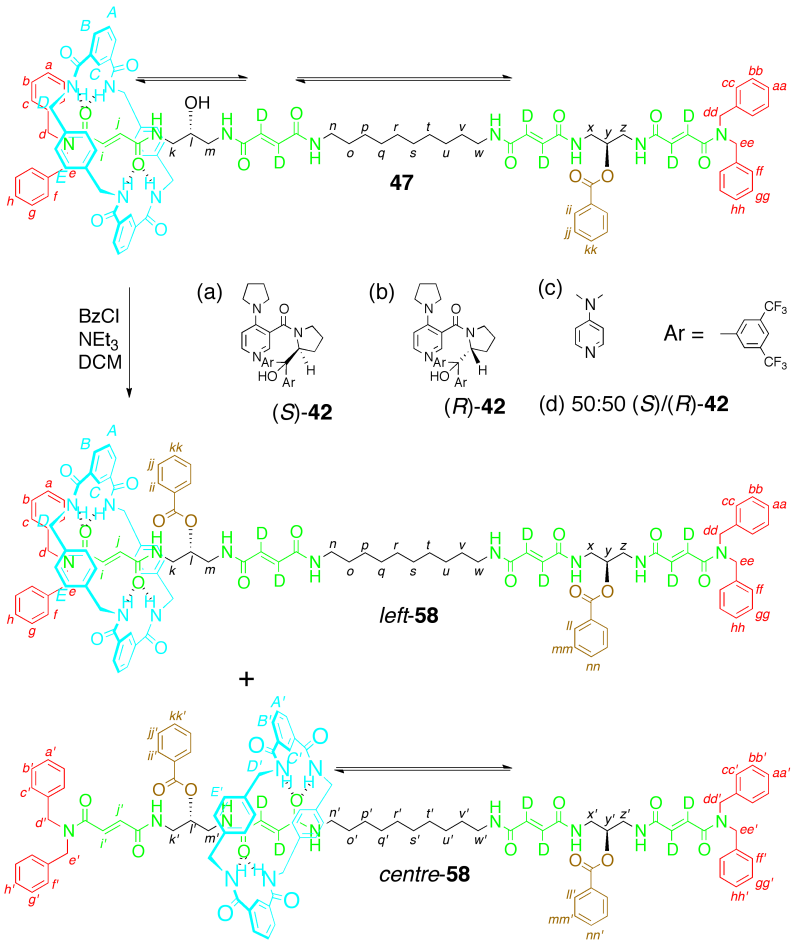

Scheme 3.8 Operation of mono-benzoylated information ratchet **47**. Reagents and conditions: BzCl (2 eq), NEt_3 (2 eq), (*S*)-**42** or (*R*)-**42** or DMAP or 50:50 (*S*)/(*R*)-**42** mixture (2 eq), DCM, 10 mM, rt, 2 h.

Mono-Benzoylated rotaxane **47** was suspended in dichloromethane, and to this suspension were added sequentially catalyst (2 eq), triethylamine (2 eq) and benzoyl chloride (2 eq). After 1 h the solvent was removed by rotary evaporation and the reaction crude was triturated once with diethyl ether, then dissolved in DMSO-d_6 for analysis by NMR spectroscopy. By solving simultaneous equations the doubly-benzoylated products were found to be formed in the following ratios:

	Catalyst	Product Distribution (±4%) *left*-**58**:*centre*-**58**
(a)	(*S*)-**42**	3:97
(b)	(*R*)-**42**	82:18
(c)	DMAP	46:54
(d)	50:50 (*S*)/(*R*)-**42** mixture	26:74

Table 3.2 Ratios observed on benzoylation of mono-benzoylated rotaxane **47** using various catalysts.

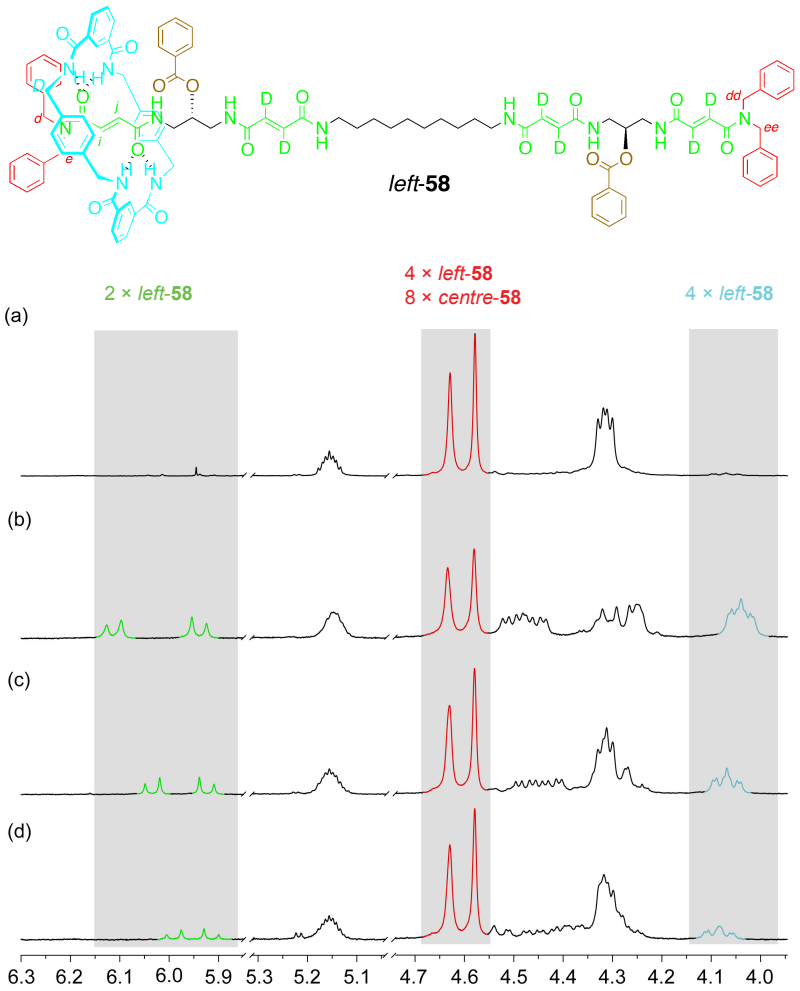

Figure 3.4 Partial ^{1}H NMR spectra (500 MHz, DMSO-d_6, 300 K) of single benzoylation of **47** in the presence of (a) (*S*)-**42**, (b) (*R*)-**42**, (c) DMAP and (d) a 50:50 (*S*)/(*R*)-**42** mixture. The peaks in the highlighted analysis regions, from left to right, correspond to the following protons: *i* and *j* when shielded by macrocycle (green); *d*, *e*, *dd* and *ee* when far from the macrocycle (red); macrocyclic D protons when near the stoppers (blue).

3.7 Markov Modelling

The methodology established in the preceding Chapter was used to derive Markov chains for the double benzoylation of rotaxane **46**.

3.7.1 Modelling of Information Ratchet 46 in the Presence of DMAP

Scheme 3.9 shows the double benzoylation of **46** in the presence of DMAP. The first benzoylation overwhelmingly occurs in such a way as to leave the macrocycle free to shuttle (96%, the sum of pathways II and III). Reactions that trap the macrocycle into the terminal compartments (pathways I and IV) are a small minority. The second benzoylation is approximately equally likely to occur with the macrocycle one one side as the other. The result, as shown in Scheme 3.10, is approximately half the macrocycle in the central compartment, and the other half equally distributed between the two equivalent terminal compartments.

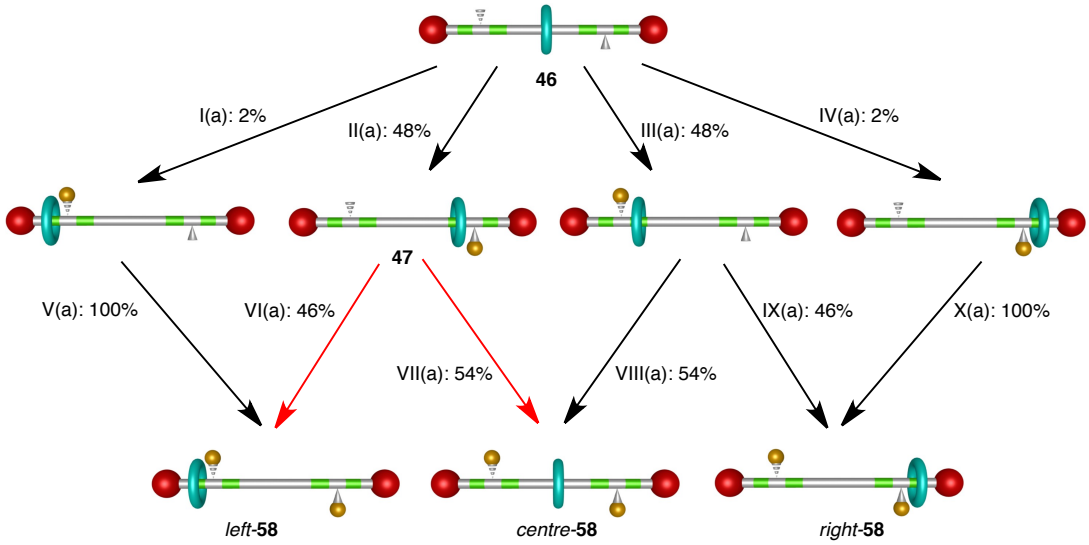

Scheme 3.9 Markov chain for the operation of information ratchet **46** in the presence of DMAP. Values for I(a) and II(a) calculated by fitting to experimental results; values for III(a) and IV(a) are taken to be equal to values II(a) and I(a) respectively; values for V(a) and X(a) must logically be 100% under irreversible benzoylation conditions; values for VI(a) and VII(a) obtained experimentally by single benzoylation of **47**; values for VIII(a) and IX(a) are taken to be equal to values for VII(a) and VI(a) respectively. Values for transitions shown in red were obtained directly; values transitions shown in black were inferred by indirect means.

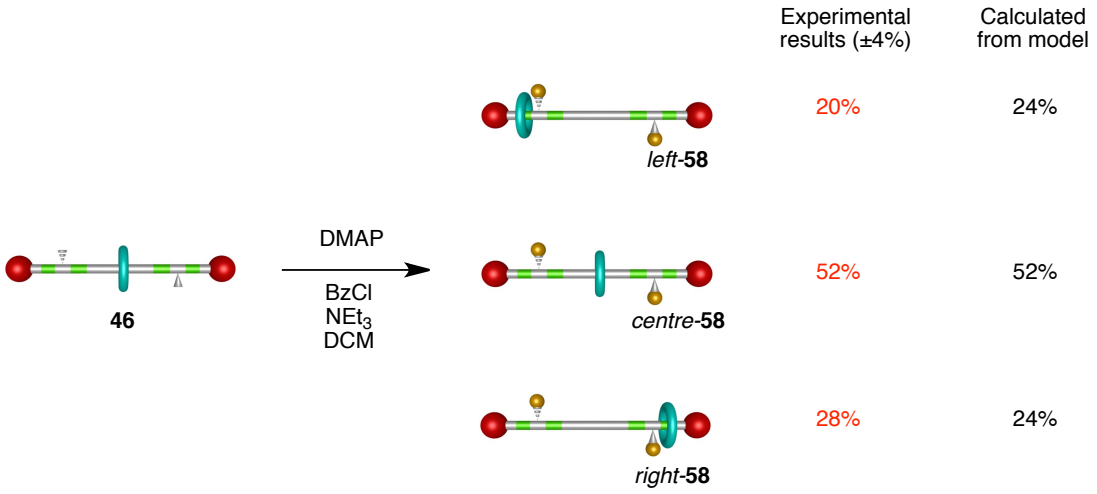

Scheme 3.10 Comparison of experimental results obtained for double benzoylation of **46** in the presence of DMAP with the results obtained with the model in Scheme 3.9.

3.7.2 Modelling of information ratchet 46 in the presence of a 50:50 (*S*)/(*R*)-42 mixture

Benzoylation in the presence of a racemic mixture of catalysts does not, in the first instance, trap the macrocycle into a terminal compartment to any detectable extent. The result of the first benzoylation is an equal mixture of two isomers with the macrocycle free to shuttle. The second benzoylation is more likely to trap the macrocycle into a terminal compartment (26%), but the most probable reactions are the ones that lead to the macrocycle occupying the central compartment.

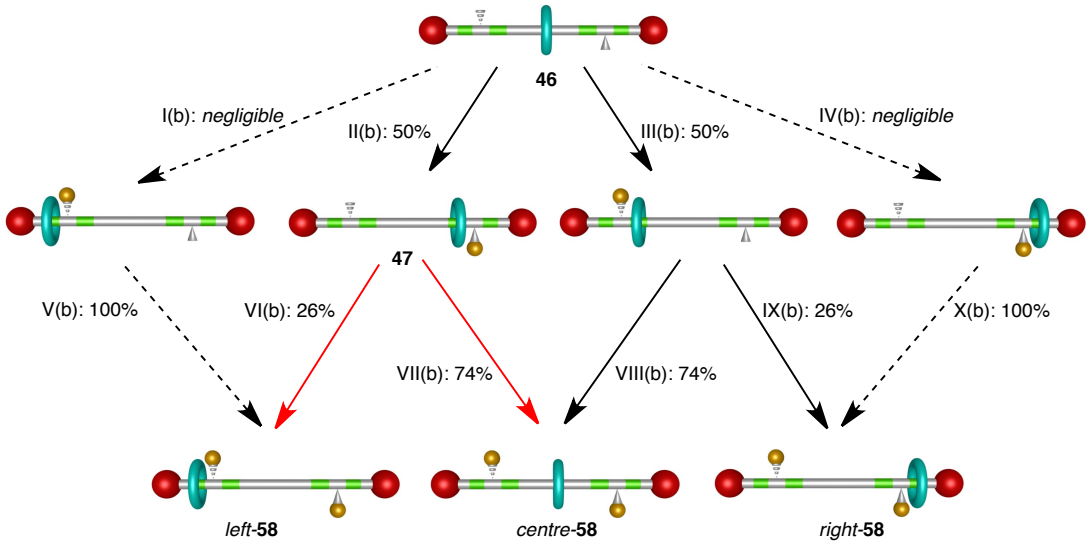

Scheme 3.11 Markov cain for the operation of information ratchet **46** in the presence of a 50:50 (*S*)/(*R*)-**42** mixture. Values for I(b) and II(b) calculated by fitting to experimental results; values for III(b) and IV(b) are taken to be equal to values II(b) and I(b) respectively; values for V(b) and X(b) must logically be 100% under irreversible benzoylation conditions; values for VI(b) and VII(b) obtained experimentally by single benzoylation of **42**; values for VIII(b) and IX(b) are taken to be equal to values for VII(b) and VI(b) respectively. Values for transitions shown in red were obtained directly; values transitions shown in black were inferred by indirect means. Dashed arrows indicate transitions which were explored to a negligible extent.

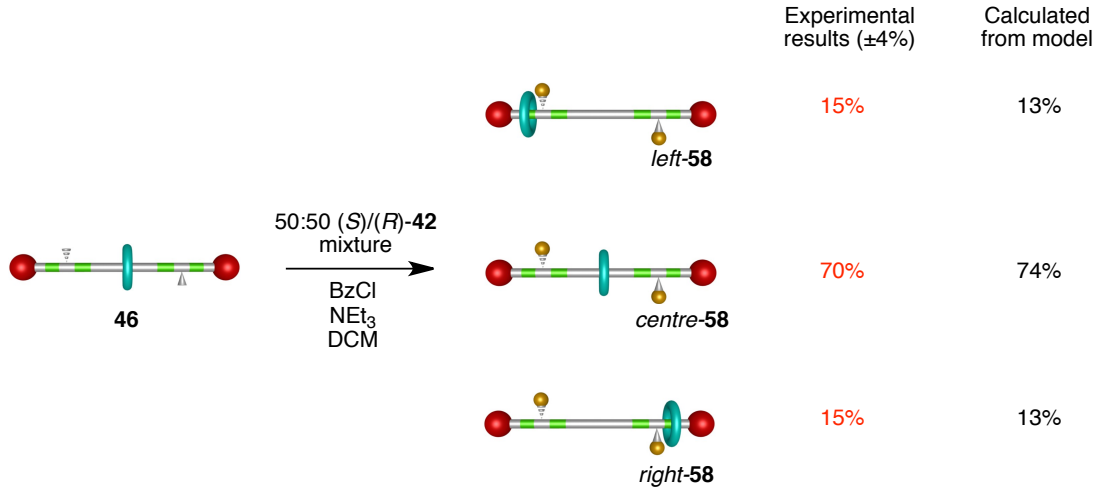

Scheme 3.12 Comparison of experimental results obtained for double benzoylation of **46** in the presence of a 50:50 (*S*)/(*R*)-**42** mixture with the results obtained with the model in Scheme 3.11.

3.7.3 Modelling of Information Ratchet 46 in the Presence of (*S*)-42

Where achiral or racemic mixtures of catalysts reacted with the rotaxane's two chiral centres equally, the effect of a single enantiomer was quite different. The predominant pathway is III, which accounts for 94% of the first instance benzoylations. The complementary pathway II makes up the remaining 6%. After the first benzoylation, the majority of the macrocycles are able to shuttle between the central and right-hand compartment; a second benzoylation results in most of the macrocycle (82%) trapped in the terminal compartment. For the minor product (6%) that was the result of pathway II, the directional discrimination is even more pronounced: 97% of the macrocycles are directed into the rightmost compartment available by the second benzoylation reaction.

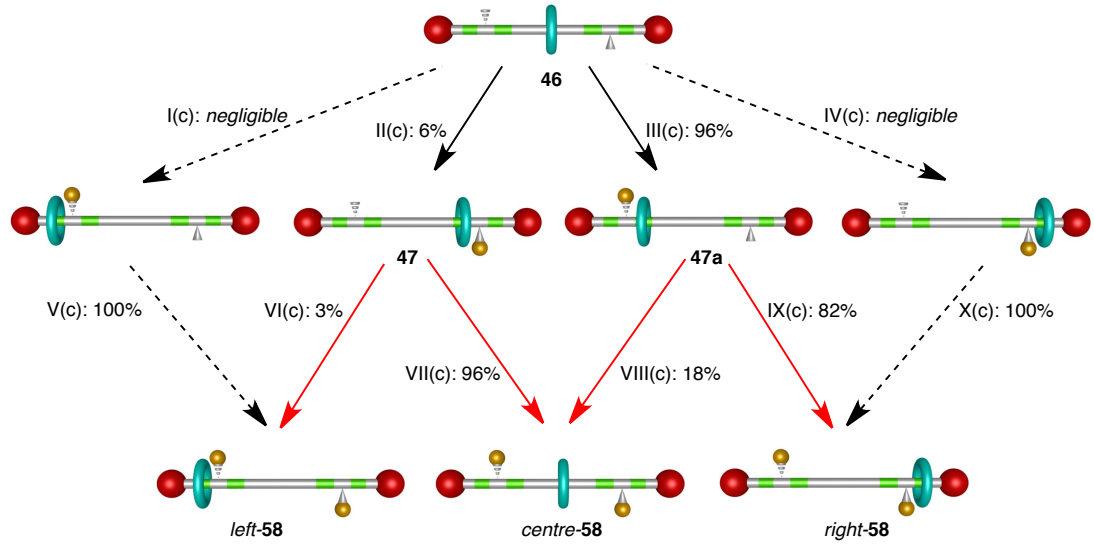

Scheme 3.13 Markov chain for the operation of information ratchet **46** in the presence of (*S*)-**42**. Contributions from I(c) and IV(c) are negligible (see Scheme 3.11); values for II(c) and III(c) were calculated by fitting to experimental data of benzoylation of **46**; values for V(c) and X(c) must logically be 100% under irreversible benzoylation conditions; values for VI(c) and VII(c) obtained experimentally by single benzoylation of **47** in the presence of (*S*)-**42**; values for VIII(c) and IX(c) obtained experimentally by single benzoylation of **47** in the presence of (*R*)-**42**. Values for transitions shown in red were obtained directly; values transitions shown in black were inferred by indirect means. Dashed arrows indicate transitions which were explored to a negligible extent.

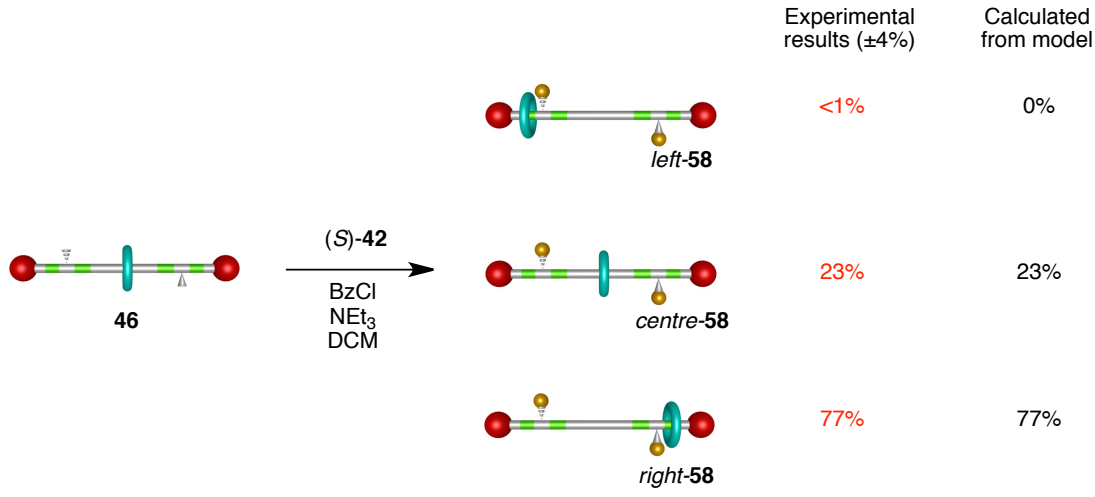

Scheme 3.14 Comparison of experimental results obtained for double benzoylation of **46** in the presence of (*S*)-**42** with the results obtained with the model in Scheme 3.13.

3.8 Comparison: Thermodynamics and Kinetics

Comparison of the behaviour of the present system's **46** and the previous Chapter's **25** reveals the product distribution to be the result of a complex interplay of kinetic and thermodynamic effects. Briefly summarised, these are:

1. When free to shuttle, **25**'s macrocycle has a thermodynamic preference for terminal binding environments. In **46**, the central compartment is favoured over the two terminal compartments.

2. Benzoylation reactions that trap the macrocycle into a terminal compartment are kinetically disfavoured, probably for steric reasons.

3. Macrocycle shuttling is fast on the timescale of benzoylation reactions. As such, a freely shuttling macrocycle is able to have a strong influence on the rate of benzoylation of hydroxyl groups far from the macrocycle's preferred position.

4. Benzoylation near a fumaramide group reduces the fumaramide group's ability to bind with the macrocycle, probably for steric reasons.

The rationale for these conclusions about the rotaxanes' properties is explained over the next few sections.

3.8.1 Equilibrium Distribution

A macrocycle freely shuttling on either **46** or **25** is unlikely to occupy the three compartments equally. For the macrocycle, the central compartment is an environment very different from the two terminal ones; different patterns of hydrogen bond donors and acceptors are available. Therefore a thermodynamic preference for occupancy of either the terminal or the central compartments is to be expected, and this will have consequences for the ratio of products formed when the macrocycle becomes kinetically locked on operation.

This ratio of products formed on benzoylation is unlikely to reflect the equilibrium distribution exactly under any circumstances; nevertheless, DMAP, being achiral, will at least bring with it no confounding factors resulting from stereochemistry. In Leigh and coworkers' 2008 paper, NMR spectroscopy studies of unsymmetrical rotaxane **5** (Figure 1.6) indicated that at equilibrium the macrocycle resided over the fumaramide binding site approximately 75% of the time, and over the succinamide binding site only 25% of the time. Benzoylation of this system resulted in a 75:25 mixture of products that reflected the equilibrium preference for the system; this suggests that DMAP does allow the benzoylation to take place irrespective of the position of the macrocycle. While there is no guarantee that such fidelity will continue to be expressed in the more complicated systems of **46** and **25**, benzoylation in the presence of DMAP might be expected to give the most accurate picture of the equilibrium distribution of macrocycles over positions of the thread.

Consider only the short three-compartment rotaxane **25**. The diol and the mono-benzoylated forms of the rotaxane both mostly yield terminally-positioned products when acylated in the presence of DMAP, suggesting a bias towards terminal-station occupancy at equilibrium. This hypothesis was confirmed by NMR spectroscopy (see Figure 2.6 in the previous Chapter).

Unfortunately, equivalent NMR spectra for **46** at equilibrium were not obtained because no suitable triplet of compounds was found that was sufficiently soluble in deuterated DCM. Nevertheless, consideration of the Markov chains suggests that the same logic applies to **46**, although the distribution of macrocycles in this system appears to be different. Here, the effect of benzoylation with DMAP is reversed, with *centre*-**58** being the dominant product. This is not unexpected, however: **46**'s central compartment possesses two fumaramide binding sites, not just one; **46**'s macrocycle is therefore likely to spend much more of its time in the central compartment than **25**'s does, and the ratio obtained from benzoylation reactions to trap it is likely to reflect this.

3.8.2 "Trapping" Reactions

It appears, then, that benzoylation with DMAP captures the macrocycles in something like their equilibrium distribution. The next thing to determine is just how close DMAP gets to this equilibrium value. Does the reaction occur 'blindly', benzoylating irrespective of where the macrocycle happens to be at the time? Or does DMAP bring with it its own preferences for terminal or central occupancy?

Consider the class of events that might be called "trapping" reactions. The first benzoylation on a diol rotaxane either can occur in such a way as to leave the macrocycle free to shuttle (transitions II and III), or can kinetically trap it into one of the terminal compartments (transitions I and IV). This second kind of benzoylation, when it occurs, effectively fixes the future of the rotaxane: a molecule of **46** with the macrocycle trapped in the left compartment can only ever become a molecule of *left*-**58**, as indicated by the 100% probability of transition for processes V and X in the above Markov chains.

Rotaxane	Catalyst	Probability that first benzoylation traps macrocycle
25	DMAP	50%
25	50:50 (*S*)/(*R*)-**42** mixture	*Negligible*
25	(*S*)-**42**	*Negligible*
46	DMAP	4%
46	50:50 (*S*)/(*R*)-**42** mixture	*Negligible*
46	(*S*)-**42**	*Negligible*

Table 3.3 Comparison of the probabilities of trapping reactions (sum of transitions I and IV) on both rotaxanes using various catalysts.

Examination of the data (Table 3.3) shows that trapping reactions are disfavoured, perhaps for steric reasons. The macrocycle residing in the terminal compartment partially occludes the nearby hydroxyl group, making benzoylation there unlikely; therefore, when there is an opportunity for benzoylation to occur elsewhere, it generally will. The only apparent exception is **25** benzoylated in the presence of DMAP, where trapping reactions, while still a minority, represent a more significant percentage of the first-instance benzoylations. Recall from the previous section, however, that at equilibrium the macrocycle on **25** spends the majority of its time in the terminal compartments. The trapping reactions here are more likely to occur simply because there is at any given moment more rotaxane available to react in this way. While the kinetically disfavoured trapping reactions can occur on **25** because they are thermodynamically favourable, the equivalent reactions on **46** are unlikely because they are both kinetically *and* thermodynamically disfavoured.

3.8.3 The Effect of Using a Chiral Catalyst

First-instance benzoylation reactions that trap the macrocycle into a terminal compartment do not occur to any noticeable extent, on either rotaxane **25** or **46**, when a chiral catalyst is used. If the reason for the general unfavourability of trapping reactions is a steric clash between the DMAP/benzoyl chloride conjugate and the macrocycle, then this is unsurprising. The chiral catalyst is a much larger than DMAP, and can be expected to be less able to react with a partially blocked hydroxyl group.

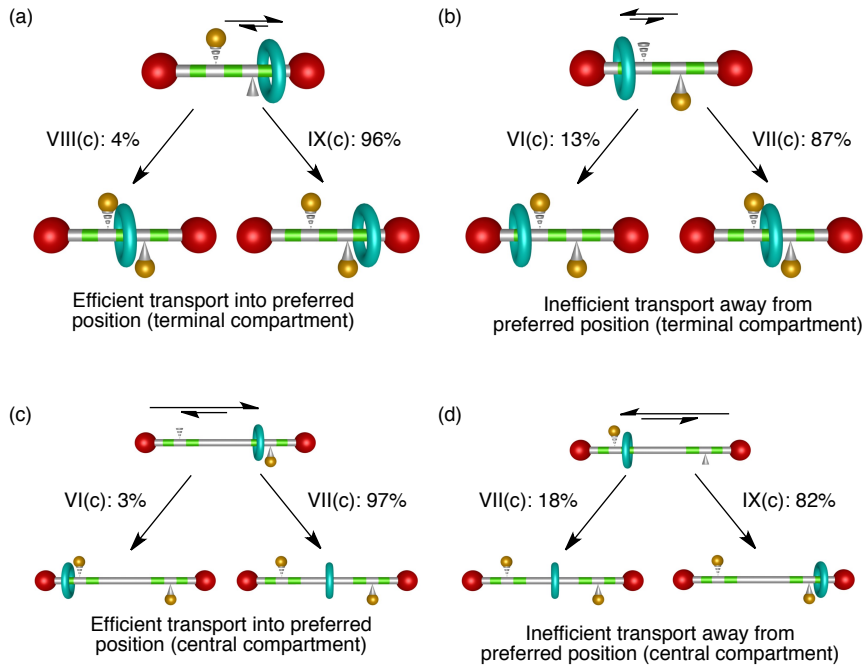

Scheme 3.15 Comparison of the second benzoylations of rotaxanes **25** and **46** in the presence of (*S*)-**42**. The handedness of the catalyst directs the macrocycle into the rightmost compartment. In cases (a) and (c), the direction of transport agrees with the thermodynamic bias inherent in the rotaxane, resulting in highly efficient transport. In (b) and (d), the catalyst directs the macrocycle into an unfavourable position, resulting in reduced transport efficiency.

Comparison of the way the second benzoylation proceeds in rotaxanes **25** and **46** gives other clues to the trade-offs between kinetics and thermodynamics in the system. The final distribution of products is shown to be the end result of

the chiral catalyst's kinetic modification of an already existing thermodynamic bias.

Scheme 3.15 displays the possible second benzoylations, catalysed by (*S*)-**42**, that occur on the mono-benzoylated forms of **25** and **46** (ignoring those with macrocycles already trapped; their future is already fixed). In all cases, the macrocycle is successfully driven to the right; but the degree of success varies. This variation is readily comprehensible when one considers the likely equilibrium distribution of the macrocycles. In (a) and (c), the position of the macrocycle favoured by the catalyst for benzoylation also happens to be where the macrocycle finds a thermodynamic minimum – in the terminal compartment for the short rotaxane, and in the central compartment for the long one. For directional transport to succeed in (b) and (d), the benzoylation reaction must occur when the macrocycle is far from where it is likely to spend the majority of its time. As a consequence, the directional discrimination is much less effective in (b) and (d), where the chiral catalyst is effectively fighting against the rotaxane's inherent bias, than in (a) and (c), where the two effects are in concordance.

3.8.4 Timescale of the Reactions

The difference in probability between transitions II and III on both rotaxanes in the presence of (*S*)-**42** is striking. Under chiral conditions, the benzoylation appears to occur more readily on one chiral centre than on the other. It is tempting to invoke the different stereochemistries of the two hydroxyl groups – the one on the left is (*S*), the one on the right is (*R*),[5] and the two can be expected to react at different rates in a chiral environment; but this on its own is unsatisfactory. Consideration of the thread without the macrocycle shows that the chiral centre is not particularly well-expressed. Although the atoms bearing

the hydroxyl group are nominally (*S*) and (*R*), the thread is symmetrical over a distance of six atoms on either side of the carbon bearing the hydroxyl group. This makes the prospect of significant discrimination by a chiral catalyst solely on the grounds of the different chiralities of the hydroxyl groups less plausible.

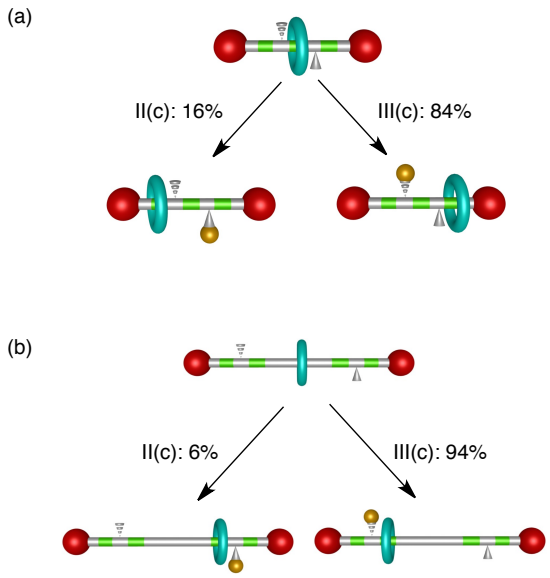

Scheme 3.16 Discrimination shown in first-instance benzoylation using chiral catalyst (*S*)-**42**.

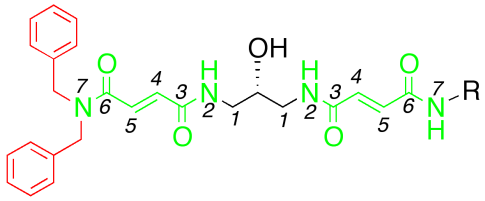

Figure 3.5 The environment surrounding the chiral centre is highly symmetrical over short distances.

It is only when the macrocycle is nearby that the chirality of the hydroxyl groups becomes chemically relevant. Ensuring such close residence was in fact a design requirement of the system published by Leigh and coworkers in 2008,[1] and is still the reason that the present systems were designed with fumaramide

binding sites on both sides of the chiral centre. While the macrocycle on a two-station system can only ever be close at hand, it is an open question how the macrocycle affects the rate of benzoylation from far away on longer systems.

Without invoking such long-range influences, it is necessary to consider how much time a freely shuttling macrocycle is likely to spend close to the site of benzoylation. Studies on related systems have shown frequencies of shuttling of several thousand Hz at room temperature in halogenated solvents.[6] If shuttling is sufficiently fast compared to the benzoylation, the layout of these systems ensures that there will always be *some* macrocycle available to lend expression of chirality to the hydroxyl groups. Indeed, there is some suggestion from the percentages shown in Scheme 3.16 that the macrocycle in **25** exerts less influence than the macrocycle in **46**; this is in line with the hypothesis that the macrocycle spends most of its time in the terminal compartments of **25** (far from the reacting hydroxyl group) but in the central compartment of **46** (close to the hydroxyl group).

3.8.5 The Effect of Benzoyl Groups on Nearby Fumaramide Binding Sites

One further issue remains to be addressed. It has already been established that reactions that trap the macrocycle in the terminal compartments are kinetically disfavoured, and that a strong thermodynamic bias towards terminal compartments is required to make them occur to any noticeable extent in the first-instance benzoylation. Why then is it that this unfavourable reaction becomes significantly more likely to occur in the second round of benzoylations?

		Percentage of macrocycles that are trapped in a terminal compartment by benzoylation	
Rotaxane	**Catalyst**	**First benzoylation**	**Second benzoylation**
25	DMAP	50%	64%
46	DMAP	4%	46%
25	50:50 (*S*)/(*R*)-**42** mixture	*Negligible*	26%
46	50:50 (*S*)/(*R*)-**42** mixture	*Negligible*	47%

Table 3.4 Evidence that the thermodynamic favourability of the terminal binding sites increases after the first benzoylation reaction.

Table 3.4 gives the percentage of reactions at each stage that lead to a terminally-locked macrocycle. As has already been established, benzoylation with DMAP appears to reflect the equilibrium distribution of macrocycles over positions on the thread. The table indicates that the first benzoylation *changes* the equilibrium distribution, making the terminal binding sites thermodynamically more favourable.

A small increase in the occupancy of the terminal compartments is probably inevitable after the first benzoylation, since the number of compartments accessible to the macrocycle has decreased by one. Nevertheless, the increase is significant enough to demand a more thorough explanation. A more likely explanation is that a benzoyl group effectively poisons the nearby fumaramide groups for macrocycle binding. The steric bulk of a nearby benzoyl group could disrupt efficient binding of the macrocycle to the fumaramide group, reducing the macrocycle's thermodynamic preference for that site. The effect of such a disruption would be expected to be most pronounced for **46**: since the terminal compartments have been shown by NMR spectroscopy studies on **25** to be thermodynamic sinks, the only reason that the macrocycle prefers the central

compartment of **46** is the availability of *two* fumaramide binding sites; if one of these binding sites was made unavailable, the equilibrium distribution might make the terminal compartment a more favourable environment for the macrocycle than the central one.

The addition of a benzoyl group to **46** raises the energy of one of the minima and makes the central compartment as a whole less favourable. At equilibrium, a greater number of macrocycles is found in the remaining terminal compartment, and the second benzoylation is able to trap many of these macrocycles. The trapping is still more effective with DMAP than with the chiral DMAP analogues, presumably because of the difference in size between these two acylation catalysts.

3.9 Summary and Outlook

A three-compartment information ratchet system incorporating a long alkyl spacer has been successfully synthesised and operated, and has been found to be almost as effective at directional macrocycle transport as the previous Chapter's molecule despite having both the spacer and an extra binding site. The distance over which the transport occurs has been increased by the length of a decane spacer. This spacer was able to offset the solubility penalty for incorporating an extra fumaramide binding site, and strongly indicates that it would be possible to design much longer systems with many repeat units in the same molecule.

More importantly, comparison between the long rotaxane **46** and its shorter predecessor **25** has permitted the construction of a much more satisfactory theory of how these machines work in detail. The complex tradeoffs between thermodynamics and kinetics in these systems are now well understood. It is hoped that this understanding will lead directly to the development of longer and more complicated molecular machines, capable of ratcheting particles over much longer distances, to perform a variety of tasks.

3.10 Experimental Section

Many of the compounds documented in this Chapter are chiral or adopt chiral conformations. The resulting inequivalent nuclei are in some instances observed as a complex series of signals, although the same compound may also exhibit simpler signals under different conditions (different solvent, temperature, concentration, etc). Where possible, the signals have been assigned unambiguously and where non-equivalence occurred it is noted in the experimental assignments. Signals for carbons adjacent to deuterons on fumaramide residues were not observed by ^{13}C NMR spectroscopy.

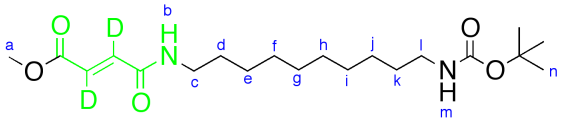

51

To a stirred, cooled (0 °C) solution of **35** (1.14 g, 8.64 mmol) in anhydrous DMF (100 mL) under N_2 was added sequentially **52** (1.2 eq, 10.34 mmol, 2.82 g), DIPEA (1.2 eq, 10.34 mmol, 1.76 mL), HOBt (1.2 eq, 10.34 mmol, 1.40 g) and TBTU (1.2 eq, 10.34 mmol, 3.32 g). The mixture was allowed to reach room temperature with stirring over 12 h, diluted with saturated $NaHCO_3$ (100 mL) and extracted into 3:1 $CHCl_3$/IPA (3 × 100 mL). The combined organic fractions were washed with saturated $NaHCO_3$ (3 × 50 mL), HCl (1 M, 3 × 50 mL) and brine (3 × 50 mL), then dried over $MgSO_4$ and concentrated under reduced pressure by coevaporation with toluene. Flash chromatography (1% MeOH in DCM) gave **51** as a white solid (2.20 g, 65%). M.p. 93–94 °C. ^{1}H NMR (400 MHz, $CDCl_3$): δ = 6.45 (br, 1H, H_b), 4.59 (br, 1H, H_m), 3.59 (s, 3H, H_a), 3.32 (dd, 2H, *J* = 13.3, 6.8, H_c), 3.07 (dd, 2H, *J* = 11.8, 5.5, H_l), 1.59–1.48 (m, 2H, H_d), 1.41 (s, 11H, H_k + H_n), 1.24 (br, 12H, H_e + H_f + H_g + H_h + H_i + H_j); ^{13}C NMR (125 MHz, $CDCl_3$): δ = 166.2 (C), 163.5 (C), 156.1 (C), 136.6 (CD), 129.3 (CD) 79.0, 52.1, 40.6, 39.9, 30.0 (×2), 29.3 (×2), 29.2 (×2), 28.4, 26.8, 26.7. LR-MS (ESI): m/z = 409 $[M+Na]^+$;

HR-MS (ESI): m/z = 387.2819 $[M+H]^+$ (calculated for $C_{20}H_{34}D_2N_2O_5H$ = 387.2823).

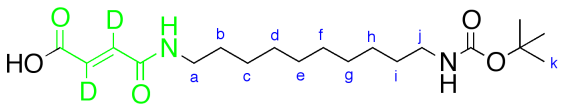

53

To a stirred solution of **51** (300 mg, 0.75 mmol) in 3:1 THF/H_2O (10.1 mL) was added LiOH·H_2O (2 eq, 1.50 mmol, 63 mg). After 25 mins the mixture was diluted with HCl (1 M, 10 mL) and extracted into 3:1 $CHCl_3$/IPA (3 × 15 mL). The combined organic fractions were washed with HCl (1 M, 3 × 5 mL) and brine (3 × 5 mL), dried over $MgSO_4$ and concentrated under reduced pressure to give **53** as a white low-melting solid (279 mg, *quant.*). ^{1}H NMR (500 MHz, 1:1 CD_3OD/ CDCl3): δ = 3.47 (t, 2H, *J* = 7.2, H_a), 3.24 (t, 2H, *J* = 7.1, H_j), 1.81–1.70 (m, 2H, H_b), 1.70–1.59 (m, 11H, H_i + H_k), 1.59–1.41 (m, 12H, H_c + H_d + H_e + H_f + Hg + H_h); ^{13}C NMR (125 MHz, 1:1 $CD_3OD/CDCl_3$): δ = 167.6, 164.8, 157.0, 78.9, 40.3, 39.7, 29.7, 29.3 (×2), 29.1 (×2), 28.9, 28.0, 26.8, 26.6. LR-MS (ESI): m/z = 393 $[M+Na]^+$; HR-MS (ESI, negative mode): m/z = 369.2388 $[M–H]^-$ (calculated for $C_{19}H_{33}N_2O_5$ = 369.2395).

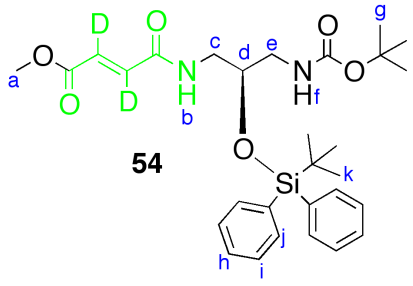

54

To a stirred, cooled (0 °C) solution of **35** (1.14 g, 8.64 mmol) in anhydrous DMF (103 mL) under N_2 was added sequentially amine **34** (1.2 eq, 10.34 mmol, 2.82 g), DIPEA (1.2 eq, 10.34 mmol, 1.76 mL), HOBt (1.2 eq, 10.34 mmol, 1.40 g) and TBTU (1.2 eq, 10.34 mmol, 3.32 g). The mixture was allowed to reach room temperature with stirring over 12 h, diluted with saturated $NaHCO_3$ (100 mL)

and extracted into 3:1 $CHCl_3$/IPA (3 × 100 mL). The combined organic fractions were washed with saturated $NaHCO_3$ (3 × 50 mL), HCl (1 M, 3 × 50 mL) and brine (3 × 50 mL), then dried over $MgSO_4$ and concentrated under reduced pressure by coevaporation with toluene. Flash chromatography (1% MeOH in DCM) gave **54** as a white solid (2.20 g, 85%). M.p. 131–132 °C. $[\alpha]_D^{20}$ = +31.1 (c = 1.10, DCM). ^{1}H NMR (400 MHz, $CDCl_3$): δ = 7.66 (t, 4H, *J* = 7.9, H_i), 7.54–7.32 (m, 6H, H_h + H_j), 6.70–6.58 (m, 1H, H_b), 4.94–4.76 (m, 1H, H_f), 3.90 (dt, 1H, *J* = 10.0, 4.9, H_d), 3.80 (s, 3H, H_a), 3.71–3.56 (m, 1H, H_c), 3.31 (ddd, 1H, *J* = 14.4, 8.1, 3.3, H_e), 3.14–3.00 (m, 1H, H_c), 2.92 (dt, 1H, *J* = 14.5, 5.0, H_e), 1.43 (s, 9H, H_g), 1.09 (s, 9H, H_k); ^{13}C NMR (100 MHz, $CDCl_3$): δ = 166.1 (C), 163.7 (C), 156.9 (C), 135.8 (CH), 133.5 (C), 130.2 (CH), 128.1 (CH), 80.0 (C), 70.7 (CH), 60.5 (C), 52.3 (CH_3), 43.1 (CH_2), 41.6 (CH_2), 28.5 (CH_3), 27.1 (CH_3). LR-MS (ESI): m/z = 565.3 $[M+Na]^+$; HR-MS (ESI, negative mode): m/z = 543.2845 $[M–H]^-$ (calculated for $C_{29}H_{38}D_2N_2O_6SiH$ = 543.2854).

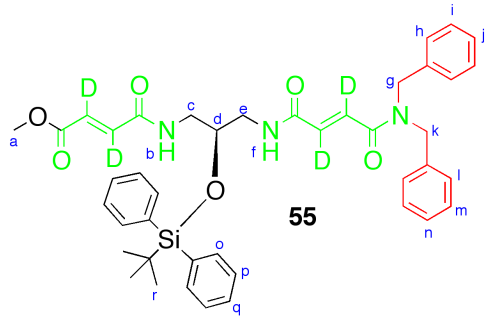

To a stirred solution of **54** (400 mg, 0.74 mmol, 1.2 eq) in anhydrous DCM (24.6 mL) in a loosely-sealed round-bottomed flask was added TFA (6.15 mL). After 16 h the mixture was diluted with aqueous NaOH (1 M) until basic and extracted into DCM (3 × 50 mL). The combined organic fractions were dried over $MgSO_4$ and the solvent was removed under reduced pressure. The obtained residue was redissolved in anhydrous DMF (6.2 mL) under N_2 and cooled to 0 °C. Acid **32** (1 eq, 0.615 mmol, 182 mg), DIPEA (1.2 eq, 0.74 mmol, 125 µL), HOBt (1.2 eq, 0.74 mmol, 99 mg) and TBTU (1.2 eq, 0.74 mmol, 237 mg) were added. After allowing the reaction to reach room temperature with stirring over 16 h the reaction mixture was diluted with saturated $NaHCO_3$ (10 mL) and extracted into

DCM (4 × 15 mL). The combined organic fractions were washed with saturated $NaHCO_3$ (3 × 10 mL), HCl (1 M, 3 × 10 mL) and brine (3 × 10 mL), then dried over $MgSO_4$ and the solvent was removed by coevaporation with toluene under reduced pressure. Flash chromatography (1:1.5 PE/EtOAc) gave **55** as a yellow solid (375 mg, 85%). M.p. 83–84 °C. $[\alpha]_D^{20}$ = –7.1 (c = 1.10, 1:1 MeOH/DCM). ^{1}H NMR (400 MHz, $CDCl_3$): δ = 7.66 (dt, 4H, J = 8.0, 1.5, H_p), 7.52–7.27 (m, 12H, H_i + H_j + H_m + H_n + H_o + H_q), 7.25–7.20 (m, 2H, H_h), 7.19–7.11 (m, 2H, H_l), 6.51 (dd, 1H, *J* = 7.5, 5.1, H_f), 6.30 (dd, 1H, *J* = 7.8, 5.0, H_b), 4.73–4.44 (m, 4H, H_g + H_k), 4.06–3.95 (m, 1H, H_d), 3.78 (s, 3H, H_a), 3.71–3.61 (m, 2H, H_c), 3.00–2.89 (m, 2H, H_e), 1.09 (s, 9H, H_r); ^{13}C NMR (100 MHz, $CDCl_3$): δ = 166.3, 166.2, 165.4, 164.7, 136.3, 135.8, 135.7, 133.2 (×2), 129.9 (×2), 128.9, 128.6, 128.0, 127.7, 126.6, 70.0, 51.8 (×2), 50.2, 42.7, 42.5, 26.6, 19.0. LR-MS (ESI): m/z 722 $[M+H]^+$; HR-MS (ESI): m/z = 722.3556 $[M+H]^+$ (calculated for $C_{42}H_{43}D_4N_3O_6SiH$ = 722.3558).

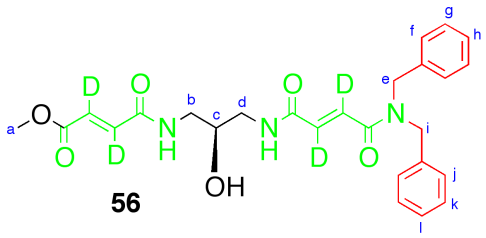

56

To a stirred solution of **55** (307 mg, 0.43 mmol) in dry THF (4.2 mL) was added TBAF (2 eq, 0.85 mmol, 0.85 mL of 1 M solution in THF). After 18 h the reaction mixture was diluted with EtOAc (80 mL) and washed with sodium citrate (5 × 10 mL), then dried over $MgSO_4$ and concentrated under reduced pressure. Flash chromatography (pure DCM increasing to pure 1:1 DCM/MeOH) gave **56** as a colourless solid (206 mg, *quant.*). M.p. 153–154 °C. $[\alpha]_D^{20}$ = +19.0 (c = 0.25, DCM). ^{1}H NMR (400 MHz, $CDCl_3$): δ = 7.38–7.27 (m, 6H, H_g + H_h + H_k + H_l), 7.18 (d, 2H, *J* = 6.5, H_f), 7.13 (d, 2H, *J* = 6.6, H_j), 4.62 (s, 2H, H_e), 4.55 (s, 2H, H_i), 3.89–3.77 (m, 1H, H_c), 3.73 (s, 3H, H_a), 3.42–3.17 (m, 4H, H_b + H_d); ^{13}C NMR (100 MHz, CDCl3): δ = 168.0, 167.1, 166.2, 166.0, 136.9, 136.4, 129.5, 129.3, 128.7, 128.5, 128.3, 127.3, 69.3, 50.9, 49.1, 48.7, 43.8, 43.7. LR-MS (ESI): m/z 484 $[M+H]^+$; HR-MS (ESI): m/z = 484.2366 $[M+H]^+$ (calculated for $C_{26}H_{25}D_4N_3O_6H$ = 484.2380).

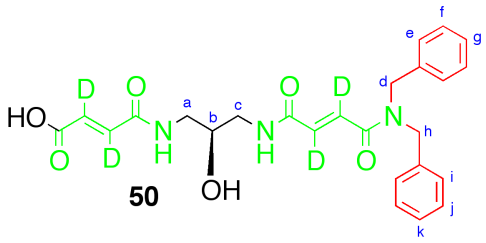

To a stirred solution of **56** (43 mg, 89 µmol) in 3:1 THF/H_2O (1.33 mL) was added LiOH·H_2O (2 eq, 178 µmol, 7.5 mg). After 25 mins the mixture was diluted with HCl (1 M, 2 mL) and extracted into 3:1 $CHCl_3$/IPA (3 × 5 mL). The combined organic fractions were washed once with water (3 mL), dried over $MgSO_4$ and concentrated under reduced pressure to give **50** as a white solid (42 mg, *quant.*). M.p. 143–144 °C. $[\alpha]_D^{20}$ = +66.7 (c = 0.27, DMSO). ^{1}H NMR (400 MHz, 3:1 CD_3OD/CDCl3): δ = 7.30–7.16 (m, 6H, H_f + H_g + H_j + H_k), 7.13 (d, 2H, *J* = 6.9, H_e), 7.08 (d, 2H, *J* = 7.2, H_i), 4.63 (s, 2H, H_d or H_h), 4.60 (s, 2H, H_d or H_h), 3.75 (m, 1H, H_b), 3.24 (m, 4H, H_a + H_c); ^{13}C NMR (125 MHz, 1:1 CD_3OD/CDCl3): δ = 167.3, 166.4, 165.6, 165.4, 137.3, 136.2, 135.8, 128.9, 128.6, 128.0, 127.6, 126.6, 68.7, 50.3 (×2), 43.1, 43.0. LR-MS (ESI): m/z 470 $[M+H]^+$; HR-MS (ESI): m/z = 470.2212 $[M+H]^+$ (calculated for $C_{25}H_{23}D_4N_3O_6H$ = 470.2224).

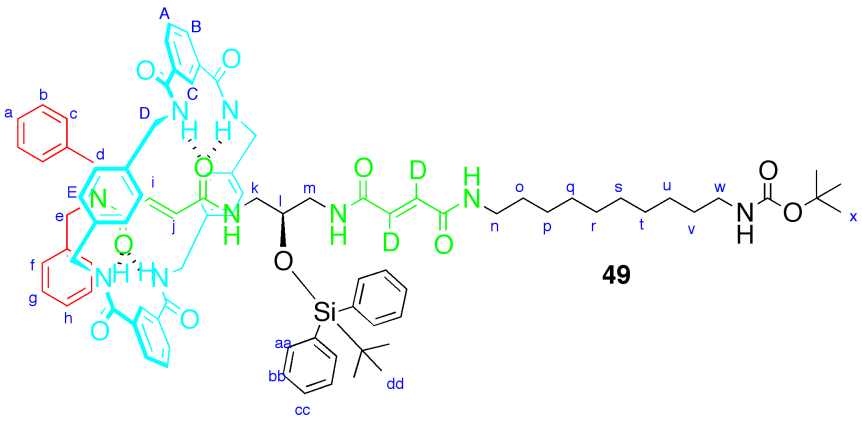

To a stirred solution of **28** (400 mg, 0.15 mmol, 1.07 eq) in anhydrous DCM (6 mL) in a loosely-sealed round-bottomed flask was added TFA (1.5 mL). After 16 h the mixture was diluted with aqueous NaOH (1 M) until basic and extracted

into DCM (3 × 20 mL). The combined organic fractions were dried over $MgSO_4$ and the solvent was removed under reduced pressure. The obtained residue was redissolved in anhydrous DMF (1.4 mL) under N_2. To this solution was added sequentially **53** (1 eq, 52 mg, 0.14 mmol), DIPEA (1.2 eq, 0.17 mmol, 29 µL), HOBt (1.2 eq, 0.17 mmol, 23 mg) and TBTU (1.2 eq, 0.17 mmol, 54 mg). The mixture was allowed to reach room temperature with stirring over 12 h, diluted with saturated $NaHCO_3$ (2 mL) and extracted into 3:1 $CHCl_3$/IPA (3 × 6 mL). The combined organic fractions were washed with saturated $NaHCO_3$ (3 × 1 mL), HCl (1 M, 3 × 1 mL) and brine (3 × 1 mL), then dried over $MgSO_4$ and concentrated under reduced pressure by coevaporation with toluene. Flash chromatography (2:1 EtOAc/PE) gave **49** as a slightly yellow oil (117 mg, 56%). $[\alpha]_D^{20}$ = +15.2 (c = 0.5, 1:1 MeOH/DCM). ^{1}H NMR (400 MHz, $CDCl_3$): δ = 8.53 (s, 2H, H_C), 8.26–8.20 (m, 4H, H_B), 7.76–7.69 (m, 6H, H_A + H_{bb}), 7.45–7.30 (m, 9H, H_a + H_b + H_{aa} + H_{cc}), 7.27 (dd, 2H, *J* = 7.6, 1.8, H_c), 7.17 (t, 1H, J = 7.4, H_h), 7.09 (t, 2H, *J* = 7.5, H_g), 6.90 (dd, 8H, *J* = 26.8, 8.0, H_E), 6.78 (d, 2H, *J* = 7.3, H_f), 5.94 (s, 2H, H_i + H_j), 4.58–4.31 (m, 8H, H_D + H_d + H_e), 4.28–4.11 (m, 4H, H_D), 4.00 (td, 1H, *J* = 8.6, 4.2, H_l), 3.58–3.30 (m, 5H, H_k + H_m + H_w), 3.10 (t, 2H, *J* = 7.1, H_n), 3.04–2.93 (m, 1H, H_k), 1.68 (dt, 2H, *J* = 14.3, 7.1, H_o), 1.58–1.48 (m, 11H, H_v + H_x), 1.48–1.30 (m, 12H, H_p + H_q + H_r + H_s + H_t + H_u), 1.12 (s, 9H, H_{dd}); ^{13}C NMR (125 MHz, $CDCl_3$): δ = 168.2 (×2), 167.3, 166.9, 166.8, 166.2, 138.3, 138.2, 137.8, 136.8, 136.6, 135.8, 134.9, 134.8, 134.6, 132.5, 131.2, 130.4, 130.3, 130.0 (×2), 129.9, 129.8, 129.7, 129.6, 129.1 (×2), 128.9, 128.8 (×2), 128.7, 128.5, 126.7, 125.6, 71.2, 52.9, 52.5, 51.5, 50.0, 44.7, 44.5, 43.7, 40.7, 38.9, 30.4, 30.3, 30.2, 30.1 (×2), 30.0, 28.5, 27.9, 27.8, 27.4, 27.3, 27.2, 27.1. LR-MS (ESI): m/z 697 $[M–Boc]^{2+}$; observed peaks are consistent with theoretical isotope distribution.

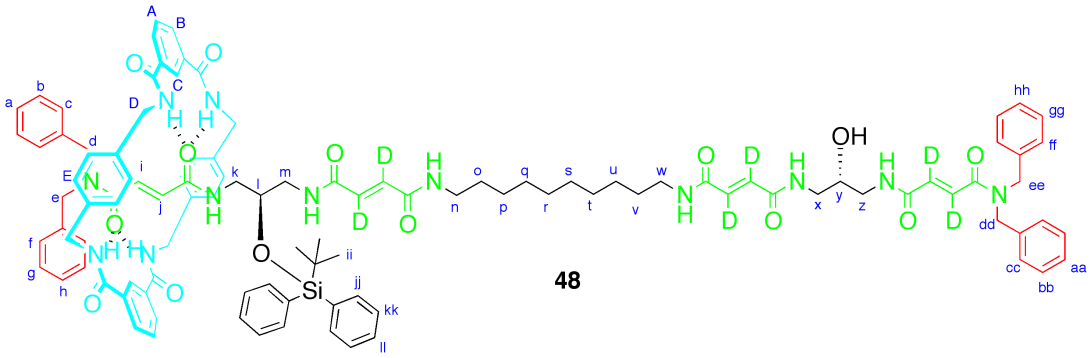

48

To a stirred solution of **49** (191 mg, 0.13 mmol, 1.2 eq) in anhydrous DCM (4 mL) in a loosely-sealed round-bottomed flask was added TFA (1 mL). After 16 h the mixture was concentrated under reduced pressure by coevaporation with toluene. The resulting residue was dissolved in DMF (2 mL) and cooled to 0 °C under N_2. Acid **50** (1 eq, 0.11 mmol, 50 mg), DIPEA (3 eq, 321 µmol, 55 µL), HOBt (1.2 eq, 0.13 mmol, 17 mg) and TBTU (1.2 eq, 0.13 mmol, 41 mg) were added sequentially. The reaction mixture was allowed to reach room temperature with stirring over 16 h then was diluted with saturated $NaHCO_3$ solution (5 mL) and extracted into 3:1 chloroform/IPA (3 × 15 mL). The combined organic fractions were washed with saturated $NaHCO_3$ (3 × 5 mL), HCl (1 M, 3 × 5 mL) and brine (3 × 5 mL) then dried over $MgSO_4$ and concentrated under reduced pressure. Flash chromatography (pure DCM increasing to 4% MeOH in DCM) gave **48** as a white solid (177 mg, 90%). On heating the product decomposed at 250 °C. $[\alpha]_D^{20}$ = +10.7 (c = 0.38, DCM). ^{1}H NMR (500 MHz, 1:1 $CD_3OD/CDCl_3$): δ = 8.46 (s, 2H, H_C), 8.20–8.10 (m, 4H, H_B), 7.74–7.61 (m, 6H, H_A + H_{kk}), 7.38–7.12 (m, 14H, H_g + H_h + H_{aa} + H_{bb} + H_{cc} + H_{jj} + H_{ll}), 7.09 (t, 1H, *J* = 7.4, H_a), 7.02 (t, 2H, *J* = 7.5, H_b), 6.83 (m, 10H, H_E + H_f), 6.71 (d, 2H, H_c), 5.87 (s, 2H, H_i + H_j), 4.66 (s, 2H, H_{dd} or H_{ee}), 4.62 (s, 2H, H_{dd} or H_{ee}), 4.57–4.19 (m, 8H, H_D + H_d + H_e), 4.19–4.08 (m, 4H, H_D), 3.93 (dd, 1H, *J* = 8.7, 4.3, H_y), 3.88–3.81 (m, 1H, H_l), 3.50–3.14 (m, 11H, H_k + H_m + H_n + H_w + H_x + H_z), 2.91 (dd, 1H, *J* = 13.7, 9.3, H_k), 1.64–1.51 (m, 4H, H_o + H_v), 1.46–1.12 (m, 12H, H_p + H_q + H_r + H_s + H_t + H_u), 1.04 (s, 9H, H_{ii}); ^{13}C NMR (125 MHz, 1:1 $CD_3OD/CDCl_3$): δ = 168.0 (×2), 167.5, 167.4, 166.8, 166.6, 166.5, 166.4, 166.1, 165.9, 138.0, 136.6, 132.4 (×2), 130.2, 130.1, 129.8 (×3), 129.7, 129.5, 129.0, 128.7 (×3), 128.6, 128.5, 127.6, 126.4, 125.2, 71.1, 69.6, 59.3, 54.4, 52.6, 52.3, 51.3, 49.7, 44.5 (×3),

44.4, 44.3, 44.2, 43.1, 43.0, 40.6, 40.5, 30.3, 30.4, 30.0, 27.8, 27.3, 24.5, 20.5, 19.8. LR-MS (ESI): m/z 922 $[M+2H]^{2+}$; observed peaks consistent with theoretical isotope pattern.

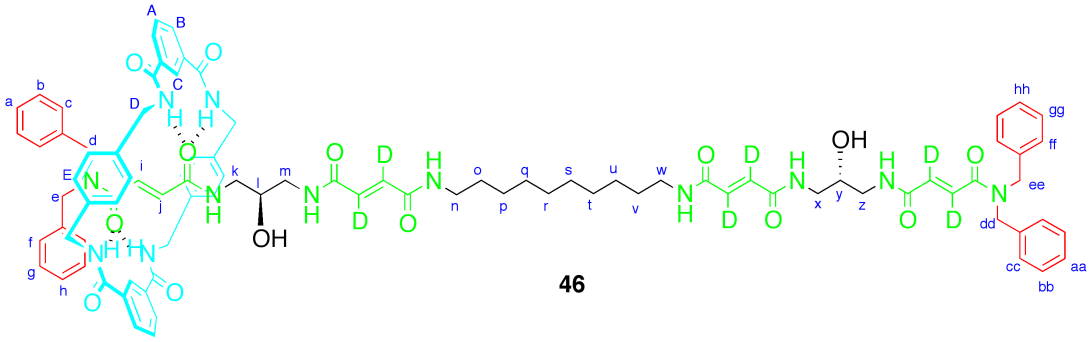

46

To a stirred solution of **48** (82 mg, 39 μmol) in DCM (0.39 mL) was added HF·py (0.52 mL of a 70% in pyridine solution) and the mixture was stirred for 16 h, then cooled to 0 °C and diluted with DCM (10 mL). TMSOMe (4.8 mL) was added followed by HCl (1 M, 10 mL), and the mixture was extracted into 3:1 $CHCl_3$/IPA (3 × 30 mL). The combined organic fractions were dried over $MgSO_4$ and concentrated under reduced pressure. Flash chromatography (neat EtOAc, then 6:1 DCM/MeOH) gave diol rotaxane **46** as a colourless solid (53 mg, 84%). M.p. 154–155 °C. ^{1}H NMR (400 MHz, 1:1 $CD_3OD/CDCl_3$): δ = 8.77 (s, 2H, H_C), 8.31 (dd, 4H, *J* = 7.8, H_B), 7.78 (t, 2H, *J* = 7.7, H_A), 7.59–7.45 (m, 6H, H_a + H_b + H_{gg} + H_{hh}), 7.45–7.29 (m, 10H, H_f, H_g, H_h, H_{aa}, H_{bb}, H_{cc}), 7.27–7.11 (m, 12H, H_E + H_c + H_{ff}), 7.11–6.74 (m, 2H, H_i + H_j), 4.55 (s, 8H, H_d + H_e + H_{dd} + H_{ee}), 4.32 (s, 4H, H_D)4.11–3.93 (m, 2H, H_l + H_y), 3.53–3.21 (m, 12H, H_k + H_m + H_n + H_w + H_x + H_z), 1.79–1.63 (m, 4H, H_o + H_v), 1.54–1.40 (m, 12H, H_p + H_q + H_r + H_s + H_t + H_u); ^{13}C NMR (125 MHz, $CDCl_3$): δ = 167.7, 166.9, 166.8, 166.7, 166.3, 165.7, 137.7, 137.6, 136.9, 136.1, 135.1, 134.2, 132.1, 129.9, 129.7 (×3), 129.6, 129.5, 129.3, 129.1, 128.7, 128.5 (×3), 128.3, 127.3, 126.9, 125.0, 69.4, 66.5, 44.3, 44.0, 43.9, 20.3, 30.2, 29.9, 29.7, 29.6, 27.4. LR-MS (ESI): m/z = 803 $[M+2H]^{2+}$; HR-MS (ESI): m/z = 803.4075 $[M+2H]^{2+}$ (calculated for $C_{92}H_{98}N_{12}O_{14}$ = 803.4080).

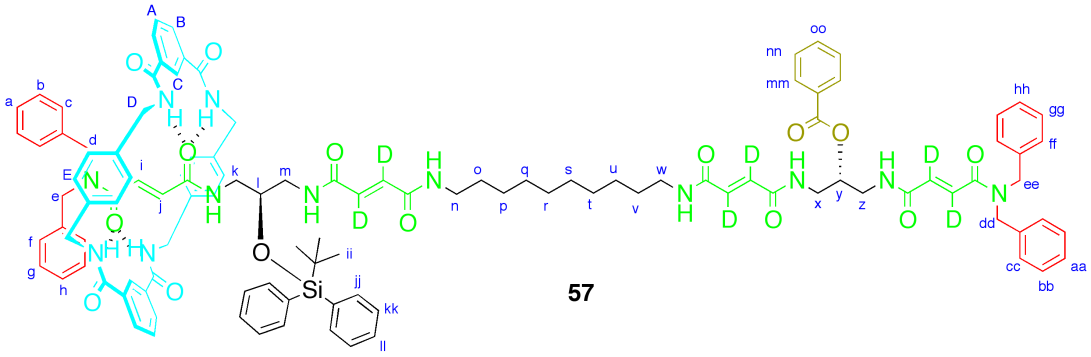

57

To a stirred solution of **48** (164 mg, 89 µmol), DMAP (5 eq, 444 µmol, 54 mg) and triethylamine (5 eq, 444 µmol, 62 mg) in DCM (9 mL) was added benzoyl chloride (5 eq, 444 µmol, 62 mg). After 2 h the mixture was concentrated under reduced pressure. Preparative TLC (5% MeOH in DCM) afforded **57** as a colourless solid (52 mg, 30%). M.p. 122–123 °C. $[\alpha]_D^{20}$ = +16.0 (c = 0.15, DCM). ^{1}H NMR (500 MHz, 1:1 $CD_3OD/CDCl_3$): δ = 8.45 (s, 2H, H_C), 8.16 (t, 4H, *J* = 7.3, H_B), 8.01 (d, 2H, *J* = 7.2, H_{nn}), 7.69–7.58 (m, 6H, H_A + H_{kk}), 7.58–7.50 (m, 1H, H_{oo}), 7.45–7.06 (m, 26H, H_a + H_f + H_g + H_h + H_{aa} + H_{bb} + H_{cc} + H_{ff} + H_{gg} + H_{hh} + H_{jj} + H_{ll} + H_{mm}), 7.02 (t, 2H, *J* = 7.5, H_b), 6.83 (d, 4H, J = 7.9, H_E), 6.77–6.58 (m, 6H, H_E + H_c), 5.91–5.81 (m, 2H, H_i + H_j), 5.27 (p, 1H, *J* = 5.5, H_y), 4.68–3.96 (m, 16H, H_D + H_d + H_e + H_{dd} + H_{ee}), 3.78 (td, 1H, *J* = 8.3, 3.8, H_l), 3.72–3.53 (m, 4H, H_x + H_z), 3.49–3.35 (m, 5H, H_k + H_m + H_w), 3.25 (t, 2H, *J* = 7.1, H_n), 2.81 (dd, 1H, *J* = 13.3, 9.4, H_k), 1.62 (dt, 2H, *J* = 14.5, 7.2, H_v), 1.57–1.44 (m, 2H, H_o), 1.44–1.26 (m, 12H, H_p + H_q + H_r + H_s + H_t + H_u), 1.04 (s, 9H, H_{ii}); ^{13}C NMR (125 MHz, 1:1 $CD_3OD/CDCl_3$): δ = 167.7, 167.6, 167.3, 167.0 (×2), 166.6, 166.3, 166.2, 165.7, 165.4, 137.7, 137.6, 136.9 (×2), 136.4, 136.3 (×2), 135.9, 134.3 (×2), 134.2, 133.9, 133.7, 133.3, 133.1 (×2), 132.3, 132.2, 132.1, 132.0, 130.8, 130.3, 130.0, 129.7, 129.6, 129.5, 129.3 (×2), 128.9, 128.7, 128.5 (×2), 128.4, 128.3, 127.3 (×2), 126.9, 126.1, 124.7, 72.3, 70.8, 52.1, 52.0, 44.1 (×2), 42.1, 40.9, 40.4, 40.3, 32.5, 30.3, 30.0, 30.0, 29.8 (×2), 29.6 (×2), 27.5, 27.2, 19.6, 14.2. LR-MS (ESI): m/z 975 $[M+2H]^{2+}$; HR-MS (ESI): m/z = 974.9808 $[M+2H]^{2+}$ (calculated for $C_{115}H_{120}D_6O_{15}N_{12}Si$ = 974.9815).

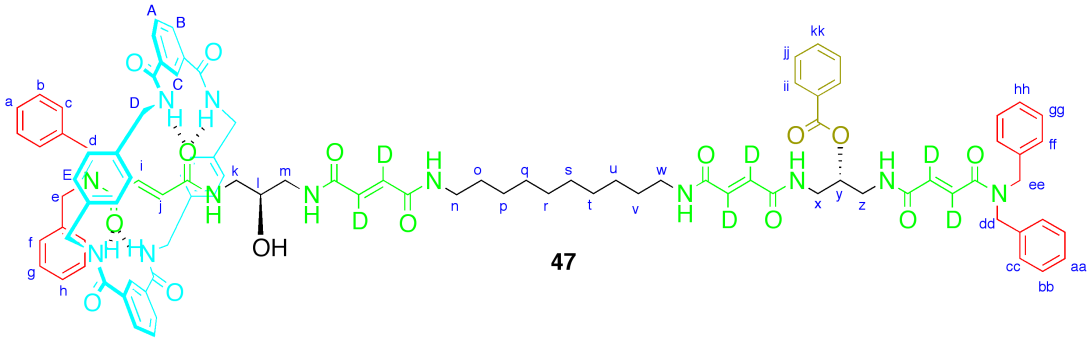

47

To a stirred solution of **57** (47 mg, 24 μmol) in DCM (620 μL) was added HF·py (200 μL of a 70% in pyridine solution) and the mixture was stirred for 16 h, then cooled to 0 °C and diluted with DCM (2 mL). TMSOMe (1.5 mL) was added followed by HCl (1 M, 10 mL), and the mixture was extracted into 3:1 $CHCl_3$/IPA (3 × 5 mL). The combined organic fractions were dried over $MgSO_4$ and concentrated under reduced pressure. Purification by preparative TLC (EtOAc) gave mono-benzoylated rotaxane **47** as a colourless solid (27 mg, 66%). M.p. 157 °C. $[\alpha]_D^{20}$ = +28.0 (c = 0.50, 1:1 CD_3OD:$CDCl_3$). ^1H NMR (400 MHz, 1:1 CD_3OD/$CDCl_3$): δ = 8.60 (s, 2H, H_C), 8.13 (dd, 4H, *J* = 7.8, 1.6, H_B), 8.00 (d, 2H, *J* = 7.2, H_{jj}), 7.64–7.49 (m, 4H, H_A + H_{ii}), 7.37–7.10 (m, 20H, H_a + H_b + H_f + H_g + H_h + H_{aa} + H_{bb} + H_{cc} + H_{ff} + H_{gg} + H_{hh} + H_{kk}), 7.08–6.97 (m, 8H, H_E), 6.95–6.85 (m, 2H, H_c), 6.53 (dd, 2H, *J* = 60.7, 14.5, H_i + H_j), 5.30–5.21 (m, 1H, H_y), 4.59–4.11 (m, 16H, H_D + H_d + H_e + H_{dd} + H_{ee}), 3.86 (m, 1H, H_l), 3.69–3.45 (m, 8H, H_k + H_m + H_x + H_z), 3.20 (dd, 4H, *J* = 7.2, 14.4, H_n + H_w), 1.57–1.44 (m, 4H, H_o + H_v), 1.37–1.22 (m, 12H, H_p + H_q + H_r + H_s + H_t + H_u); ^{13}C NMR (125 MHz, $CDCl_3$): δ = 167.9 (×2), 167.1 (×2), 166.9, 166.8 (×2), 166.5, 166.3, 166.0, 165.9 (×3), 137.8, 137.7, 137.0, 136.5, 136.0, 134.9, 134.4, 134.0, 132.1, 130.4, 130.3, 129.9, 129.8, 129.6 (×2), 129.5, 129.4 (×2), 129.0 (×2), 128.8, 128.6 (×3), 128.3, 127.4, 126.8, 125.3, 72.6, 69.4, 51.7, 51.0, 50.7, 49.6, 49.5 (×2), 49.3, 44.4, 44.2, 44.0, 41.1 (×3), 41.0, 30.2, 30.0, 29.8, 29.7, 27.6. LR-MS (ESI): m/z = 974 $[M+2H]^{2+}$; observed peaks consistent with theoretical isotope distribution.

3.10.1 General Method for the Operation of 46

To a stirred suspension of diol **46** (4 mg, 2.50 μmol) in DCM (0.25 mL) was added catalyst (4 eq, 10.0 μmol), triethylamine (4 eq, 10.0 μmol, 1.36 mg) and benzoyl chloride (4 eq, 10.0 μmol, 1 mg). After 1 h the reaction mixture was concentrated under reduced pressure and triturated with Et_2O (1 × 2 mL). Residual Et_2O was removed under reduced pressure and the entire crude mixture was dissolved in DMSO-d_6 for analysis by NMR spectroscopy.

3.10.2 General Method for the Operation of 47

The method used in the previous Chapter was followed. To a stirred suspension of mono-benzoylated rotaxane **47** (5.6 mg, 3.3 μmol) in DCM (0.33 mL) was added catalyst (2 eq, 6.6 μmol), triethylamine (2 eq, 6.6 μmol, 0.66 mg) and benzoyl chloride (2 eq, 6.6 μmol, 0.92 mg). After 1 h the reaction mixture was concentrated under reduced pressure and triturated with Et_2O (1 × 2 mL). Residual Et_2O was removed under reduced pressure and the entire crude mixture was dissolved in DMSO-d_6 for analysis by NMR spectroscopy.

3.11 References and Notes

1. Alvarez-Pérez, M.; Goldup, S. M.; Leigh, D. A.; Slawin, A. M. Z. A chemically-driven molecular information ratchet. *J. Am. Chem. Soc.* **2008**, *130*, 1836–1838.

2. "Extensibility". In *A Dictionary of Computing*; Daintith, J.; Wright, E., Eds.; Oxford University Press: Oxford, United Kingdom, 2008.

3. Ghanem, M. A.; Chretien, J.-M.; Pinczewska, A.; Kilburn, J. D.; Bartlett, P. N. Covalent modification of glassy carbon surface with organic redox probes through diamine linkers using electrochemical and solid-phase synthesis methodologies. *J. Mater. Chem.* **2008**, *18*, 4917–4927.

4. Niwayama, S. Highly efficient selective monohydrolysis of symmetric diesters. *J. Org. Chem.* **2000**, *65*, 5834–5836.

5. Neglecting deuterium, which has been shown by Leigh and coworkers in 2008 (see *Ref.* 1) not to noticeably affect the directional discrimination in information ratchets.

6. Lane, A. S.; Leigh, D. A.; Murphy, A. Peptide-based molecular shuttles. *J. Am. Chem. Soc.* **1997**, *119*, 11092–11093.

Chapter Four

Progress Towards Highly Extended Information Ratchets

Acknowledgements

Miriam Wilson, Dr Jordi Solà are gratefully acknowledged for their assistance in the preparation of compounds **68** and **73** and the large-scale preparation of several building blocks whose syntheses were developed in previous Chapters. MALDI mass spectrometry was performed by Dr Logan Mackay. Dr Craig Robertson is gratefully acknowledged for his examination and proofreading of this Chapter.

Synopsis

Having established a general theory for the operation of a class of linear molecular information ratchets, the task now becomes extending the technology to operate over increasingly large distances. Much promise was shown by the work of the previous Chapter, in which the incorporation of an alkyl spacer successfully offset the solubility penalty for adding an extra fumaramide binding site. A four-gate, five-compartment rotaxane was designed as a candidate information ratchet system.

The synthesis initially showed promise. However, as the precursors' size increased, so did their properties as gelators, and their solubility in organic solvents decreased rapidly. In the final stages of the synthesis these problems became insurmountable, necessitating a redesign. Work on a three-gate, four-compartment molecule proceeded more smoothly, and although the final steps were costly, the synthesis was successfully completed. Operation and characterisation of this rotaxane is ongoing in our research group, but the early indications are that the molecule does indeed function as an information ratchet, and that directional transport is achieved over long distances on the molecular level.

4.1 Introduction

The work of the previous Chapters has been to increase the distance over which a rotaxane-based molecular machine may transport its Brownian macrocycle by using an information ratchet mechanism. Along the way, discoveries have been made which have shed much light on the way in which these molecular machines function. In the course of this investigation, the question that arose was: how far could this technology be pushed? Would it be possible to construct longer or perhaps even polymeric rotaxanes, with multiple repeat units and sites of directional discrimination, that are capable of long-distance directional transport?

As an important milestone in the construction of increasingly powerful linear information ratchets, an ambitious new target was proposed: a five-compartment linear information ratchet (Figure 4.1).

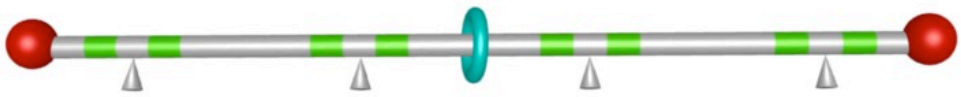

Figure 4.1 Cartoon representation of an unprotected four-gate, five-compartment information ratchet.

The molecule envisaged would be able to directionally transport a Brownian macrocycle over five compartments representing three chemically different environments. Alkyl spacers incorporated into the thread would serve to offset the solubility penalty for the extra binding sites, an effect demonstrated in the previous Chapters. The use of four chiral repeat units would also have interesting implications for the notion of cumulative transport, as shown schematically in Scheme 4.1.

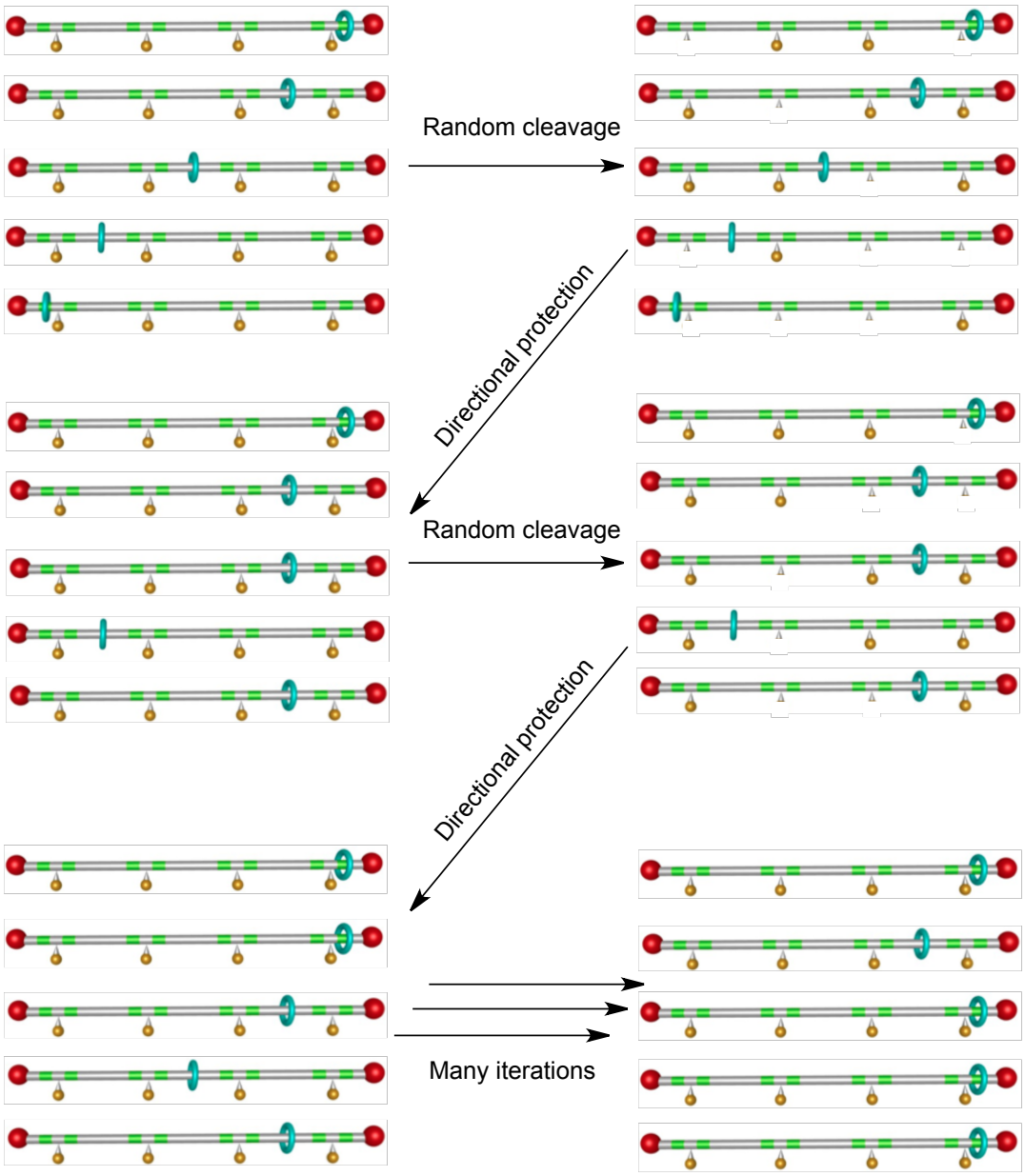

Scheme 4.1 Starting from a pure starting material (*top left*), it is possible to drive the population of macrocycles cumulatively to the right by successive cycles of random partial deprotection followed by total reprotection with directional discrimination. Because retrograde motion of the macrocycle is prohibited by this peristaltic mechanism, the transport efficiency after several operations is likely to be greater than what would have been obtained had all the protecting groups been removed at once, and then reprotected in one step.

In Scheme 4.1, a form of stochastic pumping[1] is used to drive the population of macrocycles to the right. The starting state in the top left corner has the entire population of macrocycles locked into the leftmost compartment. Cleavage of some fraction of the protecting groups (say, 50%) will randomly liberate some

of the macrocycles to further shuttling, giving them an opportunity to move one or more compartments to the right under chiral protection conditions. Successive cycling of these two steps (random cleavage, directional protection) in a manner strongly reminiscent of a peristaltic pump will result in enrichment of the population of macrocycles in the rightmost compartment.

This kind of cumulative work could never be realised in a simple two-compartment system, because cleavage of a rotaxane's sole protecting group would effectively return that rotaxane to its starting state.[2] While a two-gate, three-compartment system could in principle be used as a substrate, there are practical limitations to how well the effect would be expressed. However many cycles of operation are used, the maximum amount of macrocycle that can be transported to the rightmost compartment is given by the effectiveness of directional discrimination at the rightmost chiral centre. This effectiveness has already been quantified in Chapter Two for the short three-compartment system **25** and in Chapter Three for a three-compartment system incorporating an alkyl spacer **46**. The maximum efficiency attainable by these systems is the ratio given by the single benzoylation of mono-benzoylated rotaxanes **26** and **47** using chiral catalysts. In these experiments, the entire population of macrocycles is forced to choose between the terminal compartment and the one adjacent to it; this is exactly equivalent to the theoretical end-point of a cleavage/reprotection cycling process on these systems.

Successive operations of the previous Chapter's system would have a theoretical ceiling of *left*/*centre*/*right* 0:18:82, a ratio that is not much of an improvement over the value of 0:23:77 attainable through a simple double benzoylation. Chapter Two's system might do better: many operations would be expected to drive the ratio from 0:21:79 to as much as 0:4:96, but even this represents a movement of only 17% of the macrocycles after several cycles. A further complication that counts against using these systems as substrates is that multiple deprotections on the thread might in some instances allow the

macrocycle to slip backwards. This makes the theoretical best-case scenario, in which the entire population of macrocycles is forced to choose between only the two rightmost compartments, less likely to occur even under ideal conditions. The theoretical upper bound for successful cumulative transport in these two-compartment systems is likely to be somewhat lower than stated for this reason; how much lower depends on the fraction of protecting groups cleaved.

For these reasons, in order for the full potential of cumulative directional transport to be realised, a rotaxane with more than three compartments must be synthesised. While a four-compartment system was a desirable target, the number of unique chemical environments experienced by the macrocycle would still only be two (a terminal-compartment environment and a non-terminal compartment environment). Increasing the number of compartments from four to five immediately adds an extra environment (a distinct central compartment) with what was expected to be only a small increase in synthetic effort. The directional transport of a macrocycle across a landscape of three distinct binding environments would be an important demonstration of the robustness and universality of these extended information ratchet systems.

As a test substrate for such exciting potential uses, the synthesis of the five-compartment system was undertaken.

4.2 First Design

The design of the five-compartment system builds on the work described in the previous Chapter; it simply extends diol rotaxane **46** to include two extra repeat units, each repeat unit bearing a chiral centre surrounded by two fumaramide residues and an alkyl spacer to increase solubility (Figure 4.2).

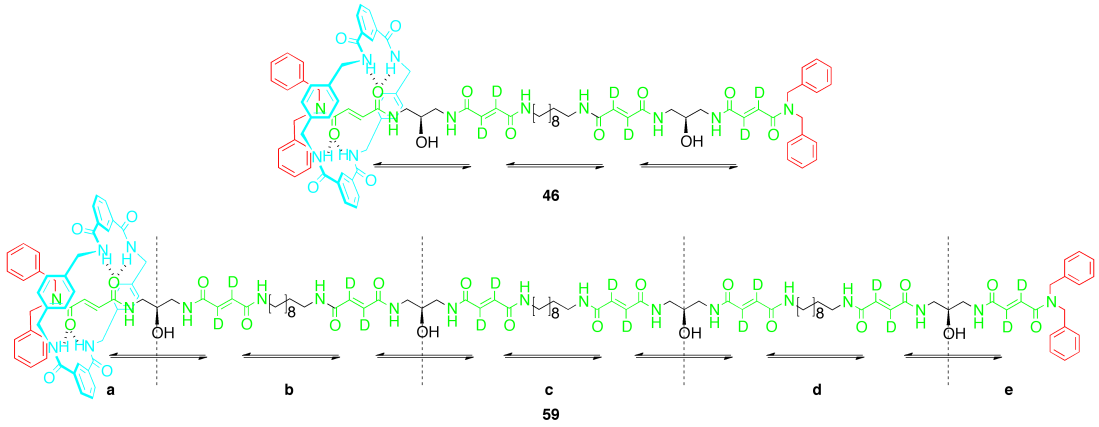

Figure 4.2 Adding two repeat units to **46** affords **59**, a five-compartment molecular information ratchet. Equilibrium arrows denote macrocycle shuttling.

Several features of **59** are worthy of consideration. Firstly, the four chiral carbon each have an absolute configuration of (*R*).[3] However, it is the chirality of the carbon-atom/macrocycle complex that determines the direction of transport, and not the chirality of the carbon atom in isolation. A macrocycle on one side of the chiral centre is chemically different from a macrocycle on the other side in a chiral environment, and a chiral catalyst can be expected to acylate the hydroxyl groups at different rates depending on the position of the macrocycle. The residues from the chiral building blocks have been arranged in such a way that the macrocycle always encounters the same local configuration of atoms when it encounters a prochiral centre. As a result the local expression of chirality is constant, ensuring that the directional movement caused by

benzoylation with a chiral catalyst will always occur in the same direction, irrespective of which compartment the macrocycle happens to be in.

A second consideration is that the quadruple benzoylation of **59** is expected to give, not three, but *five* kinetically locked positional isomers **60a–e**, as shown in Scheme 4.2. Some of these positional isomers are expected to be inseparable (**60a** from **60e**, **60b** from **60d**) and others indistinguishable (**60b** from **60c** and **60d**), by most analytical techniques. It is not necessary, however, for the exact distribution of macrocycles over the thread to be known before declaring the rotaxane a successful information ratchet. Instead, we will concern ourselves with the efficiency of delivery to the terminal compartments. This figure will be given by the integration of the NMR signals for the fumaric protons that are shielded by the macrocycle. If different enantiomers of the catalyst generate products with significantly different amounts of macrocycle in the nondeuterated (leftmost) compartment, an information ratchet mechanism will have been demonstrated. Additionally, in order to show that cumulative work has been done by a partial deprotection/reprotection cycle, it will be necessary only to observe an increase in the occupancy of the destination compartment, again easily quantifiable by NMR spectroscopy.

In Scheme 4.2, quadruple benzoylation of **59** is shown to generate a mixture of five positional isomers. As in earlier Chapters, the efficiency of the machine will be determined by examining the composition of the mixture. Because of the expected difficulties of separating and distinguishing the different positional isomers, our knowledge of the precise composition of the product mixture is likely to be incomplete. Analysis by NMR spectroscopy will allow the accurate determination of the absolute amounts of **60a** and **60e** by comparing them to an internal standard on the molecule, perhaps the macrocyclic *C* protons. The sum of **60a** and **60e** will be given by the amount of shielding of the stopper protons when the macrocycle is in the terminal compartments, and the difference between **60a** and **60e** will be given by the degree of shielding of the two fumaric

protons in **60a** (a deuterated fumaramide group will be shielded instead in **2e**). The relative amounts of **60b**, **60c** and **60d** will be difficult to assess, however, because of the likely similarity between these compounds' spectra. While the earlier machines' success was measured by examining the distribution of the macrocycle over the whole of the thread, the metric by which this system's usefulness is measured will be the transport efficiency: the percentage of macrocycle that is successfully directed into that terminal compartment specified by the handedness of the catalyst employed.

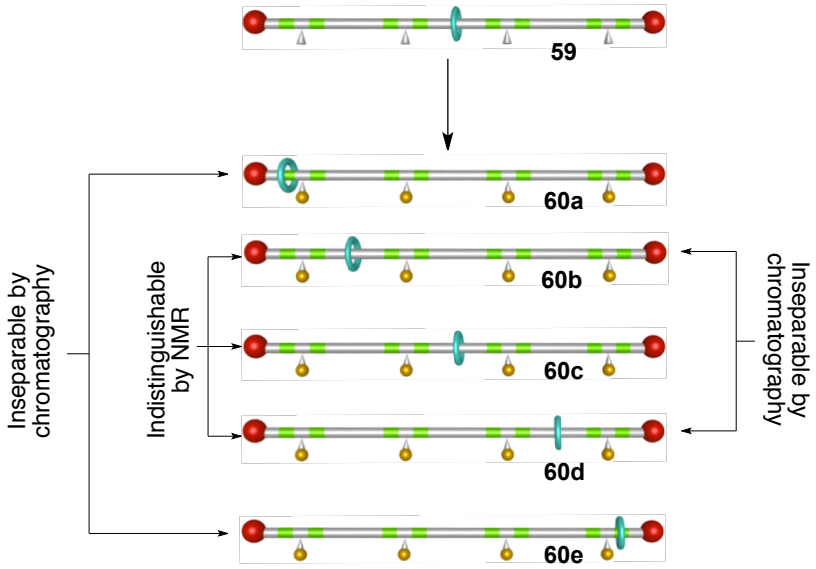

Scheme 4.2 Quadruple benzoylation of **59** is expected to yield five positional isomers **60a–e**. Isomers **60b** and **60d** will be inseparable by chromatographic techniques and indistinguishable by NMR; isomers **60a** and **60c** will likewise be inseparable, but may be distinguished from one another by the use of deuterium labelling.

One final consideration is that the tool for mathematical analysis used in the three-compartment systems – the Markov chain – will probably not be used here. This results from two factors: firstly, our likely ignorance of the exact distribution of macrocycles over the central part of the thread; and secondly, the increased complexity of the system, which will make the number of transitions to be calculated very large. In these information ratchet systems, the number of transitions (whose values are not automatically 100%) is equal to $G \times 2^G$, where G is the number of gates (hydroxyl groups); for systems with increasingly large

numbers of gates, the number of transitions rapidly becomes enormous. These problems are theoretically surmountable by synthesising every possible intermediate and performing many experiments to determine ratios at every stage, but this would impracticable in the time available.

Despite these limitations on our likely understanding of the internal mechanisms of a five-compartment system, extended systems like **59** are important test substrates for long-distance directional transport; they also afford a possible means by which *cumulative* work of the kind demonstrated in Scheme 4.1 could be done. By monitoring the number of macrocycles in the leftmost, nondeuterated compartment, the efficiency of delivery could be easily quantified both for a single operation and over a number of deprotection/ reprotection cycles.

4.3 Retrosynthesis

Although it is a much larger molecule than those presented in earlier Chapters, the target molecule **59** was designed according to the principle of extensibility introduced in Chapter Three, and was consequently highly modular. The structure could be broken down into a number of shared building blocks which, once prepared in sufficient quantity, might be combined in a number of possible ways. This left the synthetic strategy rather open.

As illustrated in Scheme 4.3, information ratchet rotaxane **59** was to be constructed from four simple molecules already prepared in the synthesis of earlier systems – **28**, **54**, **51** and **32**. These starting materials could be joined in various combinations *via* standard peptidic coupling reactions to give the three

precursors **49**, **62** and **63** shown in square brackets. The decision to divide the target molecule into three similarly-sized parts in this way was intended to avoid solubility problems by keeping the intermediates functionally simple for as long as possible. Nevertheless, it was understood at the outset that the modularity of the design afforded many routes to the production of **59**, and that the synthesis was flexible enough for these intermediates to be bypassed by following an alternative path if they proved difficult to make. The approach proposed in Scheme 4.3 has the additional advantage that the synthesis of the left third of the molecule, rotaxane **49**, has already been explored and optimised in the previous Chapter.

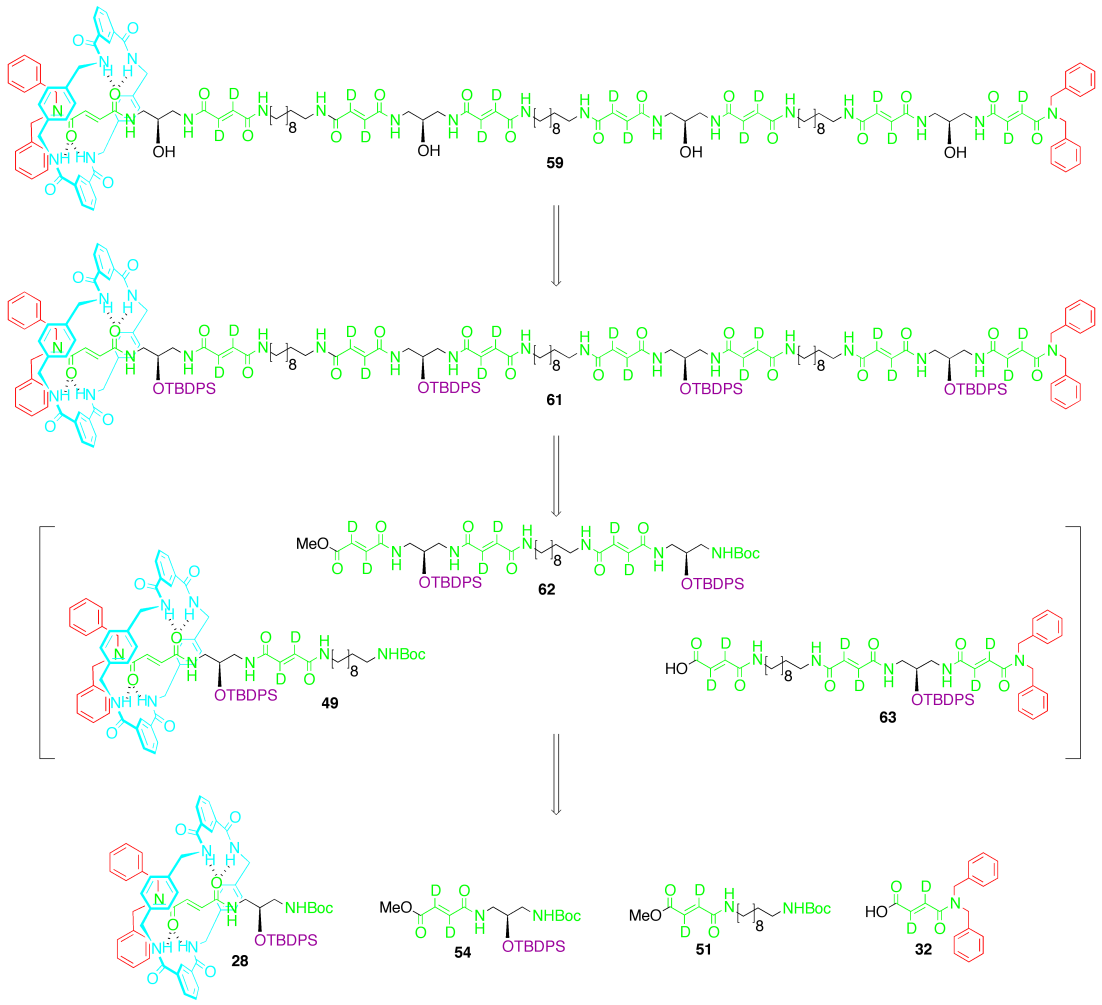

Scheme 4.3 Retrosynthetic analysis of **59**.

Several synthetic steps were eliminated by the decision not to cleave silyl groups individually as they are introduced, but to leave them in place until the end. Retention of the TBDPS groups was also expected to increase the solubility of the intermediates. As a consequence of this decision, the final step of the synthesis would be a quadruple desilylation reaction in the presence of a fluoride source, perhaps TBAF but more probably HF as a solution in pyridine, as difficulties have been encountered removing TBAF salts from the products of related reactions (see Chapter Two).

4.4 Synthesis

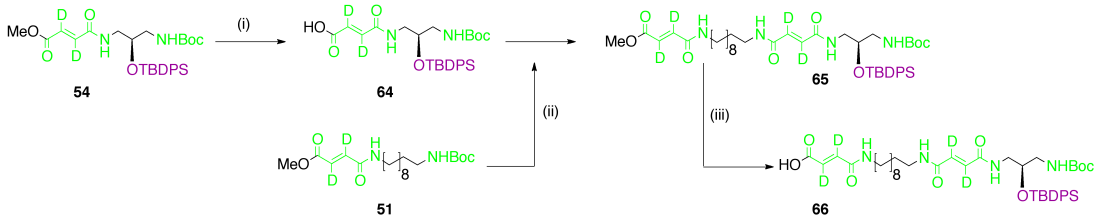

Scheme 4.4 (i) LiOH·H_2O, 3:1 THF/H_2O, rt, 1 h, *quant.*; (ii) (a) TFA, DCM, rt, 16 h, *quant.*; (b) **51**, TBTU, HOBt, DIPEA, DMF, 16 h, 0 °C to rt, 80%; (iii) LiOH·H_2O, 3:1 THF/H_2O, rt, 1 h, *quant.*

Chiral building block **54** was saponified under standard conditions and quantitatively furnished acid **64**. This was destined to be coupled to the deprotected amine form of spacer unit **51**, but this deprotection reaction was initially rather problematic. The Boc group was removed by stirring in a loosely-sealed vessel with a mixture of 4:1 DCM/TFA overnight at room temperature, and both TLC and mass spectrometry confirmed that the reaction had proceeded cleanly; unfortunately the standard work-up procedure (dilution with 1 M aqueous sodium hydroxide until basic, then extraction into an organic

solvent) led to decomposition of the product. This problem was overcome by eliminating the aqueous work-up altogether: removal of the DCM/TFA mixture by coevaporation with toluene under reduced pressure afforded the TFA salt of the desired amine. No decomposition was observed by mass spectrometry or NMR spectroscopy. The subsequent coupling with **64** was performed with a higher excess of DIPEA than usual (3 equivalents rather than the normal 1.2) to free the amine for the reaction. The peptidic coupling proceeded smoothly, affording **65** in 80% yield. This important synthetic intermediate represents the repeat unit in **59**, bearing both a Boc-protected amine and a carboxylic acid masked as a methyl ester – two different handles for extension. The acid **66** was prepared from **65** by a one-hour saponification reaction under standard conditions.

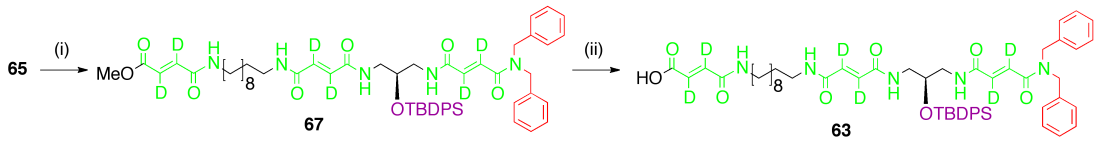

Scheme 4.5 (i) (a) Repeat unit **65**, TFA, DCM, rt, 16 h, *quant.*; (b) Acid **32**, TBTU, HOBt, DIPEA, DMF, 16 h, 0 °C to rt, 60%; (ii) $LiOH{\cdot}H_2O$, 3:1 THF/H_2O, rt, 1 h, *quant.*

The next stage of the synthesis made use of **65**'s other synthetic handle, the Boc-protected amine. The Boc group was cleaved with TFA in DCM as before, and coupled, as a TFA salt, with the bulky stopper group **32** (the synthesis of which is described in Chapter Two). The coupling reaction furnished **63** in a moderate yield, which was then saponified over the course of an hour to complete the right third of the target molecule, acid **63**, in quantitative yield.

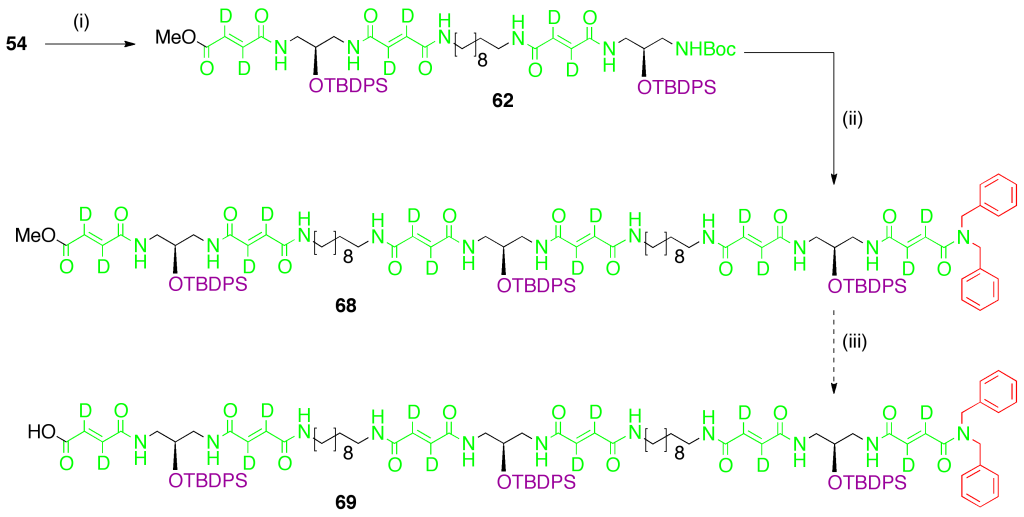

Scheme 4.6 (i) (a) TFA, DCM, 16 h, *quant.*; (b) Acid **66**, TBTU, HOBt, DIPEA, DMF, 16 h, rt, 50%; (ii) (a) TFA, DCM, TIPS, 40 min; (b) Acid **32**, TBTU, HOBt, DIPEA, DMF, 16 h, 0 °C to rt, 26% (over 2 steps); (iii) $LiOH{\cdot}H_2O$, DMSO, rt, 24 h, trace.

Fragment **54** was treated with a TFA/DCM mixture to cleave the Boc group, and the resulting primary amine used without purification in a coupling reaction with acid **66** to give the middle module **62**. This reaction did not proceed smoothly. As these molecules' length increased, so did their tendencies to act as powerful organogelators. Often the reaction mixture would form a gel as soon as the acid and amine shared a flask; at other times no gelation was initially observed, but after leaving overnight the mixture was so viscous the stirrer bar was unable to rotate. It was found that performing the reaction at higher dilution and without the usual cooling helped to an extent, but yields were poor; the molecules' low solubility also served to make both the work-up and purification by column chromatography challenging.

Once the central module **62** had been obtained, the next step was to cleave the Boc group and couple the resulting amine to module **32**. As usual, the initial approach in cleavage of the Boc group was to dissolve the compound in 4:1 DCM/TFA in a loosely-sealed vessel and leave the reaction stirring overnight. This procedure, however, led to decomposition of **62**. On investigation by NMR spectroscopy and mass spectrometry, the decomposition product was shown to

be the result of a desilylation: the TFA had cleaved the TBDPS group while leaving Boc group untouched. This was a surprise as both the protecting group literature and our own experience with these groups led us to think the desilylation reaction was unlikely; nevertheless, precedents were found to exist.[4]

Fortunately, mass spectrometry also indicated that there existed at least some of the desired product, suggesting that the Boc cleavage and the desilylation were occurring simultaneously. This prompted an attempt to accelerate the Boc removal over the desilylation by adding the cation scavenger TIPS.[5] After 40 minutes the reaction was halted by removal of the solvent by coevaporation with toluene under reduced pressure and TIPS was removed by trituration with hexane. Evidence from NMR spectroscopy confirmed that the Boc group had been cleaved with negligible loss of TBDPS. The resulting amine was used without purification for the next step: coupling the middle module to acid **32**. As for the previous coupling, a combination of low solubility and powerful gelation effects reduced the yield significantly. Amide **68**'s excellent properties as an emulsifier made the work-up of the coupling difficult. Purification was achieved in the first instance by centrifugation in 1:1 DCM/methanol, exploiting the fact that **68** was most likely to be the least soluble substance in the flask; this was followed by purification by preparative TLC which afforded **68** in a disappointingly low yield of 26%.

Amide **68** was found to insoluble in most organic solvents, to the extent that the NMR spectra used to confirm purity could be taken only in DMSO-d_6. Unfortunately **68** also proved insoluble in the 3:1 THF/water mixture used for saponification reactions, and no saponified product **69** was detected even after stirring for several days (for more soluble compounds, these reactions complete after approximately 40 minutes). A number of different solvents and stoichiometries to use for the reaction were screened. At best, only trace amounts of conversion to product was observed using when using DMSO as a

solvent, even with a great excess of lithium hydroxide and extending the reaction time to over 48 hours. While the product was faintly detectable by mass spectrometry, NMR spectroscopy indicated that the reaction was far from complete.

With **68** so insoluble in both organic and aqueous solvents, there seemed little hope that the carboxylic acid **69** would be any easier to work with even if it were able to be isolated. Since the synthetic route would then require a peptidic coupling to another large moiety containing even more hydrogen bond donors and acceptors – to be followed, still, by a quadruple desilylation that would only increase the hydrogen bonding potential – it became obvious that the target molecule was beyond our abilities to make. Consequently the synthesis of the five-compartment rotaxane **59** was put on hold indefinitely pending a rethink of the design.

4.5 Second Design

The synthesis of the five-compartment information ratchet was abandoned for reasons of solubility. The introduction of alkyl spacers did increase the solubility of many of the precursors encountered in the synthesis; nevertheless, it was not enough to enable the system to be extended indefinitely. An increase in length still incurred a decrease in solubility, and although the severity of the gradient had been noticeably lessened, solubility still defined the limit of how long these systems can be.

While we were unsuccessful in producing a five-compartment rotaxane, there was still a chance that a *four*-compartment system would be short enough, and

carry sufficiently few hydrogen bond donors and acceptors, to avoid the gelation problems that halted the synthesis of **59**. The attempt to synthesise the five-compartment system furnished us with a number of useful building blocks that would dramatically reduce the synthetic effort for this system. The design of the four-compartment system is shown in Figure 4.3.

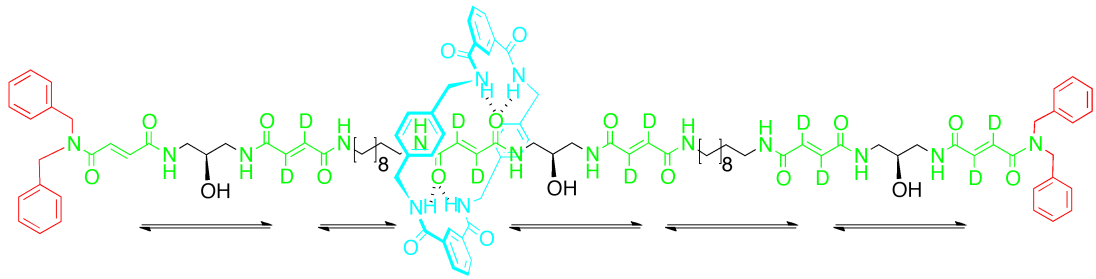

70

Figure 4.3 Four-compartment molecular information ratchet **70**.

The proposed ratchet **70** is based on the five-compartment one; it merely makes use of one fewer repeat unit. As in the previous system, the macrocycle's position will only be known exactly when it is close enough to disrupt the NMR signals for the stopper protons (positional isomers **71a** and **71d**). The fumaric protons in **71a** will be shielded by the macrocycle, allowing the relative quantities of **71a** and **71d** to be determined in the product mixture. The relative quantities of **71b** and **71c** are not expected to be assignable because they will not be sufficiently distinguishable either by spectroscopy or by chromatography (they are enantiomers if the deuterium atoms are discounted, however, and in principle may be resolved by chiral HPLC).

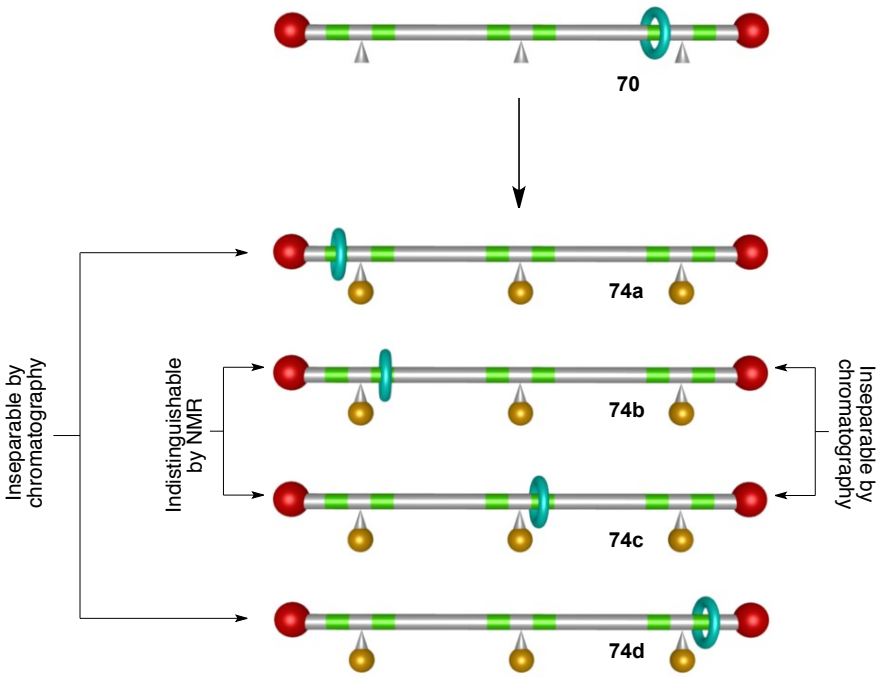

Scheme 4.7 Triple benzoylation of **70** is expected to generate four positional isomers **71a–d**, two of which will be indistinguishable by NMR spectroscopy and inseparable by chromatography.

4.6 Retrosynthesis

The retrosynthesis of **70** is shown in Scheme 4.8. The building blocks common to the synthesis of the five-compartment rotaxane offered a number of possible retrosyntheses. The route selected disconnected **70** into two fragments of similar size. Rotaxane **73** was reachable in one step from previously synthesised precursors **28** and **65**. Acid **63** had already been produced in the synthesis of the five-compartment system.

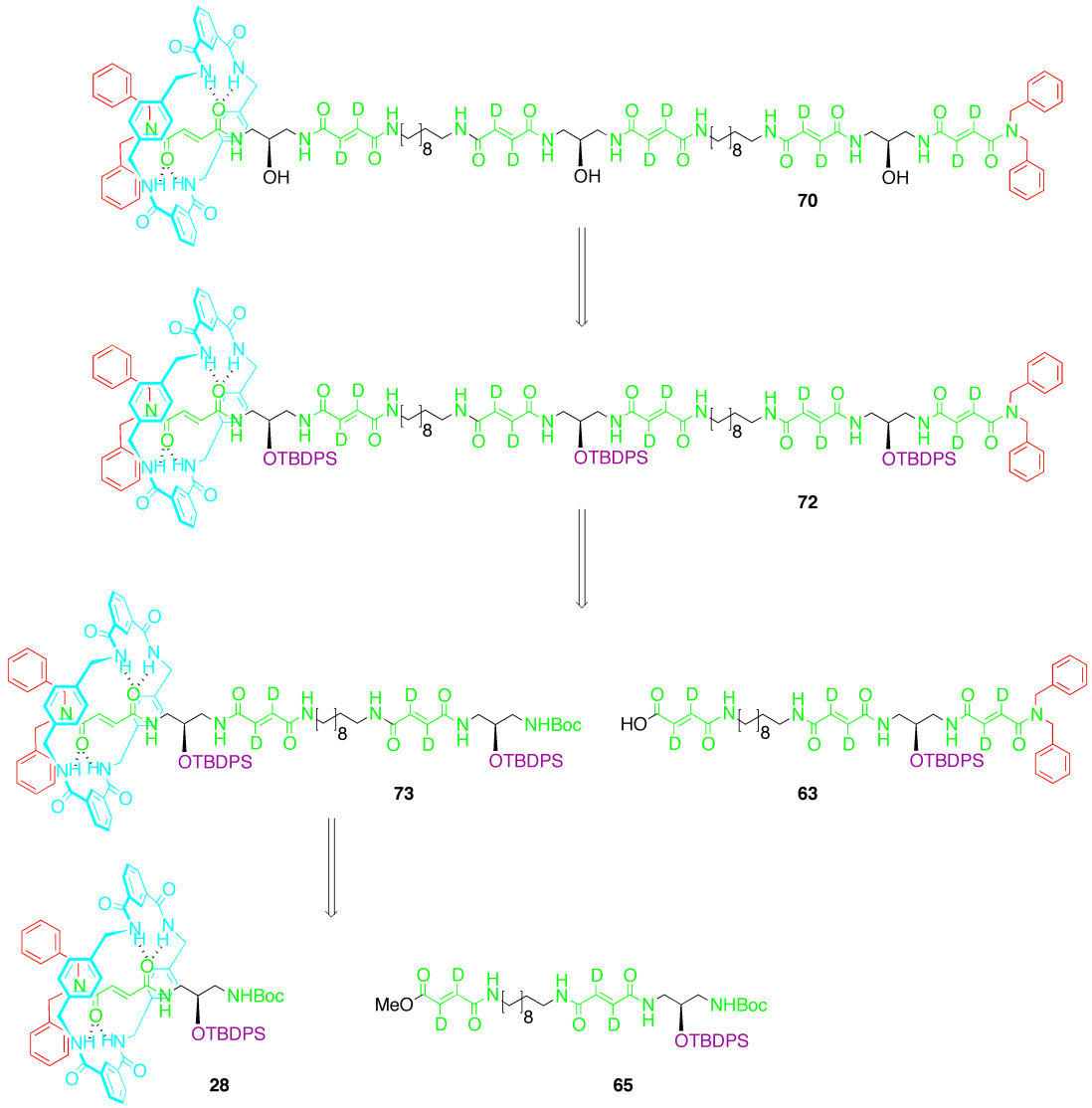

Scheme 4.8 Retrosynthetic analysis of **70**; compounds **28**, **63** and **65** had already been prepared in the course of the synthesis of **59**.

4.7 Synthesis

The Boc group of previously prepared rotaxane **28** was cleaved under standard conditions with a 4:1 DCM/TFA mixture and coupled to acid **66**, already synthesised for the five-compartment system, in the presence of TBTU, HOBt and DIPEA. The peptidic coupling reactions in this synthesis were performed without the usual cooling in an ice bath; this approach prevented the gelation of the reaction mixture which had been a a major problem in the preparation of these linear, multiply hydrogen-bonding molecules. Purification by column chromatography afforded **73** in an acceptable yield. Next, **73** was treated with a 4:1 TFA/DCM mixture to cleave the Boc group; TIPS was added to accelerate the reaction over cleavage of the silyl groups. A reaction time of 40 minutes was sufficient to remove the Boc group, and no loss of TBDPS was detected by either mass spectrometry or NMR spectroscopy.

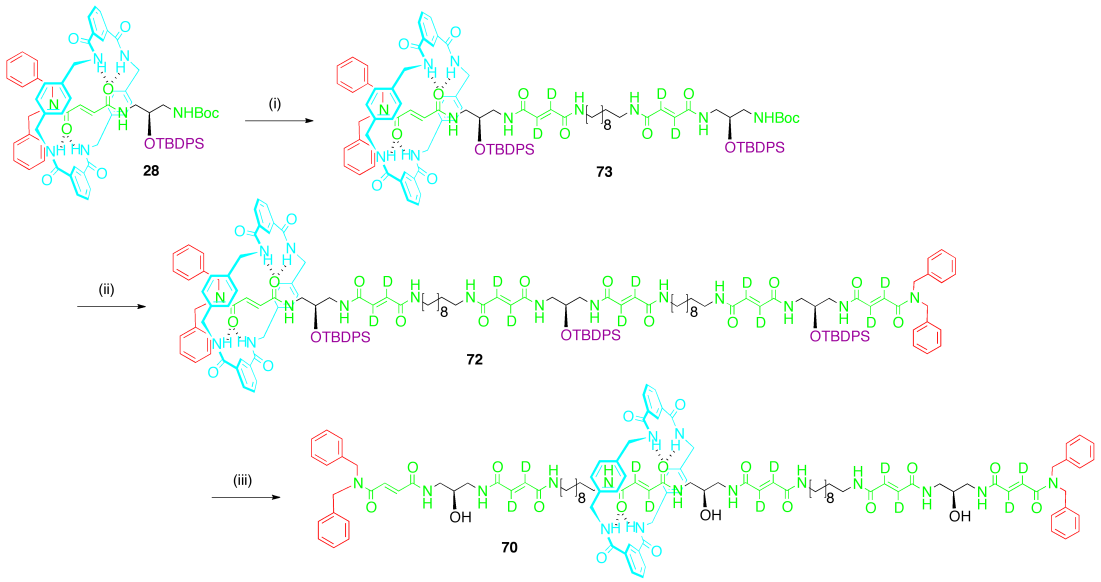

Scheme 4.9 (a) TFA, DCM, rt, 16 h, *quant.*; (b) Acid **66**, TBTU, HOBt, DIPEA, rt, 52%; (ii) (a) TFA, DCM, TIPS, rt, 40 min; (b) Acid **63**, TBTU, HOBt, DIPEA, DMF, rt, 42%; (iii) HF·py, DCM, rt, 16 h, 59%.

The crude primary amine form of **73** was used without further purification and coupled at room temperature to acid **63**. As had been observed before with related compounds, **72**'s low solubility made purification difficult and costly, but was eventually obtained with an isolated yield of 42%. Cleavage of the three silyl protecting groups was performed in a single step by treatment with hydrogen fluoride in a solution of pyridine. Purification (a combination of trituration with a 1:1 methanol/DCM mixture and preparative TLC) incurred further losses; the highest yield obtained for the final compound was 59%. Triol **70** was so insoluble as to be undetectable by NMR in any solvent except DMSO-d_6, but NMR spectroscopy and mass spectrometry confirmed the formation of the desired product.

4.8 Operation of Information Ratchet 70 and Analysis

The benzoylation of **70** was initially performed using the same reaction conditions as in the previous Chapters, in DCM, with two equivalents per hydroxyl group of catalyst, triethylamine and benzoyl chloride. Both chiral catalysts, (*S*)-**42** and (*R*)-**42**, were used. Our first experiments indicated that the benzoylation reaction occurs extremely slowly in this case. While the double benzoylation of three-compartment diols **25** or **46** occurred in a matter of minutes, analysis of the triple benzoylation of **70** showed significant amounts of starting material present after many days, even with the use of a great excess of benzoyl chloride than employed previously. Attempts to drive the reaction to completion by heating in a microwave at 60 °C for 2 h were unsuccessful.

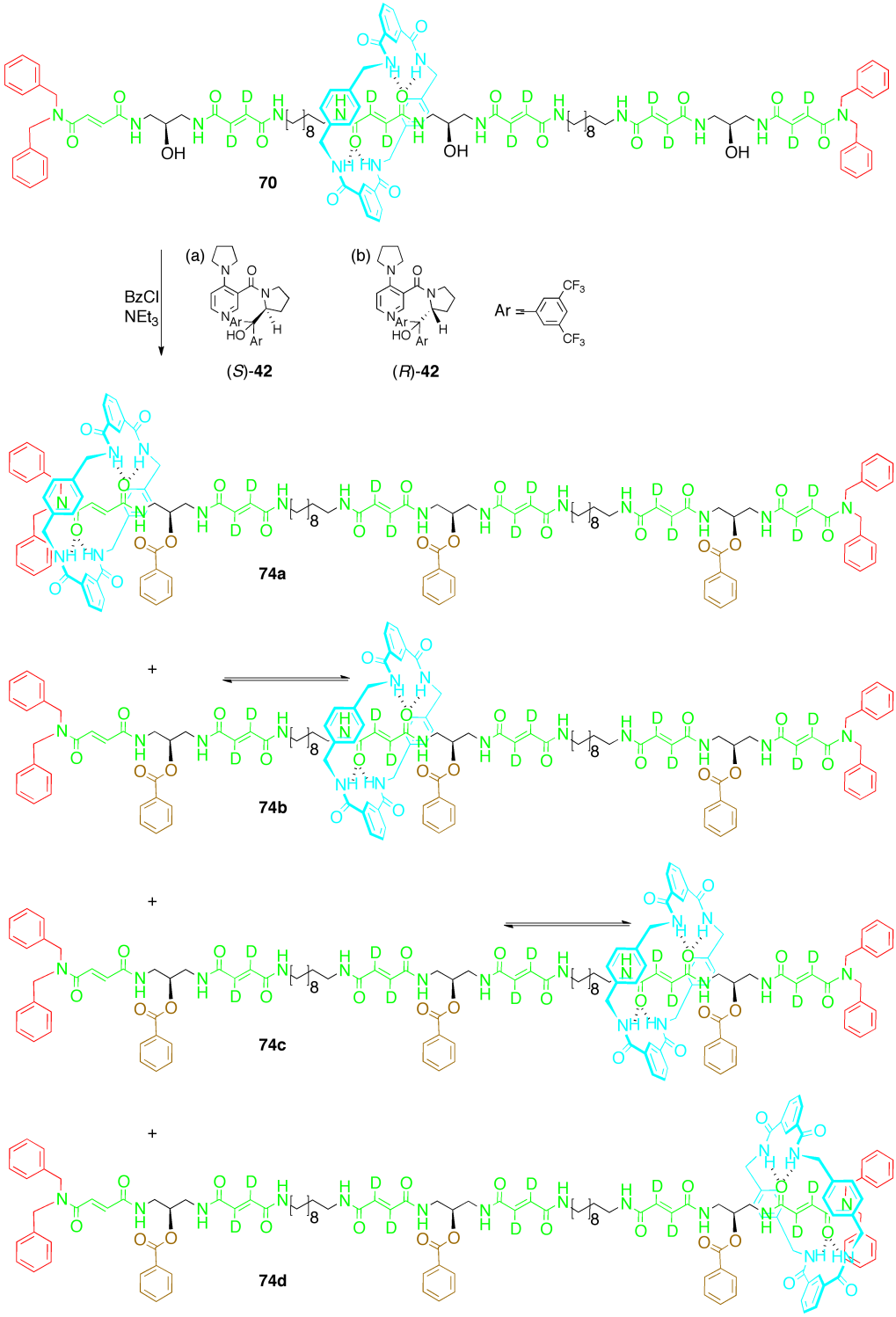

Scheme 4.10 Operation of diol information ratchet **70** was expected to give a mixture of four products **74a–d**.

4.8.1 Evidence from NMR Spectroscopy

Analysis by NMR spectroscopy of reaction mixtures in DMSO-d_6 confirmed that benzoylation was occurring to some extent: resonance signals at 7.9 ppm, 7.6 ppm and 7.4 ppm are consistent with a benzoyl group bound to the thread, as shown by the spectra of doubly benzoylated three-compartment rotaxanes **25** and **46**; it appears from the integration that up to a third of the available hydroxyl groups have been benzoylated. It is also apparent that at least some of the macrocycle has been successfully trapped into terminal compartments. This is shown by the resonance signal at 4.15 ppm, highlighted in blue in Figure 4.4, which correspond to *macrocyclic protons near the stoppers*. The most arresting evidence, however, is the presence at 6.0 ppm of peaks characteristic of a fumaramide residue shielded by a macrocycle. The peaks' sharpness and chemical shift both indicate that they are caused by a kinetically locked macrocycle, not one free to shuttle. Crucially, these shielded fumaric signals occur only when (*R*)-**42** is used as a catalyst; they are absent when (*S*)-**42** is used, although the benzoyl peaks remain. This is the necessary and sufficient criterion to show that, in those molecules of **70** which undergo benzoylation, directional discrimination driven by an information ratchet mechanism has taken place. Triol **70** is indisputably an information ratchet, although admittedly only a partially successful one.

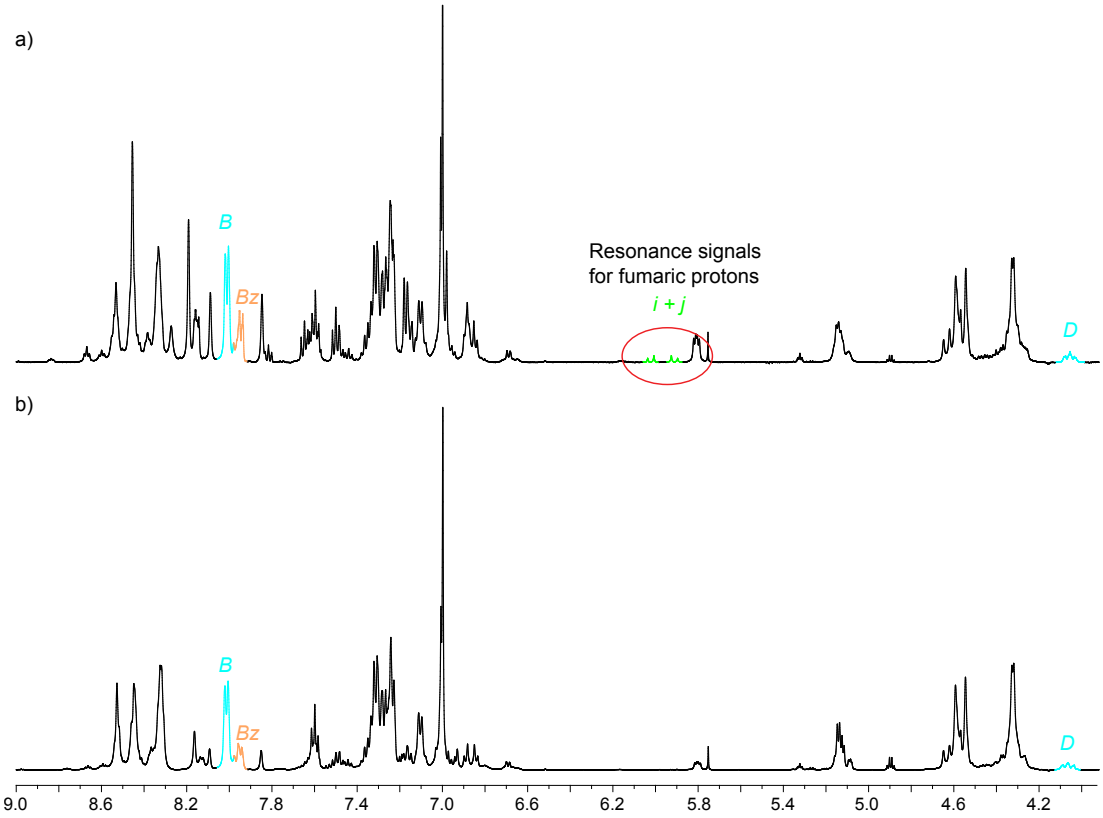

Figure 4.4. Partial ^{1}H NMR (500 Mhz, DMSO-d_6) of benzoylation attempts using (a) (*R*)-**42** and (b) (*S*)-**42** as catalysts. Macrocyclic *B* peaks (integrated as 4H) are shown in blue. Benzoyl group peaks are shown in orange, and have integrals much less than the expected 6H, indicating that the benzoylation is not complete. With both catalysts, macrocyclic *D* peaks at 4.1 ppm (blue) confirm the presence of macrocycle kinetically locked into a terminal compartment. Shielded fumaric signals for protons *i* and *j* at 5.9 ppm (highlighted in green) are present when (*R*)-**42** is used, but not when (*S*)-**42** is used, indicating that the direction of macrocycle transport depends on the handedness of the chiral catalyst. The presence of shielded fumaric protons does not necessarily indicate **74a**, and may instead be due to other, partially-benzoylated species (see Figure 4.5).

It is important to note that the observation of shielded fumaric protons does not necessarily indicate the presence of **74a**. All that is known about the species responsible for the signals is that there is a macrocycle in the leftmost compartment, and that this macrocycle is trapped by at least one benzoyl group. The possible compounds that could account for the signal are shown in Figure 4.5. The signal is likely to have been produced by a mixture of these compounds.

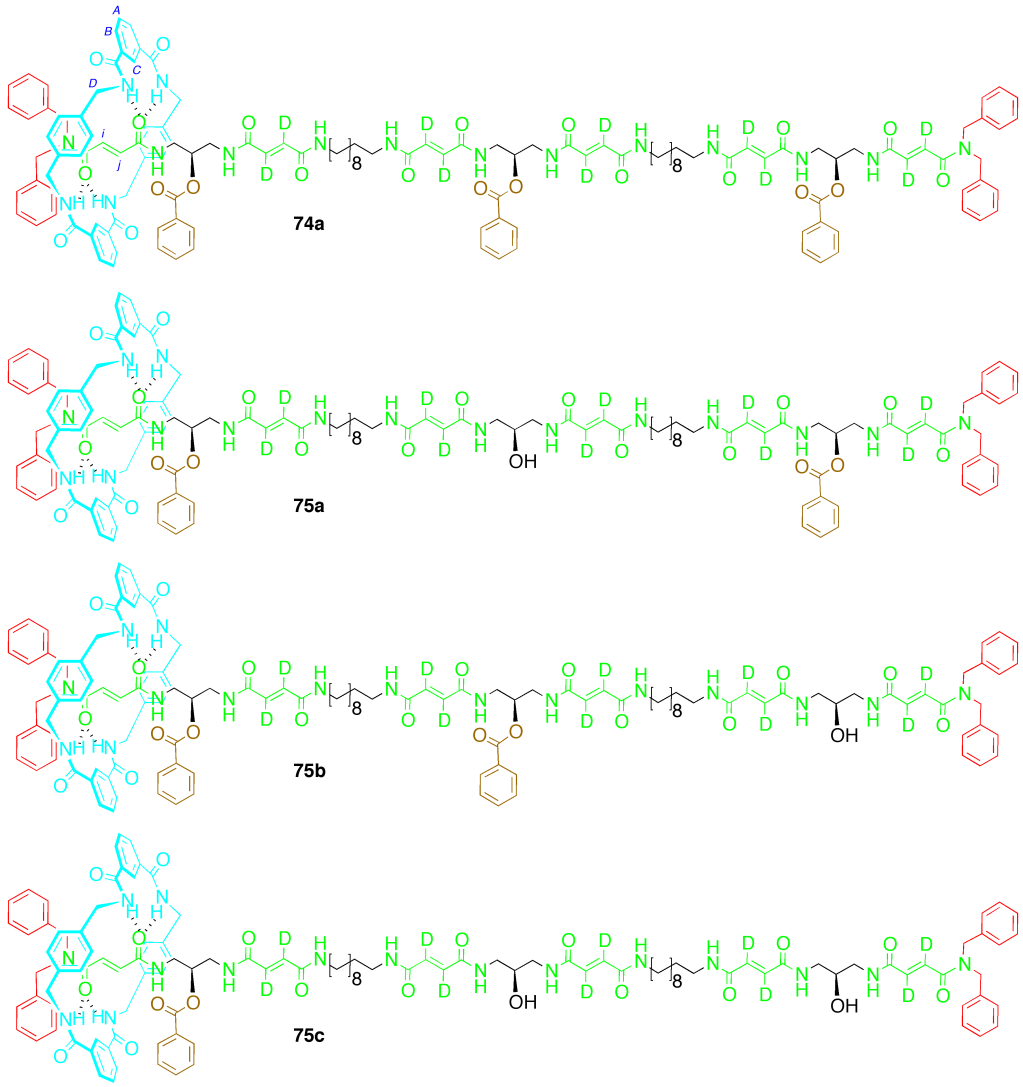

Figure 4.5 Four products resulting from the full or partial benzoylation of **70** are capable of generating the signal observed at 5.9 ppm. It is likely that the crude reaction product contains a mixture of all four, but **75c**, with the lowest molecular weight, is the only form detectable by MALDI mass spectrometry.

4.8.2 Evidence from Mass Spectrometry

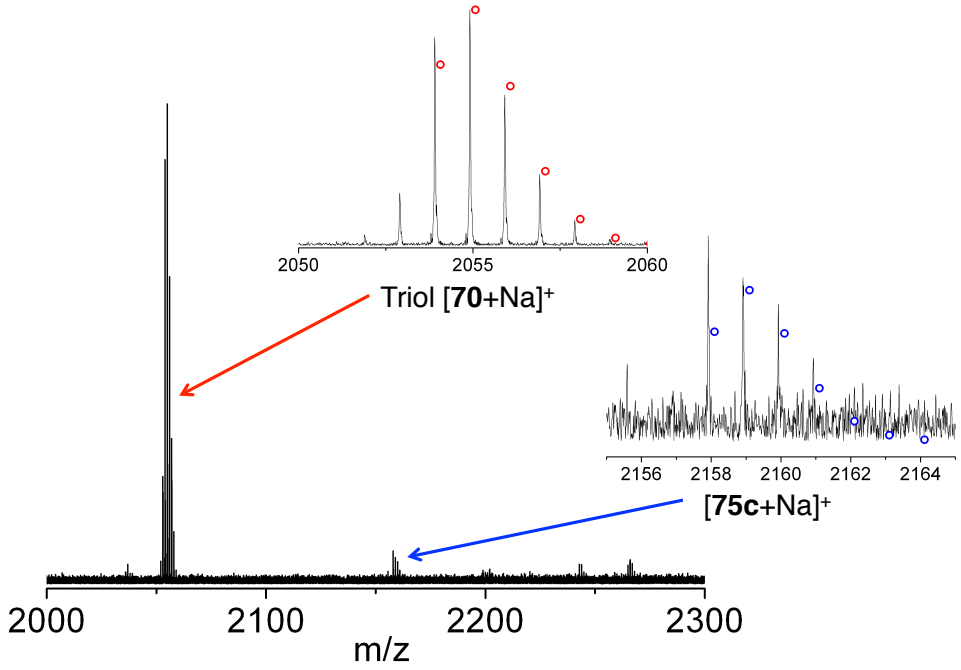

Figure 4.6 MALDI mass spectrum of a typical attempt at the benzoylation of triol **70**. A large amount of unreacted triol is detected as a monosodiated cation (theoretical isotope distribution overlaid in red). A much smaller peak corresponds to the mono-benzoylated product **75c**, again observed as a monosodiated cation (theoretical isotope distribution overlaid in blue). No doubly- or triply-benzoylated forms of **70** were detected.

Electrospray ionisation mass spectrometry (positive and negative modes) of the crude reaction mixture showed no identifiable peaks; either the compounds do not ionise sufficiently well with this technique, or they are so insoluble in organic solvents that the quantities that passed through the filter were not sufficient for a spectrum to be obtained. MALDI mass spectrometry (Figure 4.6) partially overcame these problems, and the ability to take a mass spectrum from a specific part of a TLC plate proved invaluable in identifying the components of the mixture.[6] Resonance signals corresponding to the starting material **70** were clearly visible. A cluster of peaks around m/z = 2159 Da corresponding to singly benzoylated **70** was observed as a minor constituent. No doubly- or triply-benzoylated **70** was detected. Nevertheless, it is clear that MALDI mass

spectrometry does not provide a quantitative analysis of the contents of the reaction vessel. NMR spectroscopy shows the existence of more benzoylated product than is detected by mass spectrometry. It would appear that the mono-benzoylated **70** is less likely to be detect by MALDI mass spectrometry than the triol. Doubly- or triply-benzoylated **70** are likely to be even more difficult to observe, either as a result of poor ionisability or easy fragmentation using this technique.

The data from NMR and mass spectrometry appear to be in conflict with certain aspects of the mechanism of action proposed for diols **25** and **46**. The evidence presented in Chapters Two and Three suggests that the chiral DMAP analogues (*S*)-**42** and (*R*)-**42** do not catalyse reactions that trap the macrocycle into a terminal compartment in the first instance. Here, however, there is evidence of macrocycles locked into terminal compartments by single benzoylations, and *no* evidence (by mass spectrometry) of multiple benzoylations on the same thread. This analysis suggests that **70** undergoes a type of reaction that appears forbidden in shorter systems, and an alternative explanation seems necessary.

One possible theory might be that single benzoylation of **70** poisons the substrate to further reactions, perhaps for reasons of solubility. Experience with short three-compartment rotaxane **25** lends plausibility to the theory, as for some positional isomers the solubility of **25** *decreased* on protection of its hydroxyl groups. This theory predicts, however, that the principal constituent of the reaction mixture would be singly-benzoylated **70**. The presence of a large amount of starting material **70** detectable by MALDI mass spectrometry is evidence against the theory. In order for the benzoylation of hydroxyl groups to be as high as 33% (as indicated by NMR), and for there still to be free triol **70** in solution, there logically must also be doubly- and triply-benzoylated forms of **70** present in the mixture that are not detected by mass spectrometry.

When the shielded fumaric protons are detected on use of (*R*)-**42**, they most probably result from a mixture of singly-, doubly- or triply-benzoylated **70**. Our experience of the previous Chapters' systems suggests that in the first instance, benzoylation occurs far from the macrocycle. The central or rightmost hydroxyl groups would be the first the be benzoylated, leaving the macrocycle free to shuttle. A later benzoylation reaction would then succeed in trapping some of the macrocycle into the terminal compartment. Even in the most successful experiments, these multiple benzoylations have been a minority, since at most a third of the available hydroxyl groups being protected in this way. Nevertheless, when they do occur, directional transport of the macrocycle is a statistically likely result. The direction of this transport depends on the handedness of the catalyst employed. Based on the evidence so far obtained, **70** is a working four-compartment information ratchet.

4.9 Summary and Outlook

Attempts to operate the four-compartment information ratchet **70** have demonstrated that multiple benzoylation reactions occur on the same thread, and that the macrocycle is at least to some extent directionally transported by these reactions. Unfortunately, the low reactivity of **70** towards benzoyl chloride, presumably a consequence of its very low solubility in organic solvents, means that the results are not reproducible. At the time of writing no triple benzoylation has successfully been driven to completion, either by raising the temperature or by increasing the number of equivalents.

Work is ongoing in our group to develop a fully reproducible and efficient technique for the operation of **70**. Variation of temperature or solvent might lead to an improved reaction yield for benzoylation, although there is a delicate

trade-off to be made: the hydrogen bonding that must be broken in order to solubilise the molecule is also what the information ratchet mechanism depends on in order to function. The macrocycle binds to its stations through hydrogen bonds that would be disrupted in highly polar media, effectively limiting the range of conditions that might be expected to work. The same applies for temperature: performing the reaction in a high-boiling solvent at elevated temperature might successfully solubilise the molecules, but will also increase the likelihood of errors as the magnitude of the entropy term increases.[7] It is hoped that conditions may be found that overcome the reactivity problems without disturbing the macrocycle-thread interactions. If such conditions are not found, a redesign will be required to solubilise the molecule.

The preliminary results from this Chapter are encouraging, however. It is hoped that either the design presented here or one very similar may soon be made to overcome the solubility problems and realise long-distance directional transport of a Brownian macrocycle *via* a chemically-driven information ratchet process. The work on increasingly long and complex information ratchets will continue into the future.

4.10 Experimental Section

Many of the compounds documented in this Chapter are chiral or adopt chiral conformations. The resulting inequivalent nuclei are in some instances observed as a complex series of signals, although the same compound may also exhibit simpler signals under different conditions (different solvent, temperature, concentration, etc). Where possible, the signals have been assigned unambiguously and where non-equivalence occurred it is noted in the experimental assignments. Signals for carbons adjacent to deuterons on fumaramide residues were not observed by ^{13}C NMR spectroscopy.

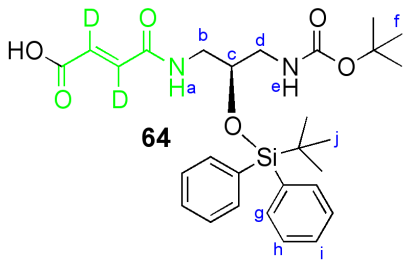

64

To a stirred solution of **54** (680 mg, 1.25 mmol) in 3:1 THF/H_2O (20 mL) was added LiOH·H_2O (2 eq, 2.5 mmol, 105 mg). After 40 mins the mixture was diluted with HCl (1 M, 10 mL) and extracted into 3:1 $CHCl_3$/IPA (3 × 30 mL). The combined organic fractions were washed with HCl (1 M, 3 × 10 mL) and brine (3 × 10 mL), dried over $MgSO_4$ and concentrated under reduced pressure to give **64** as a colourless solid (660 mg, *quant.*). M.p. 110 °C. $[\alpha]_D^{20}$ = +31.0 (c = 0.90, DCM). ^{1}H NMR (500 MHz, $CDCl_3$): δ = 7.73–7.47 (m, 4H, H_h), 7.42–7.27 (m, 6H, H_g + H_i), 7.26–7.20 (m, 1H, H_a), 4.87–4.74 (m, 1H, H_e), 3.83 (dd, 1H, *J* = 8.5, 3.7, H_c), 3.77–3.61 (m, 1H, H_b), 3.43–3.27 (m, 1H, H_d), 3.02 (ddd, 1H, *J* = 13.4, 8.7, 4.5, H_b), 2.89 (dt, 1H, *J* = 14.8, 3.7, H_d), 1.36 (s, 9H, H_f), 1.01 (s, 9H, H_j); ^{13}C NMR (125 MHz, 1:1 CD_3OD/$CDCl_3$): 167.2, 164.5, 156.6, 135.5, 133.2, 129.8, 127.6, 70.4,

43.0, 42.1, 41.2, 27.9, 26.6, 19.0 LR-MS (ESI, negative mode): m/z = 527 $[M–H]^-$; observed peaks consistent with theoretical isotope distribution.

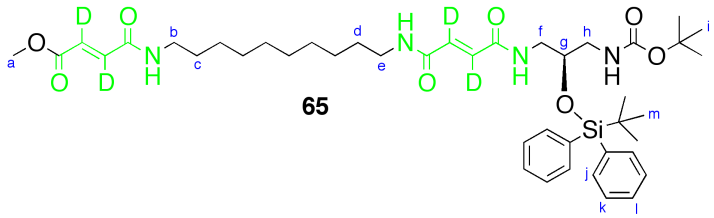

To a stirred solution of amide **51** (457 mg, 1.18 mmol, 1 eq) in anhydrous DCM (24.6 mL) in a loosely-sealed round-bottomed flask was added TFA (1.5 mL) and TIPS (0.1 mL). After 2 h the and the solvent was removed by coevaporation with toluene under reduced pressure. The obtained residue was triturated (×3) with hexane, redissolved in anhydrous DMF (12 mL) under N_2 and cooled to 0 °C. Acid **64** (1 eq, 1.18 mmol, 623 mg), DIPEA (3 eq, 3.54 mmol, 604 µL), HOBt (1.2 eq, 2.36 mmol, 319 mg) and TBTU (1.2 eq, 2.36 mmol, 758 mg) were added. After allowing the reaction to reach room temperature with stirring over 16 h the reaction mixture was diluted with saturated $NaHCO_3$ (12 mL) and extracted into 3:1 $CHCl_3$/IPA (3 × 25 mL). The combined organic fractions were washed with saturated $NaHCO_3$ (3 × 5 mL), HCl (1 M, 3 × 5 mL) and brine (3 × 5 mL), then dried over $MgSO_4$ and the solvent was removed by coevaporation with toluene under reduced pressure. Flash chromatography (1% MeOH in DCM) gave **65** as a white solid (754 mg, 80%). M.p. 173–174 °C. $[\alpha]_D^{20}$ = +29.1 (c = 0.10, 1:1 MeOH/DCM). ^{1}H NMR (400 MHz, $CDCl_3$): δ = 7.89 (dd, 4H, *J* = 8.1, 1.7, H_k), 7.69–7.56 (m, 6H, H_j + H_l), 4.12 (q, 1H, *J* = 5.1, H_g), 4.00 (s, 3H, H_a), 3.60–3.51 (m, 2H, H_f), 3.48 (t, 4H, *J* = 7.2, H_b + H_e), 3.33 (t, 2H, *J* = 5.4, H_h), 1.82–1.68 (m, 4H, H_c + H_d), 1.61 (s, 9H, H_i), 1.58–1.45 (m, 12H, H_{alkyl}), 1.28 (s, 9H, H_m); ^{13}C NMR (100 MHz, $CDCl_3$ with 1 drop CD_3OD): δ = 170.6, 169.6, 168.7, 168.1, 160.5, 139.6, 137.2, 133.9, 131.7, 83.6, 74.5, 56.1, 47.0, 46.3, 43.8 (×2), 43.7, 33.3, 33.2, 33.1, 33.0 (×2), 32.9 (×2), 32.1, 30.8, 23.1. LR-MS (ESI): m/z = 722 $[M+H]^+$; observed peaks consistent with theoretical isotope distribution.

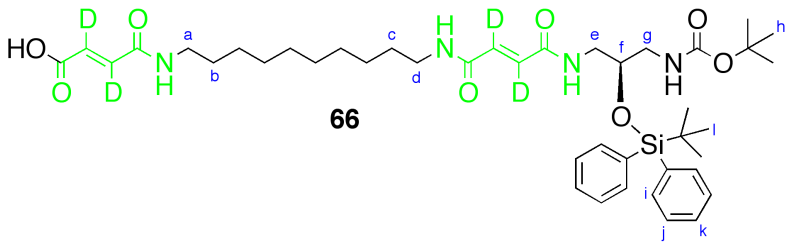

66

To a stirred solution of **65** (187 mg, 0.24 mmol) in 3:1 THF/H_2O (3 mL) was added LiOH·H_2O (2 eq, 0.48 mmol, 20 mg). After 45 mins the mixture was diluted with HCl (1 M, 3 mL) and extracted into 3:1 $CHCl_3$/IPA (3 × 5 mL). The combined organic fractions were washed with HCl (1 M, 3 × 2 mL) and brine (3 × 2 mL), dried over $MgSO_4$ and concentrated under reduced pressure to give **66** as a white solid (184 mg, *quant.*). M.p. 236–237 °C. $[\alpha]_D^{20}$ = +30.3 (c = 0.20, 1:1 CD_3OD:$CDCl_3$). ^{1}H NMR (500 MHz, 1:1 CD_3OD/$CDCl_3$): δ = 7.67–7.54 (m, 4H, H_j), 7.47–7.21 (m, 6H, H_i + H_k), 4.00 (dq, 1H, *J* = 10.1, 5.0, H_f), 3.28–3.22 (m, 2H, H_e), 3.19 (t, 4H, *J* = 7.1, H_a + H_d), 2.88–2.70 (m, 2H, H_g), 1.51–1.39 (m, 4H, H_b + H_c), 1.34–1.16 (m, 21H, H_{alkyl} + H_h), 1.04 (s, 9H, H_l); ^{13}C NMR (125 MHz, 1:1 CD_3OD/ $CDCl_3$): δ = 166.1, 165.7, 164.6, 164.0, 163.5, 136.3, 133.9, 130.5, 128.3, 70.8, 70.6, 52.4, 50.6, 49.2, 43.1 (×2), 43.0, 40.6, 40.4, 40.2, 39.2, 29.4, 29.2, 27.2, 26.9, 19.2. LR-MS (ESI): m/z = 783 $[M+H]^+$; observed peaks consistent with theoretical isotope distribution.

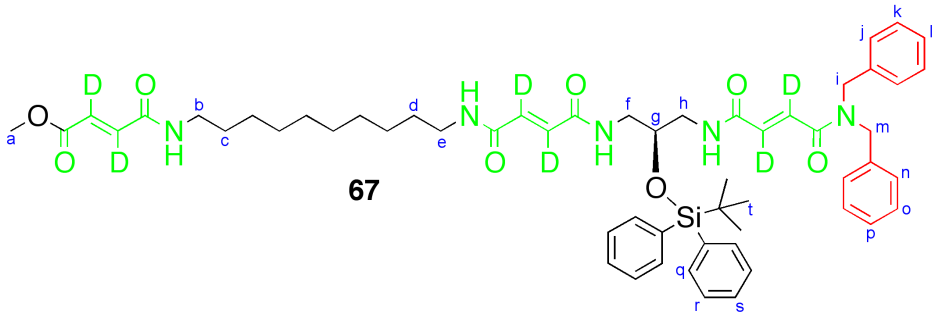

67

To a stirred solution of **65** (465 mg, 0.58 mmol, 1 eq) in anhydrous DCM (20 mL) in a loosely-sealed round-bottomed flask was added TFA (5 mL) and TIPS (0.1 mL). After 16 h the solvent was removed by coevaporation with toluene

under reduced pressure. The obtained residue was triturated with hexane then redissolved in anhydrous DMF (5.8 mL) under N_2 and cooled to 0 °C. Acid **32** (1 eq, 0.58 mmol, 172 mg), DIPEA (3 eq, 1.74 mmol, 300 µL), HOBt (1.2 eq, 0 .70 mmol, 95 mg) and TBTU (1.2 eq, 0.70 mmol, 225 mg) were added. After allowing the reaction to reach room temperature with stirring over 16 h the reaction mixture was diluted with saturated $NaHCO_3$ (15 mL) and extracted into 3:1 $CHCl_3$/IPA (4 × 25 mL). The combined organic fractions were washed with saturated $NaHCO_3$ (3 × 10 mL), HCl (1 M, 3 × 10 mL) and brine (3 × 10 mL), then dried over $MgSO_4$ and the solvent was removed by coevaporation with toluene under reduced pressure. Flash chromatography (neat DCM increasing to 2% MeOH in DCM) gave **67** as a yellow solid (342 mg, 60%). M.p. 134-135 °C. $[\alpha]_D^{20}$ = +34.0 (c = 1.02, 1:1 CD_3OD/DCM). ^1H NMR (400 MHz, 1:1 CD_3OD/$CDCl_3$): δ = 7.70 (d, 4H, *J* = 6.9, H_r), 7.49–7.30 (m, 12H, H_k + H_l + H_o + H_p + H_q + H_s), 7.27 (d, 2H, *J* = 6.8, H_h), 7.21 (d, 2H, *J* = 7.1, H_l), 4.67 (d, 4H, *J* = 13.2, H_i + H_m), 4.06 (quint, 1H, *J* = 5.5, H_g), 3.78 (s, 3H, Ha), 3.41–4.44 (m, 4H, H_e + H_g), 3.30 (t, 4H, *J* = 7.1, H_b + H_e), 1.64–1.51 (m, 4H, H_c + H_d), 1.46–1.26 (m, 12H, H_{alkyl}), 1.09 (s, 9H, H_t); ^{13}C NMR (125 MHz, 1:1 CD_3OD/$CDCl_3$): δ = 166.2, 166.0 165.5, 165.0, 164.8, 164.2, 136.0, 135.4 (×2), 132.9, 130.8, 129.6, 128.6, 128.3, 127.8, 127.4, 127.3, 126.4, 69.8, 66.0, 65.7, 64.0, 51.5, 49.9, 48.3, 42.4, 39.6, 39.5, 39.4, 29.2, 29.0, 28.8, 28.7, 26.5, 26.3, 18.7. LR-MS (ESI): m/z = 976 $[M+H]^+$; observed peaks consistent with theoretical isotope distribution.

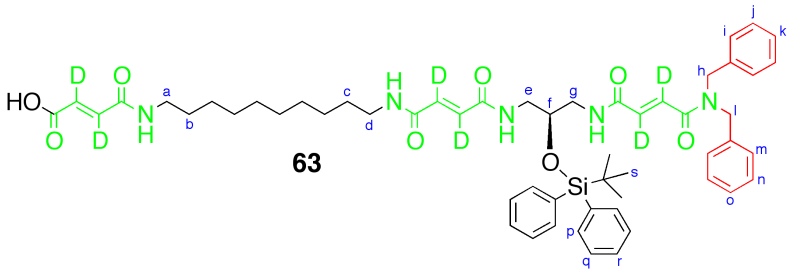

63

To a stirred solution of **67** (100 mg, 102 µmol) in 3:1 THF/H_2O (1.4 mL) was added LiOH·H_2O (2 eq, 204 µmol, 8.6 mg). After 20 mins the mixture was diluted with HCl (1 M, 10 mL) and extracted into 3:1 $CHCl_3$/IPA (3 × 15 mL). The

combined organic fractions were washed with HCl (1 M, 3 × 5 mL) and brine (3 × 5 mL), dried over $MgSO_4$ and concentrated under reduced pressure to give **63** as a white solid (98 mg, *quant.*). M.p. 167–169 °C. $[\alpha]_D^{20}$ = +35.5 (c = 0.31, DMSO). ^{1}H NMR (400 MHz, DMSO-d_6): δ = 7.60 (d, 4H, J = 8.2, H_q), 7.47–7.22 (m, 14H, H_i + H_j + H_k + H_n + H_o + H_p + H_r), 7.17 (d, 2H, J = 7.4, H_m), 4.61 (d, 4H, J = 17.1, H_h + H_l), 3.68–3.55 (m, 1H, H_f), 3.29–3.06 (m, 3H, H_e + H_g), 3.16–300 (m, 5H, H_a + H_d + H_g), 1.53–1.34 (m, 4H, H_b + H_c), 1.34–1.14 (m, 12H, H_{alkyl}), 0.96 (s, 9H, H_s); ^{13}C NMR (125 MHz, DMSO-d_6): δ = 166.6, 165.4 (×2), 164.0, 163.1 (×2), 137.4, 137.2, 135.6, 135.1, 134.7, 128.9, 128.6, 128.0, 127.8, 127.6, 127.4, 126.6, 70.4, 68.3, 62.9, 62.3, 50.2, 48.8, 32.4, 31.5, 29.2, 28.9, 26.9, 26.6, 25.4, 22.3, 19.0, 18.9, 14.0. LR-MS (ESI): m/z = 829 $[M+H]^+$; observed peaks consistent with theoretical isotope distribution.

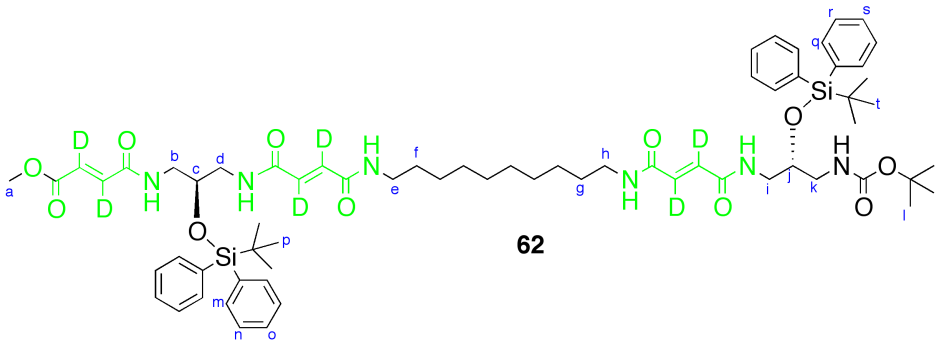

62

To a stirred solution of **54** (150 mg, 0.34 mmol, 1.2 eq) and TIPS (0.1 mL) in anhydrous DCM (9 mL) in a round-bottomed flask was added TFA (2.25 mL). After 16 h the solvent was removed by coevaporation with toluene under reduced pressure. The obtained residue was triturated with hexane and redissolved in anhydrous DMF (15 mL) under N_2 and cooled to 0 °C. Acid **66** (1 eq, 0.29 mmol, 223 mg), DIPEA (1.2 eq, 0.34 mmol, 250 µL), HOBt (1.2 eq, 0.34 mmol, 46 mg) and TBTU (1.2 eq, 0.34 mmol, 109 mg) were added. After allowing the reaction to reach room temperature with stirring over 16 h the reaction mixture was diluted with saturated $NaHCO_3$ (10 mL) and extracted into

DCM (4 × 15 mL). The combined organic fractions were washed with saturated $NaHCO_3$ (3 × 10 mL), HCl (1 M, 3 × 10 mL) and brine (3 × 10 mL), then dried over $MgSO_4$ and the solvent was removed by coevaporation with toluene under reduced pressure. Flash chromatography (2% MeOH in DCM) gave **62** as a yellow solid (172 mg, 50%). M.p. 156–157 °C. $[\alpha]_D^{20}$ = –7.3 (c = 1.10, DCM). ^{1}H NMR (400 MHz, 1:1 $CD_3OD/CDCl_3$): δ = 7.69–7.64 (m, 8H, H_n + H_r), 7.41 (dq, 12H, *J* = 13.9, 6.8, H_m + H_o + H_q + H_s), 4.01 (dq, 1H, *J* = 10.9, 5.4, H_j), 3.95–3.85 (m, 1H, H_c), 3.80 (s, 3H, H_a), 3.38–3.30 (m 6H, H_d + H_i + H_k), 3.27 (t, 4H, *J* = 7.2, H_e + H_h), 3.12 (d, 2H, *J* = 4.9, H_b), 1.58–1.48 (m, 4H, H_f + H_g), 1.40 (s, 9H, H_l), 1.37–1.28 (br, 12H, H_{alkyl}), 1.06 (s, 18H, H_p + H_t); ^{13}C NMR (125 MHz, 1:1 $CD_3OD/CDCl_3$): δ = 166.9, 166.7, 166.4, 166.3, 165.7, 165.4, 165.3, 136.3, 134.0, 133.9, 133.8, 132.2, 130.6, 130.5, 128.4, 71.2, 70.7, 52.6, 43.8, 43.3, 43.2, 43.1, 40.5, 40.4, 40.1, 30.0, 29.8, 29.6, 29.1, 28.6, 27.5, 27.3 (×3), 26.5 (×4). LR-MS (ESI): m/z = 1207 $[M+H]^+$; HR-MS (ESI): m/z = 1207.6788 $[M+H]^+$ (calculated for $C_{66}H_{86}D_6N_6O_{11}Si_2H$ = 1207.6812).

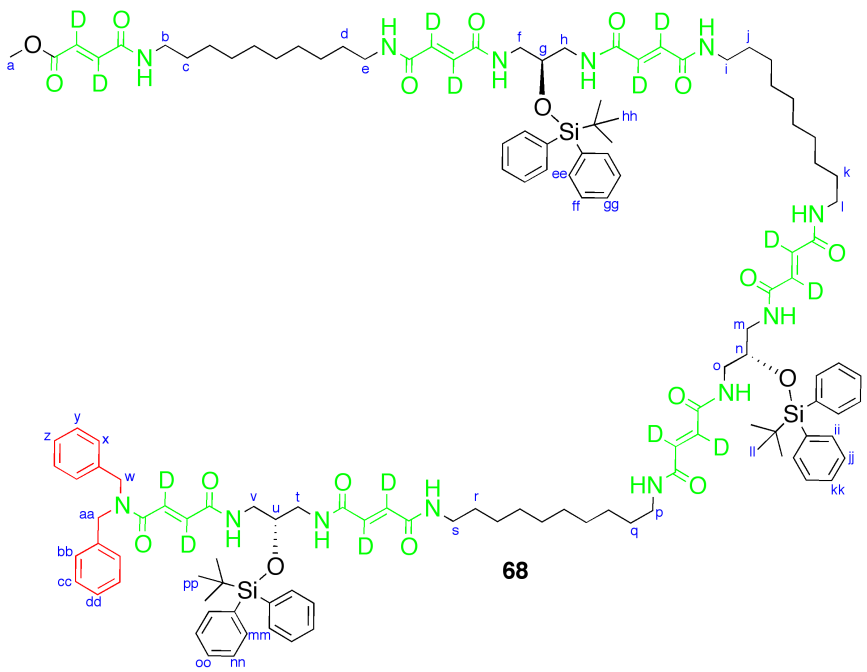

68

To a stirred solution of **62** (165 mg, 0.13 mmol, 1.2 eq) and TIPS (0.1 mL) in anhydrous DCM (2 mL) in a loosely-sealed round-bottomed flask was added

TFA (0.5 mL). After 16 h the solvent was removed by coevaporation with toluene under reduced pressure. The obtained residue was triturated with hexane then redissolved in anhydrous DMF (20 mL) under N_2 and cooled to 0 °C. Acid **32** (1 eq, 0.113 mmol, 35 mg), DIPEA (3 eq, 0.283 mmol, 48 µL), HOBt (1.2 eq, 0.113 mmol, 15 mg) and TBTU (1.2 eq, 0.113 mmol, 36 mg) were added. After allowing the reaction to reach room temperature with stirring over 16 h the reaction mixture was diluted with saturated $NaHCO_3$ (20 mL) and extracted into 3:1 IPA/$CHCl_3$ (4 × 100 mL). The combined organic fractions were washed with saturated $NaHCO_3$ (3 × 30 mL), HCl (1 M, 3 × 30 mL) and brine (3 × 30 mL), then dried over $MgSO_4$ and the solvent was removed by coevaporation with toluene under reduced pressure. The crude reaction mixture was triturated with a 1:1 DCM/MeOH mixture with centrifugation (×3). Flash chromatography (5% MeOH in DCM) followed by preparative TLC (eluent: 10% MeOH in DCM, × 4) gave **68** as a white solid (29 mg, 26%). The compound decomposed on heating at 214 °C. $[\alpha]_D^{20}$ = +27.3 (c = 0.10, DMSO). ^{1}H NMR (500 MHz, DMSO-d_6): δ = 7.60 (t, 12H, J = 7.4, H_{ff} + H_{jj} + H_{nn}), 7.48–7.22 (m, 22H, H_x + H_z + H_{dd} + H_{ee} + H_{gg} + H_{ii} + H_{kk} + H_{mm} + H_{oo}), 7.16 (d, 2H, J = 7.5, H_{bb}), 4.61 (dd, 4H, J = 21.7, 4.3, 4H, H_w + H_{aa}), 3.98–3.89 (m, 3H, H_g + H_n + H_u), 3.72 (s, 3H, H_a), 3.27–3.15 (m, 12H, H_f + H_h + H_m + H_o + H_t + H_v), 3.15–3.05 (m, 12H, H_b + H_e + H_i + H_l + H_p + H_s), 1.47–1.32 (m, 12H, H_c + H_d + H_j + H_k + H_q + H_r), 1.31–1.14 (m, 36H, H_{alkyl}), 1.04–0.90 (m, 27H, H_{hh} + H_{ll} + H_{pp}). ^{13}C NMR (125 MHz, DMSO-d_6): δ = 166.0, 165.7, 164.6, 164.5 (×4), 164.2, 164.0 (×4), 163.5 (×2), 137.8, 137.6, 135.9, 133.8, 130.3, 129.2, 129.0, 128.2, 128.1, 127.9, 127.7, 126.9, 70.8, 70.7, 70.6, 52.5, 50.6, 49.3, 43.1 (×2), 43.0 (×4), 40.6, 40.4, 40.3 40.1, 40.0, 39.2, 29.4 (×4), 29.2 (×2), 27.2 (×2), 26.9 (br, ×18), 19.3 (×3). LR-MS (ESI): m/z 1030 $[M+2H]^{2+}$; observed peaks consistent with theoretical isotope distribution.

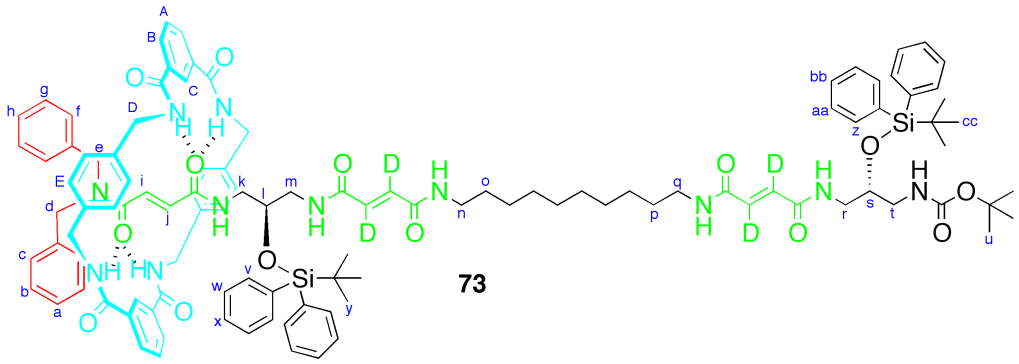

73

To a stirred solution of **28** (350 mg, 0.28 mmol, 1.2 eq) in anhydrous DCM (9 mL) in a loosely-sealed round-bottomed flask was added TFA (6.15 mL). After 16 h the solvent was removed by coevaporation with toluene under reduced pressure. The obtained residue was redissolved in anhydrous DMF (2.5 mL) under N_2 and **66** (1 eq, 0.235 mmol, 184 mg), DIPEA (3 eq, 0.71 mmol, 120 µL), HOBt (1.2 eq, 0.28 mmol, 38 mg) and TBTU (1.2 eq, 0.28 mmol, 90 mg) were added. After 16 h the reaction mixture was diluted with saturated $NaHCO_3$ (4 mL) and extracted into 3:1 $CHCl_3$/IPA (4 × 5 mL). The combined organic fractions were washed with saturated $NaHCO_3$ (3 × 5 mL), HCl (1 M, 3 × 5 mL) and brine (3 × 5 mL), then dried over $MgSO_4$ and the solvent was removed by coevaporation with toluene under reduced pressure. Flash chromatography (3% MeOH in DCM) gave **73** as a low-melting white solid (234 mg, 52%). $[\alpha]_D^{20}$ = –75.3 (c = 1.00, DCM). ^{1}H NMR (400 MHz, 1:1 $CD_3OD/CDCl_3$): δ = 8.75 (s, 2H, H_C), 8.45 (t, 4H, *J* = 7.4, H_B), 7.95 (m, 10H, H_A+ H_w + H_{aa}), 7.75–7.36 (m, 18H, H_a + H_b + H_c + H_h + H_v + H_x + H_z + H_{bb}), 7.31 (t, 2H, *J* = 7.5, H_g), 7.12 (d, 4H, *J* = 8.0, H_E), 7.05–6.95 (m, 6H, H_E + H_f), 6.15 (s, 2H, H_i + H_j), 4.85–4.32 (m, 12H, H_D + H_d + H_e), 4.85–4.32 (m, 1H, H_s), 4.12–4.04 (m, 1H, H_l), 3.83–3.52 (m, 10H, H_m, H_n, H_q, H_r, H_t), 3.41 (t, 2H, *J* = 5.1, H_k), 1.96–1.87 (m, 2H, H_o), 1.87–1.76 (m, 2H, H_p), 1.67 (s, 9H, H_u), 1.65–1.56 (m, 12H, H_{alkyl}), 1.36 (s, 9H, H_{cc}), 1.33 (s, 9H, H_y); ^{13}C NMR (100 MHz, $CDCl_3$): δ = 167.8, 167.4, 166.4, 166.0 (×2), 165.9, 165.6, 165.5, 137.8 (×2), 137.1, 136.5, 136.4 (×2), 136.0, 134.4 (×2), 134.2, 134.1 (×2), 133.9, 133.4, 132.4, 132.3, 130.9 (×2), 132.3, 130.9 (×2), 130.6, 130.1, 129.9, 71.4, 70.9, 52.3, 52.1, 44.4 (×2), 44.3, 44.1, 43.4, 42.5, 40.6, 40.5, 40.4, 30.1 (×2), 29.9, 29.8, 29.7,

28.7, 27.6 (×2), 27.3 (×2), 19.8, 19.7; LR-MS (ESI): m/z = 952 $[M+2H]^{2+}$; observed peaks consistent with theoretical isotope distribution.

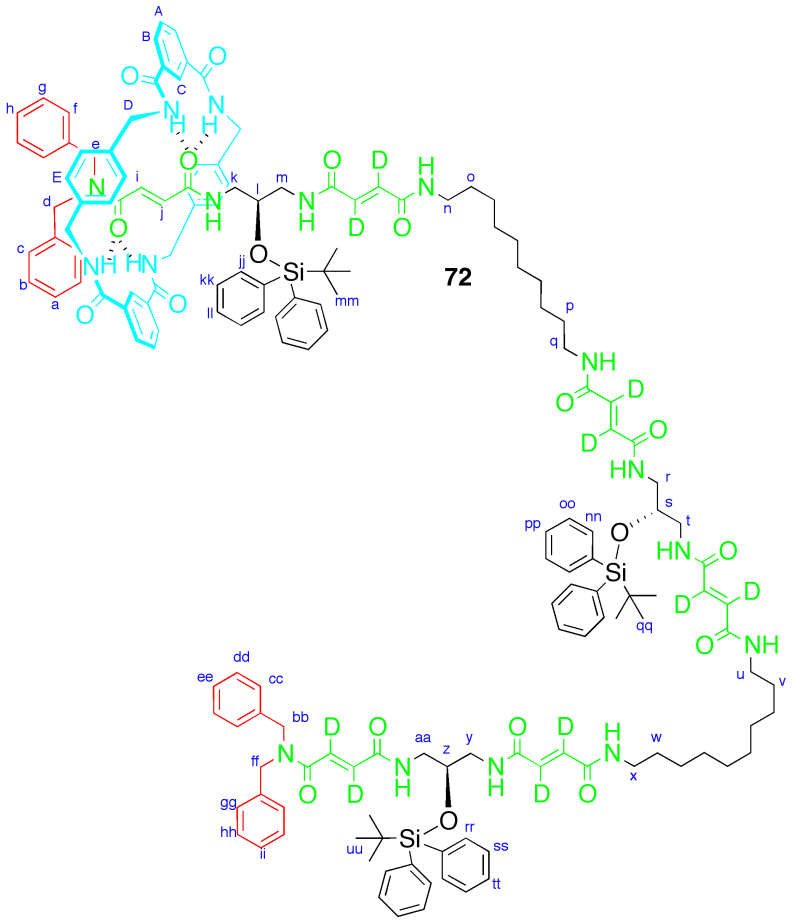

To a stirred solution of **73** (110 mg, 58 µmol, 1 eq) in anhydrous DCM (8 mL) in a loosely-sealed round-bottomed flask was added TFA (2 mL) and TIPS (0.1 mL). After 40 min the solvent was removed by coevaporation with toluene under reduced pressure. The obtained residue was redissolved in anhydrous DMF (2 mL) under N_2 and **63** (1 eq, 58 µmol, 56 mg), DIPEA (3 eq, 174 µmol, 30 µL), HOBt (1.9 eq, 110 µmol, 15 mg) and TBTU (1.7 eq, 99 µmol, 15 mg) were added. After 16 h the reaction mixture was diluted with saturated $NaHCO_3$ (10 mL) and extracted into $CHCl_3$/IPA (4 × 20 mL). The combined organic fractions were washed with saturated $NaHCO_3$ (3 × 10 mL), HCl (1 M, 3 × 10 mL) and brine (3 × 10 mL), then dried over $MgSO_4$ and the solvent was removed by

coevaporation with toluene under reduced pressure. The residue obtained was purified by trituration with MeOH and flash chromatography (3% MeOH in DCM) to give **72** as a white solid (67 mg, 42%). M.p. 220-221 °C. $[\alpha]_D^{20}$ = +19.5 (c = 0.25, 1:1 DCM/MeOH). ^{1}H NMR (500 MHz, 1:2 $CD_3OD/CDCl_3$): δ = 8.44 (s, 2H, H_C), 8.16 (m, 4H, H_B), 7.67–7.58 (m, 14H, $H_A + H_{kk} + H_{oo} + H_{ss}$), 7.42–7.16 (m, 31H, $H_a + H_b + H_{cc} + H_{dd} + H_{ee} + H_{gg} + H_{hh} + H_{ii} + H_{jj} + H_{ll} + H_{nn} + H_{pp} + H_{rr} + H_{tt}$), 7.16–7.07 (m, 3H, $H_c + H_h$), 7.02 (t, 2H, *J* = 7.5, H_g), 6.80 (d, 4H, *J* = 8.0, H_E), 6.66 (t, 6H, *J* = 7.8, $H_E + H_f$), 5.89–5.78 (m, 2H, $H_i + H_j$), 4.67–4.00 (br, 16H, $H_D + H_d + H_e + H_{bb} + H_{ff}$), 3.97 (dt, 3H, *J* = 10.4, 5.3, $H_l + H_s + H_z$), 3.74–3.58 (m, 3H, $H_k + H_m$), 3.47–3.30 (m, 8H, $H_m + H_r + H_t + H_y + H_{aa}$), 3.30–3.20 (m, 12H, $H_n + H_q + H_r + H_t + H_u + H_x$), 2.81–2.68 (m, 1H, H_k), 1.57–1.45 (m, 8H, $H_o + H_p + H_v + H_w$), 1.46–1.13 (br, 24H, H_{alkyl}), 1.05 (d, 18H, *J* = 2.9, $H_{qq} + H_{uu}$), 1.03 (s, 9H, H_{mm}); ^{13}C NMR (125 MHz, 1:2 $CD_3OD/CDCl_3$): δ = 166.9, 166.6, 166.2, 165.8, 165.7, 165.6, 165.2, 165.1, 165.0, 164.9, 164.8, 164.7, 164.6, 135.8, 135.7 (×2), 134.0, 133.9, 133.8, 133.7, 131.9, 131.7, 131.6, 131.5 (×2), 131.4 (×2), 130.4 (×2), 130.2, 130.1, 129.5, 129.1 (×2), 128.9 (×2), 128.8, 128.4, 128.2, 128.1, 128.0, 127.9, 127.8, 126.8, 126.1, 125.4, 125.0, 124.5, 124.0, 70.4, 70.2, 69.8, 69.7, 69.4, 69.2, 67.1, 67.0, 66.8, 66.7, 51.5 (×2), 50.3, 43.7, 43.6, 43.5, 42.7, 42.6, 41.1, 41.0 (×2), 40.2, 40.0 (×2), 39.9, 39.8, 29.8, 29.7, 29.6, 29.5 (×2), 29.3 (×2), 29.2, 29.1, 28.8, 27.1, 27.0, 26.8, 16.2. LR-MS (ESI): m/z = 1374 $[M+2H]^{2+}$; observed peaks consistent with theoretical isotope distribution.

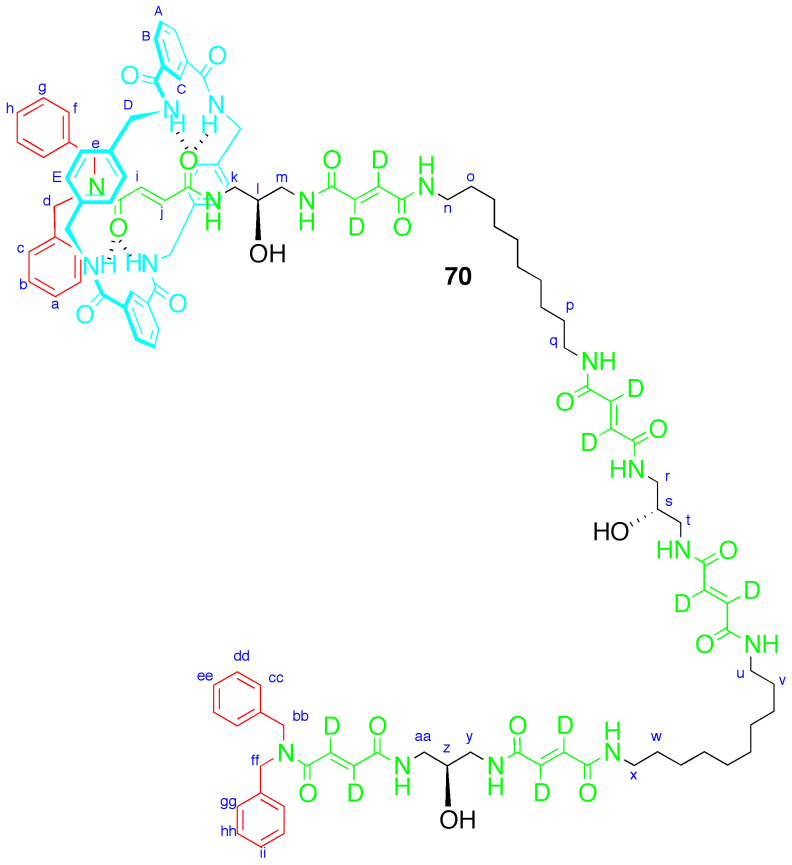

To a stirred solution of **72** (56 mg, 20.4 μmol) in a 1:1 DCM/MeOH mixture (1.5 mL) was added HF·py (0.50 mL of a 70% in pyridine solution) and the mixture was stirred for 16 h, then cooled to 0 °C and diluted with DCM (10 mL). TMSOMe (4.8 mL) was added followed by HCl (1 M, 10 mL), and the mixture was extracted into 3:1 $CHCl_3$/IPA (3 × 50 mL). The combined organic fractions were dried over $MgSO_4$ and concentrated under reduced pressure. The resulting crude was dissolved in DMSO and precipitated into a methanol vortex; filtration gave **70** as a white solid (24 mg, 60%). M.p. 173–174 °C. ^{1}H NMR (500 MHz, DMSO-d_6): δ = 8.54–8.47 (m, 4H, H_C + NH), 8.43 (t, 4H, J = 5.5, NH), 8.35–8.23 (m, 8H, NH), 8.02 (d, 4H, J = 7.7, H_B), 7.61 (t, 2H, J = 7.7, H_A), 7.36–7.21 (m, 18H, H_a + H_b + H_f + H_g + H_h + H_i + H_j + H_{cc} + H_{dd} + H_{ee} + H_{hh} + H_{ii}), 7.11 (d, 4H, J = 7.5, H_c + H_{gg}), 6.99 (s, 8H, H_E), 4.66–4.50 (m, 8H, H_d + H_e + H_{bb} + H_{ff}), 4.39–4.25 (m, 8H, H_D), 3.70–3.55 (m, 3H, H_l + H_s + H_z), 3.28–3.18 (m, 8H, H_n + H_q + H_u + H_x), 3.10–3.00 (12H, H_k + H_m + H_r + H_t + H_y + H_{aa}), 1.20–1.08 (m, 24H, H_{alkyl}); ^{13}C NMR (125 MHz, DMSO-d_6): δ = 166.7, 166.1, 165.7, 164.9, 164.5, 164.1, 163.9, 137.8, 137.4, 134.6, 132.4, 132.0, 131.0, 129.4, 129.2 (×3), 129.0, 128.4, 127.8, 127.4, 126.7,

125.6, 68.6, 55.6, 50.7, 49.5, 45.3, 43.8, 43.7, 42.6, 41.5, 29.7, 29.3, 26.9, 26.7, 25.9, 22.7, 16.8, 16.4, 14.6. LR-MS (ESI): m/z = 2055 $[M+Na]^+$; HR-MS (MALDI): m/z = 2055.0719 $[M+Na]^+$ (calculated for $C_{113}H_{126}D_{10}N_{16}O_{19}Na$ = 2055.0727).

4.11 References and Notes

1. Reimann, P. Brownian motors: noisy transport far from equilibrium. *Phys. Rep.* **2002**, *361*, 57–265.

2. This would not be true if deprotection occurred in a non-random fashion. If, for example, the rate of deprotection 'ahead' of the macrocycle was faster than deprotection 'behind' it, reprotection would enrich the population of successfully transported macrocycles even in a two-compartment system. In fact, this enrichment would still take place even if the protection reaction occurred completely at random with respect to the macrocycle's position; only one stimulus (linking or unlinking) needs to be biased in order for directional transport to occur.

3. Some stereochemical ambiguity is introduced when displaying the alkyl groups truncated in this fashion. The style chosen here is meant to capture the modularity of the design and show that the directional discrimination will be the same at every chiral centre; this is at the expense of showing the actual orientation of the bonds, some of which would point into the paper if the alkyl groups were drawn fully extended.

4. Hu, J. D.; Miller, M. J. Total synthesis of a mycobactin S, a siderophore and growth promoter of *Mycobacterium smegmatis*, and determination of its growth inhibitory activity against *Mycobacterium tuberculosis*. *J. Am. Chem. Soc.* **1997**, *119*, 3462–3468.

5. Pearson, D. A.; Blanchette, M.; Baker, M. L.; Guindon, C. A. Trialkylsilanes as scavengers for the trifluoroacetic-acid deblocking of protecting groups in peptide-synthesis. *Tetrahedron Lett.* **1989**, *30*, 2739–2742.

6. Method for matrix coating adapted from Goodwin, R. J. A.; Dungworth, J. C.; Cobb, S. R.; Pitt, A. R. Time-dependent evolution of tissue markers by MALDI-MS imaging. *Proteomics* **2008**, *8*, 3801–3809. A 10 mL solution of 10 mg mL^{-1} CHCA in 50% acetonitrile, 50% H_2O, 0.1% TFA was spray coated using a pneumatic TLC sprayer (Sigma Aldrich). The sprayer was held 30 cm from the target during matrix coating and sections were allowed to dry between coating cycles. The data was acquired in positive ion mode. Each analysis was the result of 200 laser shots, using a laser spot diameter of 60 μm and a power level of 20%. Ions were detected between m/z 200 Da and 3500 Da.

7. Bennett, C. H. The thermodynamics of computation – a review. *Int. J. Theor. Phys.* **1982**, *21*, 905-940.